AD_____

Award Number: W81XWH-09-1-0658

TITLE: New Advanced Technologies in Stem Cell Therapy

PRINCIPAL INVESTIGATOR: Johnny Huard, Ph.D.

CONTRACTING ORGANIZATION: The University of Pittsburgh
Pittsburgh, PA 15213

REPORT DATE: September 2013

TYPE OF REPORT: Annual

PREPARED FOR: U.S. Army Medical Research and Materiel Command
Fort Detrick, Maryland 21702-5012

DISTRIBUTION STATEMENT: Approved for public release; distribution unlimited

REPORT DOCUMENTATION PAGE

Form Approved
OMB No. 0704-0188

1. REPORT DATE *(DD-MM-YYYY)*	**2. REPORT TYPE**	**3. DATES COVERED** *(From - To)*
September 2013	Annual	1 September 2012 - 31 August 2013

4. TITLE AND SUBTITLE

New Advanced Technologies in Stem Cell Therapy

5a. CONTRACT NUMBER

5b. GRANT NUMBER
W81XWH-09-1-0658

5c. PROGRAM ELEMENT NUMBER

6. AUTHOR(S)
Johnny Huard, Ph.D.
Ira Fox, M.D.
David Permutter, M.D.
E-Mail: jhuard@pitt.edu

5d. PROJECT NUMBER

5e. TASK NUMBER

5f. WORK UNIT NUMBER

7. PERFORMING ORGANIZATION NAME(S) AND ADDRESS(ES)
The University of Pittsburgh
Pittsburgh, PA 15213

8. PERFORMING ORGANIZATION REPORT NUMBER

9. SPONSORING / MONITORING AGENCY NAME(S) AND ADDRESS(ES)
U.S. Army Medical Research and Materiel Command
Fort Detrick, Maryland 21702-5012

10. SPONSOR/MONITOR'S ACRONYM(S)

11. SPONSOR/MONITOR'S REPORT NUMBER(S)

12. DISTRIBUTION / AVAILABILITY STATEMENT
Approved for Public Release; Distribution Unlimited

13. SUPPLEMENTARY NOTES

14. ABSTRACT

Please see the following two pages.

15. SUBJECT TERMS

Project 1: Duchenne Muscular Dystrophy (DMD), human muscle-derived cells (hMDC), myoendothelial cells, pericytes, hMDC transplantation, angiogenesis

Project 2: Hepatacyte transplantation, inducible pluripotent stem (iPS)cells, alpha-1-antitrypsin (AT) deficiency, PiZ mice

16. SECURITY CLASSIFICATION OF:			**17. LIMITATION OF ABSTRACT**	**18. NUMBER OF PAGES**	**19a. NAME OF RESPONSIBLE PERSON**
a. REPORT	**b. ABSTRACT**	**c. THIS PAGE**			USAMRMC
U	U	U	UU	171	**19b. TELEPHONE NUMBER** *(include area code)*

Abstracts

Project 1

Background: We have isolated and characterized a population of skeletal muscle-derived stem cells (MDSCs) that display a greatly improved skeletal and cardiac muscle transplantation capacity when compared to skeletal muscle myoblasts. The MDSCs' ability to withstand oxidative and inflammatory stresses appears to be the single most important factor for their improved transplantation capacity. Although the true origin of MDSCs remains unclear, their high degree of similarity with blood vessel-derived stem cells suggests their potential origin could be from the vascular wall. We have recently isolated two distinct populations of cells from the vasculature of human skeletal muscle known collectively as human skeletal muscle-derived cells (hMDCs). The two populations are myo-endothelial cells and pericytes and both can repair skeletal and cardiac muscles in a more effective manner than myoblasts, as is observed with murine MDSCs.

In the current proposal we intend to evaluate and compare the regeneration capacity of these two hMDC populations after their implantation into the skeletal muscle of immunodeficient/dystrophic (SCID/mdx) mice. We will then investigate the influence that sex has on the regeneration and repair capacity of the hMDCs endowed with the greatest regeneration capacity (either myo-entothelial cells or pericytes). Finally we will investigate the influence that age plays on the regeneration capacity of the cells.

Study Design: We will investigate the effects of cell survival, proliferation, resistance to stress, and neo-angiogenesis on the regeneration capacity of the hMDCs implanted into the skeletal muscle of SCID/mdx mice Since we have observed that female murine MDSCs display an improved transplantation capacity in skeletal muscle when compared to male MDSCs, we will determine the influence that sex has on the hMDCs. Due to the fact that MDSCs isolated from aged mice have a lower skeletal muscle regeneration index than MDSCs isolated from young mice, we will also investigate the influence that donor and host age has on the isolated hMDCs.

Relevance: This project will enable us to further assess the feasibility of using hMDC transplantation to improve the function of skeletal muscle that has been damaged by Duchenne muscular dystrophy (DMD) and other muscle degenerative disorders and injury.

Technical Objective #1: To compare the regeneration capacities of human muscle-derived myo-endo cells and pericytes when implanted in the skeletal muscle of *SCID/mdx* mice and select the optimal cell type to proceed with Technical Objectives 2 and 3.

Hypothesis 1: A differential regeneration capacity will be observed in skeletal muscle of SCID/mdx mice between myo-endo cells and pericytes.

Technical Objective #2: To investigate the influence of sex on the regeneration/repair capacity of the hMDCs implanted in the skeletal muscle of *SCID/mdx* mice.

Hypothesis 2: After implantation into skeletal muscle, the hMDCs cells (myo-endo cells or pericytes) endowed with the highest regenerating potential in skeletal muscle will be influenced by the sex of the donor, due to a differential ability to resist stressful conditions.

Technical Objective #3: To investigate the influence of age on the regeneration/repair capacity of hMDCs implanted in the skeletal muscle of *SCID/mdx* mice.

Hypothesis 3: After implantation into skeletal muscle, the hMDCs cells (myo-endo cells or pericytes) endowed with the highest regenerating potential in skeletal muscle will be influenced by the age of the donor due to a differential ability to induce angiogenesis.

Project 2

Background: Hepatocyte transplantation holds great promise as an alternative to whole organ liver transplantation. Unfortunately, the availability of human hepatocytes is limited. We have shown that functionally normal hepatocytes can be generated from human ES cells (hES). Since human skin fibroblasts can now be genetically modified to produce (iPS) cells with characteristics nearly identical to hES cells, it may be possible to generate hepatocytes from patients using their own cells. We believe the PiZ transgenic mouse model of alpha-1-antitrypsin (AT) deficiency is critical for evaluating the efficacy of stem cell therapies, as hepatocytes without the mutant protein have a selective hepatic repopulation advantage in these mice, and the

PiZ mouse recapitulates the slowly progressing type of disease that affects most patients with chronic liver diseases.

Objective/Hypothesis: Both of the main obstacles to transplantation of stem cells for the treatment of liver disease (the number of livers available and the immunological barrier) might be addressed if liver cells could be generated de novo from precursor cells of the individual to be treated.

Study Design: We will determine the extent to which human patient-specific, inducible pluripotent stem (iPS) cells can be differentiated into primary human hepatocytes. We will then determine the extent to which the PiZ mouse model of AT deficiency can be developed as a platform for pre-clinical testing of hepatic stem cells. Finally, we will identify specific molecules responsible for regenerative and fibrotic signals in the PiZ mouse model of liver disease.

Relevance: This project will determine the extent to which patient-specific hepatic stem cells can be used for regeneration and repair of injuries to the liver and liver failure. A more complete understanding of the mechanisms by which donor stem cells can reduce liver injury and toxin and/or cancer risk should enhance the number of areas where hepatic stem cell transplantation might be effectively applied.

Technical Objective #1: *Determine the extent to which human patient-specific, inducible pluripotent stem (iPS) cells can be differentiated into primary human hepatocytes.*

Hypothesis: Protocols that successfully differentiate mouse and human embryonic stem (ES) cells toward a hepatocyte phenotype will be effective in differentiating human skin cell-derived iPS cells into liver cells.

Technical Objective #2: Determine the extent to which the PiZ mouse model of alpha-1-antitrypsin (AT) deficiency can be developed as a platform for pre-clinical testing of hepatic stem cell transplantation as a treatment for severe liver injury and disease.

Hypothesis: *iPS cells differentiated toward a hepatocyte phenotype can engraft and respond normally to proliferative signals in the livers of PiZ mice.*

Technical Objective #3: Utilize laser-capture microdissection, coupled with high-density oligonucleotide array techniques as well as double-label immunofluorescence techniques to identify specific molecules responsible for regenerative and fibrotic signals in the PiZ mouse model of liver disease.

Hypothesis: *Transplantation of donor stem cells can ameliorate liver injury and cancer risk in liver disease.*

Table of Contents

Sub-Project 1: Muscle stem cell transplantation for Duchenne muscular dystrophy
PI: Johnny Huard

INTRODUCTION:
We have isolated and characterized a population of skeletal muscle-derived stem cells (MDSCs) that display an improved skeletal and cardiac muscle repair upon transplantation when compared to skeletal muscle myoblasts. The MDSCs' ability to withstand oxidative and inflammatory stresses appears to be the most important factor for their improved transplantation capacity. Although the true origin of MDSCs remains unclear, their high degree of similarity with blood vessel-derived cells (myo-endothelial and perivascular cells) suggests their potential origin could be from the vascular wall. We have also isolated two distinct populations of cells from the vasculature of human skeletal muscle known collectively as human skeletal muscle-derived cells (hMDCs). The two populations are myoendothelial cells and pericytes and they both can repair skeletal and cardiac muscles in a more effective manner than myoblasts, as is observed with murine MDSCs. In the current proposal we have evaluated and compared the regeneration capacity of these two hMDC populations in vitro and after their implantation into the skeletal muscle of cardiotoxin (ctx) injured immunodeficient mice. We are now in the process of investigating the influence that sex has on the regeneration and repair capacity of the hMDCs endowed with the greatest regeneration capacity which we have determined to be the myoentothelial cell population. Finally we will investigate the influence that age plays on the regeneration capacity of the cells. We will investigate the effects of cell survival, proliferation, resistance to stress, and neo-angiogenesis induction on the regeneration capacity of the hMDCs implanted into the skeletal muscle of SCID/*mdx* mice since this model is more relevant to DMD than the ctx injury model previously used. Since we have observed that female murine MDSCs display an improved transplantation capacity in skeletal muscle when compared to male MDSCs, we will determine the influence that sex has on the hMDCs. Due to the fact that MDSCs isolated from aged mice have a lower skeletal muscle regeneration index than MDSCs isolated from young mice, we will also investigate the influence that donor and host age has on the isolated hMDCs. This project will enable us to further assess the feasibility of using hMDC transplantation to improve the function of skeletal muscle that has been damaged by Duchenne muscular dystrophy (DMD) and other muscle degenerative disorders and injury.

During the last 4 years we were involved with the characterization of 2 populations of hMDCs, myoendothelial cells and pericytes and demonstrated that the myoendothelial cells and pericytes could repair skeletal and cardiac muscle more effectively than myoblasts. As previously reported, several aspects of the first aim of the project were completed, namely the fluorescent-activated cell sorting (FACS) of the myoendothelial cells, pericytes and myoblasts from cryopreserved human progenitor skeletal muscle cells (hPSMCs); comparisons of the *in vitro* myogenic potential of these populations; and the transplantation of the populations into cardiotoxin-injured skeletal muscle of SCID mice to assess their *in vivo* regenerative capacity. The results showed that the myoendothelial cells possessed a better in vitro myogenic differentiation capacity, as well as, a better in vivo engraftment capacity when transplanted into cardiotoxin injured skeletal muscle using an antibody against human spectrin. During the 2nd year of funding we demonstrated on a minimal number of experimental animals that proliferation and myogenic differentiation capacities were greater in the younger experimental animals and that oxidative stress resistance is reduced in MDC's isolated from older individuals. We were also involved with optimizing the media type for MDC expansion and were attempting to identify an optimal dystrophin antibody to use for the in vivo detection of human MDCs in our mouse model of DMD that is also immunocompromised (SCID/mdx). Unfortunately, all but one of the antibodies tested continued to have high levels of background. More importantly was the fact that even after identifying antibodies with reduced background, preliminary studies, where we injected hMDCs into SCID/mdx mice, showed levels of engraftment that were not high. Another tangential study performed during year 3's performance period showed that the immunomodulary properties of MDCs was associated with a reduction in NF-kB/p65 signally and that MDCs with reduced p65 expression could improve the histopathology of a model of DMD that has no dystrophin or utrophin expression, also known as the dKO (double Knock-Out) mouse, when injected IP. The current year's major focus (Year 4) was to continue to determine why we were experiencing the transplantation difficulties

with the SCID/mdx mice. It was imperative to determine why the SCID/mdx mice were generating such high levels of background when injected with hMDCs Unfortunately our aged SCID/mdx colony has diminished substantially and we are currently in the process of aging additional mice .We have been aging this colony of mice for 2 years in order to carry out the remaining aims of this grant, which outlined experiments to compare the transplantation efficiency of old and young hMDCs injected into old and young host SCID/mdx animals; however, while continuing to age the mice we will utilize younger SCID/mdx mice and the dKO model that we described in last year's report as well as SCID mice with a ctx injury which we described previously.

BODY:

Statement of Work:

Technical Objective #1: To compare the regeneration capacities of human muscle-derived myoendothelial cells and pericytes when implanted in the skeletal muscle of dystrophic mice and select the optimal cell type to proceed with Technical Objectives 2 and 3.

Hypothesis 1: A differential regeneration capacity will be observed in the skeletal muscle of SCID/mdx mice between myoendothelial cells and pericytes.

Technical Objective #2: To investigate the influence of sex on the regeneration/repair capacity of the hMDCs implanted in the skeletal muscle of dystrophic mice.

Hypothesis 2: After implantation into skeletal muscle, the hMDCs cells endowed with the highest regenerating potential in skeletal muscle will be influenced by the sex of the donor, due to a differential ability to resist stressful conditions.

Technical Objective #3: To investigate the influence of age on the regeneration/repair capacity of hMDCs implanted in the skeletal muscle of dystrophic mice.

Hypothesis 3: After implantation into skeletal muscle, the hMDCs cells endowed with the highest regenerating potential in skeletal muscle will be influenced by the age of the donor due to a differential ability to induce angiogenesis.

Progress made from 9-1-12 to 8-31-13

Below is outlined the progress that we made last year in an attempt to work out the difficulties we have been experiencing with the transplantation of our human MDCs into the SCID/mdx model, which was proposed to be utilized as a DMD model to test the transplantation efficiency of several hMDC populations. Besides the proposed human cell types of pericytes and myo-endo cells we utilized human MDCs isolated via the preplate technique, which is a population of cells that is more heterogeneous in nature and contains both the myo-endo cell and pericyte sub-populations. We also compared these latter three populations to another human cell population isolated from dental pulp and amniotic fluidto determine if the engraftment problems were related to the stem cell type. Moreover we performed a study to see if we could improve the cells transplantation efficiency by activating the Notch signally pathway, which has been described previously to be necessary for maintaining the stem cell niche in skeletal muscle. Finally, in an attempt to further improve engraftment efficiency we grew the cells on a variety of different substrates with varying degrees of surface elasticity to improve their expansion. Below is a summary of our findings.

Human muscle derived stem cells for muscle regeneration:

Isolation of hMDSCs

Human skeletal muscle tissues obtained from 2 male donors (21 and 23 years old) and 2 female donors (30 and 76 years old) were purchased from the National Disease Research Interchange (NDRI). hMDSCs were isolated using our previously described modified pre-plate technique. Cells were seeded at a density of 1000 cell/cm^2, passaged every 3 days and maintained at less than 50% confluence.

Surface marker expression of the preplate isolated hMDSCs

The marker profile of the cells from each donor was analyzed by flow cytometry using anti-human fluorochrome-conjugated antibodies/ligands: CD45-APC-Cy7, CD56-PE-Cy7, CD90-APC, CD146-FITC, UEA-1R-PE, CD44-PE, CD73-PE, CD105-PE.

Stem cell gene expression by the isolated hMDSCs

The expression of stem cell genes POU class 5 homeobox 1 (POU5F1 or OCT4) and the Nanog homeobox (NANOG) and SRY (sex determining region Y)-box 2 (SOX2) were tested using semiquantitative RT-PCR.

Multipotent differentiation capacities of the hMDSCs

hMDSCs were tested for their myogenic, adipogenic, chondrogenic and osteogenic differentiation capacities in vitro.

Construction of Lenti-GFP and hMDSCs transduction to track the fate of the injected cells

We constructed lenti-GFP vector under the control of CMV promoter. Lenti-GFP virus was packaged in GP293T cells. In order to test whether hMDSCs could efficiently regenerate muscle in vivo, we transduced hMDSCs at passage 10 with lenti-GFP virus. The lenti-GFP transduced cells were then subjected to flow cytometry cell sorting for GFP at passage 3 post transduction and further expanded in proliferation medium for in vivo muscle injection.

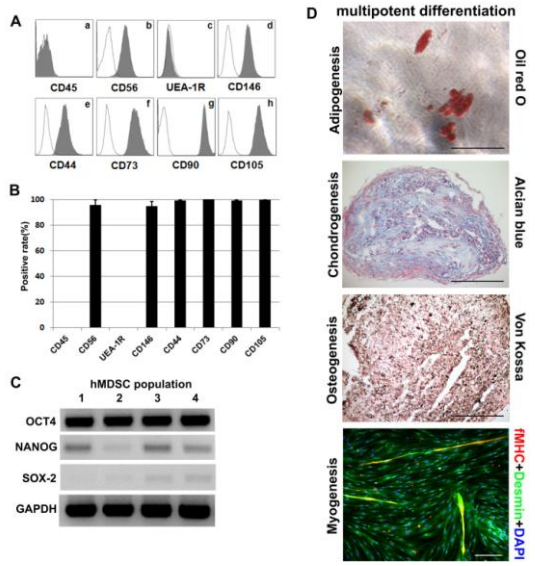

Fig.1. Characterization of the hMDSCs. **A.** Flow cytometry analysis of hMDSC surface markers revealed robust expression of CD56, CD146, CD44, CD73, CD90, CD105 but not CD45 or UEA-1R. **B.** Quantification of cell lineage marker expression in hMDSCs from 4 donors demonstrated consistency in their cell marker expression profiles. **C.** RT-PCR results of stem cell markers. Cells from each donor expressed the stem cell markers OCT4 and NANOG, but only faint expression of SOX-2 was detected in cells from two donors (3 and 4). D. Multipotent differentiation of hMDSCs. hMDSCs undergo adipogenesis(oil red staining), chondrogenesis(Alcian blue staining), osteogenesis (von Kossa staining) and myogenesis as shown by fMHC and desmin immunofluoresence. Scale bars represent 200μm.

In vivo muscle regeneration

SCID/mdx mice at 8 weeks were divided into two groups(n=4): Group 1: MDXSCID injected with hMDSCs-lenti-GFP 5×10^5 cells in the gastrocnemius; Group2, MDXSCID mice were first injured with cardiotoxin 30μl(4μM), 24 hrs later, 5×10^5 hMDSCs-lenti-GFP cells were injected into the same gastrocnemius muscle that was injured with cardiotoxin(CTX). Mice were sacrificed at 14days after injection, gastrocnemius muscle were dissected and snap frozen in 2-methyle-butane that was precooled in liquid nitrogen. Crysections were performed and immunofluorescent staining of dystrophin-GFP and fMHC-GFP were performed.

Results

Characterization of hMDSCs

hMDSCs isolated by a modified pre-plate technique were characterized by flow cytometry for several cell lineage markers, including CD45 (leukocytes/hematopoietic cells), CD56 (myogenic cells), *Ulex europaeus agglutinin I receptor* (UEA-1R, endothelial cells), CD146 (pericytes/endothelial cells) as well as classic mesenchymal stem/stromal cell (MSC) markers: CD44, CD73, CD90, and CD105. We found that hMDSCs robustly expressed CD56, CD146, and four MSC markers (more than 99% positive) but not CD45 or UEA-1R (**Fig. 1A**). Quantitative analysis revealed a consistent marker expression profile in all the hMDSC populations examined (**Fig.1B**). RT-PCR results revealed that cells from all donors expressed the stem cell markers OCT4 and NANOG, while cells from two of the donors (23 y/o male and 76 y/o female) slightly expressed SOX-2 (**Fig.1C**). In vitro differentiation assays indicated that the hMDSCs could undergo adipogenic, chondrogenic, osteogenic and myogenic differentiation as shown by oil red O staining, Alcian blue staining, von Kossa staining and fMHC and desmin immunofluorescence respectively (**Fig. 1D**).

Lenti-GFP transduction efficiency

The transduction efficiency of lenti-GFP was approximately 85%. After GFP sorting, the GFP positive cells were approximately 95-99%. Some cells lost GFP over time; however, the majority of the cells maintained GFP transgene expression during cell expansion (Figure 2A).

hMDSCs engrafted in the skeletal muscle of SCID/mdx mice

Our results showed no dystrophin–GFP double positive fibers or fMHC –GFP double positive fibers; however, we did find GFP positive central nucleated muscle fibers along the GFP positive hMDC clusters in both the non-injury and CTX injured groups. There were no statistical differences in the number of central nucleated muscle fibers between the groups. We therefore conclude, as we have in the past experiments, that the hMDCs could engraft in the SCID/mdx mice but only minimal muscle regeneration was observed (Figure 2B).

Conclusion

We found that the hMDCs isolated by the preplate technique expressed mesenchymal stem cell markers CD73, CD90, CD105 and CD44. They also uniquely expressed the myogenic marker CD56 and the pericyte marker CD146. As they could undergo adipogenic, chondrogenic, osteogenic and myogenic differentiation, we speculate that they are mesenchymal stem cells of muscle origin. The in vivo results indicated that they could engraft within the muscle; however, their regeneration capacities were low. Therefore, the co-injection of myogenic growth factors or ex vivo enhancing myogenic transcription factors or other cellular enhancement protocols are perhaps required to increase the muscle regeneration capacity of the hMDCs within this model of DMD.

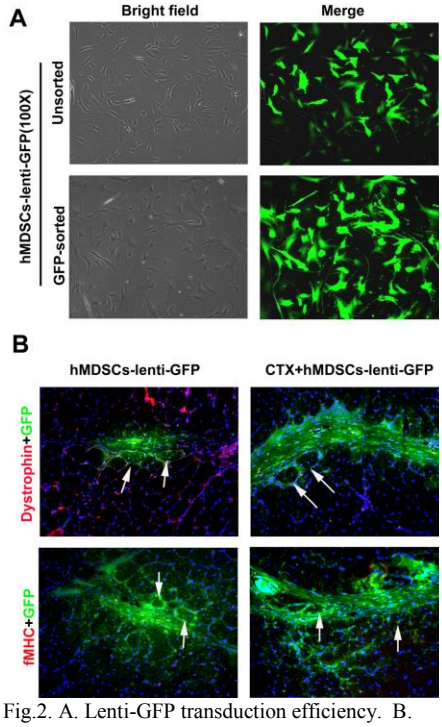

Fig.2. A. Lenti-GFP transduction efficiency. B. hMDSCs fused with very few muscle fibers two weeks after gastrocnemius injection in either non-injured or carditoxin injured dystrophic muscle. We did not find any dystrophin-GFP double positive cells or fast myosin heavy chain double positive cells. We did find very few central nucleated GFP positive cells near the GFP positive cell clusters in the injection site (white arrows). All pictures were taken at 200X magnification.

Enhanced myogenic potential of human dental pulp and amniotic fluid stem cells by use of a demethylation agent and conditioned media.

Duchenne muscular dystrophy (DMD) is a X-linked genetic disease that is caused by a lack of dystrophin which results in severe muscle degeneration and leads to early death by the mid-twenties. Cell therapy can be used to reintroduce dystrophin to repair damaged muscle fibers.

Human dental pulp (hDPSCs) and amniotic fluid stem cells (hAFSCs) may represent alternative cell sources that are less controversial than the use of embryonic stem cells. HDPSCs can be isolated from the adult human dental pulp of the third molars during routine extraction. HAFSCs, represent 1% of the cells in human amniocentesis specimens and can be isolated by immunoselection of the c-Kit (CD117) antigen positive population via magnetic cell sorting (MACS). HDPSCs and hAFSCs have been shown to possess self-renewal and multipotent capacities (1,2); therefore, they may represent promising cell populations for developing therapies for treating DMD. This study evaluated the myogenic potential of hDPSCs and hAFSCs using different conditions which optimized the most effective protocol to differentiate the cells towards a myogenic lineage.

Human DPSCs were isolated as described by Riccio et al (3). The STRO-1+ DPSC population was obtained by magnetic cell sorting. AFSCs were isolated as previously described by De Coppi et al (2): hAFSCs cultures, from supernumerary amniocentesis specimens, were subjected to c-Kit immuno-selection by MACS technology.

To test the ability of hAFSCs and hDPSCs to form new myotubes, the cells were differentiated in a direct co-culture system with C2C12 myoblasts. Human cells and C2C12 cells, seeded at a 10:1 ratio, were maintained in proliferation medium (PM: DMEM High Glucose + 10% FBS) until confluent, the medium was then replaced with fusion medium (FM: DMEM High Glucose + 1% FBS + 10nM insulin). To evaluate whether hAFSCs and hDPSCs could be committed to the myogenic lineage, cells were seeded at 3000 cells/cm2 in PM until confluent. Subsequently, the medium was replaced with low serum differentiation medium supplemented with 10µM 5-Aza-2'-deoxycytidine (5-Aza) for 24 hours, to induce DNA demethylation. After removing 5-Aza, medium was replaced with low serum differentiation medium (fusion medium) supplemented with 10 nM insulin. Cells were differentiated in a) low serum medium plus 10 nM insulin and b) pre-filtered conditioned FM from the C2C12 culture + fresh differentiation medium + 10 nM insulin. To determine myogenic differentiation, staining for human Nuclei (huNu) and myosin heavy chain (MyHC) was performed. Myogenic differentiation after demethylation was verified by myogenin and MyHC immune-fluorescent (IF) staining. Human cells were processed for IF staining as previously described (3).

Figure 3

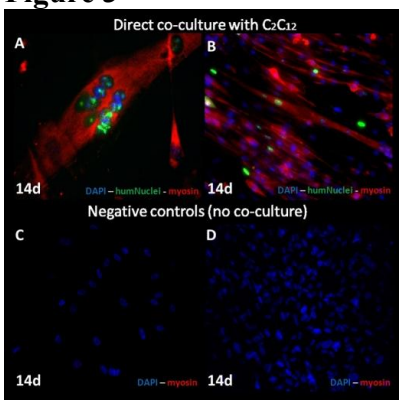

When differentiated in direct co-culture with C2C12 cells, human AFSCs and DPSCs were able to undergo myogenic differentiation, as demonstrated by the positive staining of the myotubes with anti-huNu ab (**Fig. 3A-B**). Human cells which were not co-cultured with C2C12 did not undergo myogenic differentiation and did not fuse in myotubes (**Fig. 3C-D**).

Data from the IF analysis of myogenic differentiation after treatment with 10µM 5-Aza showed that hAFSCs are driven toward a myogenic lineage and express myogenin, a myogenic differentiation marker, after 14 days of differentiation (**Fig. 4A**), while the hDPSCs underwent myogenic differentiation expressing myogenin after 21 days of differentiation under the same conditions (**Fig. 4C**). Moreover, some hAFSCs also showed positive staining for MyHC (**Fig. 4B**). Immunofluorescence labeling also showed that when conditioned medium from the differentiating C2C12 cells was added to fresh myogenic medium, the human cells pre-treated with 5-Aza started to express myogenin after 14 and 21 days of differentiation (**Fig. 4D-4F**) respectively. Furthermore, some of the hAFSCs also showed positive staining for MyHC (**Fig. 4E**). Cells not demethylated demonstrated no positive staining for muscle specific markers (**Fig. 4G-H**).

Figure 4

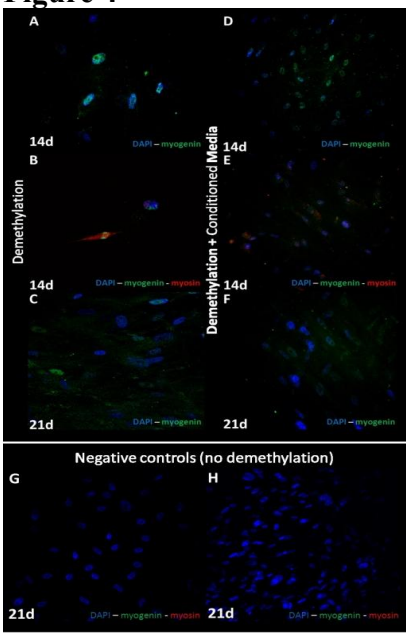

Figure 5

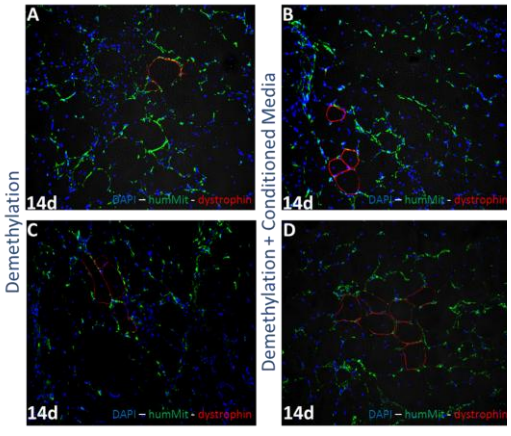

In vitro pre-differentiated hDPSCs and hAFSCs were injected into the gastrocnemius muscles of 8-10 week old SCID/mdx mice. The muscles were harvested 14 days after injection, snap frozen in liquid N2 and cryosectioned. Immunofluorescent labeling of muscle cryosections using an anti-human mitochondrial (humMit) antibody showed engraftment by both the hDPSCs (**Fig.5A-B**) and hAFSCs (**Fig.5C-D**). Interestingly, the double IF staining of humMit and dystrophin revealed the presence of human cells in some dystrophin-positive muscle fibers, as shown in **Fig.5.**

The IF image data in this study demonstrated that the hAFSCs and

hDPSCs stem cell populations could actively participate in the formation of myotubes. These human cells were capable of fusing with murine C2C12, as demonstrated by the positive IF staining of the multi-nucleated cells to anti-huNu ab. These results showed the potential of these cells for skeletal muscle repair. This study demonstrated that demethylation treatment could effectively induce a myogenic commitment of hAFSCs and hDPSCs, in two different conditions, as shown by IF staining: hAFSCs underwent myogenic differentiation earlier than hDPSCs, and reached a more mature differentiation status as shown by their expression of MyHC. The *in vivo* results suggest that hAFSCs and hDPSCs represent a potential, non-controversial sources of stem cells that could be very useful for translational strategies to enhance the repair of injured skeletal muscle in DMD patients; however, these cell population were also very limited in their ability to engraft and produce human dystrophin in the SCID/mdx model as was observed with the myo-endo and pericyte populations indicated that the poor expression of dystrophin is not exclusively a hMDC related phenomenon. This study also demonstrated the utility of demethylation to induce hAFSCs and hDPSCs to differentiate towards the myogenic lineage in vitro and, to a very limited degree, engraft and produce dystrophin. The positive fibers observed were very few and could represent revertant myofibers. We therefore conclude that like the myo-endo, pericytes, and preplate isolated MDCs, the hAFSCs and hDPSCs could engraft but could only participate in myofiber regeneration and dystrophin production to a very limited degree, if at all.

Improving the efficacy of human cell transplantation into dystrophic muscle by activating Notch signaling.

It is believed that optimized mechanisms for the regulation of muscle stem cells are naturally inherent in the stem cell niche in healthy skeletal muscle (7-9). The stem cell niche in skeletal muscle is the nest of quiescent stem cells beneath the basal lamina of myofibers, and is critical for maintaining the stemness and self-renewal of stem cells (7). In diseased or aged skeletal muscle, the proper function of the stem cell niche is impaired, resulting in the loss of the cells' self-renewal and regeneration capacities (7). It is notable that the activation of Notch signaling has been identified as a key molecular signature of the native stem cell niche in skeletal muscle, and is needed for the colonization of stem cells in the niche and asymmetric cell division (10-12). Therefore, we suggested that the transplantation of human muscle cells could be greatly improved by activating Notch signaling in the cells.

Methods:

Mouse model: immune-deficient mdx mice (SCID/mdx, female, 8 weeks old) were used in the study.
Preparation of PCL scaffold: PCL (polycaprolactone) was prepared and provided by Dr. Jin Gao in Dr. Yadong Wang's lab, according to a procedure described previously.
DLL1 conjugation to PCL: DLL1 (mouse): Fc (human) (rec) (Enzolifesciences) was chemically conjugated with PCL following the procedure previously described by Zhang et al (13). Briefly, aminolysis of PCL was conducted first and then DLL1 was immobilized to aminated PCL with the help of heterobifunctional crosslinker Sulfosuccinimidyl-4-(*N*-maleimidomethyl) cyclohexane-1-carboxylate (Sulfo-SMCC).
Cell seeding into PCL: Cell seeding was conducted by injecting 0.1 x10^5 human GFP labeled MDCs into the DLL-conjugated PCL or control PCL constructs (a size of around 2 x 2 x1mm) and cultured in medium. Cell suspensions were aspirated in a syringe with a 20G needle and injected into the scaffold once per every 1mm distance. Half of the culture medium was then carefully added to each well and allowed to incubate for 4 hours, prior to adding the remaining half of the medium.
Implantation of Jagged1 treated cells:
Human muscle-derived cells were treated with Jagged1 peptide (CDDYYYGFGCNKFCRPR) (10nM) in proliferation medium for 2 days in vitro, and then injected into the left GM muscles of 8-week old SCID/mdx mice (3x10^5 cells). The same numbers of cells without treatment were injected into the right GM muscles of the same SCID/mdx mice to serve as a control.
Histology and Immunohistochemistry: The frozen skeletal muscles were cryosectioned at a thickness of 10 microns and processed for histological analysis. Expansion and engraftment of muscle stem cells were identified by immuno-staining with antibodies against human lamin A/C and utrophin.

To find out the effect of Notch activation *in vitro*, and to mimick the in vivo growth environment, GFP-labeled human muscle stem cells were seeded in 3D constructs made of PCL (polycaprolactone), which were chemically conjugated with an activating Notch ligand [DLL1 (mouse): Fc (human) (rec)] following a procedure previously described by Zhang et al (13). Specifically, 2 µg DLL1 (mouse): Fc (human) (rec) was dissolved in 50µL of PBS and incubated with Sulf-SMCC treated PCL construct (size: 2 x 2 x 1 mm). Cell seeding was conducted by injecting of 0.2 x10^5 GFP labeled human muscle stem cells into the DLL-conjugated PCL or control PCL constructs and cultured in medium. At day 3 after cell seeding, there was a clearly increased number of GFP labeled human muscle stem cells observed in DLL1-conjugated P CL (**Figure 6**). This observation indicated that the activation of Notch signaling in human muscle stem cells could promote their proliferation.

Figure 6

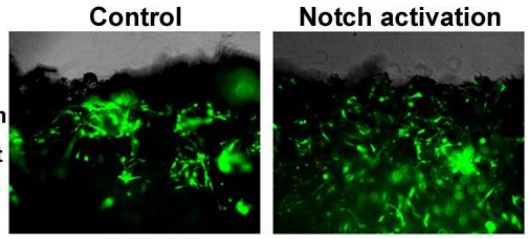

We further tested the effect of Notch activation in human muscle-derived cells *in vivo*, by transplanting the Notch activator (Jagged1) treated cells into the skeletal muscle of SCID/mdx mice. Human muscle-derived cells were treated with Jagged1 peptide (CDDYYYGFGCNKFCRPR) (10nM) in proliferation medium for 2 days in vitro, and then injected into the Gastrocnemius (GM) muscles of 8-week old SCID/mdx mice (3x10^5 cells). Cells without treatment were also injected in to GM muscle of SCID/mdx mice to serve as a control. Ten days after the cell transplantation, muscle tissues were harvested and immuno-stained with antibodies against human lamin A/C and utrophin. Compared to the skeletal muscle transplanted with the untreated control cells, there were more utrophin-positive myofibers and larger cell engraftment observed in the skeletal muscle transplanted with the Notch-activated human muscle cells (**Figure 7**). Our results indicated that the transplantation of human MDCs into dystrophic muscle could potentially be improved by activating Notch signaling prior to their implantation.

Figure 7

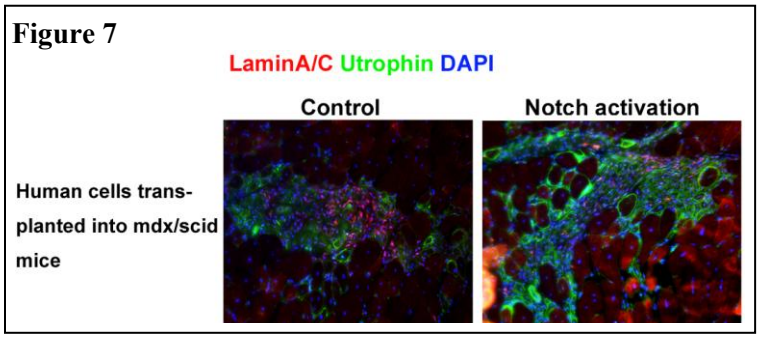

Proliferation and Differentiation Capacities of Muscle Derived Stem/Progenitor Cells Cultured on Polydimethylsiloxane Substrates of Varying Elastic Modulus and Protein Coating

Introduction:

In this proof of concept study we utilized muscle derived stem/progenitor cells (MDSPCs) which are multipotent murine cells that display a capacity for long term proliferation. These cells have been utilized to regenerate bone (14), cartilage (15), skeletal (14) and cardiac muscles[3], as well as ameliorate the effects of aging[4]. MDSPCs are isolated and cultured on collagen I coated polystyrene flasks, but recent publications have shown that culturing progenitor cells on substrates with anatomically relevant elasticities and protein coatings can vastly alter their ability to proliferate and differentiate *in vitro* as well as engraft *in vivo* (18-20). Polydimethylsiloxane (PDMS) blends have shown to be a readily tunable substrate creating reproducible culture surfaces at anatomically relevant elasticities (20). These blends can be adjusted across three orders-of-magnitude, surpassing what is capable with other hydrogel or PDMS systems. This study was designed to observe the effects of altering the culture surface conditions on MDSPCs *in vitro* and determine how to translate these findings to improve tissue regeneration with MDSPCs *in vivo*.

Methods:

Creating variable stiffness PDMS substrates and protein coated culture surfaces: PDMS substrates and protein coatings were prepared using previously defined methods7. Briefly, blends of Sylgard 527 and Sylgard 184 (Dow Corning) were mixed to create PDMS substrates with elastic modulus of 5 kPa, 50 kPa, 830 kPa, and 1.72 MPa. These blends were cured in 12 well plates with one of each protein coating, collagen type I (Col-1), collagen type IV and laminin (Col-4/Lam), or fibronectin (FN).

Proliferation of MDSPCs: MDSPC proliferation was investigated for 3 days on 12-well plates using a Live Cell Imaging (LCI) system. Time-lapse images were acquired every 15 minutes over 72 hours and cell numbers quantified at 6-hour intervals using ImageJ (NIH). Counts were averaged for each time point from at least 6 separate images and experiments were performed in duplicate.

Myogenic differentiation of MDSPCs: Myogenic differentiation potential was assessed by inducing *in vitro* myotubes formation after switching the proliferation medium (Dulbecco's modified Eagle's medium [DMEM] containing 10% fetal bovine serum [FBS], 10% horse serum, 1% Penicillin/Streptomycin, and 0.5% chick embryo extract) to fusion medium (DMEM containing 2% FBS and 1% penicillin/streptomycin). After 2-3 days, cells were fixed in cold methanol and immunostained for skeletal fast myosin heavy chain (f-MyHC)-positive myotubes (1:400, Sigma) and counterstained with DAPI (1:1000, Sigma). Images were taken on a Leica DM-IRB inverted microscope with a 20x objective.

Results:

Culture surfaces with PDMS substrates and protein coatings increase the proliferative capacity of MDSPCs: MDSPCs were observed on 13 separate combinations of protein coating and substrate elastic modulus, including the negative control of tissue culture plastic with no substrate or coating, to evaluate their effects on rate of proliferation (**Figure 8**).

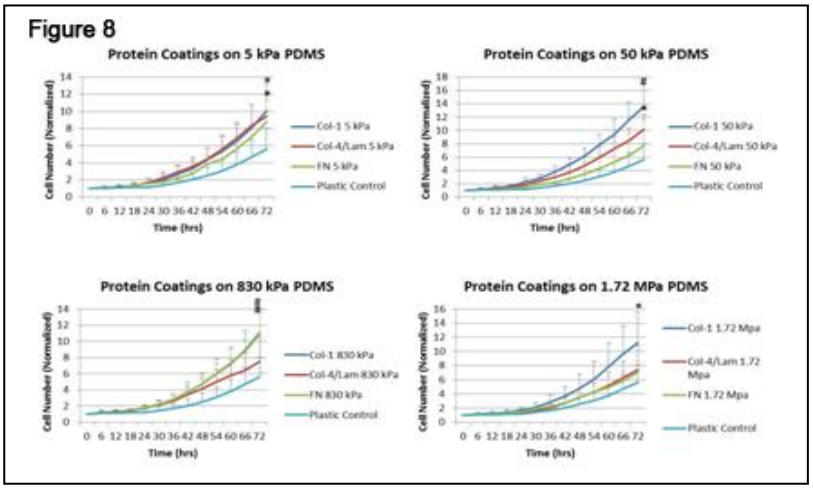

Significance in comparison to the negative control (plastic) is denoted with * ($p < 0.05$) and # ($p<0.001$). The highest proliferation rate from each group of substrate elastic modulus came from the condition including the coating of collagen type I. The combination of collagen type I coating on the 50 kPa PDMS provided the optimal condition for MDSPC proliferation.

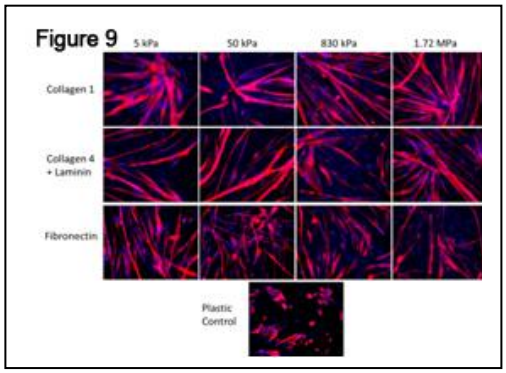

Qualitative differences in myotube formation between substrate elasticities and protein coatings: MDSPCs were differentiated into myotubes on the various PDMS substrates and protein coatings for 2-3 days, displaying a dynamic range of myotube dimensions (**Figure 9**). MDSPCs cultured on collagen type I and collagen type IV/laminin coatings created more robust and elongated myotubes. Myotubes formed on stiffer substrates (830 kPa and 1.72 MPa) were more numerous, but also more slender, than their broader counterparts formed on softer PDMS.

After these initial findings utilizing murine MDSPCs we initiated experiments using human MDCs, specifically human myo-endo cells, employing the same parameters outlined above for the murine MDSPCs. As above, both the proliferation and differentiation (fusion) capacities were analyzed as the endpoint measurement abilities of the cells. In regard to the proliferation capacities of the MDCs we found that the most highly proliferative cells were found in the collagen 4/laminin coated plates with a rigidity of 1.72 MPa and the lowest proliferative capacity was observed in the fibronectin coated plates with a rigidity of 5kPa (Figure 10). In regard to the

effects on the differentiation (myogenic fusion), the substrate that promoted the highest fusion was seen in the collagen I coated plates with a rigidity of 5kPa and the lowest fusion index was observed with the fibronectin substrate with a rigidity of 50kPa (Figures 11A and 11B).

Figure 10

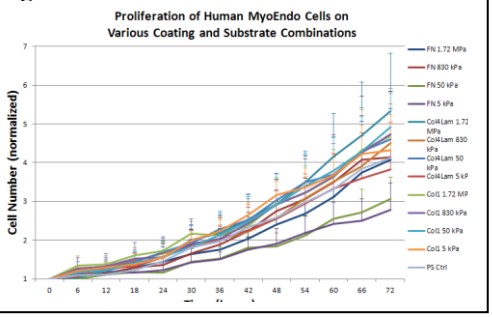

Figure 11

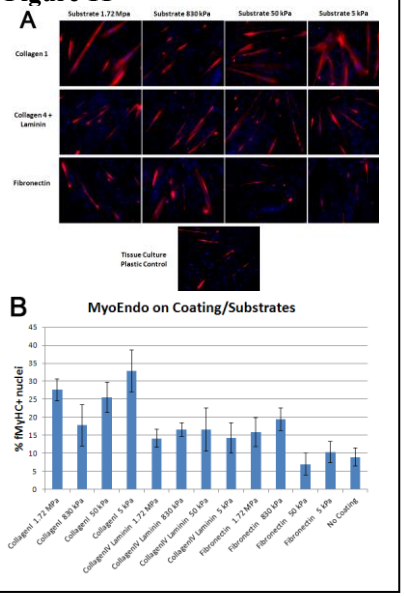

Discussion:

These findings support the view that optimizing the *in vitro* environment, by modulating the surface culture conditions with a variable stiffness PDMS substrate and protein coatings; can augment stem cell proliferation and differentiation capacities. Culture methods such as this may be used to prime MDSPCs towards specific lineages, by simulating tissue conditions of their natural niche, to improve cellular engraftment for therapeutic cell transplantations. The object of proliferating the cells in vitro is to expand the number of cells without promoting their differentiation into more mature lineages; therefore, we suspect that the optimal substrate is probably the fibronectin coated on plates with a 50kPa rigidity. Future cell therapies implemented for tissue repair may significantly benefit from the application of primary cells isolated and expanded on PDMS surfaces with protein coatings. Future in vivo studies are planned to test if modulating the cells in vitro expansion can affect their engraftment and regeneration capacities in injured and diseased skeletal muscle.

Progress made from 9-1-11 to 8-31-12

SCID/mdx mice skeletal muscle generates high levels of background when immunostained with an antibody against "human dystrophin".

An ongoing problem exists with the animal model that we were intending to utilize for our transplantation efficiency experiments on aged and young animals using aged and young hMDCs. It is a mouse model that is both deficient in murine dystrophin (mdx) and is immune-compromised (SCID, lacking both T and B cell functional activity). The purpose of utilizing this model was to demonstrate muscle regeneration in a dystrophic animal without eliciting a cellular immune response. When originally created this model demonstrated excellent grafting capacities and very little immune response, however, over the past year we have been experiencing a problem with this model, in that all the anti-human dystrophin antibodies we have been using have been giving us very high levels of background in the skeletal muscle of these mice. Originally we thought that it was a cross reactivity with the cells injected, but soon discovered the antibody was binding in vivo even when only PBS was being injected. The following is a summary of the work we performed over the past year to try and elucidate and correct this problem.

In this 1st set of experiments human myoendothelial (myoendo) cells, pericyte, and preplate cells purchased from Cook Myosite, Inc. were injected into 8 week old SCID/mdx mice and compared with mice injected with vehicle alone (PBS) or not injected at all. The mice were sacrificed 2 weeks post-transplantation. The following is the resulting data which shows very limited engraftment overall and no significance between the groups Figure 1.

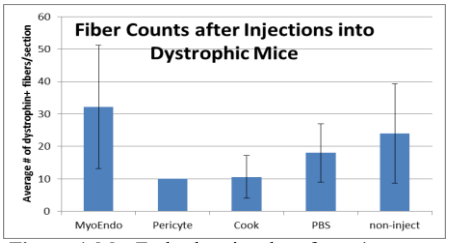

Figure 1 MyoEndo data is taken from 4 separate donor populations injected into 12 separate muscles. Pericyte data is taken from 1 muscle. Cook Myosite data is taken from 1 donor population and 5 muscles. PBS data was taken from 6 separate muscles. Non-injected data was taken from 4 different muscles.

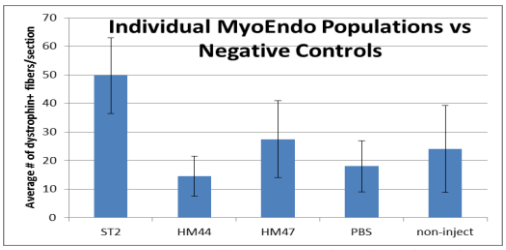

Figure 2: ST2 MyoEndo (69 M) data is taken from 5 separate muscles. HM44 MyoEndo (26 F) data is taken from 4 separate muscle. HM47 MyoEndo (16 M) data is taken from 2 separate muscles. PBS data was taken from 6 separate muscles. Non-injected data was taken from 4 different muscles. Significance between ST2 and PBS ($P > 0.005$); and between ST2 and non-injected ($P > 0.05$) was observed.

Since previous data indicated that the myoendo populations appeared superior to the pericytes and cells 3 separate populations of the myoendo cells were compared. The data can be seen in Figure 2. Again even when comparing all the populations of myoendo cells we have isolated, only the ST2 population showed any significance in myofiber regeneration; however the number of regenerated myofibers were barely above that observed for revertancy as seen in the PBS and non-injected muscles

Comparison of "dystrophin-positive" myofibers in SCID/mdx after injecting either STS2 myoendo cells in PBS or PBS alone. As is evident in this figure, positive fibers can be seen in both muscles indicating cross reactivity of the antibody with some membrane bound molecule in both the cell injected and PBS injected muscles (Figure 3).

Figure 3

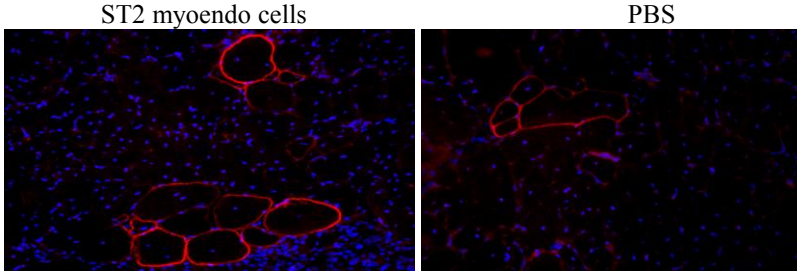

In order to confirm that the cells were actually present in the injected muscle after transplantation we used a retrovirus to label the cells with GFP and 2 days after injecting the cells the mice were sacrificed and the muscles were analyzed for GFP and dystrophin (Figure 4A). Some of the transplanted muscles were allowed to go 14 days prior to harvesting the muscles in order to see if additional time was required for the injected cells to fuse and begin expressing dystrophin (Figure 4B). To confirm that GFP was truly positive in these sections an anti-GFP antibody was used to detect GFP expression (Figure 4C, white). We have concluded from these data that the injected cells were engrafting but not producing dystrophin; so what are the cells doing?

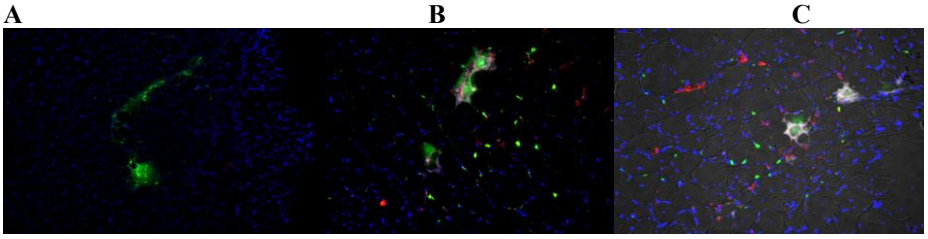

Figure 4: MDCs expressing GFP (green); A and B, anti-GFP (white), C; anti-Dystrophin (red), DAPI (blue)

In order to observe the regenerative processes, if any, in the SCID/mdx skeletal muscle after hMDC injection, we stained the muscles with an antibody against embryonic skeletal myosin heavy chain. Interestingly all the muscles injected, including the PBS injected control, demonstrated a massive amount of myofiber regeneration and there was no difference in the numbers of eMyHC expressing myofibers between any of the groups as can be seen in figure 5.

In a related set of experiments which confirmed the positive engraftment of the hMDCs and the lack of dystrophin expression, we had injected hMDCs that were being cultured using Platelet-Rich Plasma (PRP) in place of Fetal Bovine Serum (FBS). This experiment was intended to

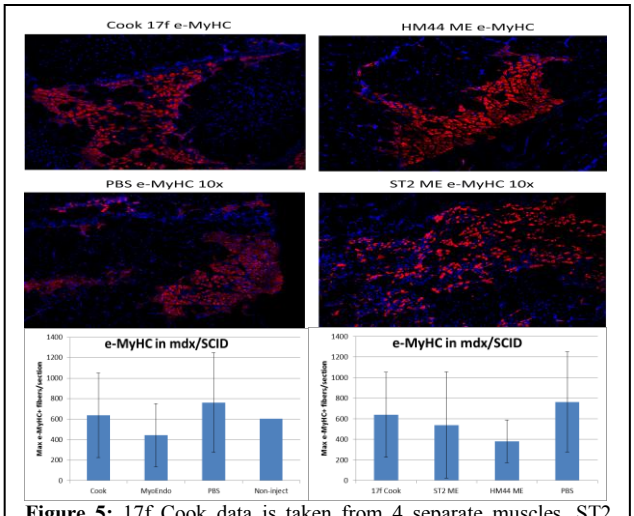

Figure 5: 17f Cook data is taken from 4 separate muscles, ST2 MyoEndo data is taken from 2 separate muscles, HM44, MyoEndo data is taken from 3 separate muscles, PBS data is taken from 4 separate muscles.

explore the use of an autologously-derived material to expand isolated hMDCs, which would have tremendous benefits for clinical applications of the hMDCs. In this experiment PRP-expanded and FBS-expanded hMDCs were injected into Mdx-SCID mouse muscles damaged with cardiotoxin. 4 weeks after cell injection, human major histocompatability complex I (hMHC-I) positive myofibers (red) could be detected in the injured muscles (**Figure 6**). The human MHC-I (red) expressed both on the membrane and in the cytoplasm of muscle fibers. All populations of hMDCs that were expanded in PRP supplemented medium retained their ability to regenerate myofibers upon extended culture. No significant differences were found between PRP and FBS expanded hMDPCs. From the point of view of SCID/mdx skeletal muscle engraftment, the cells were readily engrafting and producing hMHC-I. This finding supports engraftment occurring, but unfortunately does not explain the lack of dystrophin expression in the transplanted muscles.

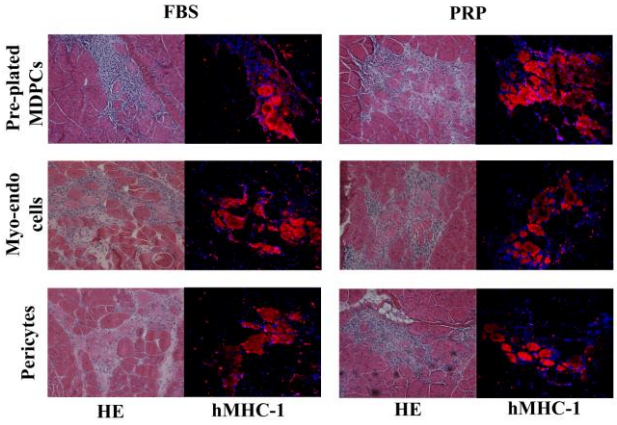

Figure 6. ***In vivo*** **myogenic potential of PRP-expanded hMPDCs.** PRP-expanded and FBS-expanded hMDPCs were also injected into Mdx-SCID mouse muscles damaged with cardiotoxin. 4 weeks after cell injection, HE staining and immuno-fluorescence staining of human MHC-fluorescence staining of human MHC-n MHC-g and immuno-fluorescence staining human MHC- I MHC- MHC myofibers can be detected in the injured muscles. All populations of hMDPCs that were expanded in PRP supplemented medium retained their ability to regenerate myofibers

In addition to the elucidation of why our SCID/mdx model was not exhibiting good engraftment with the human MDCs we have isolated, we have been performing additional tangential experiments on another model of DMD that is deficient for both dystrophin and utrophin known as the double-knock out (dKO) mouse. This model was being used because its pathophysiology more accurately resembles that of DMD patients and we felt might better accommodate the experiments outline in this grant. The following are results we have obtained using the dKO model.

Progression of muscular dystrophy in dystrophin/utrophin-/- mice is associated with rapid muscle progenitor cell exhaustion

In this study we isolated MPCs from the skeletal muscle of young (2 weeks) and old (6 weeks) dKO (dystrophin/utrophin double knock out) mice, which have a maximum lifespan of 6 to 8 weeks and is a mouse model of DMD that closely recapitulates the disease progression observed in DMD patients. We found that MPCs isolated from old dKO mice have a reduced ability to proliferate and differentiate compared to MPCs isolated from young dKO mice. In addition, Pax7 staining (a muscle progenitor cell marker) indicated that the MPC population significantly decreased during disease progression. These observations suggest that blocking the exhaustion of the MPC pool could be a new approach to improve muscle weakness in DMD patients, despite their continued lack of dystrophin expression.

Results:

1. MPCs isolated from aged dKO mice display limited proliferation ability.

We examined the proliferation kinetics of both populations *in vitro* using LCI (3) and we observed a significant reduction in the proliferation capacity of the old dKO MPCs compared to young dKO MPCs (**Figure 1**).

Figure 1

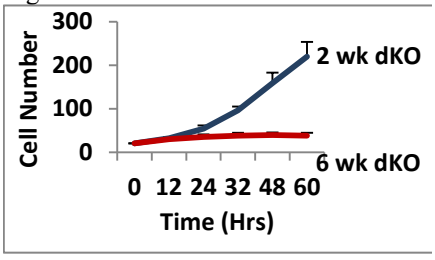

2. Pax7 positive cells undergo a rapid decline in the skeletal muscle of dKO mice during aging and disease progression.

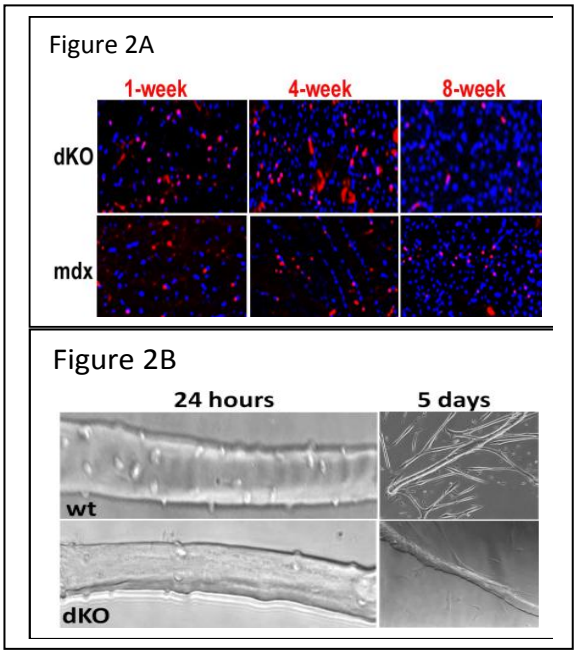

The results from the Pax7 staining showed that there is a rapid statistically significant decline in the population of Pax7 positive cells (red) in the skeletal muscle of dKO mice from 4 to 8 weeks of age in contrast to that observed in *mdx* skeletal muscle ($p<0.05$) (**Figure 2A**).

3. Isolated muscle fibers from dKO mice show a reduction in muscle progenitor cells.

The single muscle fibers were isolated from 6 weeks old dKO and WT control mice. We observed that there were more cell nuclei in the WT muscle fibers compared to the dKO muscle fibers. In addition, 5 days post-culturing, the WT muscle fibers were able to release myogenic progenitor cells forming new myotubes, in contrasts to that observed with the dKO muscle fibers. These results support both a reduction in the number and myogenic potential of the MPCs derived from the dKO mice when compared to the WT MPCs (**Figure 2B**)

4. MPCs isolated from aged dKO mice display a limited myogenic differentiation ability.

We observed that the MPCs isolated from young dKO mice formed numerous, large multi-nucleated myotubes compared to the MPCs isolated from the old dKO mice. The degree of myogenic differentiation was significantly reduced in the old dKO MPCs relative to the MPCs isolated from young dKO mice ($P < 0.001$).(**Figure 3**)

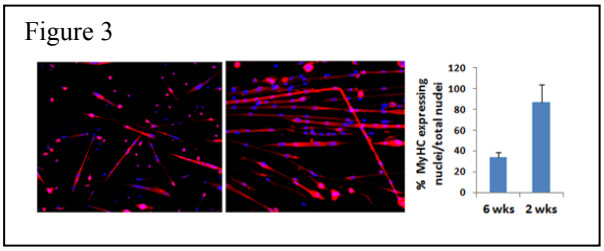

It is interesting to note that despite the lack of dystrophin at birth, the initiation of any signs of muscle weakness does not occur in DMD patients until later in childhood which happens to coincide with the exhaustion of the muscle progenitor cell pool (1). In this study we demonstrated that MPCs isolated from the skeletal muscle of old dKO mice have a reduced ability to proliferate and differentiate compared to MPCs isolated from young mice. Moreover, the numbers of Pax7 positive cells *in vivo* undergo a rapid decline in the skeletal muscle of dKO mice during aging and disease progression. Since dKO mice can only live 6-8 weeks, stem cell exhaustion could represent the main mechanism for the rapid progress of this disease. Blocking the exhaustion of muscle progenitor cells and stem cell-mediated therapy may represent a potential strategy for treating these muscle diseases. This study suggested that the exhaustion of stem cells contributes to the histopathology associated with DMD and that blocking the exhaustion of muscle progenitor cells and stem cell-mediated therapy could be used as a potential clinical strategy to treat muscle disease.

Muscle-derived cells (MDCs) responsible for myogenesis differ from MDCs involved in adipogenesis in dystrophin/utrophin-/- mice

DMD is characterized by progressive weakening of the skeletal and cardiac muscles. The predominant symptoms seen in advanced cases of DMD are sarcopenia and pseudohypertrophy with fatty infiltration in skeletal muscle. Ectopic fat accumulation in skeletal muscle can be seen not only in myopathies but also in several disorders, including obesity and ageing-related sarcopenia; however, the origin of ectopic adipocytes, nor the stimulus that trigger their formation in disease, is known. In our lab, we utilize utrophin/dystrophin double knockout (dys-/-utro-/-, dKO) mice, which better emulates the phenotype seen in DMD patients. Several types of cells, including satellite cells, can be isolated from skeletal muscle and based on a previously published preplate technique we isolated two types of cells; rapidly adhering cells (RACs) ,which are PDGFRα + mesenchymal progenitor cells, and slowly adhering cells (SACs), which are Pax7+ myogenic progenitor cells, from skeletal muscle of dKO and wild type (wt) mice. Previously, we have shown that dKO-SACs have

reduced proliferation and myogenic and adipogenic differentiation abilities compared to wt-SACs. These observations suggested that SACs in dKO mice are exhausted and potentially are the main mechanism for the rapid progress of sarcopenia; however, the cells involved in pseudohypertrophy in dKO mice remains unclear. In this study, we examined the proliferation and adipogenic differentiation capabilities of RACs since adipose cells are thought to be derived from mesenchymal stem cells. We observed increased proliferation and adipogenic differentiation capabilities in dKO-RACs compared to wt-RACs. Our results suggest that muscle progenitor cells, SACs, may be more involved in muscle fiber regeneration or degeneration while mesenchymal progenitor cells, RACs, may be the origin of the cell population that is involved in adipogenesis in dKO muscle.

Figure 1. Flow analysis of PDGFRα surface protein expression in RACs and SACs from wt and dKO mice.

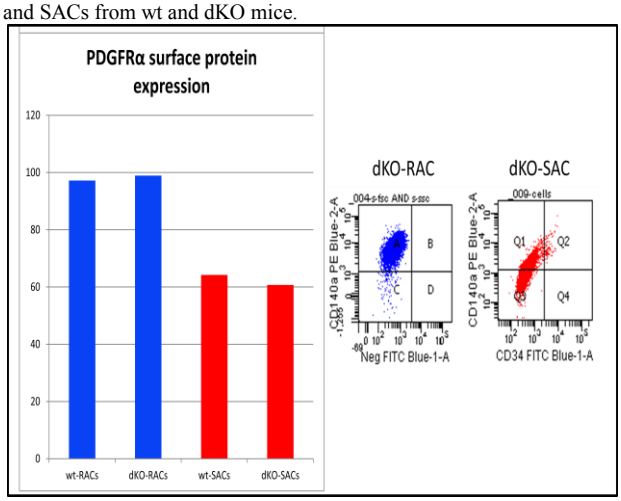

RESULTS:

dKO-RACs had increased PDGFRα expression compared to dKO-SACs. Flow cytometry analysis was used to evaluate the expression of PDGFRα, a marker for mesenchymal cells, of the RACs and SACs from both dKO and wt mice. dKO-RACs were about 98% positive for the PDGFRα surface protein, while much lower expression levels were detected in the SACs (Figure 1).

dKO-RACs displayed increased proliferation ability. The proliferation of the RACs and SACs were examined in vitro using an LCI system and MTT assay. We observed a significant increase in the proliferation of the dKO-RACs compared to the wt-RACs.

Increased in vitro adipogenic potential was detected in dKO-RACs. RACs and SACs from both dKO and wt mice were cultured in adipogenic differentiation medium for 21 days. AdipoRed staining was observed in the cytoplasm of the cells, around the nuclei. The degree of adipogenic differentiation was significantly increased in PDGFRα+ dKO-RACs compared to the dKO-SACs (Figure 2).

Figure 2. Adipogenesis of RACs and SACs. Bright field pictures and AdipoRed staining. Quantification of AdipoRed assay is shown.

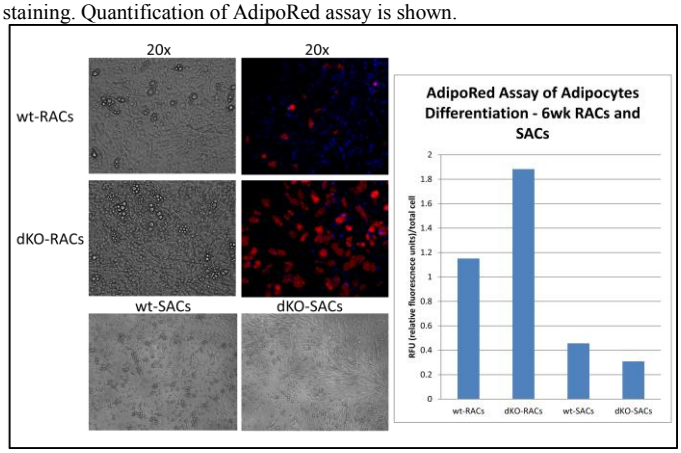

In dKO mice, an animal model of DMD, we observed severe peri-muscular adipose tissue on the surface of the gastrocneminus muscles (GM) as well as lipid accumulation inside of skeletal muscle myofibers. Intramyocellular lipid accumulation could be observed in the cardiac muscle of dKO mice; however, the source of the ectopic fat tissue within the skeletal muscle is unknown. In this study, we provide evidence that the RACs, PDGFRα + mesenchymal progenitor cells, are responsible for increased fat cell formation in the skeletal muscle of dKO mice. We observed that dKO-RACs had increased proliferation and adipogenic differentiation capabilities. This result suggests that dKO-RACs are prone to form adipocytes in skeletal muscle. This study suggests that dKO-RACs, mesenchymal progenitor cells in skeletal muscle, may contribute to adipogenesis and are responsible for ectopic fat cell formation within skeletal muscle in pathological conditions such as DMD. Therefore, targeting RACs to block adipogenesis in skeletal muscle may open new opportunities to treat muscle diseases.

RhoA signaling regulates heterotopic ossification and fatty infiltration in dystrophic skeletal muscle

Frequent heterotopic ossification (HO) or fatty infiltration is observed in the dystrophic muscle of many animal models of human Duchenne muscular dystrophy (DMD); however, little is known about the correlated molecular mechanisms involved in the process. The RhoA-Rho kinase (ROCK) signaling pathway has been shown to function as a commitment switch of the osteogenic and adipogenic differentiation of mesenchymal stem cells (MSCs). Activation of RhoA-ROCK signaling in cultured MSCs in vitro induces their osteogenesis but inhibits the potential of adipogenesis, while the application of Y-27632, a specific inhibitor of ROCK, reversed the process. Inflammation has been shown to be one of main contributors to HO, while the role of RhoA signaling in inflammation reaction has been demonstrated. The objective of the current study is to investigate the potential role of RhoA signaling in regulating HO *and* fatty infiltration in dystrophic skeletal *muscle.*

Results:

1.Skeletal muscle of dKO mice features more HO but less fatty infiltration than mdx mice (Fig. 1). Both µ-CT scan of animals (Fig. 1A) and Alizarn Red stain (Fig. 1B) of the muscle tissues revealed greatly enriched HO in the dystrophic muscles of the dKO mice. While, Oil Red O stain (Fig. 1C) and Trichrome stain (Fig. 1D) of the muscle tissues revealed reduced fatty infiltration and a number of normal muscle fibers in the muscle of dKO mice.

Figure 1

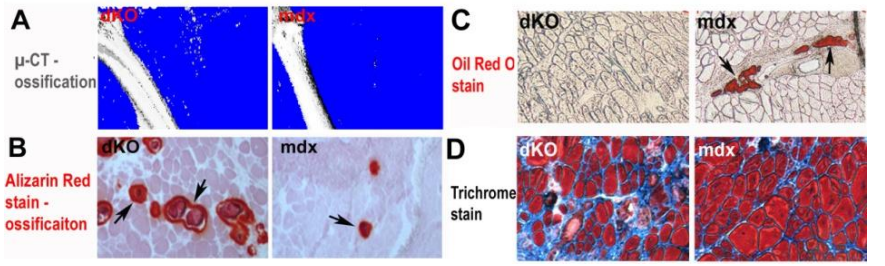

2. RhoA signaling is more activated in both skeletal muscle and muscle-derived stem cells (MDSCs) from dKO mice. Both semi-quantitative PCR and immunohistochemistry study demonstrated that RhoA signaling is more activated in the muscles of dKO mice, as well as dKO MDSCs.

Figure 2

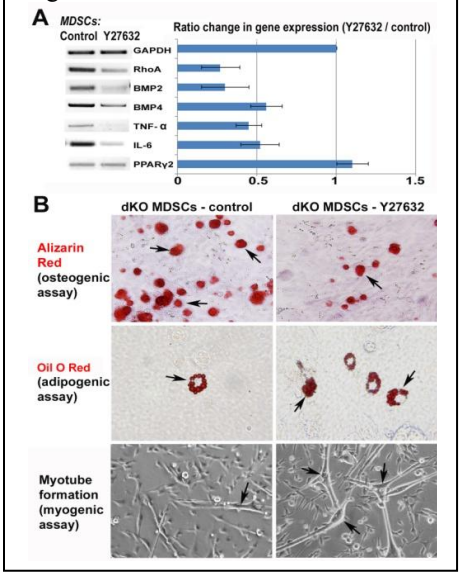

3. *In vitro* RhoA inactivation of cultured MDSCs from dKO mice decreases the osteogenesis potential and increases adipogenesis and myogenesis potential (Fig. 2). Semi-quantitative PCR study showed that Y27632 treatment *(10 µM)* of dKO-MDSCs down-regulated the expression of RhoA, BMP2 and 4, and inflammatory factors such as TNF-α and IL-6 (Fig. 2A). Osteogenesis potential was repressed while the adipogenesis and myogenesis potential of the dKO-MDSCs were increased by Y27632 (Fig. 2B).

4. RhoA inactivation in the skeletal muscle of dKO mice decreased HO and increased both fatty infiltration and muscle regeneration. GM muscles of 6 dKO mice were injected with Y27632 (5mM in 20µL of DMSO) (left limb) or control (20µL of DMSO) DMSO (right limb). Injections were conducted 3 times a week for 3 weeks. The skeletal muscles that received Y27632 injection demonstrated much slower development of HO and improved muscle regeneration, as well as reduced fibrosis formation.

These results revealed that DMD mouse models featuring different severity of muscular dystrophy may have varied potentials for developing HO or fatty infiltration in the dystrophic muscle, and RhoA signaling might be

a critical mediator of the determining these differential fates, including the progression towards HO, fatty infiltration, or normal muscle regeneration. RhoA inactivation is shown to have a great potential to repress HO and improve the phenotypes of dystrophic muscle. The status of RhoA activation in the skeletal muscle of human DMD patients and the potential effect of RhoA inactivation in human dystrophic muscle requires further investigation. This data reveals the involvement of RhoA signaling in regulating the process *of* heterotopic ossification, and indicates that RhoA may serve as a potential target for repressing injury-induced and congenital heterotopic ossification in humans.

Suppression of skeletal muscle inflammation by muscle stem cells is associated with hepatocyte growth factor in wild type and mdx;p65$^{+/-}$ mice

Persistent, unresolved inflammation can lead to secondary tissue damage. In a previous study, we reported that intramuscular (i.m.) injection of muscle-derived stem cells (MDSCs) heterozygous for the NF-kB subunit p65 (p65$^{+/-}$) reduced host inflammation and fiber necrosis seven days following muscle injury, relative to wild type (WT) MDSC injection [1]. In this investigation, we looked closer at the role of secreted factors in this observation. Using a murine cardiotoxin muscle injury model, we observed that delivery of p65$^{+/-}$ MDSCs accelerated the resolution of inflammation, relative to WT MDSCs. *In vitro* inflammation assays demonstrated that MDSCs secrete factors that modulate cytokine expression in LPS-activated macrophages, and genetic reduction of p65 enhanced this effect. Finally, deletion of one p65 allele in a murine model of Duchenne muscular dystrophy (mdx) increased the expression of the anti-inflammatory factor hepatocyte growth factor (HGF) and was associated with disease improvement.

Figure 1.

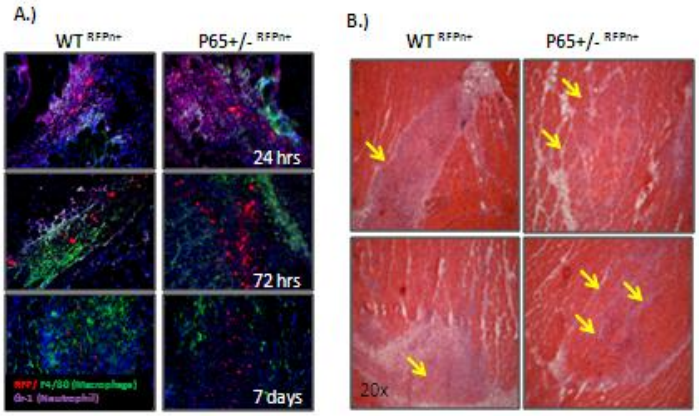

RESULTS

Confirming our previous report [1], we found that by 7 days, p65$^{+/-}$ cell engraftments were associated with reduced numbers of F4/80+ cells, compared to WT cell engraftments (Fig 1A). This can be further demonstrated histologically by H&E staining, revealing a reduction in mono-nuclear cells at sites of injury one week post injection (Fig 1B).

To look at the direct effects of MDSC-secreted factors, we performed *in vitro* inflammation assays. Briefly, RAW264.7 macrophages were activated with LPS (100ng/mL) in normal PM or WT or p65$^{+/-}$ conditioned medium (CM) (Fig 2A). The expression of the cytokines IL-1β and IL-6 was determined by real time (RT-PCR). Our results demonstrated that MDSC-CM significantly attenuates cytokine expression (Fig 2B). Although WT and p65$^{+/-}$ CM had a similar effect, we found that p65$^{+/-}$ CM exerted a stronger suppression of IL-6 expression. Previous reports have found that the activation of inflammatory macrophages is attenuated by the phosphorylation and subsequent inactivation of GSK3β [3]. By western blot, we found that upon treatment with LPS in WT-CM, the fraction of pS9-GSK3beta modestly increased within 30mins and was maintained through 24 hours. Furthermore, p65$^{+/-}$-CM demonstrated an even stronger induction of phosphorylation (Fig 2C).

Figure 2.

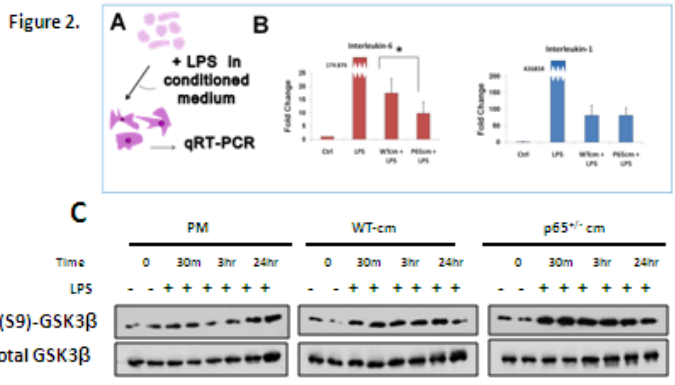

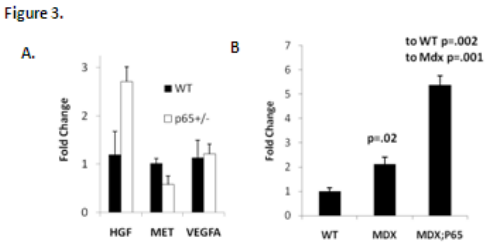

Hepatocyte growth factor (HGF) is one of the factors previously demonstrated to modulate inflammation via pS9-GSK3beta. We examined HGF expression in MDSCs and found elevated levels in $p65^{+/-}$ cells compared to the WT cells (Fig 3A). Acharyya and colleagues have reported that haploinsufficiency of p65 in an mdx background improves dystrophic pathology [4]. As we had hypothesized, HGF expression was significantly increased (Fig 3B). Based on our *in vitro* and *in vivo* inflammatory studies, HGF could be one of the contributing factors to disease improvement.

These findings indicate that NF-kB has a broader role in muscle stem and progenitor cells than previously thought, and that the anti-inflammatory molecules secreted by stem cells, such as HGF, could potentially be harnessed to control secondary pathologies of muscle diseases such as DMD.

Progress made from 9-1-10 to 8-31-11

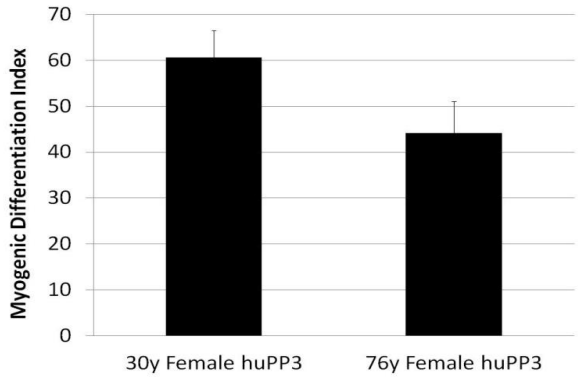

Figure 1: The MDI of two populations of human female myoendothelial cells. The MDI shows the cells isolated from the 30 year old female donor have a greater myogenic capacity than cells isolated from the 76 year old donor ($p < 0.05$).

Myogenic and proliferation capacity of young vs. old myoendothelial cells

In vitro assays to look at differences in myogenic capacities of young and old human myoendothelial cells were conducted using two cell populations one from a 30 year old female and the other from a 76 year old female. Both cell populations were derived from human skeletal muscle and isolated using our lab's pre-plate technique for stem cell isolation. Cells isolated from the latest preplate, preplate 3(PP3), were utilized in the current experiments (which means that the isolated cells adhered to the collagenated flasks between 24-48 hours after the initial muscle biopsy isolation and dissociation. For murine cell isolations, PP6 cells are able to be isolated and possess the highest multipotency and engraftment capacities as compared to PP1-PP5. To compare the myogenic capacities of the young and old cells in vitro, the cells were promoted to differentiate by placing them in low (2%) serum media for five days after which the cells were fixed and then stained for their expression of myosin heavy chain (MHC) and DAPI. The myogenic differentiation index (MDI) for each cell type was calculated by counting the number of nuclei inside MHC-stained differentiated myotubes and dividing this number by the total number of nuclei. The results shown in figure 1 indicated that the older female PP3 cells had a reduction in their myogenic potential (myotube formation) *in vitro* compared the cells isolated from the younger female biopsy. These results are being confirmed and the experiment is being repeated with human male myoendothelial cells, as well.

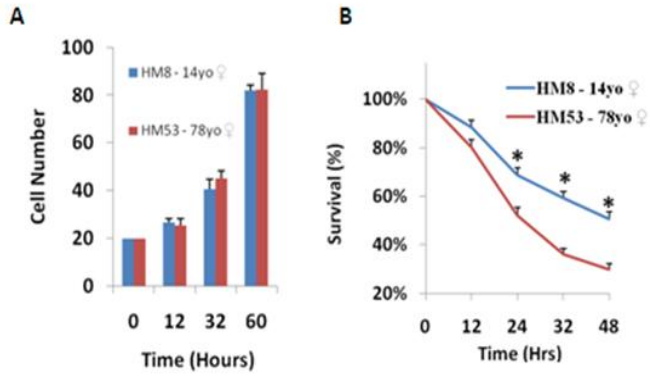

Figure2 Myoendothelial cells isolated from skeletal muscle biopsies taken from 78 year old (HM53) or 14 year old (HM8) female patients exhibit no differences in cell proliferation (A). However, aged cells are significantly less resistant to hydrogen peroxide induced (400uM) oxidative stress (B). ($p<0.05$, data represented as mean +/- s.e.m.)

In another set of experiments we isolated myoendothelial cells via FACS from the skeletal muscle of a 76 year old female (HM53) and a 14 year old female (HM8) patient. The cells were studied for their proliferative and oxidative stress resistance (exposure to 400uM hydrogen peroxide) capacities. In this study the cells were found to not differ in their proliferative capacity between HM53 and HM8 (Figure 2A); however there was a significant difference in their resistance to oxidative stress capacities at 24, 32 and 48 hrs post-exposure (Figure 2B, older cells displaying a reduction to stress resistance).
Additional studies are currently underway to increase the number of populations of young and old myoendothelial and PP3 cells (and sex) studied for their proliferation, myogenic and their stress resistance capacities.

Optimizing the culture conditions for expanding myoendothelial cells

It is of critical importance that the myoendothelial cells isolated from human skeletal muscle can be maintained in a "stem" like state when expanded in a cell monolayer. A media formulation of 10% fetal bovine serum, 10% horse serum, 1% penicillin/streptomycin and 1% chick embryo extract is normally used to culture the cells. This proliferation media (PRO) was combined with Endothelial Growth Media-2 (EGM2) media (Lonza) at a 1:1 mixture and designated PROe media. A 69 year old, male population of human myoendothelial cells (ST2) isolated via FACS were seeded on a 24-well plate at a density of 2000 cells/cm^2 of growth area. The ST2 cells had been maintained in normal proliferation media or PROe media since the cell isolation and were designated ST2 and ST2e, respectively. The 12-well plate was place on a Live Cell Imaging system (Kairos Instruments) which can capture images at different coordinates in the well and in all the seeded wells at preprogrammed time intervals, which can then be viewed after a set time as a time-lapsed movie. In the current experiment 100x images were captured every 15 minutes for a period of 108 hours. Images were analyzed using ImageJ and the data are presented in figure 3. Morphologically, the ST2e cells (3B) are smaller and less elongated than the ST2 cells and proliferate at a faster rate than ST2 cells (3C). Next, we wanted to know if the cells were able to differentiate after culture in PROe media and to compare this to cells grown under the usual culture conditions (PRO). A myogenic differentiation assay was performed, as described above, and representative images are shown in figure 4. ST2e cells not only form a greater number of myotubes but a greater number of the myotubes contained more nuclei which indicate a higher degree of maturity. These data suggest the PROe media or another variant may be more ideal for culturing human myoendothelial cells and maintaining them in a stem-like state.

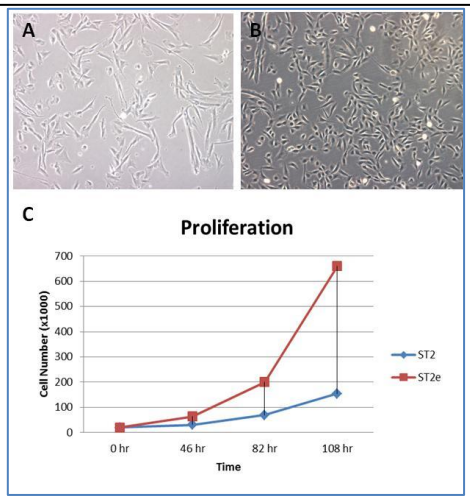

Figure 3: 100x images of human, male myoendothelial cells cultured in PRO media or PROe media. The expected doubling time of 24-36 hours is seen in the ST2 population while the ST2e cells show a doubling time of less than 24 hours (C). The morphologies of the cells are shown in A and B and indicate PROe media maintains the population in a more stem-like morphology.

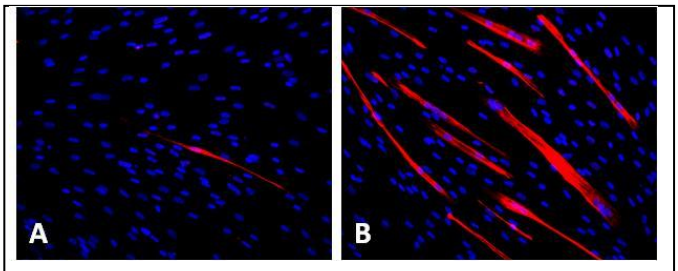

Figure 4: ST2 cells (A) and ST2e cells (B) growth in low (2%) serum media for 5 days. Cells were fixed and stained against DAPI (blue) and myosin heavy chain (red).

Identification of a dystrophin antibody for use in mdx mice

Early analysis of the first SCID/mdx tissues transplanted with human myoendothelial cells revealed a critical problem. Our group was using a polyclonal anti-dystrophin antibody (Abcam #15277) which we use for all our other mouse tissues. The initial staining of the SCID/mdx tissues showed high levels of positive staining in the PBS injected control muscles which should have been completely negative (figure 5C-D). Indeed the PBS groups had higher levels of dystrophin staining than some of the tissues tissues injected with myoendothelial

cells (5A-B). It was essential to identify a viable anti-dystrophin antibody to stain *mdx* mouse tissues. Dr. Bing Wang of the Stem Cell Research Center had created four variants (R1R2, R2N, R22R23, R24H4) of a mammalian dystrophin antibody for testing on these tissues. The results shown in figure 5 suggested variant R1R2 was the best antibody to use on the *SCID/mdx muscle* tissues (Figure 6).

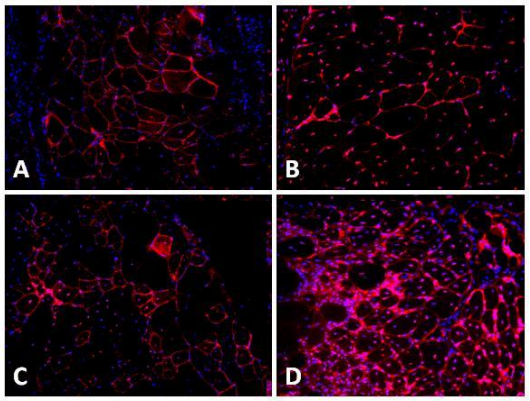

Figure 5: Mdx/SCID muscle sections stained against DAPI (blue) and mammalian dystrophin (red). (A-B) tissue transplanted with human myoendothelial cells. (C-D) tissue injected with PBS.

Effect of host sex on the regenerative capacity of old male and female myoendothelial cells

Eight week old SCID/mdx mice, male and female, were randomly assigned to 1 of 5 groups; non-injected (controls), PBS (controls), ST2, ST2e or HM49. All groups, except non-injected controls, received bilateral injections into the gastrocnemius muscles of 20 microliters of PBS or PBS containing $3x10^5$ myoendothelial cells via a 31 gauge insulin syringe. Animals were sacrificed and tissue collected 14 days post-injection. Tissues were cryosectioned and the sectioned tissues stained for dystrophin using the R1R2 variant. Analysis was performed by capturing 100x fluorescent images of the entire stained section and counting the number of positively-stained (for dystrophin) fibers present in the section. The data in figure 7 are not complete as analysis has just begun on these tissues but early evidence suggests ST2 cells (cultured in PRO media) have a greater regenerative capacity than cells grown in PROe media (ST2e). The ST2 (69 year old, male) cells showed no differences when transplanted into male or female hosts (n=3 for both). The trend for ST2e cells is for better regeneration when transplanted into female hosts but the n is low for both conditions (male host, n=1; female host, n=2). This trend is seen in the HM49 again with the HM49 (75 year old, female) injected tissues as greater regeneration is seen when the cells are transplanted into a male host. Again, the n is small (n=1 for both hosts) making further analysis

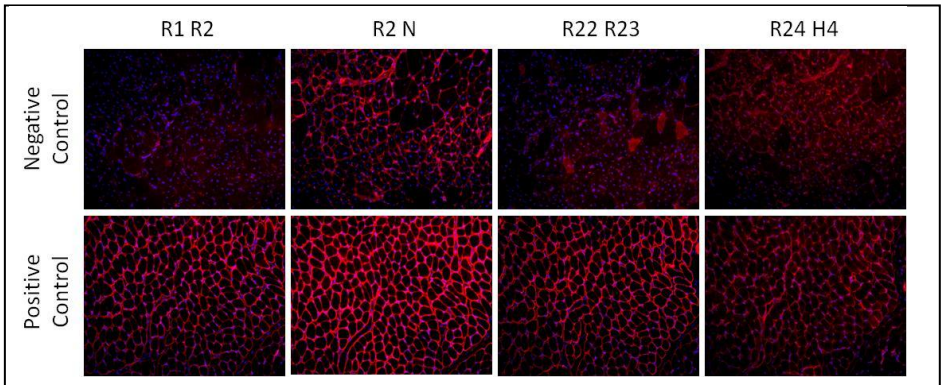

Figure 6: Testing the 4 variants of Dr. Bing Wang's polyclonal dystrophin antibody. Negative control = mdx tissue. Positive control = C57BL6 tissue. Each figure for negative or positive controls shows the identical area of the tissue. Variant R1R2 shows the lowest level of nonspecific staining.

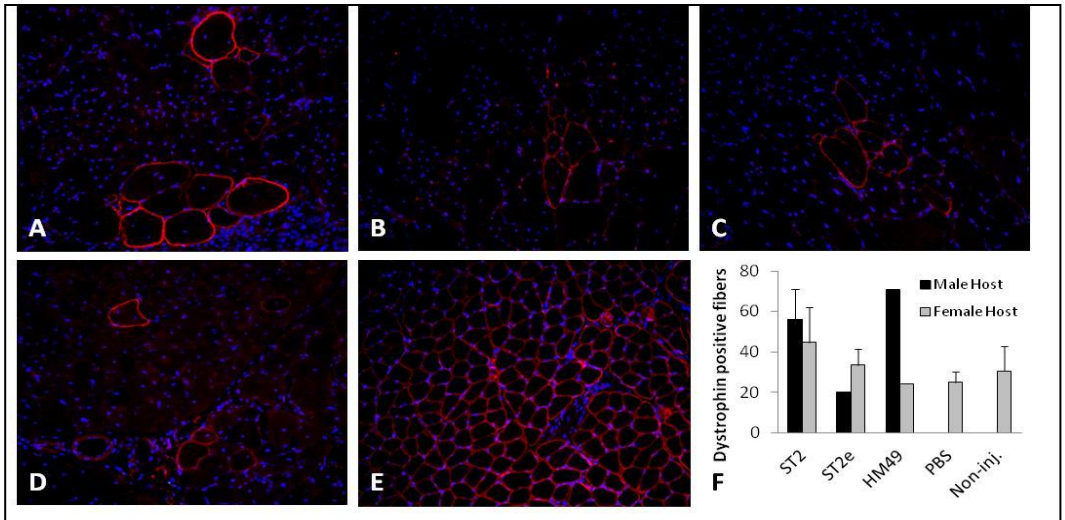

Figure 7: Analysis of tissue cryosections from *mdx/SCID* mice. Dr. Bing Wang's R1R2 dystrophin antibody (red) was used for staining. DAPI (blue) stained for nuclei. A) ST2 injected. B) ST2e injected. C) HM49 injected. D) PBS injected E) wild type (dystrophin positive) control tissue. No significant differences are seen between groups but analysis of tissues is not complete.

essential for any conclusions to be drawn. More importantly, the numbers of dystrophin positive fibers in female host tissues are all at near-background levels based on the number of revertant myofibers seen in non-injected controls. Analysis has not been performed on non-injected tissues from male hosts. Also, analysis has not yet been performed on non-injected tissues from male hosts.

Non-invasive behavioral testing to detect functional improvement following stem cell transplantation

Preliminary studies were performed on nine, 12-week old female *SCID/mdx* mice in order to test the potential use of a DigiGait™ system (Mouse Specifics, Inc., Quincy, MA) functional gait analysis system to test the functional improvement of our transplanted mice. The mice received bilateral intramuscular (gastrocnemius) injections of 20uL of PBS or 20uL PBS containing either $3x10^5$ male myoendothelial cells or $3x10^5$ male perivascular cells. This initial experiment was conducted before the determination that myoendothelial cells were the best human cell type for these studies. For non-invasive analysis of muscle function we used the DigiGait™ system (Mouse Specifics, Inc., Quincy, MA). The system consists of a treadmill with a transparent belt which had a high speed digital camera mounted ventral to the test subject. Proprietary software provide by Mouse Specifics used to analyze numerous indices of the animal's gait. A simple schematic of what the software is looking at when calculating these indices is shown in figure 8A. For our study animal gaits were examined at a velocity of 20cm/s and the ratio of the stance time to swing time was calculated. The stance and swing phases are shown in figure 8A and the analysis for the *SCID/mdx* mice is shown in 8B. The data suggest that within 2 weeks of transplantation the myoendothelial-injected mice showed a reduced "running" stride compared to the pericyte-injected mice. Since these mice were forced to move at a constant velocity subjects capable of generating more force via plantar flexion could have a ratio of stance/swing greater than 1. Since the gastrocnemious is partially responsible for plantar flexion and this muscle was the target of the transplantation, these data are encouraging and warrant further use with our other experimental animals.

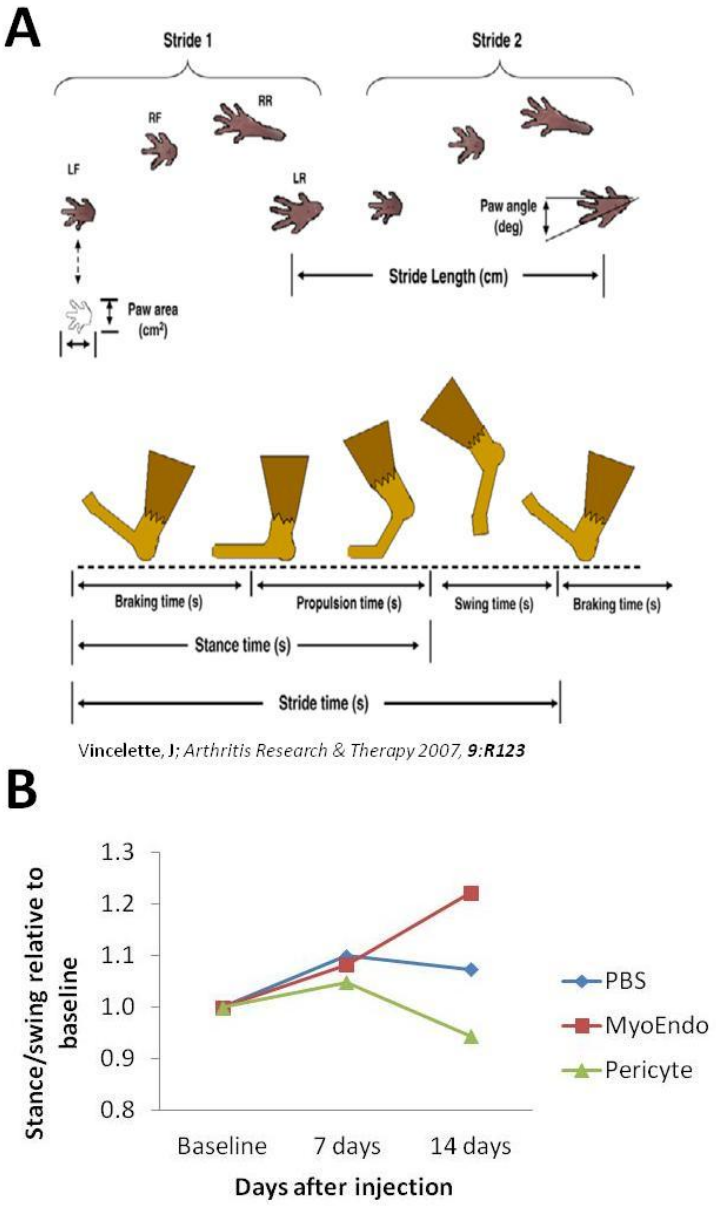

Figure 8: Non-invasive behavioral testing A) schematic of the paw areas detected by the high-speed camera as part of the DigiGait™ system. The diagram below is a visual representation of the 3 phases of a stride; braking, propulsion and swing. B) The stance phase/swing phase ratio for each group at each time point relative to each groups' baseline ratio. An increasing ratio may be indicative of increased muscle function/strength.

Immunomodulatory properties of muscle-derived stem cells associated with reduced NF-κB/p65 signaling

In this study, we examined the role of NF-kB signaling in the regenerative phenotype of muscle-derived stem cells (MDSCs) isolated from the gastrocnemius of p65 deficient mice (heterozygous, *p65+/-*) and wild type

littermates (*p65*+/+). We previously found that *p65*+/- MDSCs have enhanced cell proliferation, survival under oxidative stress, differentiation, and muscle regeneration capacity. Furthermore, we have found that *p65*+/- engraftments in wild type skeletal muscle are associated with reduced inflammation and fiber necrosis compared to *p65*+/+ MDSC engraftments. *In vitro* and *in vivo* experiments suggest that reduction of p65 signaling enhances the regenerative phenotype of MDSCs, suggesting this pathway as a candidate target to improve stem cell-based therapies for muscle disease and injury. The data presented in this study provides evidence supporting that NF-kB inhibition stimulates MDSC-mediated muscle regeneration through multiple mechanisms, including through the expression of anti-inflammatory factors that attenuate inflammation and necrosis. These experiments identify the NF-κB signaling pathway as a potential therapeutic target to enhance muscle regeneration following injury or disease (**Paper in revision. A. Lu et al. Mol. Therapy, Sept. 2011**).

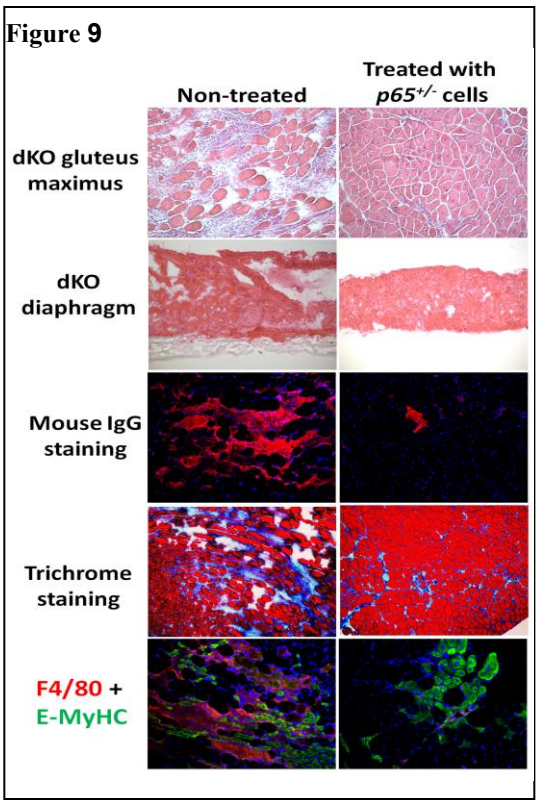

p65 +/- MDSC transplantation improves muscle histology in dKO mice after IP transplantation (Figure 9) -- MDSCs were isolated from 5 month old $p65^{+/-}$ and WT mice as previously described via a modified preplate technique. A total of 5-9 $x10^5$ viable cells or 50µl PBS were injected intraperitoneally into 5-7 day old dKO mice. Four to six weeks after transplantation, the muscles were harvested and cryosections were prepared for staining. Our preliminary data suggest that the regeneration of both the gluteus maximus and diaphragm muscles were more greatly improved in their histopathological appearance in the animals injected IP with p65-deficient MDSCs than the nontreated animals at 4 weeks post-implantation,.

Muscle cryosections were also stained for mouse IgG to determine the extent of muscle fiber necrosis.The results showed that there were less necrotic muscle fibers in the mice injected with $p65^{+/-}$ MDSCs compared to non-treated muscles (**Fig. 9**). Trichrome staining was also preformed according to the manufacturer's instructions and the results showed that there was less muscle fibrosis in the mice injected with $p65^{+/-}$ MDSCs compared to the non-treated muscles (PBS) (**Fig. 9**)

An antibody against embryonic muscle heavy chain (E-MyHC) was used to evaluate muscle regeneration and another antibody against F4/80 (macrophage marker) was used to analyze the extent of inflammation in the regenerated area. These results showed less inflammation (red, F4/80) within the regenerated area (E-MyHC (green) positive myofibers) in the muscles of mice injected with $p65^{+/-}$ MDSCs compared to the untreated muscles (**Fig. 9**). The use of NF-kappa blockade may be useful to improve the regeneration index of hMDCs in the skeletal muscle of SCID/MDX mice.

Progress made from 9-1-09 to 8-31-10

The overall goal of Technical Objective 1 is to identify the optimal human muscle derived cell type for skeletal muscle regeneration. We have completed several aspects of Technical Objective 1, namely – 1)

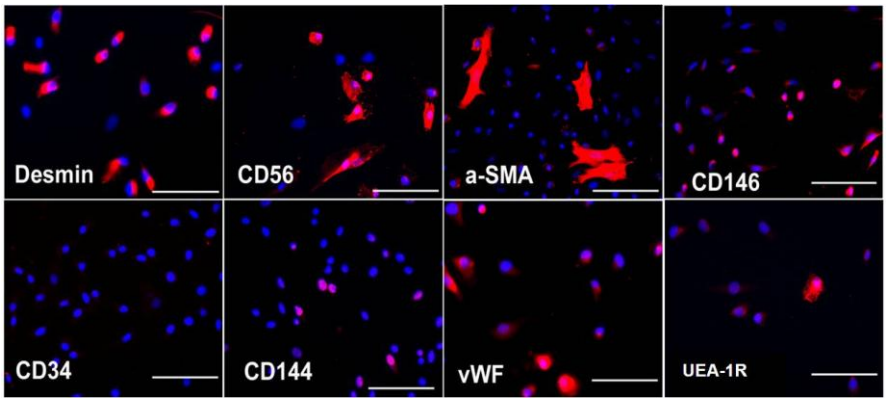

Figure 1. Differential expressions of myogenic and endothelial markers by cryopreserved human skeletal muscle cells. Immunocytochemistry revealed the diverse expressions of various cell lineage markers by cryopreserved skeletal muscle cells after expansion. Nuclei were stained blue with DAPI. (Scale bars = 100µm).

isolation of FACS-defined populations of myoblasts, myo-endothelial cells and pericytes, 2) side-by-side comparison of in vitro myogenic differentiation potential of these populations and 3) transplantation of these 3 populations to SCID/mdx animals and in vivo assessment of skeletal muscle regeneration potential of these cells.

After expansion, the cryopreserved human progenitor skeletal muscle cells (cryo-hPSMCs) were examined by immunocytochemistry for cell surface marker expression. The majority of the cryopreserved skeletal muscle cells expressed desmin and CD56, and to a lesser extent, CD146 (Figure 1). Only a fraction of cells expressed α-SMA, CD144, vWF or UEA-1R. As expected with cultured human cells, cells lacked CD34 expression. Our flow cytometry analysis quantitatively confirmed the diverse expressions of cell lineage makers by the cells: 77.1±5.7% $CD56^+$, 66.9±8.1% $CD146^+$, 11.2±2.5% UEA-$1R^+$, 0.3±0.1% $CD144^+$, 0.1% vWF^+, and no expression of CD34 and KDR (Figure 2A). Surprisingly, the number of cryo-hPSMCs positive for CD56, CD146 or UEA-1R decreased dramatically after passage 10 as compared to expression prior to passage 10 (Figure 2B).

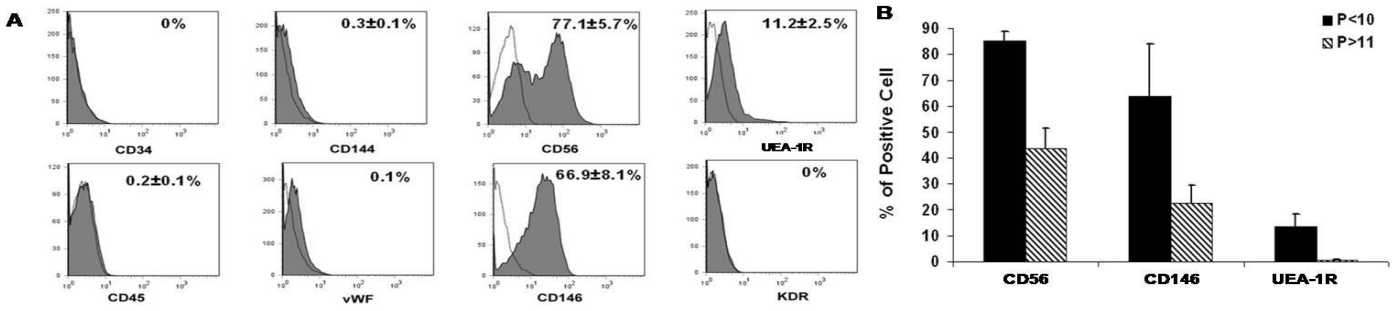

Figure 2. Differential expressions of myogenic and endothelial markers by cryopreserved human skeletal muscle cells. (A) Flow cytometry analysis quantitatively confirmed the diverse cell composition of cryopreserved skeletal muscle cells (B) The number of cryopreserved skeletal muscle cells positive for CD56, CD146, or UEA-1R decreased dramatically when cells were cultured beyond passage 10 (passage>10).

Isolation of myogenic stem/progenitor cells: Using a collection of cell lineage markers, we analyzed cryopreserved cells by flow cytometry for their expression of hematopoietic (CD45), myogenic (CD56), endothelial (UEA-1R), and perivascular (CD146) cell markers. After the exclusion of $CD45^+$ cells, four distinct cell fractions were identified, including myoblasts (Myo) ($CD56^+/CD45^-CD146^-$UEA-$1R^-$), endothelial cells (ECs) (UEA-$1R^+/CD45^-CD56^-CD146^-$), perivascular stem cells (PSCs) ($CD146^+/CD45^-CD56^-$UEA-$1R^-$), and myogenic endothelial cells (MECs) which expressed all three cell lineage markers ($CD56^+$UEA-

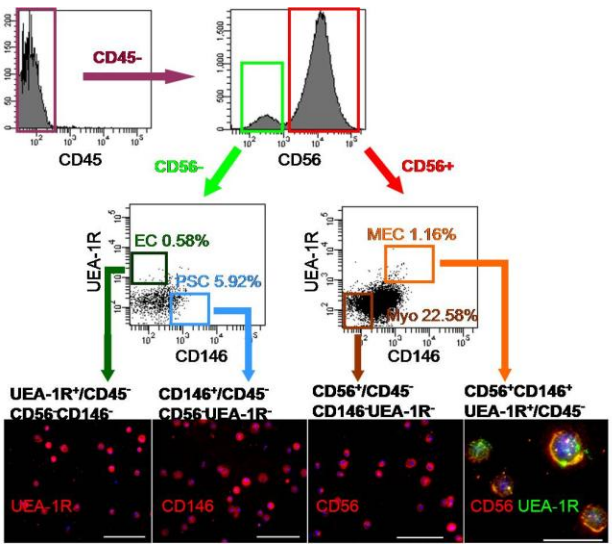

Figure 3. Identification and purification of myogenic stem cells within cryopreserved muscle cell populations. $CD45^-$ cells were separated based on CD56 expression. $CD56^+$ and $CD56^-$ populations were further gated on UEA-1R by CD146 to identify and/or sort four distinct cell populations: myogenic endothelial cells (MEC) ($CD56^+$UEA-$1R^+CD146^+/CD45^-$), myoblasts (Myo) ($CD56^+/CD45^-CD146^-$UEA-$1R^-$), perivascular stem cells (PSC) ($CD146^+/CD45^-CD56^-$UEA-$1R^-$), and endothelial cells (EC) (UEA-$1R^+/CD45^-CD56^-CD146^-$). The purities of the sorted populations were 90.73±4.82%, 92.94±1.23%, 93.86±1.72, and 94.9±0.64, respectively. Immunocytochemistry confirmed the expression of key cell lineage makers by freshly sorted cells: UEA-1R, CD146, and/or CD56. (Scale bars = 100μm except in CD56/UEA-1R double staining = 20μm)

$1R^+CD146^+/CD45^-$). The composition of long-term cultured cryopreserved muscle cells included 22.58±6.32% Myo, 0.58±0.23 % ECs, 5.92±4.66% PSCs, and 1.16±0.19% MECs (Figure 3). These four cell subsets were subsequently fractionated by FACS (Figure 3).

Next, we examined the in vitro differentiation capacity of myoendothelial cells and pericytes. Cells were stimulated for 1 week under conditions of low serum and high density and we observed a marked difference in the ability to undergo myogenic differentiation, as noted by the presence of multinucleated myotubes and positive immunostaining for myosin heavy chain (MHC) and desmin (Figure 4).

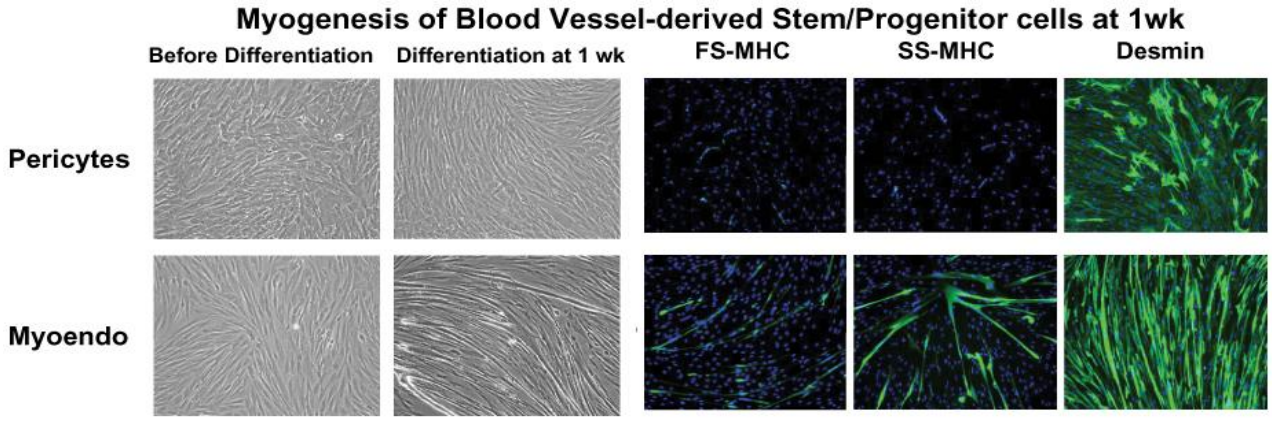

Figure 4. Myoendothelial cells displayed a higher myogenic potential as compared to pericytes. After 1 week in myogenic conditions, we find more myotubes, and greater expression of myosin heavy chain (MHC, green) and desmin (green) in the myoendothelial cell populations as compared to pericytes populations. Nuclei are DAPI stained.

Finally, to evaluate the myogenic capacities of these purified cell fractions, all freshly sorted cells were immediately transplanted into cardiotoxin-injured skeletal muscles of SCID mice (n=7 per cell fraction). Unpurified muscle cell- and saline-injected muscles were employed as controls. Mouse muscles were harvested 2 weeks post-injection, cryosectioned, and examined by immunohistochemistry to detect muscle fiber regeneration *in vivo*. An antibody against human spectrin, a myofiber cytoskeletal protein, was used to identify human cell-derived skeletal myofibers in the tissue sections. Quantitative analyses revealed that the myogenic regeneration index, indicated by human spectrin-positive skeletal myofibers per 1×10^3 injected cells, was 71.23±27.15 for MECs, 31.26±11.57 for endothelial cells (ECs), 11.44±3.79 for PSCs, 4.23±1.16 for myoblasts (Myo), and 0.55±0.36 for unsorted muscle cells (Unsort) (Figure 4). MECs exhibited the highest regeneration of human skeletal myofibers among all five cell fractions tested ($p<0.05$) (Figure 4). PSCs regenerated more myofibers than the Myo ($p>0.05$) and the Unsort ($p<0.05$) (Figure 5). Purified myoblasts displayed a higher myogenic capacity than the unsorted cells ($p<0.05$) (Figure 5).

Similar experiments are currently under way where the cell populations have been transplanted into the gastrocnemius muscles of SCID/mdx mice – a mouse model of Duchenne muscular dystrophy that is dystrophin deficient and also is immune deficient to inhibit the rejection of the injected human cell populations. These in vivo experiments will allow us to compare the myogenic potential of the cells in a DMD model verse the acute muscle injury model used above (i.e., the cardiotoxin injured mice).

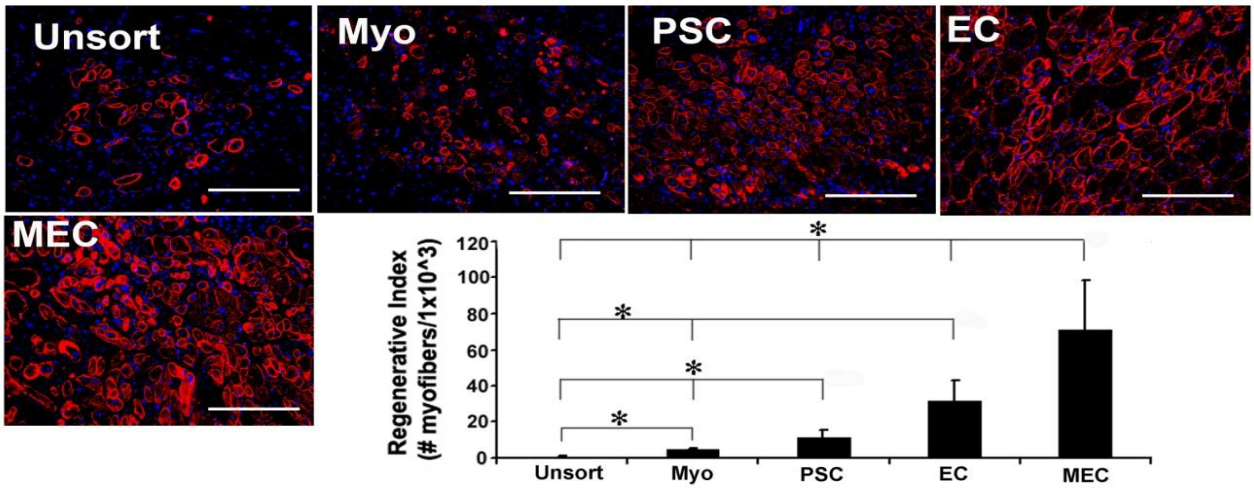

Figure 5. Comparison of myogenic regenerative capacities *in vivo*. Freshly sorted cells were transplanted into the cardiotoxin-injured skeletal muscles of SCID mice. Quantitative analyses of human spectrin-positive skeletal myofibers on tissue sections revealed that myogenic endothelial cells (MEC) mediated the highest myogenic regeneration among all five cell fractions tested (* $p<0.05$). Injection of perivascular stem cells (PSC) regenerated more human myofibers than injections of myoblasts (Myo) ($p>0.05$) and unpurified muscle cells (Unsort) (* $p<0.05$). Finally, myoblasts (Myo) displayed a higher myogenic capacity than unpurified muscle cells (Unsort) (* $p<0.05$). (Red immunostaining is spectrin, Blue nuclei are DAPI stained)

KEY RESEARCH ACCOMPLISHMENTS:

- Demonstration of prospective isolation of myoblasts, pericytes and myo-endothelial cells derived from human skeletal muscle biopsy, and from both expanded and cryopreserved populations.
- Demonstration that the myo-endothelial cells show a higher level of myogenic potential in vitro as compared to myoblasts and pericytes.
- Demonstration that both expanded and cryopreserved cells continue to show some myogenic potential in vitro.
- Demonstration that the myo-endothelial cells show a significantly higher level of skeletal muscle regeneration in vivo as compared to myoblasts and pericytes.
- Obtained preliminary evidence that PP3 cells isolated from young female skeletal muscle has a higher myogenic capacity than PP3 cells isolated from old skeletal muscle.
- Obtained preliminary evidence that myoendothelial cells isolated from young skeletal muscle is more resistant to the effects of oxidative stress than those isolated from old skeletal muscle.
- Preliminary evidence that young and old myondothelial cells possess a similar proliferation capacity.
- Optimized the growth medium for human myoendothelial cells in order to increase their proliferation rates and reduce their differentiation rates by maintaining their stem-like state in culture.
- Identified an antibody that could be used without significant background staining in our SCID/mdx model of DMD.
- Initiated studies comparing male and female myoendothelial regeneration efficiencies in vitro.
- Identified a physiological testing system (DigiGait system) that could give us excellent physiologic readouts of our transplanted animals.
- Immunomodulatory properties of muscle-derived stem cells are associated with reduced NF-κB/p65 signaling.
- p65 +/- MDSC transplantation can improve muscle histology in dKO mice (mice deficient for both utrophin and dystrophin) after IP transplantation.

- Further preliminary studies have demonstrated human muscle-derived cell engraftment in the SCID/mdx model; however, there is poor to no dystrophin expression in the transplanted muscles of these mice with any of the human population utilized.
- Engraftment has been confirmed with GFP and human MHC-1 antibodies.
- Identification of another potential model of DMD to complete the aims of this grant has led to studies using a dystrophin/utrophin-/- (double knock-out, dKO) model of DMD which has been shown to demonstrate an association between rapid muscle progenitor cell pool exhaustion with the progression of the DMD pathology.
- Further study of the dKO model led us to discover that the MDCs responsible for myogenesis differ from MDCs involved in adipogenesis in the dKO mice.
- We have also demonstrated the role of RhoA signaling in regulating the process *of* heterotopic ossification in the dystrophic muscle of dKO mice which indicates that RhoA may serve as a potential target for repressing injury-induced and congenital heterotopic ossification in humans.
- Found that NF-kB has a broader role in muscle stem and progenitor cells than previously thought, and that the anti-inflammatory molecules secreted by stem cells, such as HGF, could potentially be harnessed to control secondary pathologies of muscle diseases such as DMD.
- Preplate isolated hMDCs also exhibited poor muscle regenerative potentials as was demonstrated by the muscle-derived myo-endo and pericytes in the SCID/mdx model.
- Human dental pulp (hDPSCs) and amniotic fluid stem cells (hAFSCs) also exhibited very poor muscle regenerative potentials as was demonstrated by the muscle-derived myo-endo and pericytes in the SCID/mdx model indicating this was not a muscle stem cell related problem, but probably a problem with the ability of human cells to effectively fusein vivo.
- We found that Notch-activated human muscle cells demonstrated larger cell engraftment areas in the when transplanted into the skeletal muscle of SCID mdx indicated that the transplantation of human MDCs into dystrophic muscle could potentially be improved by activating Notch signaling prior to their implantation.
- We found that optimizing the *in vitro* environment, by modulating the surface culture conditions with a variable stiffness PDMS substrate and protein coatings; can augment stem cell proliferation and differentiation capacities which could augment the cells transplantation regenerative efficiency.

REPORTABLE OUTCOMES:

1. Chen C, Okada M, Tobita K, Crisan M, Péault B, Huard J; **Transplantation of Purified Human Skeletal Muscle-Derived Pericytes Reduce Fibrosis in Injured Ischemic Muscle Tissues**. Orthopaedic Research Society; March 6-9, 2010; New Orleans, La **(Appendix 1)**

2. Aiping Lu, Qing Yang, Minakshi Poddar, Bing Wang, Denis C. Guttridge, Paul D. Robbins, Johnny Huard; **Transplantation of p65 Deficient Stem Cells Improved the Histopathology of Skeletal Muscle in Dystrophic Mice.** Orthopaedic Research Society; 2011 ORS Annual Meeting; January 13-16, 2011; Long Beach, CA. **(Appendix 2)**

3. Proto, J., Lu, A., Robbins, P.D., Huard, J; **Immunomodulatory properties of muscle-derived stem cells associated with reduced NF-κB/p65 signaling.** Orthopaedic Research Society; 2011 ORS Annual Meeting; January 13-16, 2011; Long Beach, CA. **(Appendix 3)**

4. Aiping Lu, Jonathan Proto, Lulin Guo, Ying Tang, Mitra Lavasani, Jeremy S. Tilstra, Laura J. Niedernhofer, Bing Wang, Denis C. Guttridge, Paul D. Robbins, Johnny Huard J.H. **NF-κB negatively impacts the myogenic potential of muscle-derived stem cells.** Molecular Therapy 2012; 20(3): 661-8. PMID: 22158056 **(Appendix 4)**

5. Zheng B, Chen C, Li G, Thompson S, Poddar M, Peault B, Huard J. **Isolation of myogenic stem cells from cultures of cryopreserved human skeletal muscle.** Cell Transplantation 2012 Apr, 21(6):1087-93. PMID: 22472558 **(Appendix 5)**

6. Bo Zheng, Guangheng Li, William Chen, Bridget M Deasy, Jonathan B Pollett, Bin Sun, Lauren Drowley, Burhan Gharaibeh, Arvydas Usas, Alison Logar, Bruno Peault , Johnny Huard; **Human Myogenic Endothelial Cells Exhibit Chondrogenic and Osteogenic Potentials at the Clonal Level.** Journal of Orthopaedic Research. 2013 Jul;31(7):1089-95. PMID: 23553740 (**Appendix 6)**

7. Aiping Lu; Jonathan Proto; Xiaodong Mu; Ying Tang; Minakshi Poddar; Bing Wang; Johnny Huard**. Progression of muscular dystrophy in dystrophin/utrophin-/- mice is associated with rapid muscle progenitor cell exhaustion.** Orthopaedic Research Society; 2013 ORS Annual Meeting; January 26-30, 2013; San Antonio, TX **(Appendix 7)**

8. Jihee Sohn, Ying Tang, Bing Wang, Aiping Lu, Johnny Huard. **Muscle-derived cells (MDCs) responsible for myogenesis differ from MDCs involved in adipogenesis in dystrophin/utrophin-/- mice.** Orthopaedic Research Society; 2013 ORS Annual Meeting; January 26-30, 2013; San Antonio, TX **(Appendix 8)**

9. Xiaodong Mu, Arvydas Usas, Ying Tang, Aiping Lu, Jihee Sohn, Bing Wang, Kurt Weiss, and Johnny Huard. **RhoA signaling regulates heterotopic ossification and *fatty infiltration* in dystrophic skeletal muscle.** Orthopaedic Research Society; 2013 ORS Annual Meeting; January 26-30, 2013; San Antonio, TX **(Appendix 9)**

10. Proto, J., Tang, Y; Lu, A., Robbins, P.D., Wang, B. Huard, J. **Suppression of skeletal muscle inflammation by muscle stem cells is associated with hepatocyte growth factor in wild type and *mdx*;p65$^{+/-}$ mice.** Orthopaedic Research Society; 2013 ORS Annual Meeting; January 26-30, 2013; San Antonio, TX **(Appendix 10)**

11. Chen WC, Park T, Murray R,Zimmerlin L, Lazzari L, Huard J, Peault B. **Cellular Kinetics of Perivascular MSC Precursors**, Stem Cells International. Vol. 2013:983059 (18) 2013. (**Appendix11**)

12. Xiaodong M, Usas A, Tang Y, Lu A, Wang B, Weiss K, Huard J**. RhoA mediates defective stem cell function and heterotopic ossification in dystrophic muscle of mice**, FASEB Journal. 2013 May 23. PMID: 23704088 (**Appendix 12**)

13. Aiping Lu; Xiaodong Mu; Ying Tang; Minakshi Poddar; Jonathan D. Proto; Jihee Sohn; Nicholas Oyster; Koji Takayama; Bing Wang; Weiss Kurt; Johnny Huard, **Progression of muscular dystrophy is associated with Muscle Progenitor Cell Exhaustion and over-activated mTOR signaling (In preparation) (Appendix 13)**

14. Pisciotta, Alessandra; Lu, Aiping; Gharaibeh, Burhan; De Pol, Anto[1]; Huard, Johnny, **Enhanced myogenic potential of human dental pulp and amniotic fluid stem cells by use of a demethylation agent and conditioned media.** Orthopaedic Research Society; 2014 ORS Annual Meeting; March 15-18, 2014; New Orleans, LA (**Appendix14**)

15. Seth David Thompson, Mitra Lavasani, Bahar Ahani, Prerana Reddy, Yan Sun, Quentin, Jallerat, Adam W. Feinberg, Johnny Huard. **Proliferation and Differentiation Capacities of Muscle Derived Stem/Progenitor Cells Cultured on Polydimethylsiloxane Substrates of Varying Elastic Modulus**

and Protein Coating. Orthopaedic Research Society; 2014 ORS Annual Meeting; March 15-18, 2014; New Orleans, LA (**Appendix 15**)

CONCLUSION:

Year 1: Our results to date show that even after *in vitro* expansion and cryopreservation, primary human muscle cells harbored various subpopulations of cells. We have identified and purified to homogeneity four distinct cell populations from cryopreserved primary human muscle cells including two stem cell subpopulations: Pericytes (PSCs) ($CD146^+/CD45^-CD56^-UEA\text{-}1R^-$) and myoendothelial cells (MECs) ($CD56^+CD146^+UEA\text{-}1R^+/CD45^-$). Freshly sorted MECs, PSCs, endothelial, and myogenic cells were transplanted into the injured skeletal muscles of SCID mice to examine their myogenic efficacy. MECs displayed the highest muscle regenerative capacity among all cell subsets tested, and PSCs were superior to myoblasts and unpurified cryopreserved primary human muscle cells. These results were consistent with previous observations from the injection of cells isolated from fresh muscle biopsies. Taken together, our results suggest the presence of distinct subpopulations of highly myogenic stem/progenitor cells within expanded cryopreserved primary human muscle cells and support the feasibility of further purifying stem cell fractions from cryopreserved human cells. Most importantly, these findings infer the practicability of prospective isolation of myogenic stem/progenitor cell populations from banked human skeletal muscle cells, highlighting a new technology to further enhance the availability and efficacy of cell-mediated therapies.

Year 2: We have preliminary evidence that there are no differences in the proliferative abilities between old and young human muscle derived cells; however, there appears to be a difference in the MDCs myogenic differentiation capacity and resistance to oxidative stress. We also formulated a medium that optimizes the proliferative capacity of our human MDCs while reducing their premature myogenic differentiation and identified a non-invasive behavioral testing system to detect the functional physiological improvements of the muscles that have been transplanted with our muscle derived stem cells. Moreover, we have demonstrated that NF-κB inhibition stimulates MDSC-mediated muscle regeneration through multiple mechanisms, including through the expression of anti-inflammatory factors that attenuate inflammation and necrosis. These experiments have identified the NF-κB signaling pathway as a potential therapeutic target to enhance muscle regeneration following injury or disease. Our results have demonstrated less inflammation within the regenerating areas of muscles of mice injected with $p65^{+/-}$ MDSCs (MDSCs with ½ the expression of the NF-κB sub unit p65) compared to the untreated muscles; hence the use of NF-kappa blockade may be useful to improve the regeneration index of human muscle-derived stem cells in the skeletal muscle of SCID/MDX mice and potentially in the skeletal muscle to DMD patients.

Year 3: SCID/mdx mice skeletal muscle generates high levels of background when immunostained with an antibody against "human dystrophin", which has been an ongoing problem with this animal model. We have been performing additional tangential experiments on another model of DMD that is deficient for both dystrophin and utrophin known as the double-knock out (dKO) mouse. This model was being used because its pathophysiology more accurately resembles that of DMD patients and we felt might better accommodate the experiments outline in this grant, since we were experiencing the technical problems with the SCID/mdx model. In a set of experiments performed on the dKO mice, we demonstrated that MPCs isolated from the skeletal muscle of old dKO mice have a reduced ability to proliferate and differentiate compared to MPCs isolated from young mice. Moreover, the numbers of Pax7 positive cells *in vivo* undergo a rapid decline in the skeletal muscle of dKO mice during aging and disease progression. This study suggested that the exhaustion of stem cells contributes to the histopathology associated with DMD and that blocking the exhaustion of muscle progenitor cells and stem cell-mediated therapy could be used as a potential clinical strategy to treat muscle disease. In another set of experiments we found that dKO-RACs, mesenchymal progenitor cells in skeletal muscle, may contribute to adipogenesis and are responsible for ectopic fat cell formation within skeletal muscle in pathological conditions such as DMD. Therefore, targeting RACs to block adipogenesis in skeletal muscle may

open new opportunities to treat muscle diseases. We also found that DMD mouse models featuring different severities of muscular dystrophy may have varied potentials for developing HO or fatty infiltration in the dystrophic muscle, and RhoA signaling might be a critical mediator of the determining these differential fates, including the progression towards HO, fatty infiltration, or normal muscle regeneration. In another set of experiments we found that NF-kB has a broader role in muscle stem and progenitor cells than previously thought, and that the anti-inflammatory molecules secreted by stem cells, such as HGF, could potentially be harnessed to control secondary pathologies of muscle diseases such as DMD.

Year 4: This year's major focus was to continue to determine why we were experiencing the transplantation difficulties with the SCID/mdx mice. It was imperative to determine why the SCID/mdx mice were generating such high levels of background when injected with hMDCs and whether the hMDCs were actually engrafting and we continued to try and determine why we were experiencing the problems and to try and identifying potential ways of improving the hMDCs engraftment efficiency in this model. Besides the proposed human cell types of pericytes and myo-endo cells we utilized human MDCs isolated via the preplate technique, which is a population of cells that is more heterogeneous in nature and contains both the myo-endo cell and pericyte sub-populations. We found that the hMDCs isolated by the preplate technique expressed mesenchymal stem cell markers CD73, CD90, CD105 and CD44 and also expressed the myogenic marker CD56 and the pericyte marker CD146. The in vivo results indicated that they could engraft within the muscle; however, their muscle fiber fusion and regeneration capacities were extremely poor and no human dystrophin expression could be detected. We also compared these latter three populations to another human cell population isolated from dental pulp and amniotic fluid to determine if the engraftment problems were related to the stem cell type. This study demonstrated the utility of demethylation to induce hAFSCs and hDPSCs to differentiate towards the myogenic lineage in vitro and, to a very limited degree, engraft and produce dystrophin. The positive fibers observed were very few and could represent revertant myofibers. We therefore conclude that like the myo-endo, pericytes, and preplate isolated MDCs, the hAFSCs and hDPSCs could engraft but could only participate in myofiber regeneration to a very limited degree. Moreover we performed a study to see if we could improve the cells transplantation efficiency by activating the Notch signally pathway, which has been described previously to be necessary for maintaining the stem cell niche in skeletal muscle. We found that compared to the skeletal muscle transplanted with untreated control cells, that there were obviously more regenerating myofibers and larger cell engraftment observed in the skeletal muscle transplanted with the Notch-activated human muscle cells, which indicated that the transplantation of human MDCs into dystrophic muscle could potentially be improved by activating Notch signaling prior to their implantation. Finally, in an attempt to further improve engraftment efficiency we grew the cells on a variety of different substrates with varying degrees of surface elasticity. The findings of this study support the view that optimizing the *in vitro* environment, by modulating the surface culture conditions with a variable stiffness PDMS substrate and protein coatings; can augment stem cell proliferation and differentiation capacities. Future cell therapies implemented for tissue repair may significantly benefit from the application of primary cells isolated and expanded on PDMS surfaces with protein coatings.

REFERENCES:

1. Zhang et al. 2006. Tissue Eng 12, 2813.
2. De Coppi et al. 2007 Nat Biotechnol 25, 100.
3. Riccio et al. 2010. Eur J Histochem 54, 4.
4. N.S. Ye et al. 2006. Stem Cells Dev 15, 665.
5. Antonitsis et al. 2008 Thorac Cardiovasc Surg 56, 77.
6. Duan et al. 2010. Gen Comp Endocrinol 167, 344.
7. Boonen KJ and Post MJ, Tissue Eng Part B Rev. 2008;14(4):419-31.
8. Gopinath SD, et al., 2008;7(4):590-8.
9. Chakkalakal JV, et al., Nature. 2012;490(7420):355-60.
10. Brohl D, et al., Dev Cell. 2012;23(3):469-81.

11. Lepper C, et al., Cell Stem Cell. 2012;11(4):443-4.
12. Kuang S, et al., Cell. 2007;129(5):999-1010. PMCID: 2718740.
13. Zhang H, et al. Tissue Eng Part A. 2010;16(11):3441-8. PMCID: 2965194.
14. Lee JY, et al., *J Cell Bio* 150, 1085-1100 (2000).
15. Kuroda R, et al., *Arthritis Rheum* 54, 433-422 (2006).
16. Oshima H, etl al., *Mol Ther* 12, 1130-1141.
17. Lavasani M, et al., *Nat Comm* 3: e608 (2012).
18. Gilbert PM, et al., *Science* 329, 1078-1081 (2010).
19. Engler AJ, et al., *Cell* 126, 677-689 (2006).
20. Palchesko RN, et al., *PLoS ONE* 7(12): e51499 (2012).

APPENDICES:

Refer to Manuscripts/Reprints, Abstracts Section

MANUSCRIPTS/REPRINTS, ABSTRACTS:

1. Chen C, Okada M, Tobita K, Crisan M, Péault B, Huard J; **Transplantation of Purified Human Skeletal Muscle-Derived Pericytes Reduce Fibrosis in Injured Ischemic Muscle Tissues**. Orthopaedic Research Society; March 6-9, 2010; New Orleans, La **(Appendix 1)**
2. Aiping Lu, Qing Yang, Minakshi Poddar, Bing Wang, Denis C. Guttridge, Paul D. Robbins, Johnny Huard; **Transplantation of p65 Deficient Stem Cells Improved the Histopathology of Skeletal Muscle in Dystrophic Mice.** Orthopaedic Research Society; 2011 ORS Annual Meeting; January 13-16, 2011; Long Beach, CA. **(Appendix 2)**
3. Proto, J., Lu, A., Robbins, P.D., Huard, J; **Immunomodulatory properties of muscle-derived stem cells associated with reduced NF-κB/p65 signaling.** Orthopaedic Research Society; 2011 ORS Annual Meeting; January 13-16, 2011; Long Beach, CA. **(Appendix 3)**
4. Aiping Lu, Jonathan Proto, Lulin Guo, Ying Tang, Mitra Lavasani, Jeremy S. Tilstra, Laura J. Niedernhofer, Bing Wang, Denis C. Guttridge, Paul D. Robbins, Johnny Huard J.H. **NF-κB negatively impacts the myogenic potential of muscle-derived stem cells.** Molecular Therapy 2012; 20(3): 661-8. PMID: 22158056 **(Appendix 4)**
5. Zheng B, Chen C, Li G, Thompson S, Poddar M, Peault B, Huard J. **Isolation of myogenic stem cells from cultures of cryopreserved human skeletal muscle.** Cell Transplantation 2012 Apr, Epub ahead of print. PMID: 22472558 **(Appendix 5)**
6. Bo Zheng, Guangheng Li, William Chen, Bridget M Deasy, Jonathan B Pollett, Bin Sun, Lauren Drowley, Burhan Gharaibeh, Arvydas Usas, Alison Logar, Bruno Peault , Johnny Huard; **Human Myogenic Endothelial Cells Exhibit Chondrogenic and Osteogenic Potentials at the Clonal Level.** Journal of Orthopaedic Research (Under review) (**Appendix 6)**
7. Aiping Lu; Jonathan Proto; Xiaodong Mu; Ying Tang; Minakshi Poddar; Bing Wang; Johnny Huard**. Progression of muscular dystrophy in dystrophin/utrophin-/- mice is associated with rapid muscle progenitor cell exhaustion.** Orthopaedic Research Society; 2013 ORS Annual Meeting; January 26-30, 2013; San Antonio, TX **(Appendix 7)**
8. Jihee Sohn, Ying Tang, Bing Wang, Aiping Lu, Johnny Huard. **Muscle-derived cells (MDCs) responsible for myogenesis differ from MDCs involved in adipogenesis in dystrophin/utrophin-/- mice.** Orthopaedic Research Society; 2013 ORS Annual Meeting; January 26-30, 2013; San Antonio, TX **(Appendix 8)**
9. Xiaodong Mu, Arvydas Usas, Ying Tang, Aiping Lu, Jihee Sohn, Bing Wang, Kurt Weiss, and Johnny Huard. **RhoA signaling regulates heterotopic ossification and *fatty infiltration* in dystrophic skeletal muscle.** Orthopaedic Research Society; 2013 ORS Annual Meeting; January 26-30, 2013; San Antonio, TX **(Appendix 9)**

10. Proto, J., Tang, Y; Lu, A., Robbins, P.D., Wang, B. Huard, J. **Suppression of skeletal muscle inflammation by muscle stem cells is associated with hepatocyte growth factor in wild type and *mdx*;p65$^{+/-}$ mice.** Orthopaedic Research Society; 2013 ORS Annual Meeting; January 26-30, 2013; San Antonio, TX **(Appendix 10)**
11. Chen WC, Park T, Murray R,Zimmerlin L, Lazzari L, Huard J, Peault B. **Cellular Kinetics of Perivascular MSC Precursors**, Stem Cells International. Vol. 2013:983059 (18) 2013. (**Appendix11**)
12. Xiaodong M, Usas A, Tang Y, Lu A, Wang B, Weiss K, Huard J**. RhoA mediates defective stem cell function and heterotopic ossification in dystrophic muscle of mice**, FASEB Journal. 2013 May 23. PMID: 23704088 (**Appendix 12**)
13. Aiping Lu; Xiaodong Mu; Ying Tang; Minakshi Poddar; Jonathan D. Proto; Jihee Sohn; Nicholas Oyster; Koji Takayama; Bing Wang; Weiss Kurt; Johnny Huard, **Progression of muscular dystrophy is associated with Muscle Progenitor Cell Exhaustion and over-activated mTOR signaling (In preparation) (Appendix 13)**
14. Pisciotta, Alessandra; Lu, Aiping; Gharaibeh, Burhan; De Pol, Anto[1]; Huard, Johnny, **Enhanced myogenic potential of human dental pulp and amniotic fluid stem cells by use of a demethylation agent and conditioned media.** Orthopaedic Research Society; 2014 ORS Annual Meeting; March 15-18, 2014; New Orleans, LA (**Appendix14**)
15. Seth David Thompson, Mitra Lavasani, Bahar Ahani, Prerana Reddy, Yan Sun, Quentin, Jallerat, Adam W. Feinberg, Johnny Huard. **Proliferation and Differentiation Capacities of Muscle Derived Stem/Progenitor Cells Cultured on Polydimethylsiloxane Substrates of Varying Elastic Modulus and Protein Coating**. Orthopaedic Research Society; 2014 ORS Annual Meeting; March 15-18, 2014; New Orleans, LA (**Appendix 15**)

Sub-Project 2: Generation of human hepatocytes from patient-specific stem cells for treatment of life-threatening liver injury

PIs: David Perlmutter and Ira J. Fox

INTRODUCTION: (New data is underlined in the text of the Introduction and body.)

These studies are focused on generating human hepatocytes from patient-specific stem cells for the treatment of life-threatening liver injury. Two technical objectives were proposed: 1) Determine the extent to which human patient-specific, induced pluripotent stem (iPS) cells can be differentiated into primary human hepatocytes, and 2) Determine the extent to which the PiZ mouse model of alpha-1-antitrypsin (AT) deficiency can be developed as a platform for pre-clinical testing of hepatic stem cell transplantation as a treatment for severe liver injury and disease. In order to accomplish these objectives, we have generated 3 human iPS cell lines from normal patients and 12 iPS cell lines from patients with alpha-1-antitrypsin deficiency (ATD). These cell lines have now been characterized and 7 of which have been differentiated into hepatocytes. We have demonstrated that iPS cell-derived hepatocytes from ATD patients recapitulate the pathobiological defects observed in ATD hepatocytes. We show that there is decreased AT secretion in differentiated ATD iPS cells compared to differentiated normal iPS cells. We show that there is a decreased rate of disappearance of intracellular AT in ATD iPS cell-derived hepatocytes compared to normal iPS cell-derived hepatocytes. More importantly, ATD iPS cell-derived hepatocytes from patients with severe liver disease showed a more prominent delay in the disappearance of intracellular AT compared to those from patients with mild liver disease. We have demonstrated that iPS derived cells can be transplanted in rodents that are models of human disease and that engraftment and expansion of the derived hepatocytes corrects the disease. Finally, we have further determined the ability of donor hepatocytes to expand in the PiZ mouse, and we have generated PiZ mice on an immune-deficient background and have begun studies showing engraftment and expansion of pluripotent stem cell-derived hepatocytes in these mice.

BODY:

Technical Objective #1: Determine the extent to which human patient-specific, inducible pluripotent stem (iPS) cells can be differentiated into primary human hepatocytes.

Hypothesis: *Protocols that successfully differentiate mouse and human embryonic stem (ES) cells toward a hepatocyte phenotype will be effective in differentiating human skin cell-derived iPS cells into liver cells.*

1.1. Generation of human induced pluripotent stem cells (iPS cells).

We hypothesized that patient specific iPS cells could be generated from primary human cells, including hepatocytes, and that under appropriate conditions, the iPS cells could be induced to differentiate back to hepatocytes that could be used as cellular therapy to treat the liver defect. Here, we report the generation of multiple human iPS cell lines from primary human cells following exposure to either lentiviral, excisable lentiviral stem cell cassette or plasmid constructs carrying reprogramming factors. In **Table 1** and **2**, we characterize lines derived from normal controls, and patients with ATD. We have characterized the lines for markers of pluripotency, including alkaline phosphatase activity, nuclear NANOG, OCT3/4 and SOX2 staining, and reactivity to antibodies to the surface markers SSEA-4 and TRA1-60, and confirmed these results by qPCR. In addition, genotyping has been completed on most of the ATD and control iPS cell lines.

Table 1. List of normal iPS cell lines

Source of iPS cell line	Normal human hepatocyte (biopsy)	Normal dermal fibroblast	Normal dermal fibroblast
Vector used for iPS induction	Lentivirus	Excisable Lentiviral Stem Cell Cassette	Non-integrating plasmids
Characterization of Pluripotency			

qPCR	✔	✔	✔
Immunostaining	✔	✔	✔
Teratoma formation	✔	✔	✔
Genotype*	G/G	G/G	G/G
Name of iPS cell line	**HH1591** iPS cells (Control)	**BMC-1** iPS cells (Control)	**NF-IF** iPS cells (Control)

*** G/G: Homozygous for the wild type allele**

Table 2. List of ATD iPS cell lines

Source of iPS cell line	AT deficient human hepatocyte (Biopsy, CHP HH1764 (7/21/2010), 10(Y) M	AT deficient human hepatocyte (Biopsy, Einstein College of Medicine)	AT deficient lung fibroblast (Biopsy)	AT deficient lung fibroblast (Biopsy)	AT deficient lung fibroblast (Biopsy)	AT deficient lung fibroblast (Biopsy)
Vector used for iPS induction	Lentivirus	Non-integrating plasmids	Lentivirus	Excisable Lentiviral Stem Cell Cassette	Excisable Lentiviral Stem Cell Cassette	Excisable Lentiviral Stem Cell Cassette
Characterization of Pluripotency						
qPCR	✔	✔	✔	✔	✔	✔
Immunostaining	✔	✔	✔	✔	✔	✔
Teratoma formation	✔	✔	✔	✔	✔	✔
Genotype	A/A	A/A	A/A	A/A	A/A	A/A
Name of iPS cell line	**ATH-1** iPS cells (Severe LD ATD)	**AAT2** iPS cells (Severe LD ATD)	**AT-10 c1-6** iPS cells (Mild LD ATD) 6 other clones	**100-3-Cr-1** iPS cells (Mild LD ATD)	**102-37B-Cr-2** iPS cells (Mild LD ATD)	**103-3-Cr-1** iPS cells (Mild LD ATD)

*** A/A: Homozygous for the Z allele**

1.2. Differentiation of human iPS cells into hepatocytes.

We have now generated iPS cell-derived hepatocytes in a manner similar to what we have published[1], and using a variation on the technique described by Si-Tayeb [2]. **Figure 1** illustrates the morphologic changes that occur during differentiation. **Figure 2** shows that the differentiated H1 hES cells and ATD iPS cells exhibit several ultrastructural features seen in primary human hepatocytes.

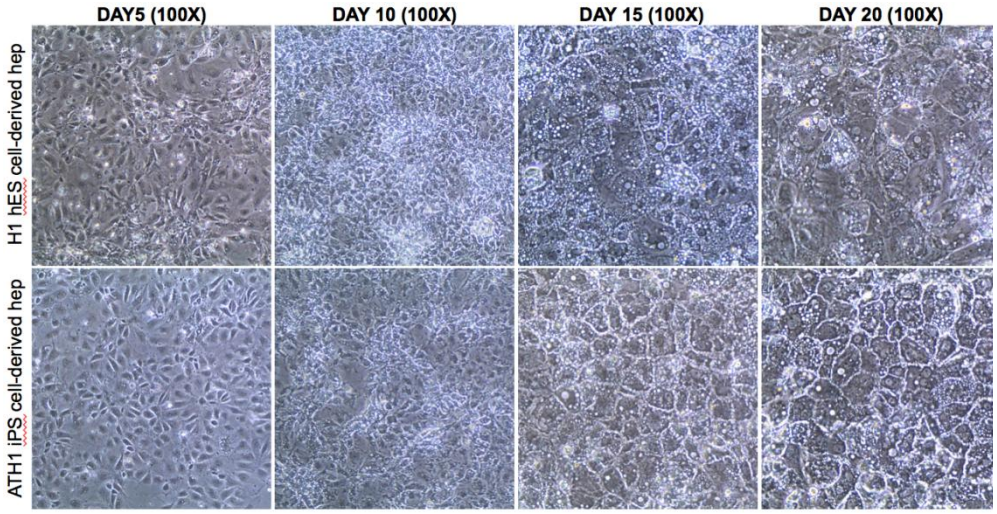

Figure 1. Morphologic changes during hepatocyte differentiation of H1 hES cell and ATD iPS cell after days 5 to 20. Morphology of iPS cells after the phase of definitive endoderm (day 5), hepatic specification (day 10), hepatic induction (day 15), and hepatic maturation (day 20).

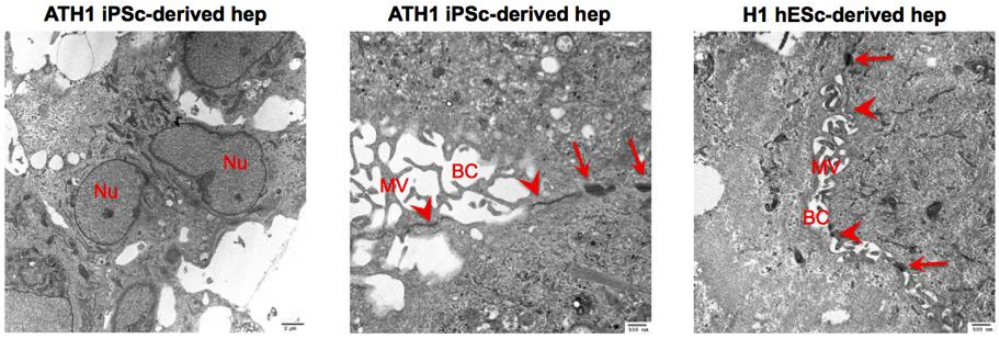

Figure 2. Electron micrograph of H1 hES cells and ATD iPS cells following hepatocyte-specific differentiation. Shown are the nuclei (Nu), bile canaliculi (BC), microvilli (MV), tight junctions (arrowhead), and desmosomes (arrow).

1.3. Analysis of differentiated ATD iPS cells.

We performed several experiments to determine whether ATD iPS cell-derived hepatocytes recapitulate the defect observed in ATD hepatocytes. In **Figure 3**, we show that differentiated cells secreted 50-65% of the albumin levels secreted by 1° human hepatocytes but ATD iPS cell-derived hepatocytes secreted only 50% of the level of AT secreted by WT iPS cell-derived or 1° human hepatocytes. In **Figure 4**, we show that similar to 1° human hepatocytes from an ATD patient with severe liver disease, electron micrograph of ATD iPS cell-derived hepatocytes showed poorly organized and markedly dilated rER. ATD is also characterized by the accumulation of the mutant AT variant within hepatocytes resulting in decreased secretion of AT. Immunofluorescent analysis of AT showed intense AT staining in ATD iPS cell-derived compared to control iPS cell-derived hepatocytes (**Figure 5**). It has been suggested that the mutant AT variant accumulates within the ER of hepatocytes in ATD patients and other model systems. We therefore sought to determine whether AT accumulates within these compartments in ATD iPS cell-derived hepatocytes by immunofluorescent staining for AT, the ER markers calnexin and calreticulin, and the Golgi marker GM130. Our data shows that AT staining colocalized with ER and Golgi markers in both ATD and control iPS cell-derived hepatocytes. Interestingly, some punctate AT staining that resembled aggregates did not colocalize with either ER or Golgi markers in ATD iHeps. In **Figure 6**, we show using a pulse-chase analysis that there is a slower rate of disappearance of intracellular AT in differentiated ATD iPS cells ($t_{1/2}$=2.1 to 4 hr) compared to control cells ($t_{1/2}$=1.4 hr). More importantly, ATD iPS cell-derived hepatocytes from patients with severe liver disease

showed a more prominent delay in the disappearance of intracellular AT (t½=3.1 to 4 hr) compared to those from patients with mild liver disease (t½=2.1 to 2.2 hr). There was no significant difference between the rates of the two iPSc clones from the mild LD patient, suggesting that the results are not an artifact of reprogramming or differentiation. These results suggest that variation in the severity of liver disease is related to genetic modifiers that affect intracellular degradation pathways.

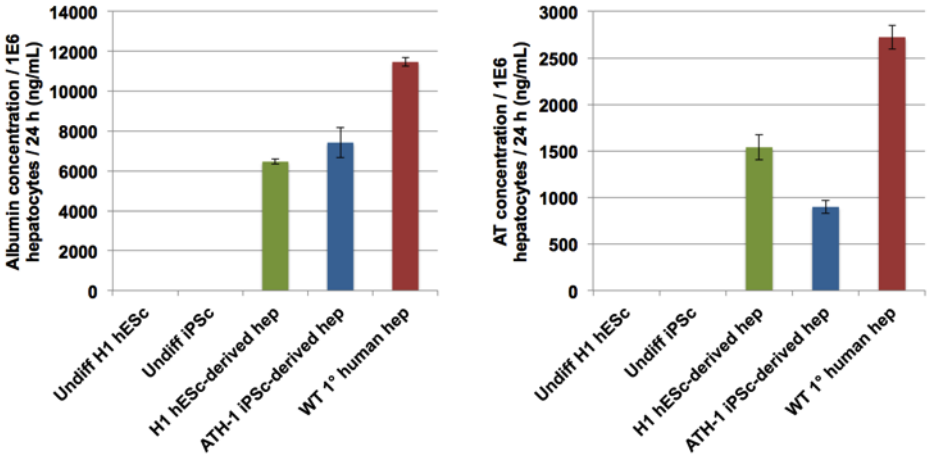

Figure 3. ELISA results following hepatocyte-specific differentiation of H1 hES cells and ATD iPS cells. Shown are the albumin and AT-specific ELISA measurements derived from the supernatant of differentiated cells over a period of 24 hours after the hepatic maturation step of differentiation compared to the results from control fresh primary human hepatocytes.

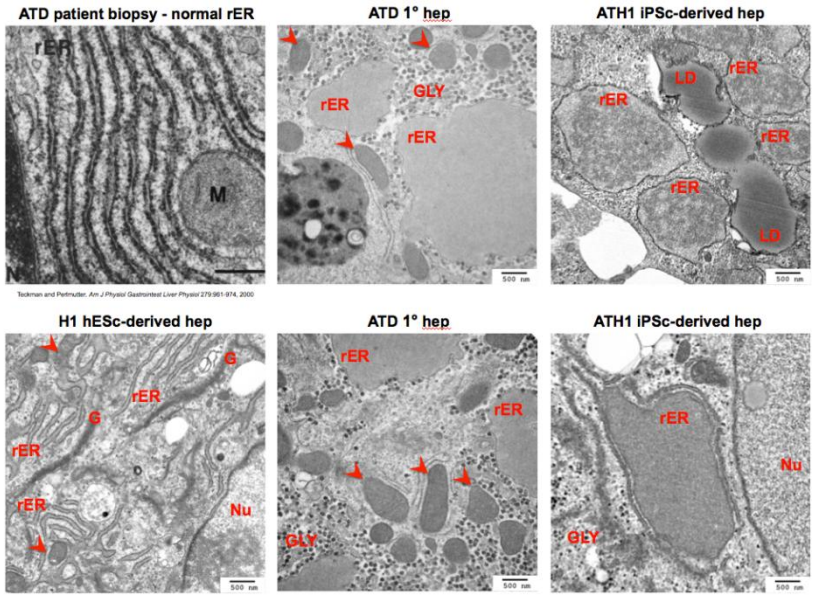

Figure 4. Electron micrograph of differentiated H1 hES cells and ATD iPS cells following hepatocyte-specific differentiation show markedly dilated rER in differentiated ATD iPS cells. Shown are the nuclei (Nu), rough endoplasmic reticulum (rER), Golgi bodies (G), lipid droplets (LD), glycogen rosettes (GLY), microvilli (MV), and mitochondria (arrowhead. For comparison, micrographs of normal and ATD 1° hepatocytes are also shown.

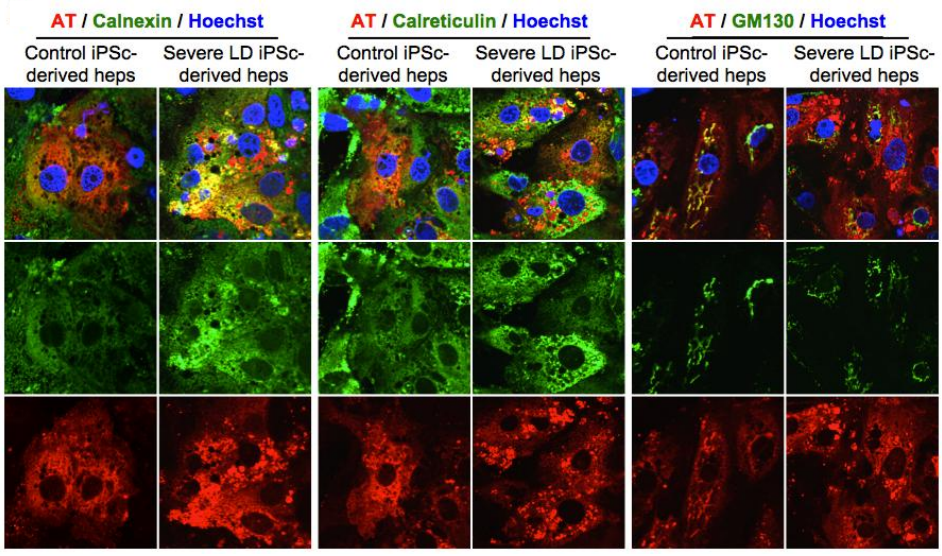

Figure 5. Double staining for AT and ER or Golgi markers in ATD iPSc-derived hepatocytes. Immunofluorescent staining of AT with calnexin, calreticulin, or GM130 (600X).

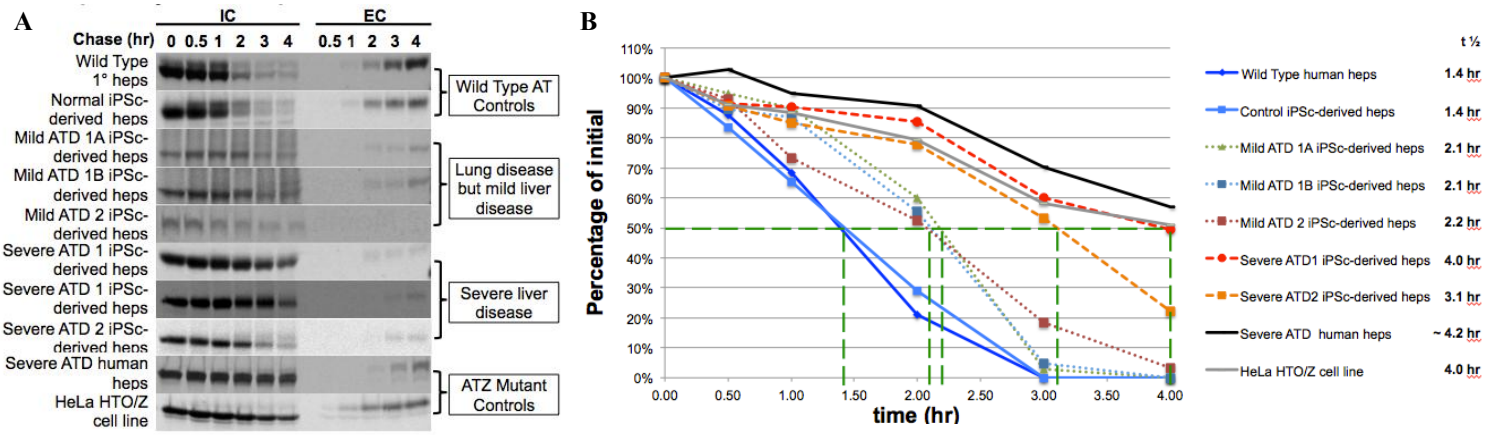

Figure 6. Pulse chase analysis of differentiated stem cells and control cells. (**A**) After cells were pulsed for 1 hour with 35S-methionine-containing medium, intracellular (IC) and extracellular (EC) fractions were collected at each of the indicated chase time points (0 to 4 hours). Samples were run on an SDS-PAGE gel and an autoradiograph was obtained. (**B**) Densitometric analysis was performed in order to calculate the half-life (t½) of the rate of disappearance of intracellular AT.

1.4. Transplantation of human iPS cell-derived hepatocytes with correction of hyperbilirubinemia in the Gunn rat model of Crigler-Najjar syndrome type 1.

To determine the extent to which stem cell-derived human hepatocytes could be engrafted in immune suppressed rat hosts, we transplanted iPS cell-derived hepatocytes into Gunn rat livers by intrasplenic injection [3]. To provide a proliferative advantage to the transplanted cells,

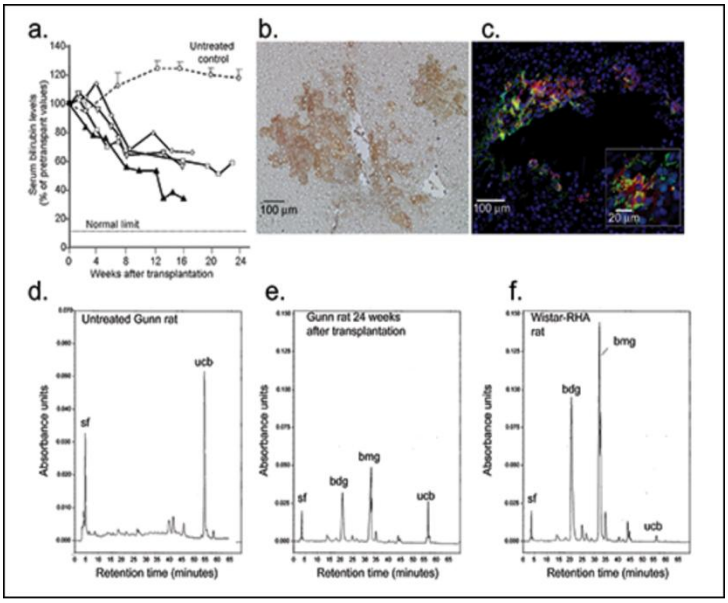

Figure 7. Effect of repopulation of the Gunn rat liver by iPS cell-derived hepatocytes. a, Serum bilirubin levels in the four recipient Gunn rats (diamond, square, open and closed triangles) at the indicated time points after transplantation of human iPS cell-derived hepatocytes are shown as percentage of pre-transplantation levels. Bilirubin levels of untreated age-matched controls are also shown (open circles, mean+SEM of 6 rats). The upper limit of serum bilirubin levels in congenic normal Wistar-RHA rats is shown as a dotted line. b and c, Representative liver sections from a recipient Gunn rat 4-6 months after transplantation of human iPS-derived hepatocytes. b, Immunohistochemical staining for human UGT1A1 showing cell clusters derived from the transplanted cells. c, Dual immunofluorescence staining showed that a majority of cells positive for human serum albumin (green) were also positive for human UGT1A1 (red). The nuclei are stained blue (DAPI). A magnified view is shown in the insert. d-f, HPLC analysis of bilirubin species excreted in the bile of a control Gunn rat, a rat receiving iPS-derived hepatocytes and a congeneic normal Wistar RHA rat is shown. sf, solvent front; ucb, unconjugated bilirubin; bdg, bilirubin diglucuronide; bmg, bilirubin monoglucuronide. Note the difference in the absorbance unit scale in panel c from that in panels d and e.

part of the host liver was irradiated (50Gy) and an adenovirus vector expressing hepatocyte growth factor was injected. For immune suppression, Tacrolimus (2mg/kg) was injected daily beginning 7 days before transplantation. After transplantation, serum bilirubin levels declined, as shown in **Figure 7**, and immuno-histochemistry of liver sections showed clusters of human albumin and UGT1A1-positive cells, and bilirubin conjugates appeared in the bile, indicating function by engrafted, UGT1A1-expressing iPS-derived hepatocytes.

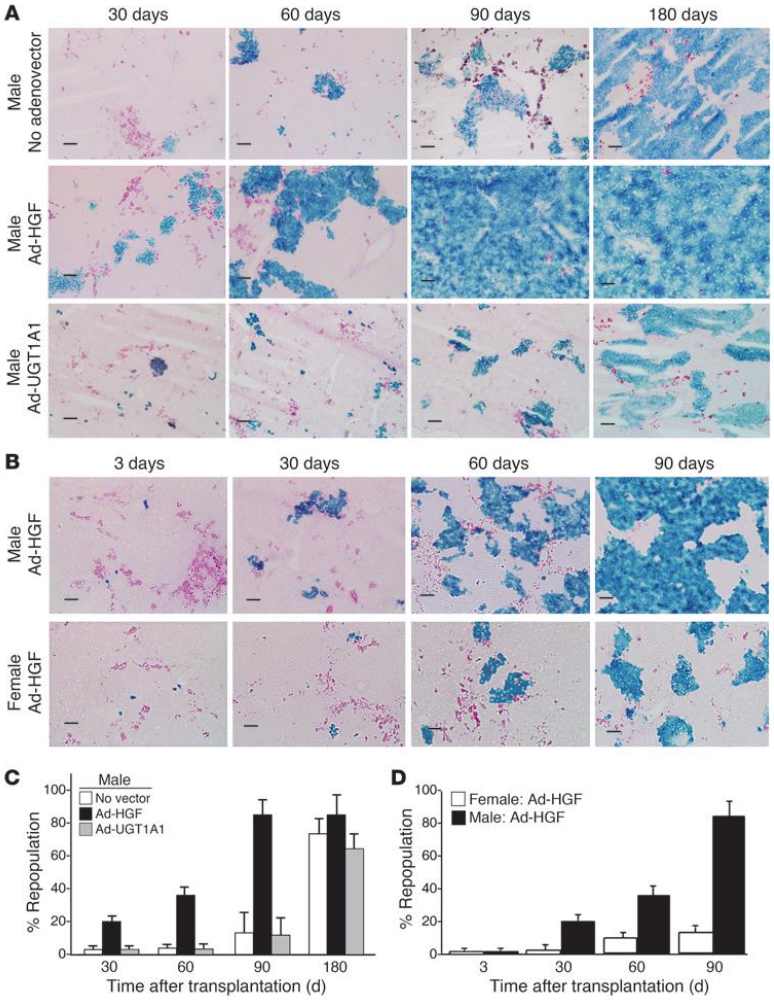

Figure 8. Kinetics of hepatic repopulation in PiZ mice. (A) Ad-HGF administration accelerated repopulation. ROSA26 mouse hepatocytes (1 × 106) were transplanted into male PiZ mice without (upper row) or with (lower row) Ad- HGF (1 × 1011 particles, i.v.). Liver sections were stained for *E. coli* β-gal (blue), and diastase plus PAS (magenta) to visualize AAT-Z globules. Scale bars: 100 μm. Data are from representative mice from each group (*n* = 6). (B) Repopulation was greater in male recipients. Male and female PiZ mice received Ad-HGF (*n* = 6). Hepatocyte transplantation and staining of liver sections were as in A. (C and D) Quantitative DNA PCR. Quantitative PCR for the *E. coli lacZ* gene was performed on DNA extracted from livers of recipient mice. Percentage of repopulation was calculated as described in the text. (C) Graphic presentation of data from experimental groups shown in A (mean ± SEM; *n* = 6 in each group), showing significantly higher repopulation in the Ad-HGF group at all time points (*P* < 0.05). (D) Data are from the experimental groups shown in B (mean ± SEM; *n* = 6 in each group), showing significantly higher repopulation in males 30, 60, and 90 days after transplantation (*P* < 0.05).

Technical Objective #2: Determine the extent to which the PiZ mouse model of alpha-1-antitrypsin (AT) deficiency can be developed as a platform for pre-clinical testing of hepatic stem cell transplantation as a treatment for severe liver injury and disease.

Hypothesis: *iPS cells differentiated toward a hepatocyte phenotype can engraft and respond normally to proliferative signals in the livers of PiZ mice.*

2.1. Hepatocyte engraftment and proliferation in AT (PiZ) transgenic mice.

In several animal models, transplanted hepatocytes have a proliferation advantage over the host liver cells, and nearly 100% of the native liver can be replaced by the donor cells [4, 5]. In AT deficiency, the abnormal Z protein can aggregate in hepatocytes and these aggregates may damage cells. Through this mechanism, AT deficiency patients may develop liver disease. Since Z protein aggregation leads to hepatocyte apoptosis, it has been hypothesized that PiM hepatocytes transplanted into PiZ livers would have a similar selective advantage and may progressively increase their relative contribution to liver mass. To examine this possibility, hepatocytes isolated from ROSA26 (beta-galactosidase transgenic mice) were transplanted into 6-8 week old human AT (hAT) transgenic mice. Three months after transplantation approximately 20% of the native liver was replaced

by ROSA26 hepatocytes, as assessed histologically by lacZ staining **(Figure 8)**. These data provide direct evidence, in an animal model, that PiM hepatocytes have the capacity to progressively replace PiZ-expressing hepatocytes following transplantation. In addition, we have accumulated direct evidence that expansion of donor hepatocytes occurs in association with specific areas in the native liver where high levels of the mutant AT protein can be found as aggregates in the host hepatocytes, presumably leading to apoptosis [6].

We then hypothesized that expression of the mutant AT-Z should reduce the capacity of the host hepatocytes to proliferate in response to mitotic stimuli, which should accelerate repopulation by transplanted wildtype cells. To test this, we examined the extent of hepatic repopulation after hepatocyte transplantation in groups of recipient PiZ mice with administration of Ad-HGF. The extent of repopulation was significantly greater at all time points in the group that received Ad-HGF. A control group that received an adenovector that expressed an irrelevant gene did not exhibit accelerated repopulation. Ninety days after transplantation 40-60% of the hepatocytes were replaced by donor cells, and in occasional PiZ recipients, the repopulation was nearly complete, so that only the bile duct epithelial cells and the non-parenchymal cells remained from the host liver **(Figure 8)**. The increased death rate of host hepatocytes, combined with a greater mitotic activity of the donor cells resulted in progressive repopulation of the host liver by the donor cells, while the liver size remained unaltered.

2.1. Human hepatocyte engraftment and proliferation in AT (PiZ)-NSG transgenic mice.

To determine the extent to which hepatic repopulation by human hepatocytes in immune-deficient PiZ mice, we transplanted 1° human hepatocytes in male PiZ-NSG mice by intrasplenic injection. To accentuate the difference in mitotic capacity, transplanted mice were injected with an adenoviral vector expressing human hepatocyte growth factor (Ad-HGF, 1x1011 pfu/mouse) within 48 hours after transplantation. **Figure 9** shows the changes in the levels of human albumin in the serum of PIZ-NSG mice transplanted with 1° human

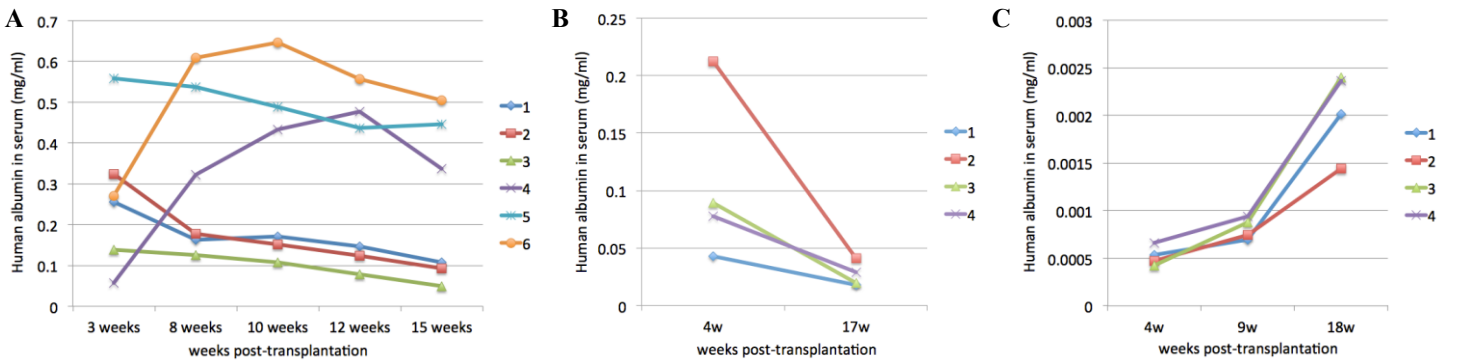

Figure 9. Human albumin levels in PiZ-NSG mouse serum transplanted with (**A**) 1-cycle chemo-treated 1° human hepatocytes (**B**) normal 1° human hepatocytes from a 6-month old donor and (**C**) 6-cycle chemo-treated 1° human hepatocytes. $1x10^6$ human hepatocytes were transplanted into each mouse by intra-splenic injection. Ad-HGF ($1x10^{10}$pfu) was injected within 48 hours post transplantation.

hepatocytes. Thus, this model did not function as desired. We will need to assess AT copy number and other means to enhance repopulation.

2.2. iPS cell-derived human hepatocyte engraftment and proliferation in immune-deficient SCID AT transgenic mice.

In last year's report we examined whether human hES cell-derived hepatocytes could engraft and proliferate spontaneously in the livers of immune deficient PiZ mice. We have now examined whether iPS-derived hepatocytes can engraft in such animals. We generated SCID/PiZ mice, and the PiZ genotype in the offspring and zygosity for the SCID mutation were determined by PCR and pyrosequencing, respectively. Human iPS cells were then differentiated to hepatocytes as described, and one million cells were transplanted into the livers of SCID/PiZ mice by intrasplenic injection. To stimulate mitosis of hepatocytes, $1x10^{11}$ adenovirus vector particles expressing hepatocyte growth factor (Ad-HGF) were injected IV into recipients one day after

transplantation. Engrafted hepatocytes were identified by immunofluorescence staining for human serum albumin (HSA). The engrafted human cells had hepatocyte-like morphology and, by three months after transplantation, engrafted iPS-derived hepatocytes were present as large colonies within the host liver **(Figure 10)**. Host cells exhibited diastase/PAS-positive AT-Z globules, but the HSA-positive human hepatocytes did not. These studies indicate that immune deficient PiZ mice are an excellent model for evaluating stem cell-derived human hepatocytes in terms of engraftment, proliferation and function [7].

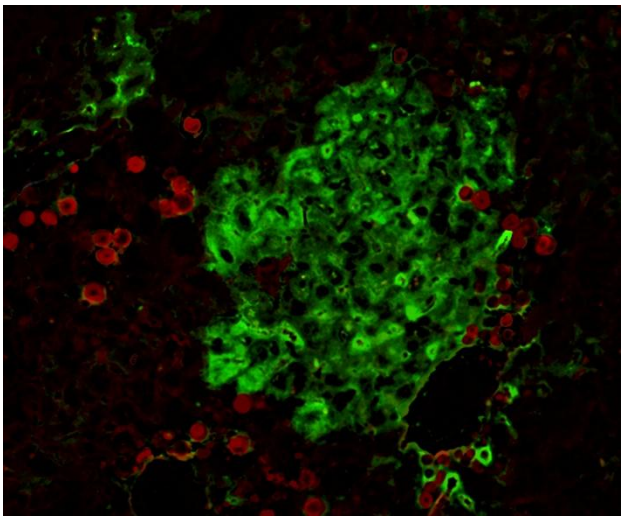

Fig 10. Transplantation of ES-derived human hepatocytes in SCID-PiZ mice. Three-months following transplantation of iPS-derived hepatocytes into immune deficient PiZ mice, immunofluorescence shows large clusters of engrafted iPS-derived hepatocytes stained green for human albumin. Red staining represents hAT globules in host hepatocytes. Nuclei are stained with Dapi (blue).

2.3. iPS cell-derived human hepatocyte engraftment and proliferation in immune-deficient AT-NSG transgenic mice.

To determine the extent to which hepatic repopulation by pluripotent stem cell-derived hepatocytes in immune-deficient PiZ mice, we transplanted normal iPSc-derived hepatocytes in male PiZ-NSG mice by intrasplenic injection. To accentuate the difference in mitotic capacity, transplanted mice were injected with an adenoviral vector expressing human hepatocyte growth factor (Ad-HGF, 1x1011 pfu/mouse) within 48 hours after transplantation. **Figure 11** shows the changes in the levels of human albumin in the serum of PIZ-NSG mice transplanted with normal iPSc-derived hepatocytes. As with transplantation with primary human hepatocytes, engraftment was not sustained in this animal model.

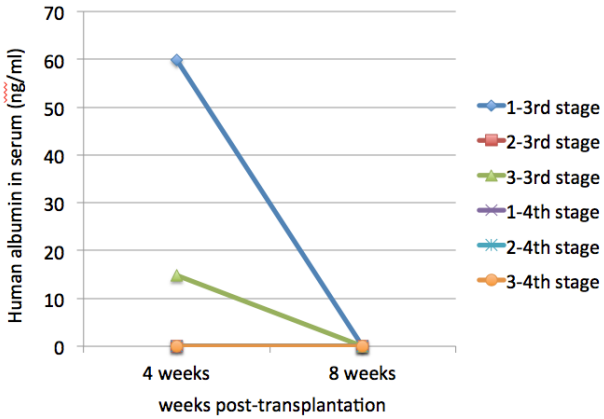

Figure 11. Human albumin levels in PiZ-NSG mouse serum transplanted with normal iPSc-derived hepatocytes. $1x10^6$ human hepatocytes were transplanted into each mouse by intra-splenic injection. Ad-HGF ($1x10^{10}$pfu) was injected within 48 hours post transplantation.

2.4. Further development of the PiZ mouse model to optimize its use for liver cell repopulation studies.

We found that accumulation of ATZ in model cell lines and in the liver of transgenic mice elicited marked activation of the transcription factor NFκB. To determine whether NFκB activation protects the liver from inflammation or carcinogenesis we mated our mouse models of AT deficiency to a mouse model in which

NFκB activation is conditionally disrupted in hepatocytes during adult life, the IKKβΔhep mouse. Our preliminary results show increased globule-containing hepatocytes, inflammatory nodules and fibrosis in the PiZ x IKKβΔhep mouse. We have also generated 2 other mouse models of AT deficiency with defects in NFκB signaling. In one we used a mouse model with NFκB activation disrupted in both hepatic parenchymal cells and hepatic macrophages, i.e. Kupfer cells. We used the IKKβΔL+H mouse that has been conditional targeted deletion of IKKβ kinase in hepatocytes and Kupfer cells. Second, we used a mouse model with targeted disruption of the NFκB p50 subunit. Our studies have shown that accumulation of ATZ leads to a unique phosphorylation of the p50 subunit and so the p50-null mouse should even more precisely elucidate the role of NFκB activation in the pathobiology of the liver in AT deficiency. Finally, we generated the Z mouse, which provides two unique features to complement the studies in the PiZ mouse: a lower level of expression of ATZ associated with milder hepatocyte necrosis and inflammation; expression of ATZ and the inflammatory reaction can be suppressed by adding doxycycline to the drinking water of the mice. These novel models will be characterized for severity of liver disease and then we will analyze liver repopulation to provide insight into how naturally occurring variation in disease severity influences repopulation of the liver.

KEY RESEARCH ACCOMPLISHMENTS:

1. Generation and characterization of iPS cell lines from control patients and patients with AT-deficiency
2. Further characterization of iPS cells during differentiation into hepatocyte-like cells
3. Determination of AT secretion by ELISA, ultrastructure by electron microscopy and rate of disappearance of intracellular AT by pulse chase analysis in ATD iPS cell-derived hepatocytes compared to controls.
4. Transplantation and expansion of human iPS-derived hepatocytes in rats, with correction of hyperbilirubinemia in the Gunn rat model of Crigler-Najjar syndrome type 1.
5. Complete repopulation of PiZ mouse livers with allogeneic hepatocytes facilitated by the use of hepatocyte growth factor administration after transplantation.
6. Engraftment and proliferation of human pluripotent stem cell-derived hepatocytes in immune-deficient SCID alpha-1-antitrypsin-deficient transgenic mice.
7. Generation of PiZ-NSG mice.
8. Preliminary studies on transplantation of primary human hepatocytes and human iPS-derived hepatocytes in PiZ-NSG mice.
9. **Further development of the PiZ mouse model to optimize its use for liver cell repopulation studies.**

REPORTABLE OUTCOMES:

1. Tafaleng E, Han B, Hale P, Chakraborty S, Soto-Gutierrez A, Nagaya M, Duncan S, Stolz D, Strom S, Roy-Chowdhury J, Perlmutter D, Fox I. The rate of disappearance of intracellular α-1-antitrypsin correlates with liver disease severity in iPSc-derived hepatocytes generated from PIZZ α-1-antitrypsin deficiency patients. AASLD Liver Meeting 2013.
2. Tafaleng E, Han B, Hale P, Chakraborty S, Soto-Gutierrez A, Nagaya M, Duncan S, Stolz D, Strom S, Roy-Chowdhury J, Perlmutter D, Fox I. Modeling α-1-antitrypsin deficiency using patient-derived iPSc generated hepatocytes. ISSCR Stem Cell Meeting 2013.
3. Tafaleng, EN, Watson A, Fox IJ. "Normal Hepatocyte Function and Mechanisms of Dysfunction" In: Kleinman RE, Goulet O, Mieli-Vergani G, Sanderson IR, Sherman PM, Shneider BL, eds., Walker's Pediatric Gastrointestinal Disease: Physiology, Diagnosis, Management PMPH—USA. PMPH-USA (People's Medical Publishing House–USA. (in press)
4. Khan Z, Tafaleng EN, Soltys KA, Fox IJ. "Congenital and Acquired Diseases of the Liver" In: Gumucio D and Samuelson L, eds. Translational Gastroenterology. John Wiley & Sons, Inc. (in press)
6. Gramignoli R, Tahan V, Dorko K, Skvorak KJ, Hansel MC, Zao W, Venkataramanan R, Ellis ECS, Jorns C, Soltys KA, Mazariegos GV, Fox IJ, Strom SC. New potential cell source for hepatocyte

transplantation: discarded livers from metabolic disease liver transplants. Stem Cell Research 2013;11:563-573.

7. Hansel MC, Gramignoli R, Blake W, Davila J, Skvorak K, Dorko K, Tahan V, Lee BR, Tafaleng E, Guzman-Lepe J, Soto-Gutierrez A, Fox IJ, Strom SC. Increased Reprogramming of Human Fetal Hepatocytes Compared With Adult Hepatocytes in Feeder-Free Conditions. Cell Transplant 2013;Feb 4.
8. Fox IJ, Duncan SA. Engineering Liver Tissue from Induced Pluripotent Stem Cells: A first step in generating new organs for transplantation? Hepatology (in press).
9. Tafaleng E, Han B, Hale P, Soto-Gutierrez A, Nagaya M, Duncan S, Stolz D, Strom S, Roy-Chowdhury J, Perlmutter D, Fox I. In vitro modeling of alpha-1-antitrypsin deficiency using induced pluripotent stem cell-derived hepatocytes from alpha-1-antitrypsin deficient patients. AASLD Liver Meeting 2012.
10. Ding J, Yannam GR, Roy-Chowdhury N, Hidvegi T, Basma H, Rennard SI, Wong RJ, Avsar Y, Guha C, Perlmutter DH, Fox IJ, Roy-Chowdhury J. Spontaneous repopulation of the liver of transgenic mice expressing mutant human alpha 1-anti-trypsin by wildtype donor hepatocytes. J Clin Invest 2011;121(5):1930-1934.
11. Roy-Chowdhury N, Chen Y, Atienza K, Chang C, Wang X, Guha C, Fox IJ, Bouhassira EE, Roy-Chowdhury J. Amelioration of hyperbilirubinemia in Gunn rats after transplantation of human hepatocytes derived from induced pluripotent stem cells. Stem Cell Reports (in revision).
12. Atienza K, Ding J, Chang C-J, Bouhassira E, Chen Y, Wang X, Avsar Y, Liu L, Guha C, Fox IJ, Salido E, Roy-Chowdhury J, Roy-Chowdhury N. Reduction of urinary oxalate excretion after transplantation of human induced pluripotent stem cell-derived hepatocytes in a mouse model of primary hyperoxaluria-1. AASLD 2011.
13. Ding J, Wang X, Neufeld D, Hansel M, Strom S, Fox IJ, Guha C, Roy-Chowdhury N, Roy-Chowdhury J. SCID/PiZ mice: a novel animal model for evaluating engraftment and proliferation of human stem cell-derived hepatocytes. AASLD 2011.
14. Avsar Y, Zhou H, Wang X, Ding J, Guha C, Fox IJ, Roy-Chowdhury N, Roy-Chowdhury J. Pharmacological enhancement of hepatocyte engraftment augments the hypobilirubinemic effect of hepatocyte transplantation in the Gunn rat model of Crigler-Najjar syndrome type 1. AASLD 2011.
15. Ito R, Fong J, Setoyama K, Gramignoli R, Tahan V, Nagaya M, Soto-Gutierrez A, Strom S, Fox IJ. Hepatocyte Xenografts Undergo Stable Long-Term Engraftment in Rats Treated with FK506 but Discordant Xenograft Albumin Secretion is 100-Fold Lower than Allograft Albumin Secretion. AST 2011.
16. Invited Speaker, iPS cell Banking Workshop, California Institute for Regenerative Medicine, San Francisco, CA, November 17-18, 2010.
17. Invited Speaker, Oregon Health and Science University Stem Cell Center, "Use of stem cells to study and treat liver disease" Portland, Oregon, February 7-8, 2011
18. Invited Speaker, AASLD Basic Research Single Topic Conference – Stem Cell in Liver Diseases and Cancer: Discovery and Promise, "Stem cells and the treatment of liver disease: understanding liver failure and cirrhosis, Atlanta, Georgia, March 19-20, 2011.
19. Invited Speaker, Yale University Stem Cell Center Seminar Series, "Stem cells and the liver" New Haven, Connecticut, March 28-29, 2011.
20. Invited Speaker, Medical College of Wisconsin, "Use of hepatocytes and stem cells to study and treat liver disease", Milwaukee, Wisconsin, May 10-11, 2011.
21. Invited Speaker, The 66th General Meeting of the Japanese Society of Gastroenterological Surgery, "Overcoming barriers to the use of hepatocytes and stem cells in treating patients with liver diseases", Nagoya, Japan, July 13-15, 2011.
22. Invited Speaker, Research Seminar Series in Developmental and Regenerative Biology, University of Kansas Medical Center, "Use of hepatocytes and stem cells to study and treat liver disease", Kansas City, Kansas, November 9-10, 2011.
23. Keynote Speaker, ISMRM Workshop on MRI-based cell tracking "Hepatocyte transplantation and the need to track engrafted cells", Miami Beach, Florida, January 29 – February 1, 2012.

24. Invited Speaker, Challenging the Paradigms: Liver Transplantation for Metabolic Disease, Children's Hospital of Pittsburgh, "Hepatocyte transplantation", Pittsburgh, PA, May 4-5, 2012.
25. Invited Speaker, American Society of Gene & Cell Therapy 15th Annual Meeting, "Overcoming barriers to successful cell therapy to treat liver disease", Philadelphia, PA May 16-19, 2012
26. Invited Speaker, 16th Maple Syrup Urine Disease Symposium, "Clinical hepatocyte transplantation for the treatment of metabolic liver diseases", Philadelphia, PA, June 28-30, 2012
27. Moderator, Mid-day Symposium: "Allotransplants, Cellular Transplants, Organ Repair, and Xenotransplants? A Debate about the Future of Organ Transplantation", American Transplant Congress, Boston, MA, June 2-6, 2012.
28. Invited Speaker, Liver Biology: Fundamental Mechanisms & Translational Application, FASEB Summer Research Conference, "Hepatocyte, stem cell transplantation, tissue engineering", Snowmass Village, Colorado, July 29 – August 3, 2012.
29. Invited Speaker, 8th Royan International Congress on Stem Cell Biology and Technology, "Overcoming barriers to the use of hepatocytes and stem cells in treating patients with liver diseases" and "Use of hepatocytes and stem cells in understanding and treating liver failure and cirrhosis", Tehran, Iran, September 5-7, 2012.
30. Invited Speaker, Masters of Surgery lecture series, Montefiore Medical Center, The University Hospital for Albert Einstein College of Medicine, "Bench to bedside: finding alternatives to organ transplantation for patients with life-threatening liver disease", New York, NY, November 4-5, 2012.
31. Faculty Member, American Association for the Study of Liver Diseases 2012 Postgraduate Course, "Tissue engineering and liver cell replacement – liver stem cells on the horizon", Boston, MA, November 10, 2012.
32. Invited Speaker, 23rd Conference of the Asian Pacific Association for the Study of the Liver (APASL 2013), "Future strategies for cellular transplantation", Singapore, June 6-10, 2013.
33. Invited Speaker, 19th Annual International Congress of ILTS, "Liver regeneration and hepatocyte repopulation", Sydney, Australia, June 14, 2013.
34. Invited Speaker, Cell Transplant Society, "Hepatocyte transplantation and regeneration in the treatment of liver disease", Milan, Italy, July 7-10, 2013.

CONCLUSIONS:

The outcomes of our studies are being accomplished as expected, and there is no change anticipated in the research plan. The intention for future studies is to attain better engraftment and more complete characterization of differentiated cells following transplantation.

REFERENCES

1. Basma H, Soto-Gutierrez A, Yannam GR, et al. Differentiation and transplantation of human embryonic stem cell-derived hepatocytes. Gastroenterology 2009;136:990-9.
2. Si-Tayeb K, Noto FK, Nagaoka M, et al. Highly efficient generation of human hepatocyte-like cells from induced pluripotent stem cells. Hepatology;51:297-305.
3. Roy-Chowdhury N, Chen Y, Atienza K, et al. Amelioration of hyperbilirubinemia in Gunn rats after transplantation of human hepatocytes derived from induced pluripotent stem cells. . AASLD 2010.
4. Overturf K, Al-Dhalimy M, Tanguay R, et al. Hepatocytes corrected by gene therapy are selected in vivo in a murine model of hereditary tyrosinaemia type I. Nat Genet 1996;12:266-73.
5. Rhim JA, Sandgren EP, Degen JL, Palmiter RD, Brinster RL. Replacement of diseased mouse liver by hepatic cell transplantation. Science 1994;263:1149-52.

6. Ding J, Yannam GR, Roy-Chowdhury N, et al. Spontaneous hepatic repopulation in transgenic mice expressing mutant human alpha1-antitrypsin by wild-type donor hepatocytes. The Journal of Clinical Investigation 2011;121:1930-4.
7. Ding J, Wang X, Neufeld DS, et al. SCID/PiZ mice: a novel animal model for evaluating engraftment and proliferation of human stem cell-derived hepatocytes. AASLD 2011.

TRANSPLANTATION OF PURIFIED HUMAN SKELETAL MUSCLE-DERIVED PERICYTES REDUCE FIBROSIS IN INJURED ISCHEMIC MUSCLE TISSUES

[1,2,4]Chien-Wen Chen, [2,4]Masaho Okada, [1,3,4,5]Kimimasa Tobita, [4]Mihaela Crisan, [3,4,5,6]Bruno Péault, [2,4,5]Johnny Huard
Department of Bioengineering[1], Orthopedic Surgery[2], Pediatrics[3], Stem Cell Research Center, Children's Hospital of Pittsburgh[4], and McGowan Institute for Regenerative Medicine[5], University of Pittsburgh and UPMC and [6]David Geffen School of Medicine, University of California at Los Angeles;
jhuard@pitt.edu

INTRODUCTION

Vascular pericytes are the mural cells that tightly encircle capillaries and microvessels throughout the body. In general, pericytes control blood vessel maturation, stability and contractility.

Multi-lineage stem/progenitor cells have been identified within virtually all organs in both human and mouse and are named diversely [1]. However, due to the retrospective discovery of these multi-lineage stem/progenitor cells in culture, the true identity of these cells *in situ* remained obscure. It has been hypothesized that vascular pericytes are indeed, or at least contain, stem/progenitor cells that are able to differentiate into bone, cartilage, fat tissue and odontoblasts [2]. Recently, we and others laboratories have shown that vascular pericytes purified from multiple human organs not only express classic MSC markers but harbor stem cell properties such as myo-, osteo-, chondro- and adipogenic potentials [2]. Consequently, pericytes are assumed to be one of the developmental origins of MSC. Human skeletal muscle-derived pericytes were not only shown to regenerate skeletal muscle fibers in dystrophic as well as cardiotoxin-injured mouse muscle but also sustain impaired cardiac function after myocardial infarction *in vivo* [2]. Nevertheless, whether transplanted vascular pericytes contribute to the reduction of fibrosis at the site of injury remains to be elucidated. Matrix metalloproteinases (MMPs) are proteolytic enzymes responsible for extracellular matrix protein degradation with an important role in tissue remodeling processes. MMP-2 and MMP-9 activities are often implicated in fibrosis [3]. Using the animal model that has been established previously, we commenced to explore whether or not pericytes influences scar tissue formation within the damaged ischemic myocardium and attempt to elucidate the mechanism(s) of action [4].

METHODS

Cell Isolation and Cell Sorting: Fresh specimens of human fetal skeletal muscle were mechanically dissociated and digested with collagenases. After lysis of erythrocytes, single cell suspension was obtained by filtering with 70-μm cell strainer. For cell sorting, cells were incubated with the following directly-conjugated antibodies: anti-CD34-PE, anti-CD45-APC, anti-CD56-PE-Cy7, and anti-CD146-FITC. For dead cell exclusion, 7-amino-actinomycin D (7-AAD) was added to stained cells before running on a FACSAria flow cytometer. Flow cytometry with an identical gating strategy was used to verify the purity of long-term cultured muscle-derived pericytes.

Animal Model of Fibrosis: Permanent ligation of the left coronary artery was performed on NOD/SCID mice under open-chest surgery. Immediately after the ligation, skeletal muscle-derived pericytes from cultures were injected into the ischemic myocardium (3×10^5 cells/heart), while the control groups received saline injections (PBS).

Histology: Masson's trichrome staining was employed to reveal myocardial fibrosis. The ratio of fibrotic area was estimated by total collagen deposition versus total sectional area using Image J software.

Hypoxic Culture: Pericytes were cultured *in vitro* under hypoxic conditions (2.5% oxygen) for 24 hours. Supernatants and cell pellets were subsequently collected for analysis.

Real-time Quantitative PCR: Real-time Quantitative PCR analysis was performed to detect gene expressions of matrix metalloproteinase-2 (MMP-2) and -9 (MMP-9) in total muscle lysates and muscle-derived pericytes cultured under normal and hypoxic conditions.

RESULTS

Purification of Human Muscle-derived Pericytes: $CD34^-45^-56^-146^{high}$ muscle-derived pericytes were sorted and cultured as previously described [2]. To ensure long-term cultured muscle-derived pericytes remain homogeneous and retain their native properties, flow cytometry was employed to examine the expression of cell surface markers used to select these cells plus alkaline phosphatase (ALP), another pericyte marker. The result shows that after long-term culturing (>10 passages), all cells remain negative for CD34, CD45 and CD56, and virtually all pericytes are positive for CD146 and ALP (Figure 1a).

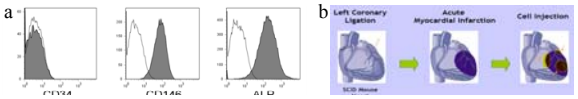

Figure 1. (a) Flow cytometry analysis of long-term cultured $CD34^-CD45^-CD56^-CD146^{high}$ pericytes . (b) Schematic depiction of transplantation of muscle-derived pericytes.

Transplantation of Muscle-derived Pericytes: Immediately after permanent ligation of the left coronary artery, muscle-derived pericytes from cultures were injected into the ischemic myocardium at a density of 3×10^5 cells/heart (Figure 1b) [4].

Scar Tissue Formation: Masson's trichrome staining revealed myocardial fibrosis after infarction with collagen deposition stained in blue (Figure 2a). Quantification at 2 weeks post injection demonstrated a 38% reduction of the fibrotic area in pericyte-injected left ventricles, compared to saline-injection (Figure 2b).

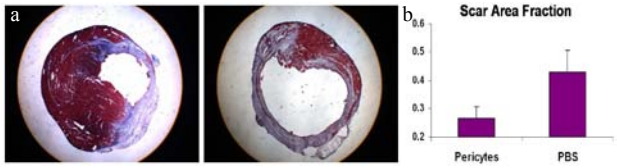

Figure 2. (a) Collagen deposition was stained blue to show the extent of myocardial fibrosis. (b) Pericyte-injected hearts had an average 38% reduction of the scar area.

Expression of MMP-2 by Muscle-derived Pericytes: Real-time quantitative PCR results revealed that cultured muscle pericytes have higher expression of MMP-2 gene than total muscle lysates, but not MMP-9. Under hypoxic culture conditions, muscle pericytes retain high expression of MMP-2 gene, while MMP-9 remained very low (Figure 3).

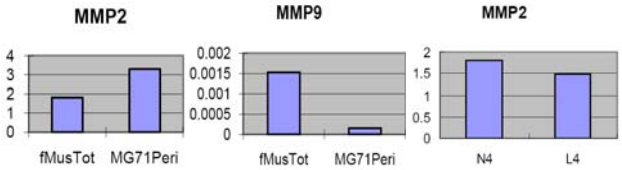

Figure 3. Real-time qPCR results of (a) MMP-2 gene (b) MMP-9 gene expression level of total muscle lysates and long-term cultured muscle pericytes. MMP-2 gene expression level was compared between muscle pericytes cultured under normoxia (N4) and hypoxia (L4).

DISCUSSION

We demonstrated that transplantation of purified skeletal muscle-derived pericytes ameliorate fibrosis in injured ischemic cardiac muscle, possibly exerting a preventative effect. Reduced MMP-2 activity has been shown to contribute to cardiac fibrosis in pathological conditions [5]. We consequently hypothesized that the high expression level of MMP-2 by muscle-derived pericytes, even under hypoxic conditions, may play a key role in pericyte-mediated reduction of fibrosis. We are currently conducting experiments to demonstrate the efficacy of muscle pericyte transplantation in diminishing chronic fibrosis. We are also investigating the influence of increased angiogenesis, a beneficial effect displayed by muscle pericytes, on reduction of fibrosis. Overall, this study will shed light on the therapeutic value of muscle-derived pericytes for the treatment of fibrosis in the injured tissues including musculoskeletal tissues.

ACKNOWLEDGMENTS

This work was partly supported by funding from the National Institutes of Health (1R21 HL083057-01A2 awarded to B.P.) and by the Henry J. Mankin Endowed Chair for Orthopaedic Research at the University of Pittsburgh (held by J.H.).

REFERENCES

1. Péault et al. Mol Ther. 2007 May;15(5):867-77.; **2.** Crisan et al. Cell Stem Cell 2008; 3(3):301-13**.;** 3. Tanriverdi-Akhisaroglu et al. Cell Biochem Funct. 2009 Mar;27(2):81-7.; 4. Okada et al. J Am Coll Cardiol. 2008; 52(23):1869-80.; 5. Van Linthout et al. Basic Res Cardiol. 2008 Jul;103(4):319-27.

Transplantation of p65 Deficient Stem Cells Improved the Histopathology of Skeletal Muscle in Dystrophic Mice

[1]Aiping Lu; [2] Qing Yang; [1]Minakshi Poddar; [1]Bing Wang; [3]Denis C. Guttridge; [4]Paul D. Robbins; [1]+ Johnny Huard
[1]+Stem Cell Research Center and Department of Orthopaedic Surgery, University of Pittsburgh, Pittsburgh, PA
[2]Department of Orthopaedic Surgery, Tongji Hospital, Huazhong University of Science and Technology, Wuhan, China
[3]Department of Molecular Virology, Immunology and Medical Genetics, Ohio State University, Columbus, OH
[4]Department of Microbiogy and Molecular Genetics. University of Pittsburgh, Pittsburgh, PA
jhuard@pitt.edu

INTRODUCTION

Duchenne muscular dystrophy (DMD) is a deadly genetic disease mainly characterized by progressive weakening of the skeletal, cardiac and diaphragmatic muscles. It is critical to find a successful therapy that will improve the histopathology of the muscles of DMD patients and restore their normal function. Recent studies have demonstrated that blocking p65, a subunit of NF-κB, enhances muscle regeneration in injured and diseased skeletal muscle [1, 2], which suggests that the NF-kB signaling pathway is a contributing factor to the dystrophic pathology in DMD patients. Previously we demonstrated that muscle derived stem cells (MDSCs) isolated from the skeletal muscles of heterozygote P65 knock-out ($P65^{+/-}$) mice showed better muscle regeneration *in vitro* and *in vivo* compared to the MDSCs isolated from wild-type (WT) mice. We also demonstrated that the transplantation of $P65^{+/-}$ MDSCs could reduce inflammation. Based on these results we performed a set of experiments to determine if these $P65^{+/-}$ MDSCs could alleviate the pathology associated with DMD more efficiently than wild-type MDSCs. When we injected $p65^{+/-}$ MDSCs intraperitoneally into dystrophin/utrophin deficient (dys-/-:utro-/-, dKO) mice, a reliable mouse model of DMD, we found that the histopathology of various skeletal muscles improved and observed a reduction in inflammation, necrosis and pathological muscle regeneration.

MATERIALS AND METHODS

Cell Isolation: MDSCs were isolated from 5 month old $P65^{+/-}$ and WT mice as previously described via a modified preplate technique [3]. The cell suspensions from both $P65^{+/-}$ and WT muscle were plated on collagen coated flasks and cultured in proliferation medium (DMEM supplemented with 10% fetal bovine serum, 10% horse serum, 0.5% chicken embryo extract and 1% Penicillin-streptomycin) until the cell number was sufficient for injection.

***Intraperitoneal injection* (IP):** A total of 5-9 $x10^5$ viable cells were suspended in 50 µl of PBS and injected IP into 5-7 days old of dKO mice. Four to six weeks after transplantation, the mice were sacrificed and their muscles were harvested and flash frozen in liquid nitrogen-cooled 2-methylbutane. 10µm serial cryosections were prepared from the frozen muscle.

Immunohistocytochemistry

Cryosections were fixed with 5% formalin, blocked with 5% Donkey serum, and then incubated with an antibody against mouse IgG (Biotinlated) to determine the extent of muscle fiber necrosis. An antibody against embryonic muscle heavy chain (E-MyHC) was used to evaluate myogenic regeneration and an antibody against F4/80 (macrophage marker) was used to analyze the extent of inflammation in the muscle tissues. Streptavidin Cy3 conjugate and Alexafluor 488 conjugated anti-mouse IgG were used as secondary antibodies. H&E staining was performed to assess myofiber morphology and fibrosis.

RESULTS

Transplantation of P65+/- MDSCs improved muscle histology

H&E showed histology improvement in various skeletal muscles including the gastrocnemius, diaphragm, thigh and tibialis anterior muscles. We observed many centrally nucleated muscle fibers (new regenerated fibers) and decreased fibrosis in the $p65^{+/-}$ MDSC injection group (**Figure 1,** thigh muscle**)**.

Transplantation of P65+/- MDSCs reduced muscle necrosis

Mouse IgG staining showed that there were less necrotic muscle fibers in the mice injected with $p65^{+/-}$ MDSCs compared to the un-treated muscle **(Figure2)**

Transplantation of $P65^{+/-}$ MDSCs reduced inflammation and pathological muscle regeneration

Less inflammation and E-MyHC positive myofibers were found in the muscles of mice injected with $p65^{+/-}$ MDSCs compared to non-treated muscle **(Figure3).**

Figure1

DKO untreated muscle **DKO muscle treated with MDSCs**

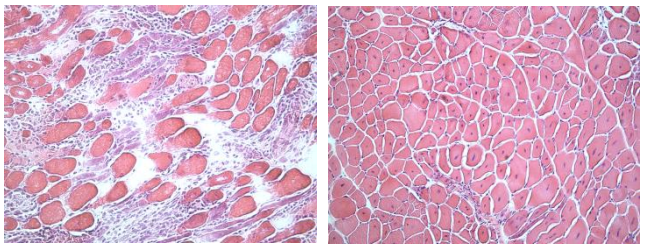

Figure2

DKO untreated muscle **DKO muscle treated with MDSCs**

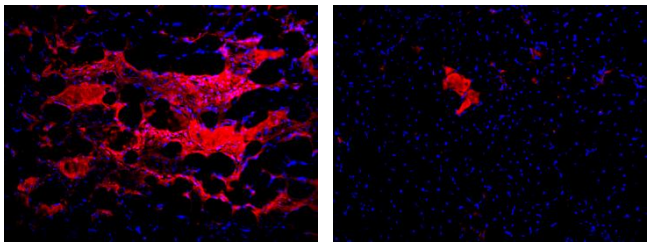

Figure3

DKO muscle nontreated **DKO muscle treated with MDSCs**

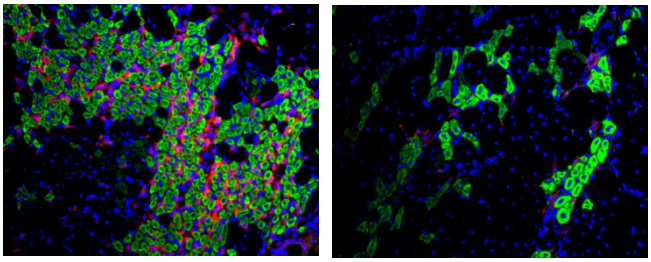

DISCUSSION

In this study we used MDSCs isolated from p65+/- mice to treat dystrophin-/-utrophin-/- mice. The up-regulation of the NF-κB pathway in these mice is associated with chronic inflammation which results in pathologies such as muscle fibrosis, necrosis, and muscle wasting. Our findings indicated that blocking p65, a subunit of NF-κB, can decrease macrophage infiltration, fibrosis formation, necrosis, and diminishes pathologic regeneration in 4 to 6 week dKO mice. We also attempted to inject the WT MDSCs isolated from normal animals; however, the results did not show an improvement in the histopathology of the mice. These results suggest that reducing the activity of the IKK/NF-κB pathway is a potential therapeutic target for the treatment of DMD. These are only preliminary data; however they are very exciting and we are planning to test additional animals in order to further confirm these results.

REFERENCES:

[1] Thaloor, D, et al Am. J.Physiol 1999; 277:C320–C329. [2] Acharyya S et al, J. Clin. Invest 2007 ; 117 :889-901. [3] Gharaibeh, et al. Nat Protoc. 2008; 3:1501-9

Immunomodulatory properties of muscle-derived stem cells associated with reduced NF-κB/p65 signaling

[1]Proto, J.; [1]Lu, A.; [2]Robbins, P.D.; [1]+Huard, J.
[1]+ Stem Cell Research Center, Children's Hospital of Pittsburgh, and Department of Orthopedic Surgery;
[2]Departments of Microbiology and Molecular Genetics, University of Pittsburgh School of Medicine, Pittsburgh, PA
jhuard@pitt.edu

INTRODUCTION

The nuclear factor kappa B (NF-kB) signal pathway has been implicated in both the normal and disease states of many different tissues. In skeletal muscle, for example, constitutive activation of inhibitor of kappa B kinase (IKKβ), a potent activator of NF-kB, leads to muscle wasting[1]. Inversely, muscle specific deletion of IKKβ in a murine model of muscular dystrophy improves dystrophic pathology and is accompanied by an increase in the number of cells fitting a muscle progenitor marker profile ($CD34^+/Sca1^-$), suggesting that NF-kB has a direct effect on muscle stem cells[2]. The NF-kB protein family includes five subunits, two of which, a p65-p50 heterodimer, are thought to play a role in blocking early myogenesis[3]. In this study, we examined the role of NF-kB signaling in the regenerative phenotype of muscle-derived stem cells (MDSCs) isolated from the gastrocnemius of p65 deficient mice (heterozygous, $p65^{+/-}$) and wild type littermates ($p65^{+/+}$). We previously found that $p65^{+/-}$ MDSCs have enhanced cell proliferation, survival under oxidative stress, differentiation, and muscle regeneration capacity. Furthermore, we have found that $p65^{+/-}$ engraftments in wild type skeletal muscle are associated with reduced inflammation and fiber necrosis compared to $p65^{+/+}$ MDSC engraftments. *In vitro* and *in vivo* experiments suggest that reduction of p65 signaling enhances the regenerative phenotype of MDSCs, suggesting this pathway as a candidate target to improve stem cell-based therapies for muscle disease and injury.

MATERIALS AND METHOD

Cell Isolation: MDSCs were isolated from five month old (n=3) $p65^{+/+}$ or $p65^{+/-}$ mice via a preplate technique [4]. A population of slowly adhering cells was obtained and expanded in DMEM containing 10% fetal bovine serum (FBS), 10% horse serum, 1% penicillin-streptomycin, and 0.5% chick embryo extract. Cells were used between passages 15 and 30.

In vivo regeneration assay: Muscle injury was induced in C57Bl/6J mice by cardiotoxin injected into gastrocnemius. One day later, MDSCs were injected into the injured muscles. Six days following transplantation, mice were sacrificed and injected muscles were harvested and snap-frozen. Serial cryosections were prepared and immunohistochemistry was performed to assess inflammation (CD14) and necrosis (IgG). The number of CD14 (+) cells was counted to assess infiltration of macrophages/monocytes. Necrosis was determined by mouse IgG staining and quantified by assessing the percentage of positively stained area.

In vitro Inflammation Model: MDSCs were grown for 24 hours in proliferation medium, after which the medium was collected and sterile filtered. RAW264.7 cells, immortal murine macrophage-like cells, were activated by exposure to 100 ng/mL LPS in either $p65^{+/+}$-, $p65^{+/-}$-, or muscle-derived fibroblast conditioned medium for 24 hours.

***Gene Expression Analysis*:** Cells were washed and RNA collected by Trizol extraction. Total RNA was reverse transcribed with Superscript III reverse transcriptase (Invitrogen) according to manufacturer's protocols. The PCR reaction was carried out with Taq Polymerase (Promega), according to manufacturer's protocols. PCR products were analyzed by electrophoresis on a 1.5% agarose gel

RESULTS

Wild type mice were injected with either $p65^{+/+}$ (Fig 1A) or $p65^{+/-}$ (Fig 1B) MDSCs in the gastrocnemius muscle and sacrificed six days later. Tissues were cryosectioned and immunostained with antibodies against CD14 to identify a monocyte/macrophage infiltrate, indicating inflammation, as well as with antibodies against mouse immunoglobulin G, a marker of necrosis. Injections of $p65^{+/-}$ cells were associated with a decrease in both necrosis and inflammation (Fig 1B-D), compared to $p65^{+/+}$ injections (Fig1A, C-D).

Figure 1.

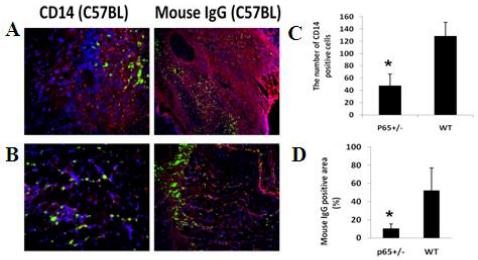

To investigate anti-inflammatory properties of MDSCs, we utilized an *in vitro* inflammation model in which RAW264.7 cells, immortal murine macrophage-like cells, are activated by LPS exposure. We found that RAW264.7 cells exposed to LPS in $p65^{+/-}$ CM expressed less IL-1 compared to controls, suggesting that p65+/- MDSCs secrete immunomodulatory factors that hinder pro-inflammatory macrophage activation.

Figure 2.

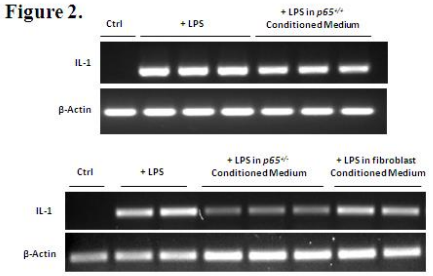

DISCUSSION

The data presented here provides evidence supporting that NF-kB inhibition stimulates MDSC-mediated muscle regeneration through multiple mechanisms, including through the expression of anti-inflammatory factors that attenuate inflammation and necrosis. These experiments identify the NF-κB signaling pathway as a potential therapeutic target to enhance muscle regeneration following injury or disease. Future directions for this project include investigating modulation of the IKK/NF-kB pathway as a means to rejuvenate the phenotype of aged muscle stem and progenitor cells. Clinical research should be conducted to test the efficacy of p65 inhibition therapy in patients suffering from muscle disorders.

REFERENCES

[1]Cai, D., et al. Cell 2004, 119:285-298. [2]Acharyya, S., et al., J Clin Invest 2007, 117:889-901. [3]Bakkar, N., et al. JCB 2008, 180(25): 787-802. [4] Gharaibeh, et al. Nat Protoc. 2008; 3:1501-9

Appendix 4

NF-κB Negatively Impacts the Myogenic Potential of Muscle-derived Stem Cells

Aiping Lu[1], Jonathan D Proto[1], Lulin Guo[1], Ying Tang[1], Mitra Lavasani[1], Jeremy S Tilstra[2], Laura J Niedernhofer[2], Bing Wang[1], Denis C Guttridge[3], Paul D Robbins[2] and Johnny Huard[1]

[1]Stem Cell Research Center, School of Medicine and Department of Orthopedic Surgery, University of Pittsburgh, Pittsburgh, Pennsylvania, USA; [2]Department of Microbiology and Molecular Genetics, University of Pittsburgh, Pittsburgh, Pennsylvania, USA; [3]Department of Molecular Virology, Immunology and Medical Genetics, The Ohio State University, Columbus, Ohio, USA

Inhibition of the inhibitor of kappa B kinase (IKK)/nuclear factor-kappa B (NF-κB) pathway enhances muscle regeneration in injured and diseased skeletal muscle, but it is unclear exactly how this pathway contributes to the regeneration process. In this study, we examined the role of NF-κB in regulating the proliferation and differentiation of muscle-derived stem cells (MDSCs). MDSCs isolated from the skeletal muscles of $p65^{+/-}$ mice (haploinsufficient for the p65 subunit of NF-κB) had enhanced proliferation and myogenic differentiation compared to MDSCs isolated from wild-type (wt) littermates. In addition, selective pharmacological inhibition of IKKβ, an upstream activator of NF-κB, enhanced wt MDSC differentiation into myotubes *in vitro*. The $p65^{+/-}$ MDSCs also displayed a higher muscle regeneration index than wt MDSCs following implantation into adult mice with muscular dystrophy. Additionally, using a muscle injury model, we observed that $p65^{+/-}$ MDSC engraftments were associated with reduced inflammation and necrosis. These results suggest that inhibition of the IKK/NF-κB pathway represents an effective approach to improve the myogenic regenerative potential of MDSCs and possibly other adult stem cell populations. Moreover, our results suggest that the improved muscle regeneration observed following inhibition of IKK/NF-κB, is mediated, at least in part, through enhanced stem cell proliferation and myogenic potential.

Received 15 April 2011; accepted 5 November 2011; published online 13 December 2011. doi:10.1038/mt.2011.261

INTRODUCTION

Nuclear factor-kappa B (NF-κB) is a ubiquitously expressed nuclear transcription factor that is evolutionarily conserved. In mammals, the NF-κB family consists of five subunits, p65 (RelA), c-Rel, RelB, p50, and p52.[1] Transcriptionally active NF-κB exists as a dimer, with the most common form being a p50–p65 heterodimer. Under nonstress conditions, the heterodimer is maintained in an inactive state in the cytoplasm via its interaction with inhibitor of kappa B (IkB) proteins. Classic NF-κB activation is mediated by IkB kinase (IKK), a large, 700–900 kDa complex consisting of two catalytic subunits, IKKα and IKKβ, and a regulatory subunit named IKKγ or NEMO (NF-κB essential modulator). In response to a variety of stimuli, including proinflammatory cytokines, bacterial products, viruses, growth factors, and oxidative stress, the complex is activated. Activated IKKβ phosphorylates IkB, leading to its polyubiquitylation and subsequent degradation by the 26S proteasome. IkB degradation allows NF-κB to translocate to the nucleus where it binds to its cognate DNA site, as well as coactivators such as CBP/p300, to induce gene expression.[2–5] Dysregulation of this pathway can result in chronic activation of IKK or NF-κB, and is seen in several pathophysiological states including cancer, rheumatoid arthritis, sepsis, muscular dystrophy, heart disease, inflammatory bowel disease, bone resorption, and both type I and II diabetes.[6,7]

The NF-κB pathway, long recognized as an important component of innate and adaptive immunity, has also more recently emerged as a key player in the regulation of skeletal muscle homeostasis.[8] Furthermore, activation of NF-κB in skeletal muscle has been linked to cachexia, muscular dystrophies, and inflammatory myopathies.[9–13] Conversely, knockout of p65, but not other subunits of NF-κB, enhances myogenic activity in MyoD-expressing mouse embryonic fibroblasts.[14] Although it is known that genetic depletion of p65 enhances muscle regeneration in both mdx and wild-type (wt) murine skeletal muscle,[13] the mechanism through which reduced of NF-κB activity positively impacts skeletal muscle remains unclear.

Given that the repair of damaged tissues is mediated by adult stem cell populations, we hypothesized that NF-κB activity negatively regulates muscle stem cell function. In this study, we specifically focus on the role of p65 in regulating muscle-derived stem cell (MDSC) growth and differentiation. This population of adult stem cells is capable of restoring muscle function.[15,16] As complete knockout of p65 ($p65^{-/-}$) results in embryonic lethality, we isolated MDSCs from the skeletal muscles (SKM) of $p65^{+/-}$ mice and wt littermates.[17] We observed that, *in vitro*, p65 haploinsuffiency was associated with increased cell proliferation and myogenic differentiation. Pharmacologic inhibition of IKK/NF-κB also enhanced myogenic

The first two authors contributed equally to the work.

Correspondence: *Johnny Huard, Stem Cell Research Center, 2 Bridgeside Point, 450 Technology Drive, Pittsburgh, Pennsylvania 15219, USA. E-mail: jhuard@pitt.edu*

differentiation. We also demonstrated that $p65^{+/-}$ MDSCs have a higher capacity for muscle regeneration after implantation into dystrophic, mdx mouse SKM. Furthermore, we show that muscle inflammation and necrosis post-injury is decreased following $p65^{+/-}$ MDSC implantation into cardiotoxin (CTX) injured SKM. These results suggest that reducing the activity of the IKK/NF-κB pathway is an effective approach to improve the myogenic potential of MDSCs and possibly other adult stem cell populations. Our results provide a novel mechanistic insight as to why the inhibition of this pathway promotes SKM healing.

RESULTS

Isolation and phenotypic characterization of MDSCs from $p65^{+/-}$ and wt mice

To examine the effect of NF-κB activity on MDSC function, we purified populations of muscle stem cells from the SKM of mice heterozygous for the p65 subunit of NF-κB ($p65^{+/-}$) and wt littermates. Using a modified preplate technique,[18] we isolated independent populations of MDSCs from three mice of each genotype. To confirm that p65 haploinsufficiency reduced basal levels of NF-κB activity, nuclear p65 was measured via ArrayScan. Nuclear, or active, p65 was found to be 30% lower in $p65^{+/-}$ than the wt MDSCs (**Figure 1a**). Upon activation, NF-κB subunits undergo post-translational modifications, such as phosphorylation, to enhance their activity.[19] Immunoblot analysis revealed that the level of phosphorylated p65 (P-p65) was also reduced; however, stimulation with tumor necrosis factor-α (TNFα) led to an increased level of P-p65 in both wt and $p65^{+/-}$ MDSCs (**Figure 1b**), demonstrating that basal, but not induced, NF-κB activity is affected by knocking-out one allele of *p65*.

To confirm the MDSC phenotype of $p65^{+/-}$ and wt cells, each population was analyzed for the expression of stem (CD34, Sca-1), myogenic (MyoD, desmin), and endothelial (CD144, CD31) cell markers by reverse transcriptase-PCR. For each of the markers, there was variability in expression between cell populations of a single genotype. However upon quantification, no significant differences were found between the different genotypes, with the exception of CD144, which was elevated in $p65^{+/-}$ MDSCs. (**Figure 2a,c,** $P < 0.05$). Such variability in marker expression has been previously reported and interpreted as evidence that these cell populations contain a mixture of stem and committed progenitor cells.[20,21] We next examined the expression of Pax7 and MyoD protein by immmunostaining, and also found no significant difference between $p65^{+/-}$ and wt cells (**Figure 2b,d**). These results suggest that genetic reduction of p65 does not dramatically alter the phenotype of MDSCs.

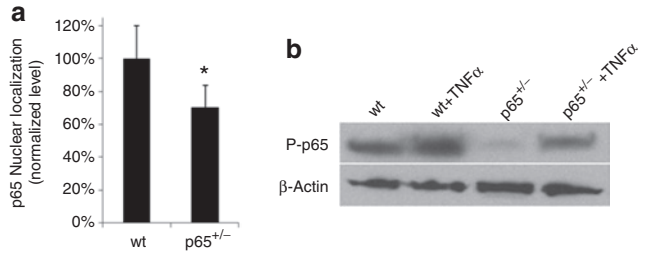

Figure 1 Muscle-derived stem cells (MDSCs) obtained from the skeletal muscles (SKM) of $p65^{+/-}$ mice have a lower level of activated p65 compared to wild-type (wt) MDSCs. (**a**) ArrayScan analysis of nuclear p65 in MDSCs isolated from $p65^{+/-}$ and wt mice. Error bars indicate "mean + SD." (**b**) Immunoblotting for phosphorylated p65 in whole cell lysates of MDSCs before and after tumor necrosis factor-α (TNFα) stimulation for 30 minutes.

$p65^{+/-}$ MDSCs proliferate faster than wt MDSCs

NF-κB is known to regulate cell division, so we investigated whether p65 reduction would alter MDSC proliferation. The three populations of $p65^{+/-}$ and wt MDSCs were plated in collagen-coated flasks and expanded in growth medium for 10–12 passages. Cells were then transferred to 24-well plates and proliferation measured using a previously described Live Cell Imaging system.[22] We observed that $p65^{+/-}$ MDSCs proliferated significantly faster than wt cells (**Figure 3a** and **Supplementary Videos S1–S2**). Equal numbers of cells were also plated on a 96-well plate and grown for three days at which point the differences in cell number were determined using an MTS assay. This assay demonstrated a similar significant increase in cell proliferation in $p65^{+/-}$ MDSCs (**Figure 3b**) suggesting that NF-κB, and in particular p65, limits the proliferation of MDSCs.

$p65^{+/-}$ MDSCs have enhanced myogenic differentiation compared to wt cells

We next measured the ability of the $p65^{+/-}$ and wt MDSCs to undergo myogenic differentiation *in vitro*. Equal numbers of cells were plated in a 24-well plate and switched to differentiation medium once the cells adhered. After 3 days the majority (80%) of the $p65^{+/-}$ cells had differentiated into myotubes, as determined by immunodetection of myosin heavy chain (**Figure 4a**). The differentiation potential of the $p65^{+/-}$ MDSCs was significantly greater than the wt MDSCs (60%; $P < 0.01$; **Figure 4b**). The difference was also demonstrated using the live cell imaging system described above (**Supplementary Videos S3–S4**). These results demonstrate that NF-κB, and in particular p65, represses MDSC differentiation *in vitro*.

Pharmacologic inhibition of IKKβ increases myogenic differentiation *in vitro*

To confirm this finding implicating NF-κB as negatively impacting MDSC differentiation, we tested whether a pharmacologic inhibitor of NF-κB could enhance MDSC myogenic potential *in vitro*. wt MDSCs were exposed to differentiation medium containing various doses of IKK-2 inhibitor IV (IKKi), a specific, reversible inhibitor of IKKβ. Cell lysates were collected at 0, 1, 14, 24, 48, and 72 hours following treatment. Accordingly, myosin heavy chain (MyHC) levels dramatically increased, beginning at 14 hours (**Figure 5a,c**). As expected, we observed a robust time-dependent decrease in P-p65 that was dose-dependent (greater at 3 μmol/l than 1 μmol/l; **Figure 5b**). We next examined NF-κB activity in wt and $p65^{+/-}$ MDSCs at various time points during myogenic differentiation by immunodetection of P-p65 and MyHC. In wt cells, beginning at 48 hours post-transition to differentiation medium, the levels of p-p65 were detectably reduced (**Figure 5d**). This occurred more rapidly (by 24 hours) in $p65^{+/-}$ cells. Similarly, accumulation of MyHC was greater at earlier time points (14 hours) in $p65^{+/-}$ cells than wt. This timeframe for MyHC accumulation is similar

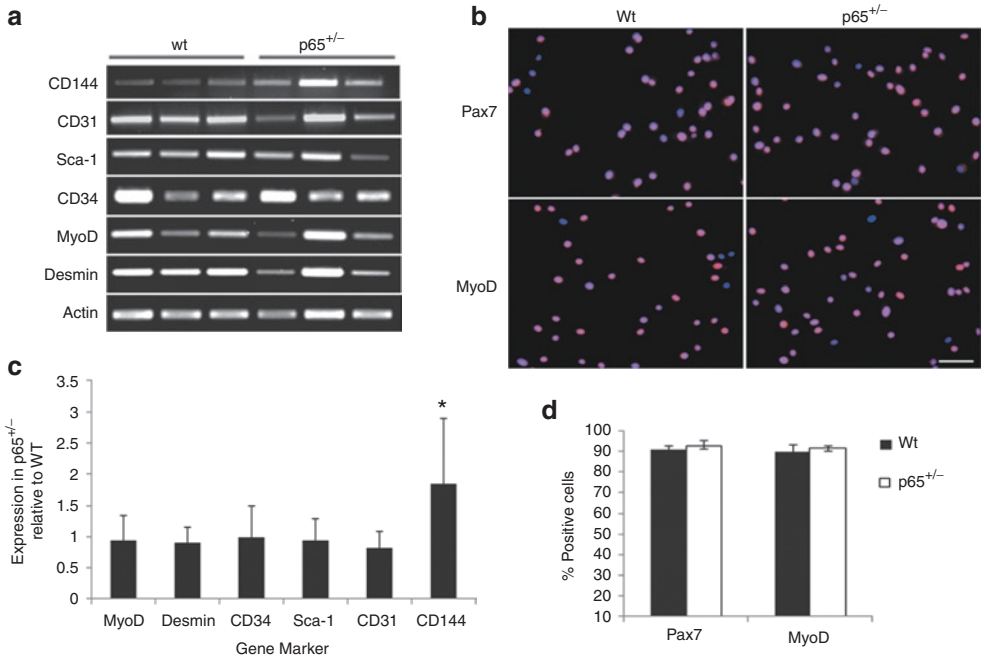

Figure 2 ***p65*$^{+/-}$ and wild-type (wt) muscle-derived stem cells (MDSCs) exhibit a similar molecular marker profile.** (**a**) RNA was isolated from three independent cell populations of each genotype. Reverse transcriptase-PCR (RT-PCR) was performed to characterize the MDSC populations for the expression of stem (CD34 and Sca-1), endothelial (CD31 and CD144) and myogenic (MyoD and desmin) cell markers. (**b**) Immunostaining for the muscle stem cell markers Pax7 and MyoD was also performed (bar = 25 µm). (**c**) Quantification of RT-PCR results. Error bars indicate "mean + SD" (n = 3 independent experiments). (**d**) Quantification of Immunostaining of Pax7 and MyoD.

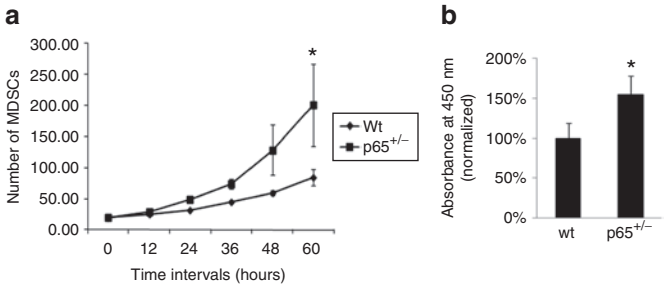

Figure 3 Muscle-derived stem cells (MDSCs) isolated from *p65*$^{+/-}$ mouse skeletal muscles (SKM) have a higher rate of proliferation than wild-type (wt) cells. (**a**) Cell proliferation rate was measured by Live Cell Imaging and (**b**) by an MTS assay ($P < 0.05$).

to that observed in wt cells treated with IKKi (Figure 5a). In order to verify that increased MyHC expression was concomitant with increased myotube formation, we treated wt MDSCs with 5 µmol/l IKKi. After 3 days, differentiation was assessed by immunofluorescence detection of MyHC. As shown in Figure 5e, compared to nontreated controls, the inhibitor caused a significant increase in myotube formation. The level of myogenic differentiation was comparable to that of *p65*$^{+/-}$ MDSCs ($P < 0.01$; Figure 5f). These results provide strong support that MDSC myogenic potential can be improved using NF-κB inhibition *ex vivo*.

p65$^{+/-}$ MDSCs have greater muscle regenerative capacity *in vivo*

To determine whether genetic depletion of p65 increases the engraftment and muscle regenerative capacity of MDSCs *in vivo*, we examined the ability of *p65*$^{+/-}$ and wt MDSCs to regenerate muscle fibers following their intramuscular implantation into an immunocompromised model of Duchenne muscular dystrophy. For these experiments, 3 × 10^5 *p65*$^{+/-}$ and wt MDSCs were injected into the gastrocnemius muscles of 8-week-old dystrophin-deficient SCID (mdx/SCID) mice. Fourteen days after implantation, significantly more dystrophin-positive myofibers were detected in the muscle injected with *p65*$^{+/-}$ MDSCs than in muscle injected with wt MDSCs ($P < 0.01$; Figure 6a,b). These results confirm our *in vitro* observations and may provide a novel mechanism as to why IKK inhibitors have been reported to improve muscle regeneration.[23]

Transplantation of *p65*$^{+/-}$ MDSCs postinjury reduces SKM inflammation and necrosis

The results above suggest that lowering basal levels of NF-κB activity increased the ability of MDSCs to engraft and differentiate following intramuscular injection (Figure 6). However, while it is possible this is mediated through enhanced proliferation and differentiation, the exact mechanism as to why more dystrophin-positive myofibers were found within the *p65*$^{+/-}$ MDSC engraftment sites remains unclear. Surrounding the engraftments of the wt MDSCs, we observed numerous cells positive for the macrophage marker CD14 as detected by immunofluorescent staining (data not shown), whereas the *p65*$^{+/-}$ MDSC engraftment sites were surrounded by fewer numbers of CD14+ cells (data not shown). As the mdx/SCID is an immunocompromised mouse model with a high level of background inflammation, we decided to further investigate this phenomenon using the well-established CTX muscle injury model in immunocompetent wt mice. In order

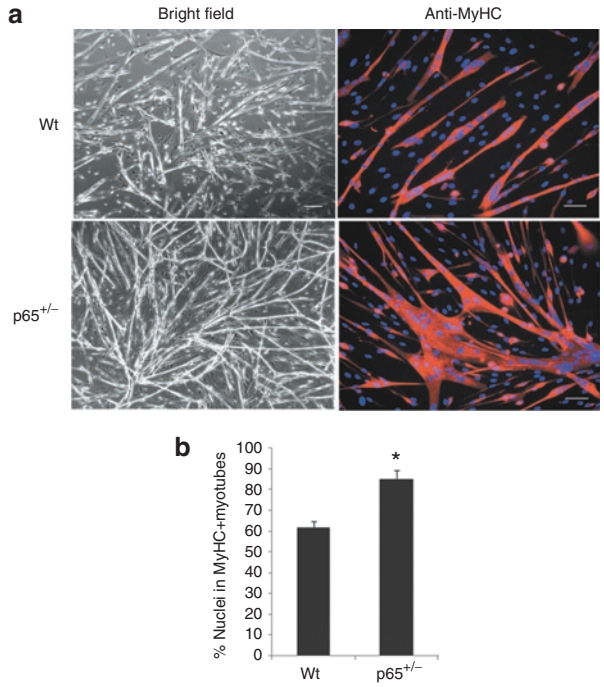

Figure 4 Myogenic differentiation is enhanced in muscle-derived stem cells (MDSCs) isolated from *p65*$^{+/-}$ mouse skeletal muscles (SKM) compared to wild-type (wt) MDSCs *in vitro*. (**a**) MDSCs were cultured in myogenic differentiation medium for 3 days, during which cell fusion into multinucleated myotubes was monitored using bright field microscopy and then confirmed by immunostaining for myosin heavy chain (MyHC-f). (**b**) Quantitation of MyHC-f positive myotubes. The percentage of differentiated myotubes was quantified as the number of nuclei in MyHC-f positive myotubes relative to the total number of nuclei. A total of three populations of *p65*$^{+/-}$ and wild-type (wt) MDSCs were tested ($P < 0.05$). In panel "**a**" all bars = 200 µm on bright field and all bars = 50 µm on MyHC immunostaining.

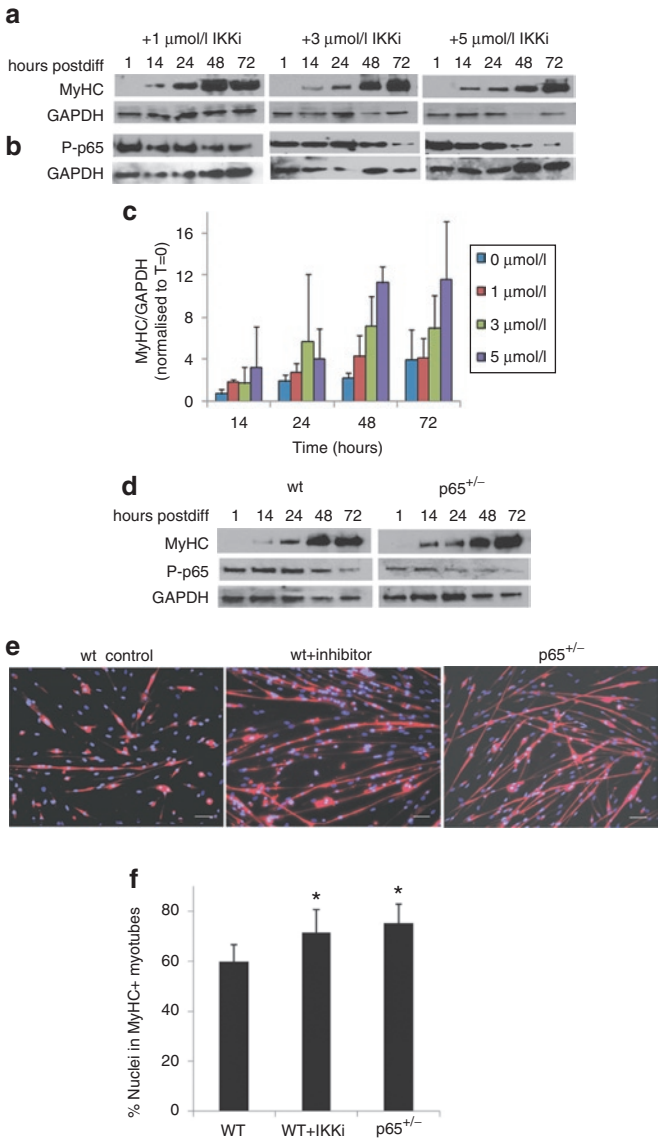

Figure 5 Muscle-derived stem cells (MDSCs) myogenic differentiation is enhanced by pharmacological inhibition of inhibitor of kappa B kinase β (IKKβ). (**a**) Western blot for myosin heavy chain (MyHC) over 72 hours of wild-type (wt) MDSCs treated with 1, 3, or 5 µmol/l IKKi during differentiation. (**b**) Western blot for P-p65 over 72 hours of wt MDSCs treated with 1, 3, or 5 µmol/l IKK inhibitor (IKKi) during differentiation. (**c**) Quantification of **b**, myosin heavy chain (MyHC-f) levels during differentiation ($n = 3$ independent experiments). (**d**) In parallel, wt and *p65*$^{+/-}$ MDSCs were cultured in differentiation medium and lysates were collected at the various time points indicated. Lysates were used for western blot for MyHC and P-p65 levels. (**e**) wt MDSCs, *p65*$^{+/-}$ MDSCs, and wt MDSCs treated with IKKi (5 µmol/l), were grown under fusion conditons for 72 hours and immunostained for MyHC-f expression (**f**) Quantification of MyHC-f staining ($P < 0.05$). In panel "**e**" all bars = 100 µm.

to confirm that transplanted *p65*$^{+/-}$ MDSCs are able to reduce inflammation in host skeletal muscle, we injected *p65*$^{+/-}$ and wt MDSCs into the gastrocnemius muscles of 8-week-old C57BL/6J mice 24 hours post-CTX injury. Six days post-transplantation, the wt MDSC engraftment area demonstrated a greater number of inflammatory cells surrounding the wt donor MDSCs than the *p65*$^{+/-}$ MDSCs. Furthermore, numerous centrally located nuclei, characteristic of regenerating muscle fibers, were found within the *p65*$^{+/-}$ MDSC injection sites. Consistent with observations made in mdx/SCID mice, the *p65*$^{+/-}$ MDSC engraftment area was associated with significantly fewer CD14+ cells than the wt MDSC engraftment area ($P < 0.01$; **Figure 7a,b**). There was also a significant (42%) reduction in tissue necrosis, as determined by quantification of mouse immunoglobulin G (IgG) staining ($P < 0.01$; **Figure 7a,c**). These results suggest that the improved engraftment and differentiation of *p65*$^{+/-}$ MDSCs is potentially due to their ability to attenuate the inflammation and necrosis that typically occurs after muscle injury.

DISCUSSION

NF-κB signaling has been implicated in the regulation of muscle degeneration and regeneration. The five mammalian NF-κB transcription factors are all expressed in skeletal muscle to modulate a variety of processes, including apoptosis, inflammation, and myoblast differentiation. Although there have been conflicting results reported as to whether NF-κB acts as a repressor or promoter of myogenesis,[8,24–29] recent results suggest that the classical NF-κB signaling pathway functions as a negative regulator of myogenesis.[14] In addition, NF-κB activation is associated with the degeneration and/or lack of regeneration of dystrophic

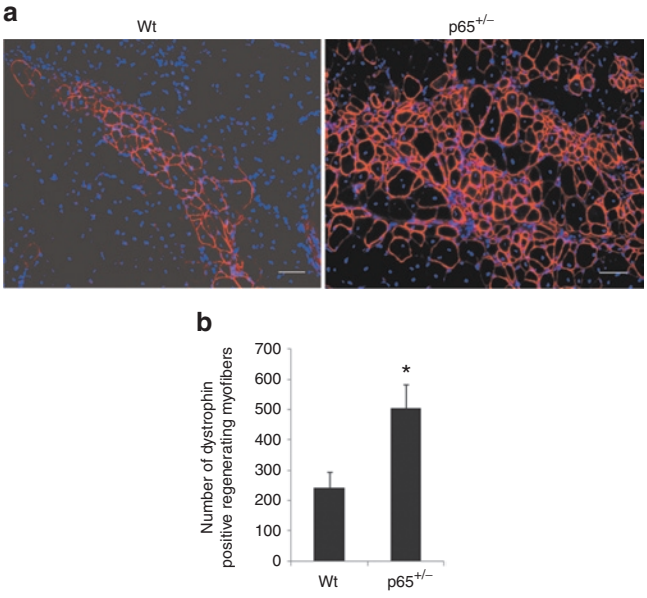

Figure 6 Heterozygous deletion of p65 promotes the regeneration capacity of muscle-derived stem cells (MDSCs). (**a**) Gastrocnemius cryosections from 8-week-old mdx/SCID mice in which $p65^{+/-}$ and wild-type (wt) MDSCs were implanted. Engraftment was determined by immunostaining for dystrophin (red). Three populations of $p65^{+/-}$ and wt MDSCs were transplanted into 12 mice in two independent experiments. (**b**) Quantitation of regenerated dystrophin-positive myofibers ($P < 0.05$). In panel "**a**" all bars = 50 µm. Error bars indicate "mean + SD" ($n = 12$).

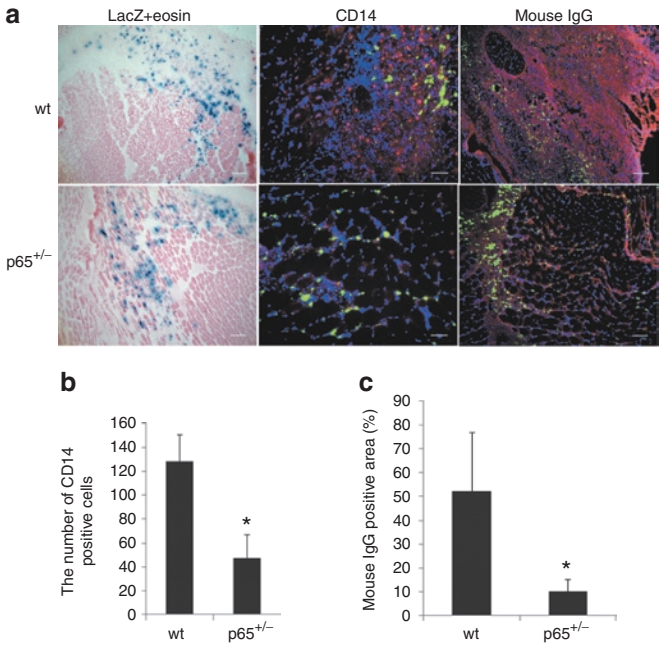

Figure 7 $p65^{+/-}$ muscle-derived stem cells (MDSCs) attenuate muscle inflammation and necrosis. (**a**) Gastrocnemius cryosections from 8-week-old C57BL/6J mice, which were injected with $p65^{+/-}$ or wild-type (wt) MDSCs 24 hours post-CTX injury. LacZ and eosin staining identified the injection area and immunostaining for CD14 (red) and mouse immunoglobulin G (IgG) (red) identified macrophages and necrotic tissue, respectively. In immunological stains, fluorescent green beads in C57BL/6J muscle sections confirmed the location of injection sites. (**b**) Quantitation of $CD14^+$ cells (the data represent six muscles per group). (**c**) Necrotic area in the gastrocnemius muscles was identified by IgG staining and quantified based on the total positive area per image (the data represent six muscles per group). In panel "**a**" all bars = 100 µm on LacZ+eosin and mouse IgG staining. All bars = 50 µm on CD14 staining.

muscle in mdx mice.[13] Thus, in this study, we examined the effect of NF-κB reduction on the proliferation and differentiation of MDSCs isolated from wt mice and mice heterozygous for p65. Although $p65^{+/-}$ MDSCs had more than a 30% reduction in p65/NF-kB levels compared to the wt MDSCs, the two genotypes expressed similar stem (CD34, Sca-1), myogenic (desmin, MyoD) and endothelial (CD144, CD31) cell markers. This result suggests that the reduction in NF-kB did not affect overall expression of MDSC markers, albeit there is some variability in stem cell marker expression between populations of the same genotype.

We observed that MDSCs with reduced p65 levels have improved proliferation compared to wt cells, suggesting that p65/NF-κB activity negatively controls MDSC expansion. More importantly, we also observed that both the rate and extent of myogenic differentiation was accelerated in MDSCs with reduced p65 and in wt MDSCs treated with an IKKβ inhibitor. Together, these data suggest that NF-κB inhibits muscle stem cell differentiation. Our results are in agreement with previous studies showing that regulation of myogenesis is dependent on p65 transcriptional activity, which is able to inhibit myogenesis.[14] It has been suggested previously that the negative effect of NF-κB on differentiation is mediated through the transcriptional activation of cyclin D1 and YinYang1 (YY1).[30,31] Interestingly, we have observed a reduction in the level of cyclin D1 in $p65^{+/-}$ MDSCs compared to wt cells, but found no difference in the level of YY1 expression (data not shown).

Recent genetic evidence supports the role of IKK/NF-κB in driving the pathogenesis of muscular dystrophy, identifying this signaling pathway a potential therapeutic target for the treatment of DMD.[13] The activity of NF-κB in dystrophic muscle is associated with not only immune cells, but also regenerative muscle fibers. Thus, we investigated whether the $p65^{+/-}$ MDSCs have a higher muscle regeneration potential than wt MDSCs after their intramuscular injection into dystrophic mdx/SCID skeletal muscles. Our results demonstrated that $p65^{+/-}$ MDSCs are more efficient at regenerating dystrophin-positive myofibers compared to wt MDSCs, which is consistent with the enhanced ability of the $p65^{+/-}$ MDSCs to differentiate in culture.

We also assessed inflammation around the engrafted site by immunofluorescent staining for CD14, a macrophage marker. While we found very few CD14+ cells within the injection sites of the $p65^{+/-}$ cells, many CD14+ cells were detected within the wt MDSC engraftment areas. As a decreased number of macrophages in the $p65^{+/-}$ cell engraftment area correlated with a reduction in necrosis, it is possible that a reduction in p65 enhances the local anti-inflammatory properties of MDSCs via regulation of paracrine factors. Several cytokines under the control of NF-κB, such as TNFα and interleukin-6 (IL-6), are potent inhibitors of myogenic differentiation.[8] Thus, taken together, these results suggest that inhibition of NF-κB/p65 may enhance myogenesis by reducing inflammation and necrosis.

During regeneration following injury, numerous paracrine factors such as myostatin, hepatocyte growth factor, and basic fibroblast growth factor play critical roles coordinating repair.[32] Other groups have demonstrated the importance of non-NF-kB proteins in muscle development and pathology. For example, myostatin acts independently of the classical TNFα and NF-kB pathway to inhibit MyoD expression and signal cachexia by reversing the IGF-1/PI3K/AKT hypertrophy pathway.[33] However, other factors, such as hepatocyte growth factor and IL-6, have been reported to activate NF-κB.[34] Given the numerous growth factors and cytokines present in damaged and regenerating muscle, the NF-κB pathway likely directs inflammation or regeneration in response to more than one factor. In summary, here we described a negative role for the p65/NF-κB signaling pathway in MDSC growth and differentiation *in vitro*, as well as muscle regeneration *in vivo*. Similarly, pharmacological inhibition of IKKβ identifies the IKK/NF-κB signaling pathway as a potential therapeutic target to improve the myogenic potential of MDSCs and muscle regeneration after injury and diseases.

MATERIALS AND METHODS

Animals. The C57BL/6J mice heterozygous for p65/RelA were originally described by Amer Beg (Cambridge, MA).[17] The mdx/SCID (C57BL/10ScSn DMD^{mdx}/J/CB17-Prkdc^{scid}/J) and C57BL/6J mice were obtained from the Jackson Laboratory (Bar Harbor, ME). All animal protocols used for these experiments were approved by the Children's Hospital of Pittsburgh's Institutional Animal Care and Use Committee.

Isolation of MDSCs from p65$^{+/-}$ mice. The mice were sacrificed at 5 months of age and muscle stem cell isolation was performed as previously described via a modified preplate technique.[18] Briefly, the SKM tissue was minced and processed through a series of enzymatic dissociations: 0.2% of collagenase type XI (Sigma-Aldrich, St Louis, MO) for 1 hour, 2.4 units/ml of dispase (Invitrogen, Carlsbad, CA) for 45 minutes, and 0.1% of trypsin-EDTA (Invitrogen) for 30 minutes at 37°C. After enzymatic dissociation, the muscle cells were centrifuged and resuspended in proliferation medium (Dulbecco's modified Eagle's medium supplemented with 10% fetal bovine serum, 10% horse serum, 0.5% chicken embryo extract, and 1% penicillin-streptomycin), and the resulting cell suspension from both $p65^{+/-}$ and wt muscle were plated in collagen type I coated flasks. Different populations of muscle-derived cells were isolated based on their adhesion characteristics. After 7 days, late preplate populations (slow-adhering cells) were obtained and cultured in proliferation medium. The slowly adhering fraction of muscle cells has been previously shown to contain MDSCs.[18] For all experiments, congenic $p65^{+/-}$ and $p65^{+/+}$ MDSCs of the same passage number were compared.

p65 staining and ArrayScan assay. Cells were fixed with 4% paraformaldehyde for 15 minutes at room temperature (RT), rinsed two times with phosphate-buffered saline (PBS), and the cells' membrane permeabilized for 10 minutes with 0.1% Triton X-100 in PBS. A 10% goat serum blocking solution was used for 1 hour and the cells were incubated with a 1:200 dilution of rabbit polyclonal anti-p65 (Abcam, Cambridge, MA) for 1 hour at RT. After washing three times, the cells were incubated for 30 minutes with Cy3-conjugated anti-rabbit IgG (1:500; Sigma-Aldrich). The nuclei were revealed by 4′,6-Diamidino-2-phenylindole (DAPI) staining. Nuclear localization of the NF-κB subunit p65 was measured via ArrayScan. This technique allows for the rapid, automated quantification of p65 and DAPI colocalization, as identified by immunocytochemistry in cells grown on a 96-well plate. Recordings were taken from multiple fields of view per well, generating data representative of each well.

Western blot assay. The cell populations isolated from $p65^{+/-}$ and wt mice were cultured in proliferation medium and stimulated with TNFα (10 ng/ml) for 30 minutes before harvesting. Cells were then lysed in Laemmli sample buffer (Bio-Rad, Hercules, CA), boiled for 5 minutes, and centrifuged at 4,000 r.p.m. for 5 minutes. Each sample was loaded on a 10% SDS-polyacrylamide gel, which was run for 2 hours and then transferred for 1.5 hours at 100 V while stirring on ice. The membrane was blocked with 5% bovine serum albumin (Sigma-Aldrich, St Louis, MO) in PBS for 1 hour and then incubated with rabbit anti-phospho-NF-κB/p65 monoclonal antibody (1:1,000; Cell Signaling, Danvers, MA) overnight at 4°C. After washing three times with Tris-buffered saline Tween-20, the membrane was incubated with goat anti-rabbit IgG (H+L) (1:5,000; Pierce, Rockford, IL) for 50 minutes at RT. Blots were developed by ECL solution (Pierce).

RT-PCR analysis. Total RNA was extracted from cells using Nucleo Spin RNA II column (Clontech, Mountain View, CA). Following isolation, complementary DNA was synthesized with SuperScript II reverse transcriptase (Invitrogen), according to the manufacturer's instructions. PCR was performed with Taq polymerase (Invitrogen) as per the manufacturer's instructions and PCR products were separated by electrophoresis with 1% agarose gels. The primers used for PCR are listed in **Table 1**. Each set of oligonucleotides was designed to span two different exons to avoid background amplification of genomic DNA. The data were quantified by densitometry using Adobe Photoshop 7.0.

Pax7 and MyoD staining. $P65^{+/-}$ and wt cells were fixed and permeabilized with 2% paraformaldehyde plus 1% Triton X-100 for 30 minutes at 4°C and rinsed two times with PBS. Cells were blocked with 5% horse serum and then incubated with a 1:100 dilution of mouse monoclonal anti-Pax7 (DSHB, Iowa City, IA) or anti-MyoD (Santa Cruz Biotechnology, Santa Cruz, CA) over night at 4°C. After washing three times, the cells were incubated for 1 hour with biotinylated anti-mouse IgG (1:300; Vector Lab, Burlingame, CA), which acted as a secondary antibody. Streptavidin 594 conjugate (1:500; Invitrogen) was added in the last step. The nuclei were revealed by DAPI staining. Negative control staining was performed by an identical procedure, with the exception that the primary antibody was omitted.

In vitro *assessment of cell proliferation.* In order to compare the proliferative potential of $p65^{+/-}$ MDSCs to wt MDSCs, we used a previously

Table 1 Primers used for RT–PCR

Gene	Forward primer	Reverse primer	Location
Sca-1	CCTACTGTGTGCAGAAAGAGC	CAGGAAGTCTTCACGTTGACC	89–331
CD34	GCAGCTTTGAGATGACATCACC	CTCAGCCTCCTCCTTTTCACA	498–715
MyoD1	ACAGTGGCGACTCAGATGCATC	GCTGCAGTCGATCTCTCAAAGC	708–1105
Desmin	AACCTGATAGACGACCTGCAG	GCTTGGACATGTCCATCTCCA	615–873
CD31	AGAGCTACGTCATTCCTCAG	GACCAAGTGTGTCACTTGAAC	474–988
CD144	CACCAACAAAAACCTGGAACA	CCACCACGATCTTGTATTCAG	425–729
β-Actin	TCAGAAGGACTCCTATGTGG	TCTTTGATGTCACGCACGAT	234–722

described Live Cell Imaging system (Kairos Instruments LLC, Pittsburgh, PA).[22] Bright field images were taken at a ×100 magnification at 10 minutes intervals over a 72-hour period in three fields of view per well, with three wells per population. The images were combined to generate a video using ImageJ software (NIH). Proliferation was assessed by counting the number of cells per field of view, over 12 hours. All six populations were also plated in 96-well plates in quadruplicate (500 cells/well) and cultured under normal conditions for 72 hours. At this time, 20 µl of CellTiter96 AQueous One Reagent (Promega, Madison, WI) was added to each well and incubated in 5% CO_2 at 37 °C. Following another 3-hour incubation, absorbance at 490 nm was read with a 96-well plate reader.

Myogenic differentiation assay and fast MyHC (MyHC-f) staining. After 15 passages, cells were plated on 24-well plates (30,000 cells/well) with Dulbecco's modified Eagle's medium supplemented with 2% fetal bovine serum to stimulate myotube formation. Three days later, immunocytochemical staining for fast skeletal MyHC was performed. After rinsing three times with PBS, cells were fixed for 2 minutes in cold methanol, blocked with 10% horse serum for 1 hour and then incubated with a mouse anti-MyHC-f (1:250; Sigma-Aldrich, clone MY-32) antibody for 2 hours at RT. The primary antibody was detected with a secondary anti-mouse IgG antibody conjugated with Cy3 (1:300; Sigma-Aldrich) for 15 minutes. The nuclei were revealed by DAPI staining. The percentage of differentiated myotubes was quantified as the number of nuclei in MyHC-f positive myotubes relative to the total number of nuclei. The myogenic differentiation was also monitored over a period of 5 days using Live Cell Imaging. The images were combined to create a video using ImageJ software (NIH).

Selective inhibition of IKKβ. To determine the effects of IKK/NF-κB inhibition on wt MDSCs during myogenic differentiation, we used IKK-2 inhibitor IV (IKKi), or 2-[(aminocarbonyl)amino]-5-(4-fluorophenyl)-3-thiophenecarboxamide (Calbiochem, San Diego, CA), a reversible competitive inhibitor of IKKβ ATP binding. Cells were plated at 10^5 cells/well in 6-well plates and exposed to IKK inhibitor in differentiation medium. Cells were treated with either 1, 3, or 5 µmol/l IKKi. Lysates were collected at 0 minute, 14, 24, 48, and 72 hours following treatment. NF-kB activity and myogenic differentation was assessed by western blot for phosphorylated NF-kB/p65 (1:1,000; Cell Signaling) and MyHC-f (1:500; Sigma-Aldrich, clone MY-32), as detailed above.

Cell implantation and dystrophin staining. MDSCs from $p65^{+/-}$ and wt muscle were grown in proliferation medium until the cell number was sufficient for injection. A total of 3×10^5 viable cells was suspended in 20 µl of Hank's balanced salts solution and injected into the gastrocnemius muscles of 8–12-week-old mdx/SCID mice using a Hamilton syringe. The same number of cells was injected into the gastrocnemius muscles of 8-week-old wt C57BL/6J mice that had been injured 1 day earlier by a 30 µl intramuscular injection of 2 µmol/l CTX (Sigma-Aldrich) in PBS. The cell suspension was mixed with green fluorescent-labeled beads before injection to detect the injection sites. Six or fourteen days after implantation, the mice were sacrificed and the gastrocnemius muscles were harvested and flash frozen in liquid nitrogen-cooled 2-methylbutane. Serial cryosections 10 µmol/l in thickness were obtained for immunohistochemical analyses. Cryosections were fixed with 5% formalin and blocked with 5% donkey serum in PBS for 1 hour, then incubated with rabbit anti-dystrophin (1:300; Abcam) for 2 hours at RT. The sections were exposed to secondary 594-conjugated anti-rabbit IgG (1:500; Invitrogen) in PBS for 30 minutes. The nuclei were revealed by DAPI staining. Immunostaining was visualized and images were taken by fluorescence microscopy (Nikon Eclipse E800; Nikon, Melville, NY). Northern Eclipse software was used for quantitative analysis of the regenerated dystrophin-positive myofibers. A series of pictures were taken, and Adobe Photoshop 7.0 was used to construct a composite picture of the dystrophin-positive myofibers, which were then manually counted.

Retroviral transduction of MDSCs. MDSCs were plated at an initial confluence of 30–40% and retrovirally transduced [in the presence of Polybrene (8 µg/ml)] to express the β-galactosidase gene (LacZ), as previously described.[35]

LacZ staining. The cryosections were fixed in 1% glutaraldehyde and incubated 3 hours with 5-bromo-4-chloro-3-indolyl β-D-galactopyranoside (X-gal) substrate at 37 °C. Sections were counterstained with Eosin.

CD14 staining. Cryosections were fixed with 5% formalin and blocked with 5% donkey serum in PBS for 1 hour, then incubated with rat anti-CD14 (1:200; Biolegend, San Diego, CA) overnight at 4 °C. This was followed by a 1-hour incubation with biotinylated anti-rat IgG (1:300; Vector Lab). Streptavidin Cy3 conjugate (1:500; Sigma-Aldrich) was added in the last step followed by several rinses in PBS. Following CD14 staining, five random pictures per slide were taken and the number of CD14+ cells was counted manually.

Mouse IgG staining and quantification of necrosis. Muscle sections were fixed with 5% formalin and blocked with 10% horse serum in PBS for 1 hour, then incubated with biotinylated anti mouse IgG (1:300; Vector Lab) for 1 hour at RT. This was followed by a 15-minute incubation with streptavidin Cy3 conjugate (1:500; Sigma-Aldrich). The nuclei were revealed by DAPI staining. The IgG positive area was measured and quantified as the percentage of mouse IgG expressing area per total area using Northern Eclipse software (Cheektowaga, NY).

Statistical analysis. All results are given as the mean ± SD. Means from $p65^{+/-}$ and wt or treated and untreated were compared using Students' *t*-test. Differences were considered statistically significant when the *P* value was < 0.05.

SUPPLEMENTARY MATERIAL

Video S1. $p65^{+/-}$ MDSC proliferation.
Video S2. wt MDSC proliferation.
Video S3. $P65^{+/-}$ MDSC differentiation.
Video S4. wt MDSC differentiation.

ACKNOWLEDGMENTS

The authors thank the members of the Huard Laboratory, especially Jenny Zhu and Bin Sun for discussions and technical advice. Special thanks go to Joseph Feduska and Bridget Deasy for live cell imaging advice. This work was supported in part by the Henry J. Mankin Endowed Chair for Orthopedic Research at the University of Pittsburgh, the William F. and Jean W. Donaldson Chair at Children's Hospital of Pittsburgh. L.J.N. is supported by NIEHS (ES016114) and NIA (AG033907). The authors do not have conflicts of interest to disclose other than the corresponding author who receives consulting fees from Cook MyoSite Inc.

REFERENCES

1. Verma, IM, Stevenson, JK, Schwarz, EM, Van Antwerp, D and Miyamoto, S (1995). Rel/NF-kappa B/I kappa B family: intimate tales of association and dissociation. *Genes Dev* **9**: 2723–2735.
2. Baeuerle, PA and Baltimore, D (1996). NF-kappa B: ten years after. *Cell* **87**: 13–20.
3. Baldwin, AS Jr (1996). The NF-kappa B and I kappa B proteins: new discoveries and insights. *Annu Rev Immunol* **14**: 649–683.
4. Li, Z and Nabel, GJ (1997). A new member of the I kappaB protein family, I kappaB epsilon, inhibits RelA (p65)-mediated NF-kappaB transcription. *Mol Cell Biol* **17**: 6184–6190.
5. Karin, M (1999). How NF-kappaB is activated: the role of the IkappaB kinase (IKK) complex. *Oncogene* **18**: 6867–6874.
6. Hayden, MS and Ghosh, S (2004). Signaling to NF-kappaB. *Genes Dev* **18**: 2195–2224.
7. Karin, M, Cao, Y, Greten, FR and Li, ZW (2002). NF-kappaB in cancer: from innocent bystander to major culprit. *Nat Rev Cancer* **2**: 301–310.
8. Langen, RC, Schols, AM, Kelders, MC, Wouters, EF and Janssen-Heininger, YM (2001). Inflammatory cytokines inhibit myogenic differentiation through activation of nuclear factor-kappaB. *FASEB J* **15**: 1169–1180.
9. Baghdiguian, S, Martin, M, Richard, I, Pons, F, Astier, C, Bourg, N *et al.* (1999). Calpain 3 deficiency is associated with myonuclear apoptosis and profound

perturbation of the IkappaB alpha/NF-kappaB pathway in limb-girdle muscular dystrophy type 2A. *Nat Med* **5**: 503–511.
10. Kumar, A, Lnu, S, Malya, R, Barron, D, Moore, J, Corry, DB *et al.* (2003). Mechanical stretch activates nuclear factor-kappaB, activator protein-1, and mitogen-activated protein kinases in lung parenchyma: implications in asthma. *FASEB J* **17**: 1800–1811.
11. Monici, MC, Aguennouz, M, Mazzeo, A, Messina, C and Vita, G (2003). Activation of nuclear factor-kappaB in inflammatory myopathies and Duchenne muscular dystrophy. *Neurology* **60**: 993–997.
12. Hunter, RB and Kandarian, SC (2004). Disruption of either the Nfkb1 or the Bcl3 gene inhibits skeletal muscle atrophy. *J Clin Invest* **114**: 1504–1511.
13. Acharyya, S, Villalta, SA, Bakkar, N, Bupha-Intr, T, Janssen, PM, Carathers, M *et al.* (2007). Interplay of IKK/NF-kappaB signaling in macrophages and myofibers promotes muscle degeneration in Duchenne muscular dystrophy. *J Clin Invest* **117**: 889–901.
14. Bakkar, N, Wang, J, Ladner, KJ, Wang, H, Dahlman, JM, Carathers, M *et al.* (2008). IKK/NF-kappaB regulates skeletal myogenesis via a signaling switch to inhibit differentiation and promote mitochondrial biogenesis. *J Cell Biol* **180**: 787–802.
15. Payne, TR, Oshima, H, Okada, M, Momoi, N, Tobita, K, Keller, BB *et al.* (2007). A relationship between vascular endothelial growth factor, angiogenesis, and cardiac repair after muscle stem cell transplantation into ischemic hearts. *J Am Coll Cardiol* **50**: 1677–1684.
16. Ambrosio, F, Ferrari, RJ, Distefano, G, Plassmeyer, JM, Carvell, GE, Deasy, BM *et al.* (2010). The synergistic effect of treadmill running on stem-cell transplantation to heal injured skeletal muscle. *Tissue Eng Part A* **16**: 839–849.
17. Beg, AA, Sha, WC, Bronson, RT, Ghosh, S and Baltimore, D (1995). Embryonic lethality and liver degeneration in mice lacking the RelA component of NF-kappa B. *Nature* **376**: 167–170.
18. Gharaibeh, B, Lu, A, Tebbets, J, Zheng, B, Feduska, J, Crisan, M *et al.* (2008). Isolation of a slowly adhering cell fraction containing stem cells from murine skeletal muscle by the preplate technique. *Nat Protoc* **3**: 1501–1509.
19. Wan, F and Lenardo, MJ (2009). Specification of DNA binding activity of NF-kappaB proteins. *Cold Spring Harb Perspect Biol* **1**: a000067.
20. Sacco, A, Doyonnas, R, Kraft, P, Vitorovic, S and Blau, HM (2008). Self-renewal and expansion of single transplanted muscle stem cells. *Nature* **456**: 502–506.
21. Jankowski, RJ, Haluszczak, C, Trucco, M and Huard, J (2001). Flow cytometric characterization of myogenic cell populations obtained via the preplate technique: potential for rapid isolation of muscle-derived stem cells. *Hum Gene Ther* **12**: 619–628.
22. Deasy, BM, Jankowski, RJ, Payne, TR, Cao, B, Goff, JP, Greenberger, JS *et al.* (2003). Modeling stem cell population growth: incorporating terms for proliferative heterogeneity. *Stem Cells* **21**: 536–545.
23. Tang, Y, Reay, DP, Salay, MN, Mi, MY, Clemens, PR, Guttridge, DC *et al.* (2010). Inhibition of the IKK/NF-?B pathway by AAV gene transfer improves muscle regeneration in older mdx mice. *Gene Ther* **17**: 1476–1483.
24. Lehtinen, SK, Rahkila, P, Helenius, M, Korhonen, P and Salminen, A (1996). Down-regulation of transcription factors AP-1, Sp-1, and NF-kappa B precedes myocyte differentiation. *Biochem Biophys Res Commun* **229**: 36–43.
25. Guttridge, DC, Albanese, C, Reuther, JY, Pestell, RG and Baldwin, AS Jr (1999). NF-kappaB controls cell growth and differentiation through transcriptional regulation of cyclin D1. *Mol Cell Biol* **19**: 5785–5799.
26. Kaliman, PA and Barannik, TV (1999). Regulation of delta-aminolevulinate synthase activity during the development of oxidative stress. *Biochemistry Mosc* **64**: 699–704.
27. Canicio, J, Ruiz-Lozano, P, Carrasco, M, Palacin, M, Chien, K, Zorzano, A *et al.* (2001). Nuclear factor kappa B-inducing kinase and Ikappa B kinase-alpha signal skeletal muscle cell differentiation. *J Biol Chem* **276**: 20228–20233.
28. Munz, B, Hildt, E, Springer, ML and Blau, HM (2002). RIP2, a checkpoint in myogenic differentiation. *Mol Cell Biol* **22**: 5879–5886.
29. Baeza-Raja, B and Muñoz-Cánoves, P (2004). p38 MAPK-induced nuclear factor-kappaB activity is required for skeletal muscle differentiation: role of interleukin-6. *Mol Biol Cell* **15**: 2013–2026.
30. Guttridge, DC, Mayo, MW, Madrid, LV, Wang, CY and Baldwin, AS Jr (2000). NF-kappaB-induced loss of MyoD messenger RNA: possible role in muscle decay and cachexia. *Science* **289**: 2363–2366.
31. Wang, H, Hertlein, E, Bakkar, N, Sun, H, Acharyya, S, Wang, J *et al.* (2007). NF-kappaB regulation of YY1 inhibits skeletal myogenesis through transcriptional silencing of myofibrillar genes. *Mol Cell Biol* **27**: 4374–4387.
32. Karalaki, M, Fili, S, Philippou, A and Koutsilieris, M (2009). Muscle regeneration: cellular and molecular events. *In Vivo* **23**: 779–796.
33. McFarlane, C, Plummer, E, Thomas, M, Hennebry, A, Ashby, M, Ling, N *et al.* (2006). Myostatin induces cachexia by activating the ubiquitin proteolytic system through an NF-kappaB-independent, FoxO1-dependent mechanism. *J Cell Physiol* **209**: 501–514.
34. Yao, P, Zhan, Y, Xu, W, Li, C, Yue, P, Xu, C *et al.* (2004). Hepatocyte growth factor-induced proliferation of hepatic stem-like cells depends on activation of NF-kappaB. *J Hepatol* **40**: 391–398.
35. Li, Y and Huard, J (2002). Differentiation of muscle-derived cells into myofibroblasts in injured skeletal muscle. *Am J Pathol* **161**: 895–907.

Appendix 5

Cell Transplantation, Vol. 21, pp. 1087–1093, 2012
Printed in the USA.

0963-6897/12 $90.00 + .00
DOI: http://dx.doi.org/10.3727/096368912X636876
E-ISSN 1555-3892
www.cognizantcommunication.com

Isolation of Myogenic Stem Cells From Cultures of Cryopreserved Human Skeletal Muscle

Bo Zheng,*[1] Chien-Wen Chen,*†[1] Guangheng Li,* Seth D. Thompson,*
Minakshi Poddar,* Bruno Péault,*‡§¶ and Johnny Huard*†

*Stem Cell Research Center, Department of Orthopaedic Surgery,
University of Pittsburgh School of Medicine and Children's Hospital of Pittsburgh of UPMC, Pittsburgh, PA, USA
†Department of Bioengineering, University of Pittsburgh Swanson School of Engineering, Pittsburgh, PA, USA
‡Department of Pediatrics, Children's Hospital of Pittsburgh of UPMC, Pittsburgh, PA, USA
§David Geffen School of Medicine, University of California at Los Angeles, Los Angeles, CA, USA
¶Center for Vascular Science and Center for Regenerative Medicine, University of Edinburgh, Edinburgh, UK

We demonstrate that subpopulations of adult human skeletal muscle-derived stem cells, myogenic endothelial cells (MECs), and perivascular stem cells (PSCs) can be simultaneously purified by fluorescence-activated cell sorting (FACS) from cryopreserved human primary skeletal muscle cell cultures (cryo-hPSMCs). For FACS isolation, we utilized a combination of cell lineage markers: the myogenic cell marker CD56, the endothelial cell marker UEA-1 receptor (UEA-1R), and the perivascular cell marker CD146. MECs expressing all three cell lineage markers ($CD56^+UEA\text{-}1R^+CD146^+/CD45^-$) and PSCs expressing only CD146 ($CD146^+/CD45^-CD56^-UEA\text{-}1R^-$) were isolated by FACS. To evaluate their myogenic capacities, the sorted cells, with and without expansion in culture, were transplanted into the cardiotoxin-injured skeletal muscles of immunodeficient mice. The purified MECs exhibited the highest regenerative capacity in the injured mouse muscles among all cell fractions tested, while PSCs remained superior to myoblasts and the unpurified primary skeletal muscle cells. Our findings show that both MECs and PSCs retain their high myogenic potentials after in vitro expansion, cryopreservation, and FACS sorting. The current study demonstrates that myogenic stem cells are prospectively isolatable from long-term cryopreserved primary skeletal muscle cell cultures. We emphasize the potential application of this new approach to extract therapeutic stem cells from human muscle cells cryogenically banked for clinical purposes.

Key words: Myogenesis; Human skeletal muscle; Myogenic endothelial cells (MECs); Perivascular stem cells (PSCs); Cell therapy

INTRODUCTION

Mammalian skeletal muscle harbors multiple stem/progenitor cell populations, which can repair and/or regenerate injured/defective tissues such as damaged/dystrophic skeletal muscles and ischemic hearts (1,2,5,7,8,10,12–19). In particular, we previously reported the identification of two subpopulations of multipotent stem cells within human skeletal muscle [i.e., myogenic endothelial cells (MECs) ($CD45^-CD34^+CD56^+CD144^+$) and perivascular stem cells (PSCs) ($CD34^-CD45^-CD56^-CD146^+$)], which exhibit multilineage mesodermal developmental potentials (6,20). These stem cell populations were specifically localized in situ within the walls of small blood vessels and can be prospectively purified by fluorescence-activated cell sorting (FACS) from fresh human skeletal muscle biopsies, through the use of a combination of positive and negative cell lineage markers (6,20). In vitro, purified MECs and PSCs displayed osteo-, chondro-, adipo-, and myogenic differentiation competence, and their high repair/regenerative capacities were not only demonstrated in injured mouse skeletal muscles but also in infarcted hearts (3,4,6,11,20). However, it has never been documented whether these stem cell fractions could persist and retain their high myogenic capacities after the cryopreservation of human primary skeletal muscle cell cultures (cryo-hPSMCs). Furthermore, MECs and PSCs have been shown to be superior to myoblasts for muscle regeneration in previously performed studies; however, it has

Received July 12, 2010; final acceptance July 10, 2011. Online prepub date: March 21, 2012.
[1]These authors provided equal contribution to this work.
Address correspondence to Johnny Huard, Ph.D., Stem Cell Research Center, Department of Orthopaedic Surgery, University of Pittsburgh School of Medicine, 206 Bridgeside Point II, 450 Technology Drive, Pittsburgh, PA, USA 15219, USA. Tel: (412) 648-2798; Fax: (412) 648-4066; E-mail: jhuard@pitt.edu

never been determined whether MECs isolated from cryopreserved, culture-expanded hPSMCs possessed the same superior regenerative capacity.

In order to identify and purify MECs and PSCs by FACS from in vitro expanded cryo-hPSMCs, we employed a collection of cell lineage markers reported in our previous studies, including the hematopoietic cell marker CD45, the myogenic cell marker CD56 (neural cell adhesion molecule; N-CAM), the perivascular cell marker CD146 (melanoma cell adhesion molecule; M-CAM/Mel-CAM/MUC18), and the endothelial cell marker UEA-1 receptor (*Ulex europaeus* agglutinin I receptor, UEA-1R) (6,20,21). UEA-1R was chosen as a substitute marker for CD34 and CD144 because these two endothelial cell markers are frequently lost during long-term culture whereas UEA-1 maintains consistent reactivity within endothelial cell lineage cultures (20,21). We hypothesized that MECs and PSCs (with and without culture expansion), purified from cryo-hPSMCs, retain their superior myogenic potential and exhibit a greater regeneration capacity of skeletal myofibers when compared to myoblasts.

MATERIALS AND METHODS

Human Muscle Biopsies and Animal Usage

In total, nine independent human skeletal muscle biopsies, from four female and five male donors (age range 4–75, mean 28), were used to obtain human primary skeletal muscle cells (hPSMCs). The procurement of human skeletal muscle biopsies from the National Disease Research Interchange (NDRI) was approved by the Institutional Review Board at the University of Pittsburgh Medical Center (UPMC). All the animal research experiments performed in this study were approved by the Animal Research and Care Committee at the Children's Hospital of Pittsburgh of UPMC (Protocol #34-05) and the University of Pittsburgh (Protocol #0810310-B2).

Cell Isolation and Cryopreservation

The human skeletal muscle biopsies were placed in Hank's Balanced Salt Solution (HBSS, Invitrogen) and transferred to the laboratory on ice. Briefly, tissues were finely minced and serially digested with 0.2% collagenase type XI, 0.25% dispase, and 0.1% trypsin, as previously described (20,21). Dispersed single cell suspensions were cultured in complete medium containing DMEM supplemented with 10% fetal bovine serum (FBS), 10% horse serum, 1% chicken embryo extract, and 1% penicillin/streptomycin (all from Invitrogen). After expansion, cells were cryopreserved at passages 2–8 in medium consisting of 50% complete culture medium and 50% freezing medium (80% FBS + 20% dimethyl sulfoxide) and stored in liquid nitrogen (21).

Flow Cytometry and Cell Sorting

To culture cryo-hPSMCs, cells were thawed and expanded for 2–6 passages. To perform flow cytometry analysis, cells were trypsinized, washed, and incubated with anti-human monoclonal antibodies/ligands: CD45-allophycocyanin-cyanine 7 (APC-Cy7), CD56-phycoerythrin-Cy7 (PE-Cy7), CD34-APC (all from Becton Dickinson), CD146-fluorescein isothiocyanate (FITC; Serotec), UEA-1-PE (Biomeda), von Willebrand factor (vWF)-FITC (US Biology), kinase insert domain receptor (also known as vascular endothelial growth factor receptor 2; VEGFR2) KDR-APC (R&D Systems), and CD144-PE (Beckman Coulter). Negative control samples received equivalent amounts of isotype-matched fluorophore-conjugated antibodies. For FACS purification, cells were incubated with CD45-APC-Cy7, CD56-PE-Cy7, CD146-FITC, UEA-1-PE, and with 7-amino-actinomycin D for dead cell exclusion. Sorted subpopulations were collected for immediate transplantation or transiently expanded in appropriate conditions as previously described (6,20).

Immunocytochemistry

For immunocytochemistry, cells were cytospun onto glass slides, fixed, and incubated with 10% serum. The following primary antibodies were used to detect cell lineage markers, including myogenic cell markers, CD56 (BD) and desmin (Sigma); perivascular cell markers, α-smooth muscle actin (Abcam) and CD146 (Cayman Chemical); endothelial cell markers/ligands, CD144 (Sigma), vWF (DAKO), CD34 (Novocastra), and biotinylated UEA-1 (Vector), followed by incubation with biotinylated secondary antibodies and/or Cy3-conjugated streptavidin (Sigma). Slides were observed and photographed on an epifluorescence microscope system (Nikon Eclipse E800).

Myogenesis In Vivo

To investigate whether the myogenic capacities of the cells were preserved, after cryopreservation, purified MECs, PSCs, myoblasts (Myos), endothelial cells (ECs), and unpurified muscle cells, without in vitro expansion, from six independent hPSMC samples were used for intramuscular injection. The newly sorted cells, on average, $11.8 \pm 5.8 \times 10^4$ $CD56^+$ Myo cells, $7.3 \pm 4.4 \times 10^4$ $CD146^+$ PSCs, $4.5 \pm 2.6 \times 10^4$ $UEA\text{-}1R^+$ ECs, and $2.9 \pm 1.7 \times 10^4$ $CD56^+UEA\text{-}1R^+CD146^+$ MECs as well as 30×10^4 corresponding unsorted cells, were resuspended in 20 μl of HBSS and used for transplantation.

To precisely measure the myogenic-regenerative capacity of each stem/progenitor cell subpopulation, newly sorted MECs, PSCs, and Myo cells were expanded in culture for 1–2 passages. Fifty thousand cells from each subpopulation as well as 5×10^4 corresponding

unsorted cells were trypsinized, washed, and resuspended in 20 μl of phosphate-buffered saline (PBS). Four individual animal experiments were performed, with each using cell populations purified from a single FACS sort of one independent cryo-hPSMC culture.

Cells were injected into a single site of the gastrocnemius muscles of severe combined immunodeficient (SCID) mice that were injured 24 h before by injecting 1 μg of cardiotoxin in 20 μl of HBSS. The untreated group received sham injections of 20 μl of HBSS or PBS only. Treated muscles were collected 2 weeks postinjection for immunohistochemical analyses. Anti-human spectrin was used to identify human cell-derived skeletal myofibers in the mouse muscles. In order to quantitatively evaluate the myogenic regenerative capacity of each subpopulation, the number of human spectrin-positive skeletal myofibers was averaged from six randomly selected sections at the site of injection in each specimen and presented as the regenerative index (per section).

Statistical Analysis

Data were summarized as average ± SE. Statistical comparison between the groups (purified cells after expansion in vitro) was performed using one-way ANOVA with a 95% confidence interval. Bonferroni pairwise multiple comparison test was performed for ANOVA post hoc analysis. Statistical analyses were performed with SigmaStat software.

RESULTS

Heterogenous Cell Composition of Human Primary Skeletal Muscle Cell Cultures (hPSMCs) After Cryopreservation and Long-Term Expansion

After expansion, the cryopreserved hPSMCs (cryo-hPSMCs) were examined by immunocytochemistry for cell surface marker expression. The majority of cryo-hPSMCs expressed desmin and CD56, and to a lesser extent, CD146 (Fig. 1). Only a fraction of cells expressed α-SMA, CD144, vWF, or UEA-1R. As predicted, the cultured human cryo-hPSMCs lacked CD34 expression. After excluding $CD45^+$ hematopoietic cells ($0.2 \pm 0.1\%$), flow cytometry analysis quantitatively confirmed the presence of cells with diverse expressions of cell lineage makers by cryo-hPSMCs: $77.1 \pm 5.7\%$ $CD56^+$, $66.9 \pm 8.1\%$ $CD146^+$, $11.2 \pm 2.5\%$ UEA-$1R^+$, $0.3 \pm 0.1\%$ $CD144^+$, 0.1% vWF^+, and null expression of CD34 and KDR (Fig. 1B). The number of cryo-hPSMCs positive for CD56, CD146, or UEA-1R decreased dramatically after passage 10 (Fig. 1C).

Isolation of Myogenic Stem/Progenitor Cells From Cryo-hPSMCs

After revealing the heterogeneous nature of cryo-hPSMCs, we analyzed these cells for the existence of previously defined subpopulations by multicolor flow cytometry, based on their expression of hematopoietic (CD45), myogenic (CD56), endothelial (UEA-1R), and perivascular (CD146) cell lineage markers (6,20). After exclusion of $CD45^+$ cells, four distinct cell fractions were identified, including myoblasts (Myo) ($CD56^+$/$CD45^-CD146^-$UEA-$1R^-$), endothelial cells (ECs) (UEA-$1R^+$/$CD45^-CD56^-CD146^-$), perivascular stem cells (PSCs) ($CD146^+$/$CD45^-CD56^-$UEA-$1R^-$), and myogenic endothelial cells (MECs), which expressed all three markers ($CD56^+$UEA-$1R^+CD146^+$/$CD45^-$). Long-term cultured cryo-hPSMCs included $22.58 \pm 6.32\%$ Myo, $0.58 \pm 0.23\%$ ECs, $5.92 \pm 4.66\%$ PSCs, and $1.16 \pm 0.19\%$ MECs (Fig. 2). These four cell subsets were subsequently fractionated by FACS, and on average we were able to recover the following number of each cell type: $25.61 \pm 9.16 \times 10^4$ $CD56^+$ Myo, $13.28 \pm 7.37 \times 10^4$ UEA-$1R^+$ ECs, $33.54 \pm 20.53 \times 10^4$ $CD146^+$ PSCs, and $3.84 \pm 0.96 \times 10^4$ $CD56^+$UEA-$1R^+CD146^+$ MECs (Fig. 2).

Purified Myogenic Stem/Progenitor Cells Retain High Myogenic Potentials In Vivo

To evaluate whether the myogenic capacity was preserved after cryopreservation, all sorted cells were immediately transplanted (without culture expansion) into the cardiotoxin-injured gastrocnemius muscles of SCID mice ($n = 6$ per cell fraction). Unpurified muscle cells and HBSS injections were employed as treated and untreated controls, respectively. Mouse muscles were harvested 2 weeks postinjection, cryosectioned, and examined by immunohistochemistry to detect muscle fiber regeneration. An antibody against human spectrin, a myofiber cytoskeletal protein, was used to identify human cell-derived skeletal myofibers in the tissue sections. All of the newly purified cell fractions regenerated human spectrin-positive myofibers in the injured mouse skeletal muscles; however, the purified fractions appeared to regenerate a greater number of muscle fibers than the unpurified cryo-hPSMCs (Fig. 3A). As expected, a lack of spectrin-expressing muscle fibers was observed in the HBSS-injected muscles (Fig. 3A).

To quantitatively measure the myogenic regenerative capacity of each purified stem/progenitor cell population, newly sorted MECs, PSCs, and Myo cells were transiently expanded in culture for 1–2 passages. Fifty thousand cells from each of the subpopulations as well as 5×10^4 corresponding unsorted cells were transplanted into the same type of muscle injury model described above ($n = 4$ per cell fraction). Phosphate-buffered saline (PBS) injections were used as negative controls. ECs were not included in this experiment due to their unstable phenotype in culture. Quantitative analyses revealed that the myogenic regenerative index,

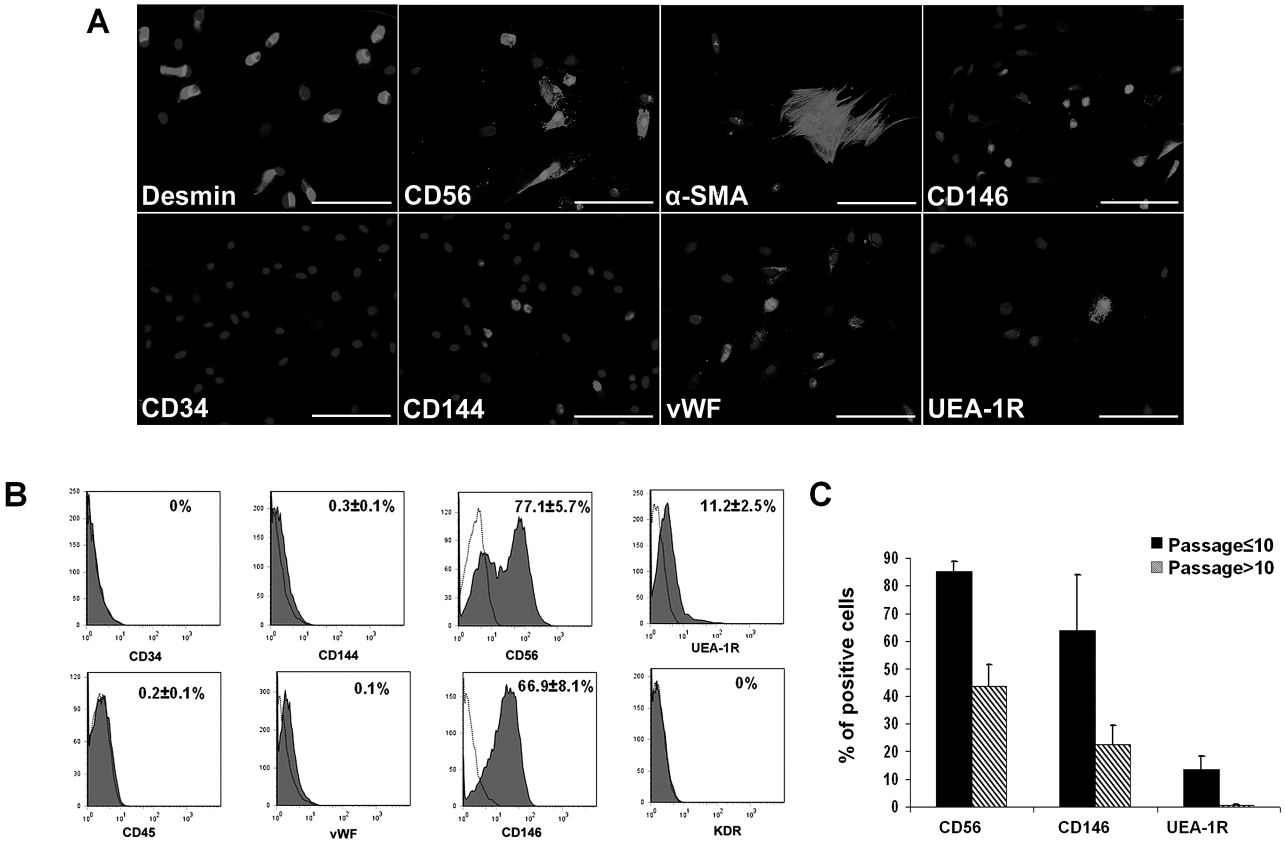

Figure 1. Expression of cell lineage markers by cryopreserved human primary skeletal muscle cells (cryo-hPSMCs). (A) Immunocytochemistry revealed the expression of various cell lineage markers (light gray) by cryo-hPSMCs after expansion. Nuclei were stained with DAPI (dark gray). (B) Flow cytometry analysis quantitatively confirmed the diverse cell composition of cryo-hPSMCs. (C) The number of cryo-hPSMCs positive for CD56, CD146, or UEA-1R decreased when cells were cultured beyond passage 10. Scale bars: 100 μm.

indicated by the average number of human spectrin-positive skeletal myofibers per muscle section, was 166.3 ± 19.2 for the MECs, 90.1 ± 8.0 for the PSCs, 45.7 ± 6.2 for the myoblasts (Myo), and 28.7 ± 8.4 for the unsorted muscle cells (Unsort) (Fig. 3B). The MECs exhibited the highest regeneration index of all four cell fractions tested ($p < 0.005$) (Fig. 3B) and the PSCs regenerated more myofibers than the Myo ($p > 0.05$) and the Unsort ($p = 0.017$) groups (Fig. 3B). Although the purified myoblasts displayed a trend of higher myogenic capacity than the unsorted cells, no statistically significant difference was observed ($p > 0.05$) (Fig. 3B).

DISCUSSION

Skeletal muscle is known to possess multiple stem/progenitor cell populations that are associated with muscle development, maintenance, and regeneration (13,18). Upon purification, muscle stem/progenitor cells in general display more robust myogenic regenerative capacities than unpurified muscle cells in animal disease models, suggesting the advantage of isolating stem cells for therapeutic purposes (6,10,13,20). More recent data have shown that there is a functional heterogeneity in myogenesis even among the muscle precursor cell pool (2).

In the present study, we demonstrated that even after in vitro expansion and cryopreservation, primary human muscle cell cultures include various subpopulations, as indicated by expression of diverse cell lineage markers. Using a modified collection of cell lineage markers (CD45, CD56, CD146, and UEA-1R), we identified and purified to homogeneity four distinct cell populations from cryo-hPSMCs, including two stem cell subpopulations: PSCs ($CD146^+/CD45^-CD56^-UEA\text{-}1R^-$) and MECs ($CD56^+CD146^+UEA\text{-}1R^+/CD45^-$) (6,20,21). Newly sorted MECs, PSCs, ECs, and Myo cells were immediately transplanted into the cardiotoxin-injured skeletal muscles of SCID mice to examine the preservation of their myogenic potential after FACS, all of which regenerated human spectrin-positive myofibers in the injured mouse

skeletal muscles. Quantitative analyses using sorted subpopulations that were minimally expanded in culture showed that the MECs displayed the highest muscle regenerative capacity among all cell subsets tested, and the PSCs were superior to myoblasts and unpurified cryo-hPSMCs.

These results were consistent with our previous observations from injections of cells isolated from fresh skeletal muscle biopsies (6,20). Taken together, our results suggest the presence of distinct subpopulations of highly myogenic stem/progenitor cells within culture-expanded, cryopreserved hPSMCs and support the feasibility of further purifying stem cell fractions from these unpurified cryopreserved human cells. Most importantly, these findings infer the practicability of prospective isolation of myogenic stem/progenitor cell populations from banked human skeletal muscle cells, highlighting a new technology to further enhance the availability and efficacy of cell-mediated therapies (9).

ACKNOWLEDGMENTS: This work was supported in part by grants to J.H from the National Institutes of Health (R01 DE013420-09) and the Department of Defense (W81XWH-09-1-0658) and from the William F. and Jean W. Donaldson Endowed Chair at the Children's Hospital of Pittsburgh, the Henry J. Mankin Endowed Chair for Orthopaedic Research at University of Pittsburgh, and by a grant to B.P. from the National Institutes of Health (R21 HL083057-01A2). The authors also wish to thank Allison Logar for her excellent technical assistance on the flow cytometry and the cell sorting and James H. Cummins for his editorial assistance in the preparation of this manuscript. The following author contributions are recognized: conception and design, collection and/or assembly of data, data analysis and interpretation, manuscript writing (B.Z.); conception and design, collection and/or

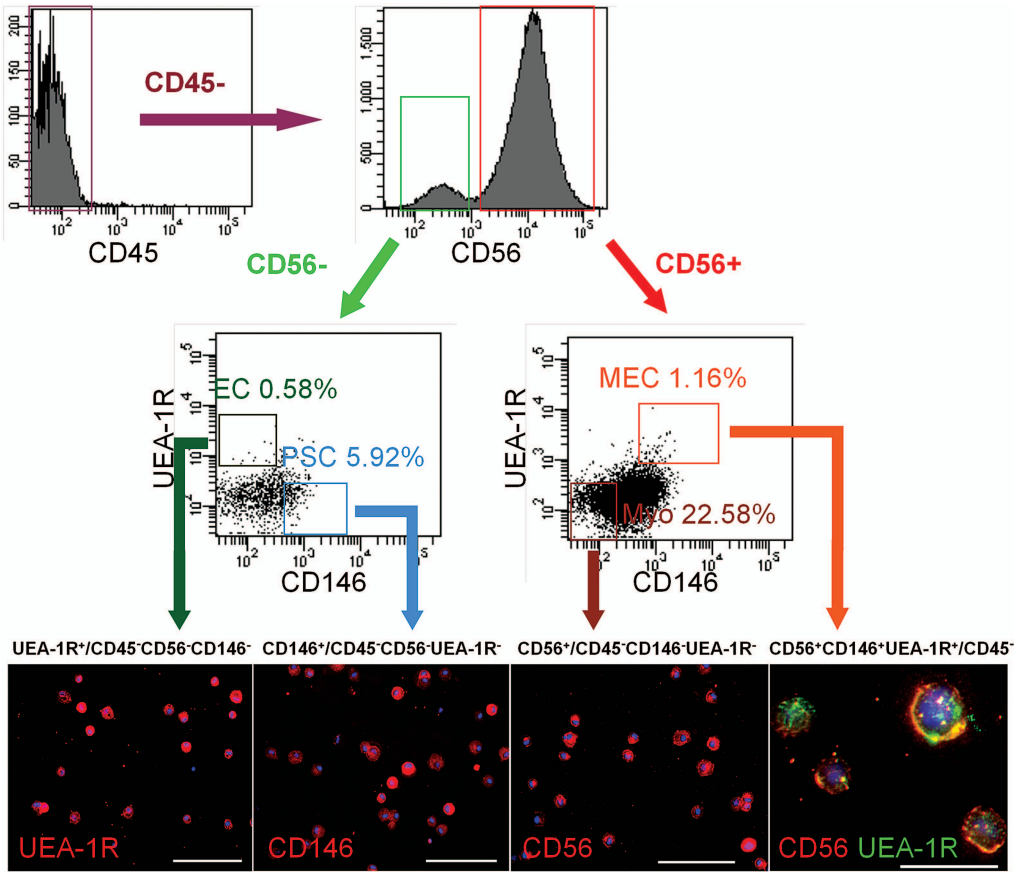

Figure 2. Identification and purification of myogenic stem cells within cryo-hPSMCs. After excluding $CD45^+$ hematopoietic cells, $CD45^-$ cells were separated based on CD56 expression. $CD56^+$ and $CD56^-$ populations were further gated on UEA-1R by CD146 to identify and/or sort four distinct cell populations: myogenic endothelial cells (MECs) ($CD56^+UEA\text{-}1R^+CD146^+/CD45^-$), myoblasts (Myos) ($CD56^+/CD45^-CD146^-UEA\text{-}1R^-$), perivascular stem cells (PSCs) ($CD146^+/CD45^-CD56^-UEA\text{-}1R^-$), and endothelial cells (ECs) ($UEA\text{-}1R^+/CD45^-CD56^-CD146^-$). The purities of the sorted populations were $90.73 \pm 4.82\%$, $92.94 \pm 1.23\%$, 93.86 ± 1.72, and 94.9 ± 0.64, respectively. Immunocytochemistry confirmed the expression of key cell lineage makers by freshly sorted cells: UEA-1R, CD146, and/or CD56. Nuclei were stained blue with DAPI. Scale bars: 100 µm; CD56/UEA-1R double staining: 20 µm.

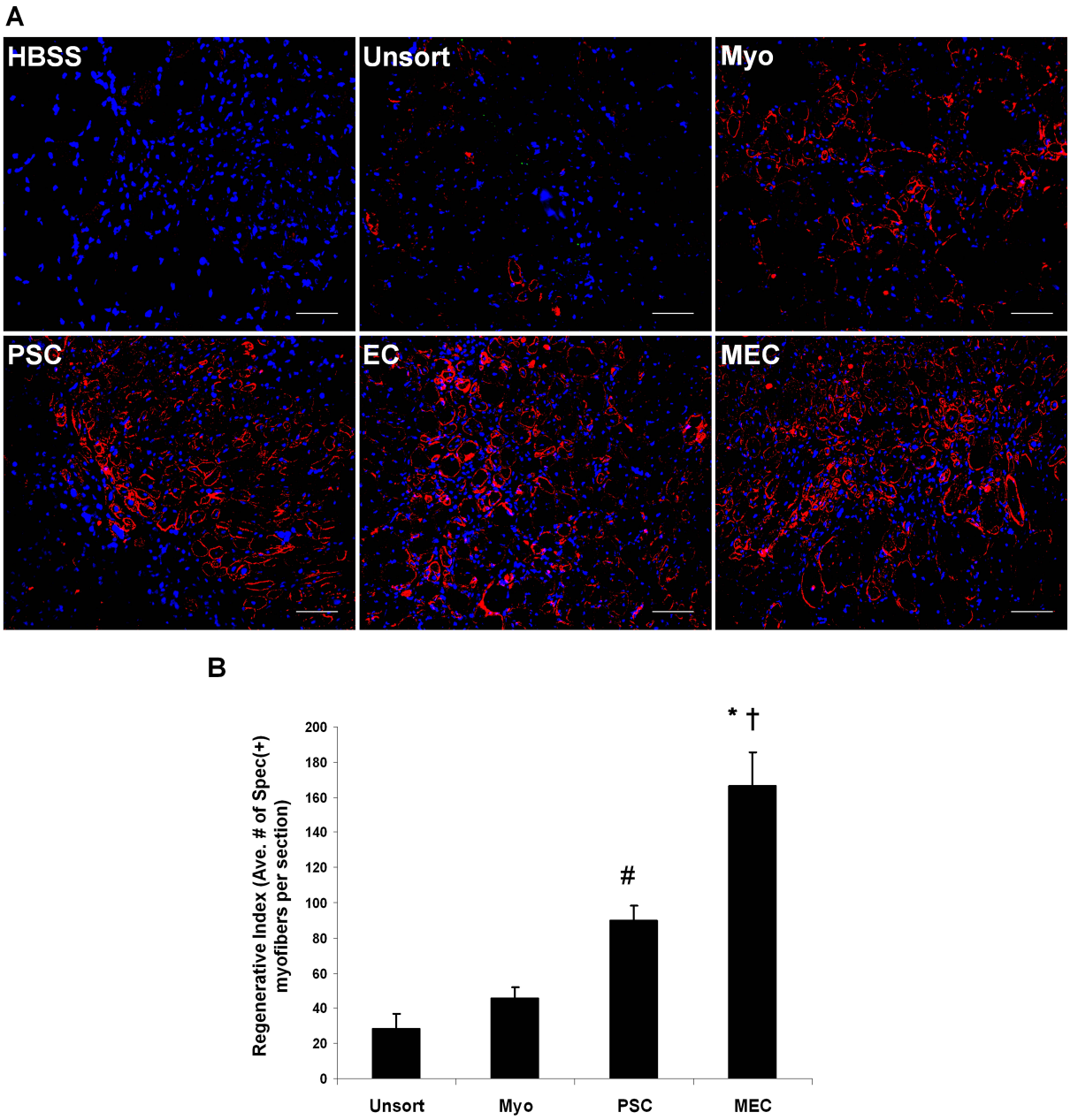

Figure 3. Comparison of myogenic regenerative capacities in vivo. (A) Representative pictures of regenerating human spectrin-positive myofibers in cardiotoxin-injured mouse skeletal muscles transplanted with newly sorted cell fractions from a single donor-derived cryo-hPSMC culture, including myogenic endothelial cells (MECs), perivascular stem cells (PSCs), endothelial cells (ECs), and myoblasts (Myos). Unsorted cryo-hPSMCs (Unsort) and HBSS were injected as treated and untreated controls respectively. Original magnification: 200×; scale bars: 50 µm. (B) Quantitative analyses of the myogenic regenerative capacities of sorted stem/progenitor cell populations. Fifty thousand cells from each cell fraction that was minimally expanded in culture were injected. Quantitative analyses of spectrin-positive human skeletal myofibers on tissue sections revealed that MECs mediated the highest myogenic regeneration among all four cell fractions tested (*$p < 0.001$ vs. Myo and Unsort; †$p = 0.004$ vs. PSC). Injection of PSCs regenerated more human myofibers than injections of Myos ($p > 0.05$) and Unsort (#$p = 0.017$). Finally, Myos displayed a trend of higher myogenic capacity than Unsort, but no significant difference was observed ($p > 0.05$).

assembly of data, data analysis and interpretation, manuscript writing (C.-W.C.); collection and/or assembly of data, data analysis, and interpretation (G.L.); collection and/or assembly of data, data analysis, and interpretation (S.D.T.); collection and/or assembly of data, data analysis and interpretation (M.P.); conception and design, financial support, data analysis and interpretation (B.P.); conception and design, financial support, data analysis and interpretation, manuscript writing, final approval of manuscript (J.H.). Dr. Johnny Huard has received remuneration from Cook Myosite, Inc. for consulting services and for royalties received from technology licensing during the period that the above research was performed. All other authors declare no conflicts of interst.

REFERENCES

1. Carr, L. K.; Steele, D.; Steele, S.; Wagner, D.; Pruchnic, R.; Jankowski, R.; Erickson, J.; Huard, J.; Chancellor, M. B. 1-year follow-up of autologous muscle-derived stem cell injection pilot study to treat stress urinary incontinence. Int. Urogynecol. J. Pelvic Floor Dysfunct. 19(6): 881–883; 2008.
2. Cerletti, M.; Jurga, S.; Witczak, C. A.; Hirshman, M. F.; Shadrach, J. L.; Goodyear, L. J.; Wagers, A. J. Highly efficient, functional engraftment of skeletal muscle stem cells in dystrophic muscles. Cell 134(1):37–47; 2008.
3. Chen, C. W.; Montelatici, E.; Crisan, M.; Corselli, M.; Huard, J.; Lazzari, L.; Péault, B. Perivascular multilineage progenitor cells in human organs: regenerative units, cytokine sources or both? Cytokine Growth Factor Rev. 20(5–6):429–434; 2009.
4. Chen, C. W.; Okada, M.; Tobita, K.; P?ault, B.; Huard, J. Purified human muscle-derived pericytes support formation of vascular structures and promote angiogenesis after myocardial infarction. Circulation 120(18 Suppl.):S1053; 2009.
5. Collins, C. A.; Zammit, P. S.; Ruiz, A. P.; Morgan, J. E.; Partridge, T. A. A population of myogenic stem cells that survives skeletal muscle aging. Stem Cells 25(4):885–894; 2007.
6. Crisan, M.; Yap, S.; Casteilla, L.; Chen, C. W.; Corselli, M.; Park, T. S.; Andriolo, G.; Sun, B.; Zheng, B.; Zhang, L.; Norotte, C.; Teng, P. N.; Traas, J.; Schugar, R.; Deasy, B. M.; Badylak, S.; Buhring, H. J.; Giacobino, J. P.; Lazzari, L.; Huard, J.; Péault, B. A perivascular origin for mesenchymal stem cells in multiple human organs. Cell Stem Cell 3(3):301–313; 2008.
7. Dellavalle, A.; Sampaolesi, M.; Tonlorenzi, R.; Tagliafico, E.; Sacchetti, B.; Perani, L.; Innocenzi, A.; Galvez, B. G.; Messina, G.; Morosetti, R.; Li, S.; Belicchi, M.; Peretti, G.; Chamberlain, J. S.; Wright, W. E.; Torrente, Y.; Ferrari, S.; Bianco, P.; Cossu, G. Pericytes of human skeletal muscle are myogenic precursors distinct from satellite cells. Nat. Cell Biol. 9(3):255–267; 2007.
8. Drowley, L.; Okada, M.; Payne, T. R.; Botta, G. P.; Oshima, H.; Keller, B. B.; Tobita, K.; Huard, J. Sex of muscle stem cells does not influence potency for cardiac cell therapy. Cell Transplant. 18(10):1137–1146; 2009.
9. Hirt-Burri, N.; de Buys Roessingh, A. S.; Scaletta, C.; Gerber, S.; Pioletti, D. P.; Applegate, L. A.; Hohlfeld, J. Human muscular fetal cells: A potential cell source for muscular therapies. Pediatr. Surg. Int. 24(1):37–47; 2008.
10. Jankowski, R. J.; Deasy, B. M.; Huard, J. Muscle-derived stem cells. Gene Ther. 9(10):642–647; 2002.
11. Okada, M.; Payne, T. R.; Zheng, B.; Oshima, H.; Momoi, N.; Tobita, K.; Keller, B. B.; Phillippi, J. A.; Péault, B.; Huard, J. Myogenic endothelial cells purified from human skeletal muscle improve cardiac function after transplantation into infarcted myocardium. J. Am. Coll. Cardiol. 52(23):1869–1880; 2008.
12. Oshima, H.; Payne, T. R.; Urish, K. L.; Sakai, T.; Ling, Y.; Gharaibeh, B.; Tobita, K.; Keller, B. B.; Cummins, J. H.; Huard, J. Differential myocardial infarct repair with muscle stem cells compared to myoblasts. Mol. Ther. 12(6):1130–1141; 2005.
13. Péault, B.; Rudnicki, M.; Torrente, Y.; Cossu, G.; Tremblay, J. P.; Partridge, T.; Gussoni, E.; Kunkel, L. M.; Huard, J. Stem and progenitor cells in skeletal muscle development, maintenance, and therapy. Mol. Ther. 15(5):867–877; 2007.
14. Pisani, D. F.; Dechesne, C. A.; Sacconi, S.; Delplace, S.; Belmonte, N.; Cochet, O.; Clement, N.; Wdziekonski, B.; Villageois, A. P.; Butori, C.; Bagnis, C.; Di Santo, J. P.; Kurzenne, J. Y.; Desnuelle, C.; Dani, C. Isolation of a highly myogenic CD34-negative subset of human skeletal muscle cells free of adipogenic potential. Stem Cells 28(4):753–764; 2010.
15. Rousseau, J.; Dumont, N.; Lebel, C.; Quenneville, S. P.; Côté, C. H.; Frenette, J.; Tremblay, J. P. Dystrophin expression following the transplantation of normal muscle precursor cells protects mdx muscle from contraction-induced damage. Cell Transplant. 19(5):589–596; 2010.
16. Seidel, M.; Borczyńska, A.; Rozwadowska, N.; Kurpisz, M. Cell-based therapy for heart failure: Skeletal myoblasts. Cell Transplant. 18(7):695–707; 2009.
17. Sherman, W.; He, K. L.; Yi, G. H.; Wang, J.; Harvey, J.; Lee, M. J.; Haimes, H.; Lee, P.; Miranda, E.; Kanwal, S.; Burkhoff, D. Myoblast transfer in ischemic heart failure: Effects on rhythm stability. Cell Transplant. 18(3):333–341; 2009.
18. Sherwood, R. I.; Christensen, J. L.; Conboy, I. M.; Conboy, M. J.; Rando, T. A.; Weissman, I. L.; Wagers, A. J. Isolation of adult mouse myogenic progenitors: Functional heterogeneity of cells within and engrafting skeletal muscle. Cell 119(4):543–554; 2004.
19. Torrente, Y.; Belicchi, M.; Marchesi, C.; Dantona, G.; Cogiamanian, F.; Pisati, F.; Gavina, M.; Giordano, R.; Tonlorenzi, R.; Fagiolari, G.; Lamperti, C.; Porretti, L.; Lopa, R.; Sampaolesi, M.; Vicentini, L.; Grimoldi, N.; Tiberio, F.; Songa, V.; Baratta, P.; Prelle, A.; Forzenigo, L.; Guglieri, M.; Pansarasa, O.; Rinaldi, C.; Mouly, V.; Butler-Browne, G. S.; Comi, G. P.; Biondetti, P.; Moggio, M.; Gaini, S. M.; Stocchetti, N.; Priori, A.; D'Angelo, M. G.; Turconi, A.; Bottinelli, R.; Cossu, G.; Rebulla, P.; Bresolin, N. Autologous transplantation of muscle-derived CD133$^+$ stem cells in Duchenne muscle patients. Cell Transplant. 16(6):563–577; 2007.
20. Zheng, B.; Cao, B. H.; Crisan, M.; Sun, B.; Li, G. H.; Logar, A.; Yap, S.; Pollett, J. B.; Drowley, L.; Cassino, T.; Gharaibeh, B.; Deasy, B. M.; Huard, J.; Péault, B. Prospective identification of myogenic endothelial cells in human skeletal muscle. Nat. Biotechnol. 25(9):1025–1034; 2007.
21. Zheng, B.; Li, G. H.; Logar, A.; Péault, B.; Huard, J. Identification of CD56+CD146+UEA-1+ cell population within cryopreserved human skeletal muscle cells which endowed with a high myogenic potential in vivo. The Orthopaedic Research Society (ORS) 54th Annual Meeting, San Francisco, CA; 2008.

Blank Page

Appendix 6

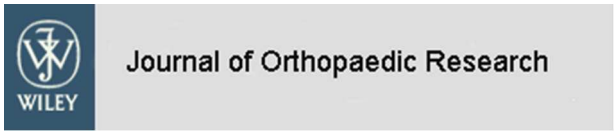

Human Myogenic Endothelial Cells Exhibit Chondrogenic and Osteogenic Potentials at the Clonal Level

Journal:	*Journal of Orthopedic Research*
Manuscript ID:	JOR-12-0639
Wiley - Manuscript type:	Research Article
Date Submitted by the Author:	29-Aug-2012
Complete List of Authors:	Zheng, Bo; Oregon Health & Science University, Li, Guangheng; University of Pittsburgh, Orthopedic Surgery Chen, William; University of Pittsburgh, Orthopedic Surgery; University of Pittsburgh, Bioengineering Deasy, Bridget; University of Pittsburgh, Orthopedic Surgery Pollett, Jonathan; Allegheny General Hospital, Cardiology Sun, Bin; University of Pittsburgh, Vascular Medicine Institute Drowley, Lauren; AstraZeneca, Gharaibeh, Burhan; University of Pittsburgh, Orthopedic Surgery Usas, Arvydas; University of Pittsburgh, Orthopedic Surgery Péault, Bruno; University of Edinburgh, Queens Medical Research Institute Huard, Johnny; Stem Cell Research Center, Dept. of Orthopaedic Surgery;
Keywords:	myogenic endothelial cells , muscle stem cells, clonal analysis, osteogenesis, chondrogenesis

Human Myogenic Endothelial Cells Exhibit Chondrogenic and Osteogenic Potentials at the Clonal Level

Bo Zheng[1,2], Guangheng Li[1,2,*], William CW Chen[1,3,*], Bridget M Deasy[1,2], Jonathan B Pollett[1], Bin Sun[1,4], Lauren Drowley[1], Burhan Gharaibeh[1], Arvydas Usas[1,2], Bruno Péault[1,4,5,6,7], Johnny Huard[1,2,5]

[1]Stem Cell Research Center, University of Pittsburgh School of Medicine

[2]Department of Orthopaedic Surgery, University of Pittsburgh School of Medicine

[3]Department of Bioengineering, University of Pittsburgh Swanson School of Engineering

[4]Department of Pediatrics, Children's Hospital of Pittsburgh of UPMC

[5]McGowan Institute for Regenerative Medicine, University of Pittsburgh

[6]David Geffen School of Medicine, University of California at Los Angeles

[7]Centre for Cardiovascular Science and MRC Centre for Regenerative Medicine, University of Edinburgh, UK

*These authors contributed equally to this work

Correspondence to:

Johnny Huard, PhD

Stem Cell Research Center, Department of Orthopaedic Surgery, School of Medicine, University of Pittsburgh, Bridgeside Point II, Suite 206, 450 Technology Drive, Pittsburgh, PA 15219

TEL: 1-412-648-2798

FAX: 1-412-648-4066

Email: jhuard@pitt.edu

Running Title: Clonal Myogenic Endothelial Cells Exhibit Osteogenic and Chondrogenic Potential

Key words: myogenic endothelial cells, muscle stem cells, clonal analysis, osteogenesis, chondrogenesis

Abstract

We have previously reported the high regenerative potential of murine muscle-derived stem cells (mMDSCs) that are capable of differentiating into multiple mesodermal cell lineages, including myogenic, endothelial, chondrocytic, and osteoblastic cells. Recently we described a putative human counterpart of mMDSCs, the myogenic endothelial cells (MECs), in adult human skeletal muscle, which efficiently repair/regenerate the injured and dystrophic skeletal muscle as well as the ischemic heart in animal disease models. Nevertheless it remained unclear whether human MECs, at the clonal level, preserve mMDSC-like chondrogenic and osteogenic potentials and classic stem cell characteristics including high proliferation and resistance to stress. Herein we demonstrated that MECs, sorted from fresh postnatal human skeletal muscle biopsies, can be grown clonally and exhibit robust resistance to oxidative stress with no tumorigeneity. MEC clones were capable of differentiating into chondrocytes and osteoblasts under inductive conditions in vitro and participated in cartilage and bone formation in vivo. Additionally, adipogenic and angiogenic potentials of clonal MECs (cMECs) were observed. Overall, our study showed that cMECs not only display typical properties of adult stem cells but also exhibit chondrogenic and osteogenic capacities in vitro and in vivo, suggesting their potential applications in articular cartilage and bone repair/regeneration.

INTRODUCTION

Recent studies suggest that stem/progenitor cell populations other than satellite cells repair/regenerate skeletal muscle.[1-7] Our group previously reported that murine muscle-derived stem cells (mMDSCs), a unique population of myogenic stem cells isolated from the slowly adhering fraction of primary muscle cells by the "preplate" technique, proliferate long-term, self-renew, and differentiate into diverse cell lineages.[8-13] mMDSCs express markers typically associated with stem cells, including CD34 and Sca-1. However, expression of these markers in mMDSCs is highly influenced by extended cell culture, leading to the difficulties of finding a valid marker profile for prospective identification and purification of native mMDSCs.

Recently, we have prospectively purified by cell sorting a unique stem cell population associated with the vasculature in the human skeletal muscle.[14] These myogenic endothelial cells (MECs) ($CD34^+/CD56^+/CD144^+/CD45^-$), which presumably represent the human counterpart of mMDSCs, can undergo long-term proliferation, multi-lineage differentiation, and repair skeletal and cardiac muscles with high efficiency, similar to mMDSCs.[14, 15] Although MECs have been characterized in our prior studies,[14, 15] the true capacity of these cells to function as multi-lineage regenerative units has not yet been fully disclosed, especially in chondrogenesis and osteogenesis. One major limitation in characterizing their multipotent potential is the likely heterogeneous nature in stemness. In the present study, we investigated whether MECs, freshly sorted from adult human skeletal muscle based on their unique cell surface marker profile, preserve chondrogenic and osteogenic potentials at the clonal level.

Our results showed that MEC clones possess stem cell characteristics equivalent to mMDSCs, including long-term proliferation with no karyotypic abnormalities and high resistance to stress. The robust ability of clonal MECs (cMECs) to differentiate into

chondrogenic and osteogenic cell lineages in vitro and in vivo was demonstrated. This clonal study of human MECs highlights their regenerative potential for integrated musculoskeletal repair and regeneration.

METHODS

Human Muscle Biopsy Procurement and Animal Research

The procurement of adult human skeletal muscle biopsies from the National Disease Research Interchange (Philadelphia, PA, USA) was approved by the Institutional Review Board at the University of Pittsburgh Medical Center (UPMC). After procurement, biopsies were immediately transported to our laboratory in Hanks' Balanced Salt Solution (HBSS) (Invitrogen, Grand Island, NY, USA) on ice. Animal experiments were approved by the Animal Research and Care Committee of the Children's Hospital of Pittsburgh of UPMC (Protocol #42-04).

Cell Isolation and Cloning

Muscle biopsies were finely minced and digested with collagenases and dispase to obtain single cell suspension as previously described.[14] Cells were immunofluorescently labeled and subject to cell sorting.[14] Details are documented in Supplementary Material.

Gene Expression Profiling

Total RNA was extracted from the 1×10^6 cells using Nucleospin RNA kit (Clontech, Mountain View, CA, USA). Details are listed in Supplementary Material. Primer sequences used for PCR are listed in Supplemental Table 1.

Cell Proliferation Analysis and Cell Survival under Oxidative Stress

For the single cell proliferation assay, cMECs were transduced with lentiviral eGFP reporter and further sorted to homogeny by FACS as previously reported.[16] To test the capacity of cMECs against oxidative stress, MEC clones were plated onto collagen-coated plates and

cultured with proliferation medium containing 400μM hydrogen peroxide (H_2O_2) and 2μl propidium iodide (1:500, PI, Sigma-Aldrich). Bright-field and fluorescent images were taken in a time-lapsed microscopic imaging system. Details are summarized in Supplementary Material.

Tumorigenesis Assay and Karyotype Analysis

To examine the tumorigenic property of cMECs in vitro, we monitored the growth of cMECs plated at different densities on 1% agar in proliferation medium. For karyotype analysis, cMEC clones were cultured for 8 weeks and harvested. The cell pellets were processed for chromosome analysis. Detail procedures are listed in Supplementary Material.

Chondrogenic and Osteogenic Differentiation in Culture and in Vivo

The details of in vitro chondrogenesis and osteogenesis are documented in Supplementary Material. To track donor cells after implantation, cMECs and unsorted cells were co-transduced with retroviral nuclear LacZ (nLacZ) reporter and subsequently with retroviral BMP4 gene as previously reported.[17] After expansion, 5×10^6 cells were seeded onto a 6×6-mm piece of Gelfoam, incubated overnight, and implanted into the gluteofemoral muscle pockets of SCID mice (8-week-old male; The Jackson Laboratory, Bar Harbor, ME, USA).

Adipogenesis in Culture and Angiogenesis in Vitro/in Vivo

The details of in vitro adipogenesis and angiogenesis as well as in vivo angiogenesis are summarized in Supplementary Material.

RESULTS

Isolation and characterization of myogenic endothelial cell clones

MECs ($CD34^+CD56^+CD144^+CD45^-$) were isolated by fluorescence activated cell sorting (FACS) from dissociated muscle biopsies as previously reported.[18] Single sorted MEC was then automatically seeded by the autoclone system of the FACSAria sorter into each well of a

collagen-coated 96-well plate (seeding density: 1 cell/well). Wells that did not contain exactly 1 cell/well were excluded from the study. A total of six MEC clones from 2 distinct muscle biopsies were obtained from 576 single-cell seeded wells. The average cloning efficiency was 1.04 %, with MECs of donor #1 and #2 having the cloning efficiency of 0.69% and 1.39% respectively. Clonal MECs (cMECs) at passage 6-15 were analyzed for their phenotypes, single cell proliferation, and multi-lineage differentiation capacity and subsequently used for transplantation experiments. Six MEC clones were individually analyzed for gene expression by RT-PCR. The results showed that genes of the lineage-specific markers were expressed in all clones at similar levels (**Figure 1A**). Notably, in addition to the late myogenic markers: desmin, m-cadherin, and CD56, we also detected expression of the early myogenic transcription factors, Pax3, Pax7, and Myf5 in all 6 clones (**Figure 1A**).

Single cells derived from MEC clones undergo clonogenic proliferation

To precisely quantitate the clonogenic potential and long-term proliferation of cMECs in culture, we performed sub-cloning analysis. MEC clones were lentivirally transduced at passage 15 to express enhanced green fluorescence protein (eGFP). Sub-cloning analysis was performed with eGFP+ cMECs individually sorted into each well of a 384-well plate by the FACSAria autoclone system (**Supplemental Figure 1**). Approximately 1/3 of all wells received exactly one cell per well; the remaining 2/3 received none. Proliferation of sub-cloned cMECs was monitored by a time-lapsed microscopic imaging system. The results showed that 73% of sub-cloned cMECs expanded to more than 8 cells, 14% divided into 2-4 cells, 12% did not divide, and 1% eventually died (**Figure 1B**). Cell doubling time and averaged cell division time were 28.1 ± 5.5 hours and 16.8 ± 2.1 hours respectively (mean±SD, n=4) (**Figure 1C**). A video of single sub-cloned cMEC proliferation was presented (**Supplemental Video**).

Gene expression, tumorigenesis, karyotype analysis, and resistance to oxidative stress

Gene expression analyses revealed that cMECs express genes associated with undifferentiated cells (GABRB3 and DNMT3B), and the stemness gene, IL6ST when compared to the unsorted human primary skeletal muscle cells (hPSMCs) (**Supplemental Table 2**). In contrast, hPSMCs expressed genes associated with myogenic differentiation including: Runx-2, Noggin, MYF5, MyoD1, Des and Actc (**Supplemental Table 2**). To assess their tumorigenesis, cMECs cultured for 2 months were analyzed for anchorage independent growth, a hallmark of transformed tumor cells. Cells were plated on a layer of 1% agar at different densities, and colony growth was scored at 2 and 3 weeks post-seeding. Non-adherent cell growth was only observed when cMECs were plated at a very high density of 2.5×10^4 cells/cm^2. Cells plated at low densities (25 and 250 cells/cm^2) and regular culture density (2,500 cells/cm^2) did not grow in an anchorage-independent manner and eventually died (**Supplemental Figure 2**). Furthermore, tumorigenesis in vivo was examined by implanting expanded cMECs into skeletal muscle pockets in the hind limbs of SCID mice. No evidence of tumor growth at 12 weeks post-transplantation was observed physically and histologically (data not shown). Finally, karyotype analyses revealed little-to-no structural (data not shown) and numerical (**Figure 1D**) abnormalities in the chromosome of all long-term cultured MEC clones.

Non-clonal MECs displayed a superior regenerative capacity in both skeletal and cardiac muscles when compared to myoblasts and/or endothelial cells, a behavior hypothesized to be associated with MECs' ability to withstand oxidative stress.[18, 19] Whether cMECs retain the resistance to oxidative stress was examined by culturing the cells in 400μM H_2O_2 and analyzing their survival every 12 hours over a 72-hour period.[20] Among five MEC clones tested, four withstood the oxidative stress to a similar or better level as non-clonal MECs, which had a

survival rate of 30.6% at 72 hours (**Supplemental Table 3**). This result suggested that cMECs in general have high resistance to extended exposure of oxidative stress.

cMECs undergo chondrogenic differentiation in vitro and in vivo

To induce chondrogenic differentiation, cMECs and hPSMCs were pellet-cultured in chondrogenic induction medium supplemented with BMP4 and TGF-β3 for up to 3 weeks. Gross morphology of pellets was compared (**Figure 2A**). The average volume of the pellets formed by cMECs was significantly larger than those formed by hPSMCs at day 7 and 21 (n=3 per group, $p<0.01$, two-tailed unpaired t test) (**Figure 2B**). Pellets were then sectioned and stained specifically for the cartilaginous matrix with Alcian blue (pH=1). cMEC pellets displayed denser blue staining when compared to hPSMC ones at all 3 time points, suggesting a robust chondrogenic potential of cMECs (**Figure 2C**). To investigate their chondrogenic potential in vivo, we co-transduced cMECs with retroviruses encoding BMP4 and nuclear LacZ (nLacZ) genes. The transduction efficiency was near 80%, revealed by the positive β-gal staining (blue) localized to the nuclei of cMECs (**Figure 2D.a**). The presence of round chondrocytes with LacZ+ nuclei (**Figure 2D.b**) and positive immunostaining for collagen type II (**Figure 2D.c**) were observed within the implanted scaffold. A few collagen type II-positive cells co-expressed β-galactosidase, confirming the presence of functional chondrogenic cells originated from donor cMECs (**Figure 2D.d**). Together these data suggest that cMECs were able to differentiate into chondrocytes in vitro and in vivo, albeit to a different extent.

cMECs undergo osteogenic differentiation in vitro and in vivo

To assay the production of mineralized extracellular matrix, cMECs were pellet-cultured in osteogenic induction medium supplemented with BMP4. Osteogenic differentiation was revealed by von Kossa staining after 7 and 21 days in culture. Compared with hPSMCs, pellets

formed by cMECs exhibited more intense mineralization (**Figure 3A**). cMEC pellets maintained in control proliferation medium with no BMP4 remained negative for von Kossa staining, suggesting no spontaneous osteogenic differentiation of cMECs without a proper inductive signal (**Figure 3A**). Mineralization within the pellet was detected by micro-computerized tomography (μCT) at 7 and 21 days (**Figure 3B**). μCT images showed that cMECs produced a significantly higher volume (**Figure 3C**) and density (**Figure 3D**) of mineralized matrix when compared to hPSMCs at both time points (n=3 per group, both $p<0.01$, two-tailed unpaired t test).

To evaluate their osteogenic potential in vivo, cMECs or hPSMCs were co-transduced with retroviruses encoding nLacZ and BMP4 genes and seeded onto a gelatin sponge (5×10^6 cells), followed by implantation into an intramuscular pocket of SCID mice. μCT imaging revealed that transduced cMECs form dense ectopic bone consistently at 2, 4, 8 and 16 weeks post-implantation while transduced hPSMCs fail to form any organized structure (**Figure 3E**). A significant difference in mineralized tissue volume between the two groups was observed at all time points (n=3 per group, all $p<0.01$, two-tailed unpaired t test) (**Figure 3F**). To track donor cMECs undergoing osteogenic differentiation, β-gal/eosin co-staining was performed on the sections of the cMEC-formed ectopic bone structure (**Figure 3G.a**). Osteogenic differentiation of donor cMECs was also confirmed by co-localization of the positive immunohistochemical signals of nLacZ and osteocalcin (**Figure 3G.b**) as well as the positive immunofluorescent signals of β-galactosidase and osteocalcin (**Figure 3G.c)**. Collectively, cMECs exhibited robust osteogenic differentiation capacity under appropriate inductive signals in vitro and in vivo.

cMECs differentiate into adipocytes and remain angiogenic in vitro and in vivo

To understand whether cMECs are able to differentiate into other mesodermal cell lineages, we examined their adipogenic potential in vitro. cMECs cultured in adipogenic induction medium were subsequently stained positive by Oil Red O, revealing the accumulated cytoplasmic lipid droplets **(Supplemental Figure 3A)**. cMECs maintained in control medium were not adipogenic **(Supplemental Figure 3B)**.

To investigate the angiogenic capacity of cMECs, Matrigel culture was used to observe the formation of capillary-like structures.[21] After incubation for 16 hours, cMECs cultured in Matrigel formed capillary-like network **(Supplemental Figure 3C)** while hPSMCs failed to form similar structures under the same condition **(Supplemental Figure 3D)**. Next we subcutaneously implanted Matrigel plugs encapsulating 1.0×10^6 cMECs, hPSMCs, or no cells into the back of SCID mice (n=4 per group). Capillary formation within the implanted plug was determined by anti-CD31 immunostaining **(Supplemental Figure 3E-G)**. The cMEC-plugs displayed significantly higher capillary density than the hPSMC-plugs ($p<0.01$, two-tailed unpaired t test) **(Supplemental Figure 3H)**. Implants with no cells exhibited no presence of CD31-positive structures. To confirm the human origin of the newly formed microvessels within the Matrigel plugs, Lamin A/C, a human nuclear specific antigen, was used to identify donor cMECs. A fraction of microvascular endothelial cells within the cMEC plugs indeed co-expressed CD31 and Lamin A/C, indicative of their human origin **(Supplemental Figure 3I-L).** These results suggest that human cMECs are not only capable of differentiating into major mesenchymal cell lineages but also retain their angiogenic capacity and participate in neovascularization in vivo after long-term culture.

DISCUSSION

Our group has previously demonstrated that mMDSCs differentiate into diverse cell lineages including bone, cartilage, muscle, endothelial, and blood cells.[8-11, 13, 22] mMDSCs repair skeletal and cardiac muscles more efficiently than myoblasts and vascular endothelial cells.[9, 11] Recently we have purified myogenic endothelial cells (MECs) from adult human skeletal muscle that co-express cell surface markers of both myogenic and endothelial cell lineages and exhibit superior regenerative capacities in injured skeletal and cardiac muscle, similar to mMDSCs.[14, 15] Nevertheless, the osteogenic and chondrogenic potentials of MECs were not fully examined at the clonal level. The present study employed the clonogenic assay to evaluate the osteogenic and chondrogenic capacities of single MEC and further characterize their stem cell properties.

We herein established a protocol that enable us to prospectively purify MEC clones from fresh human muscle biopsies directly by FACS sorting, using the previously reported combination of cell surface markers for MEC isolation.[14] RT-PCR analysis revealed that all of the MEC clones expressed genes of myogenic (desmin, CD56, Pax3, Pax7, m-cadherin and MYf5), endothelial (CD34, CD144 and vWF), smooth muscle/vascular mural (α-smooth muscle actin, PDGFR-β, NG2 and CD146), and mesenchymal stem/stromal (CD90 and CD105) cell lineages, showing consistency between clones from the two donor sources. cMECs displayed robust multipotency in vitro and in vivo, including chondrogenesis, osteogenesis, adipogenesis and angiogenesis/vasculogenesis, in addition to myogenesis reported previously.[14] Nevertheless, cMECs could not differentiate into hematopoietic cells in vitro under inductive conditions, even with the presence of OP9 stromal cells (data not shown).

MEC clones were shown to resist oxidative stress efficiently, to a similar or better level of that of non-clonal MECs. cMECs up-regulated genes associated with early progenitor cells, GABRB3 and DNMT3B, and a gene correlated to stemness, IL6ST. When compared to hPSMC,

cMECs expressed much lower level of genes associated with advanced myogenic differentiation, including Runx-2, Noggin, MyoD1, MYF5, Desmin and α-actin. The tumorigenic assay and karyotype analysis revealed no tumorigeneity in long-term expanded cMECs, suggesting the safety of this novel multi-lineage stem cell population in regenerative applications.

Our previous studies of mMDSCs indicated that these cells reside in areas that are normally occupied by capillaries running alongside myofibers.[8, 9] Similarly, MECs are associated with the vasculature in human skeletal muscle, specifically the capillaries located within the interstitial space between myofibers. The hypothesis that MECs represent a developmental intermediate between myogenic and endothelial cells was further supported by the evidence suggesting that muscle satellite cells and endothelial cells are close neighbors and privileged developmental partners.[23] Despite the unclear developmental relationship between MECs and other blood-vessel-associated stem/progenitor cells such as mesoangioblasts[24-26] and pericytes[16, 27], our data suggest that cMECs are indeed one of the multi-lineage mesodermal stem cell populations residing in a vascular niche within the adult skeletal muscle[1, 28, 29] and likely represent a human counterpart of mMDSCs.[30] Overall, these cells not only represent a promising cell source for an integrative application in musculoskeletal repair but also provide more evidence to the involvement of vasculature in post-natal musculoskeletal regeneration.

ACKNOWLEDGEMENTS

The authors wish to thank Alison Logar for her expert assistance in flow cytometry and James H. Cummins for his editorial assistance. This work was supported in part by grants from the National Institutes of Health (R01-AR049684; RO1-DE13420-06; IU54AR050733-01) and the Department of Defense (AFIRM grant W81XWH-08-2-0032) and by the William F. and Jean W. Donaldson Endowed Chair at the Children's Hospital of Pittsburgh, the Henry J. Mankin

Endowed Chair at the University of Pittsburgh, the Orris C. Hirtzel and Beatrice Dewey Hirtzel Memorial Foundation, and the Lemieux Foundation at the University of Pittsburgh. Johnny Huard received remuneration as a consultant for Cook MyoSite, Inc. during the period of this investigation. No other authors have any conflict of interest to disclose.

REFERENCES

1. Peault B, Rudnicki M, Torrente Y, Cossu G, Tremblay JP, Partridge T, et al. Stem and Progenitor Cells in Skeletal Muscle Development, Maintenance, and Therapy. Mol Ther. 2007; **15**(5): 867-77.
2. De Angelis L, Berghella L, Coletta M, Lattanzi L, Zanchi M, Cusella-De Angelis MG, et al. Skeletal myogenic progenitors originating from embryonic dorsal aorta coexpress endothelial and myogenic markers and contribute to postnatal muscle growth and regeneration. J Cell Biol. 1999; **147**(4): 869-78.
3. Ferrari G, Cusella-De Angelis G, Coletta M, Paolucci E, Stornaiuolo A, Cossu G, et al. Muscle regeneration by bone marrow-derived myogenic progenitors. Science. 1998; **279**(5356): 1528-30.
4. Sampaolesi M, Torrente Y, Innocenzi A, Tonlorenzi R, D'Antona G, Pellegrino MA, et al. Cell therapy of alpha-sarcoglycan null dystrophic mice through intra-arterial delivery of mesoangioblasts. Science. 2003; **301**(5632): 487-92.
5. Dellavalle A, Sampaolesi M, Tonlorenzi R, Tagliafico E, Sacchetti B, Perani L, et al. Pericytes of human skeletal muscle are myogenic precursors distinct from satellite cells. Nat Cell Biol. 2007; **9**(3): 255-67.
6. Crisan M, Yap S, Casteilla L, Chen C-W, Corselli M, Park TS, et al. A Perivascular Origin for Mesenchymal Stem Cells in Multiple Human Organs. Cell Stem Cell. 2008; **3**(3): 301-13.
7. Dellavalle A, Maroli G, Covarello D, Azzoni E, Innocenzi A, Perani L, et al. Pericytes resident in postnatal skeletal muscle differentiate into muscle fibres and generate satellite cells. Nat Commun. 2011; **2**: 499.
8. Lee JY, Qu-Petersen Z, Cao B, Kimura S, Jankowski R, Cummins J, et al. Clonal isolation of muscle-derived cells capable of enhancing muscle regeneration and bone healing. J Cell Biol. 2000; **150**(5): 1085-100.
9. Qu-Petersen Z, Deasy B, Jankowski R, Ikezawa M, Cummins J, Pruchnic R, et al. Identification of a novel population of muscle stem cells in mice: potential for muscle regeneration. J Cell Biol. 2002; **157**(5): 851-64.
10. Cao B, Zheng B, Jankowski RJ, Kimura S, Ikezawa M, Deasy B, et al. Muscle stem cells differentiate into haematopoietic lineages but retain myogenic potential. Nat Cell Biol. 2003; **5**(7): 640-6.
11. Payne TR, Oshima H, Sakai T, Ling Y, Gharaibeh B, Cummins J, et al. Regeneration of dystrophin-expressing myocytes in the mdx heart by skeletal muscle stem cells. Gene Ther. 2005; **12**(16): 1264-74.

12. Gharaibeh B, Lu A, Tebbets J, Zheng B, Feduska J, Crisan M, et al. Isolation of a slowly adhering cell fraction containing stem cells from murine skeletal muscle by the preplate technique. Nat Protocols. 2008; **3**(9): 1501-9.
13. Kuroda R, Usas A, Kubo S, Corsi K, Peng H, Rose T, et al. Cartilage repair using bone morphogenetic protein 4 and muscle-derived stem cells. Arthritis Rheum. 2006; **54**(2): 433-42.
14. Zheng B, Cao B, Crisan M, Sun B, Li G, Logar A, et al. Prospective identification of myogenic endothelial cells in human skeletal muscle. Nat Biotech. 2007; **25**(9): 1025-34.
15. Okada M, Payne TR, Zheng B, Oshima H, Momoi N, Tobita K, et al. Myogenic Endothelial Cells Purified From Human Skeletal Muscle Improve Cardiac Function After Transplantation Into Infarcted Myocardium. Journal of the American College of Cardiology. 2008; **52**(23): 1869-80.
16. Crisan M, Yap S, Casteilla L, Chen CW, Corselli M, Park TS, et al. A perivascular origin for mesenchymal stem cells in multiple human organs. Cell Stem Cell. 2008; **3**(3): 301-13.
17. Zheng B, Cao B, Li G, Huard J. Mouse adipose-derived stem cells undergo multilineage differentiation in vitro but primarily osteogenic and chondrogenic differentiation in vivo. Tissue Eng. 2006; **12**(7): 1891-901.
18. Zheng B, Cao B, Crisan M, Sun B, Li G, Logar A, et al. Prospective identification of myogenic endothelial cells in human skeletal muscle. Nat Biotechnol. 2007; **25**(9): 1025-34.
19. Okada M, Payne TR, Zheng B, Oshima H, Momoi N, Tobita K, et al. Myogenic endothelial cells purified from human skeletal muscle improve cardiac function after transplantation into infarcted myocardium. J Am Coll Cardiol. 2008; **52**(23): 1869-80.
20. Drowley L, Okada M, Payne TR, Botta GP, Oshima H, Keller BB, et al. Sex of muscle stem cells does not influence potency for cardiac cell therapy. Cell Transplant. 2009; **18**(10): 1137-46.
21. Wang ZZ, Au P, Chen T, Shao Y, Daheron LM, Bai H, et al. Endothelial cells derived from human embryonic stem cells form durable blood vessels in vivo. Nat Biotechnol. 2007; **25**(3): 317-8.
22. Gharaibeh B, Lu A, Tebbets J, Zheng B, Feduska J, Crisan M, et al. Isolation of a slowly adhering cell fraction containing stem cells from murine skeletal muscle by the preplate technique. Nat Protoc. 2008; **3**(9): 1501-9.
23. Christov C, Chretien F, Abou-Khalil R, Bassez G, Vallet G, Authier FJ, et al. Muscle satellite cells and endothelial cells: close neighbors and privileged partners. Mol Biol Cell. 2007; **18**(4): 1397-409.
24. Minasi MG, Riminucci M, De Angelis L, Borello U, Berarducci B, Innocenzi A, et al. The meso-angioblast: a multipotent, self-renewing cell that originates from the dorsal aorta and differentiates into most mesodermal tissues. Development. 2002; **129**(11): 2773-83.
25. Cossu G, Bianco P. Mesoangioblasts--vascular progenitors for extravascular mesodermal tissues. Curr Opin Genet Dev. 2003; **13**(5): 537-42.
26. Sampaolesi M, Blot S, D'Antona G, Granger N, Tonlorenzi R, Innocenzi A, et al. Mesoangioblast stem cells ameliorate muscle function in dystrophic dogs. Nature. 2006; **444**(7119): 574-9.
27. Dellavalle A, Sampaolesi M, Tonlorenzi R, Tagliafico E, Sacchetti B, Perani L, et al. Pericytes of human skeletal muscle are myogenic precursors distinct from satellite cells. Nat Cell Biol. 2007; **9**(3): 255-67.
28. Kuang S, Gillespie MA, Rudnicki MA. Niche regulation of muscle satellite cell self-renewal and differentiation. Cell Stem Cell. 2008; **2**(1): 22-31.

29. Voog J, Jones DL. Stem cells and the niche: a dynamic duo. Cell Stem Cell. **6**(2): 103-15.
30. Chen C-W, Corselli M, Péault B, Huard J. Human Blood-Vessel-Derived Stem Cells for Tissue Repair and Regeneration. Journal of Biomedicine and Biotechnology. 2012: Epub Feb 2.

FIGURE LEGENDS

Figure 1. Characterization of clonal myogenic endothelial cells (cMECs) in culture. (A) RT-PCR analysis was performed on all six FACS-sorted MEC clones and compared with HUVECs, cultured unsorted hPSMCs (Unsorted), and fresh skeletal muscle cell lysate (Fresh total cells). All MEC clones consistently expressed myogenic (desmin, CD56, Pax7, m-cadherin, Pax3 Myf5), endothelial (CD34, VE-cadherin, vWF), smooth muscle/vascular mural (α-smooth muscle actin, PDGFR-β, NG2, CD146), and mesenchymal stem/stromal (CD90 and CD105) cell markers. **(B)** Analysis of cMEC clonogenic proliferation capacity by sub-cloning single cells from GFP-transduced MEC clones. A total of 80 sub-cloned single GFP-positive cMEC cells (31% of 258 seeded wells) were tracked. Among them, 1% died, 12% did not divide, 14% divided to 2-4 cells, and 73% were able to form colonies (> 8 cells). **(C)** Colony growth rate (n=4) after 17 days in culture showed that the population doubling time was 28.1±5.5 hours, and the cell division time was 16.8 ±2.1 hours. **(D)** After 10 passages in culture, the majority of cMEC metaphases analyzed possess an euploid number (46) of chromosomes.

Figure 2. Chondrogenic differentiation in vitro and in vivo. (A) Gross morphology of cartilage-like pellets formed by cMECs and unsorted muscle cells after being pellet-cultured in chondrogenic medium for 3 weeks. **(B)** cMEC pellets had significantly larger volume than unsorted hPSMC pellets at day 7 and 21 (**p<0.01, Student's t-test). Data were shown as mean ± SD (n=3). **(C)** Chondrogenic differentiation is revealed by Alcian blue/nuclear fast red staining

of pellets cultured in chondrogenic medium supplemented with BMP4 and TGFβ3 at different time points (day 7, 14 and 21) (10X magnification, scale bar represents 25μm). **(D.a)** cMECs were genetically engineered to express nLacZ reporter gene. Positive staining (blue) is localized to the nuclei of the cells (scale bar represents 25μm). **(D.b)** Three weeks after transplantation, chondrogenesis in vivo by cMECs was demonstrated by co-localization of round chondrocytes with blue nuclei (arrow) after staining for β-galactosidase/eosin (scale bar represents 50μm) **(D.c)** Chondrogenesis of cMECs was also revealed by positive immunostaining for collagen type-II (red) (scale bar represents 25μm), and (**D.d**) Co-localization of collagen type-II (red) and β-galactosidase (green, arrow) signals was also detected (scale bar represents 50μm).

Figure 3. Osteogenic differentiation in vitro and in vivo. (A) von Kossa staining of cell pellets cultured in the osteogenic inductive conditions at different time points. Compared to unsorted cell pellets, cMEC pellets cultured in the osteogenic inductive medium containing BMP4 appear to display more extensive mineralization at day 7 and 21. Nevertheless, control cMEC pellets maintained in proliferation medium exhibited no mineralization (scale bar represents 250μm). **(B)** MicroCT images showed that cMEC pellets have a significantly higher **(C)** mineralized matrix volume and (**D)** mineralized matrix density when compared with unsorted cell pellets at day 7 and 21 (**$p<0.01$, Student t-test). Data were shown as mean ± SD (n=3). **(E)** cMECs or unsorted hPSMCs were retrovirally transduced to express BMP4, seeded onto Gelfoam, and implanted into the intramuscular pocket of SCID mice. MicroCT imaging demonstrated that cMEC implants appear to give rise to larger and more organized ectopic mineralized tissue than unsorted cells at all time points. **(F)** There is a significant difference of mineralized tissue volume between the two groups ($p<0.01$ at all time points, Student's t-test). Data were shown as mean ± SEM (n=3). Osteogenesis in vivo by cMECs was also confirmed by co-localization of

(G.a) β-galactosidase-positive nuclei (blue) within eosin-positive cells and **(G.b)** positive immunohistochemical staining for β-galactosidase (blue) and osteocalcin (brown) in the newly formed mineralized tissue as well as **(G.c)** co-localized immunofluorescent staining of osteocalcin (red) and β-galactosidase (green, arrow) (scale bar represents 50μm).

Figure 1

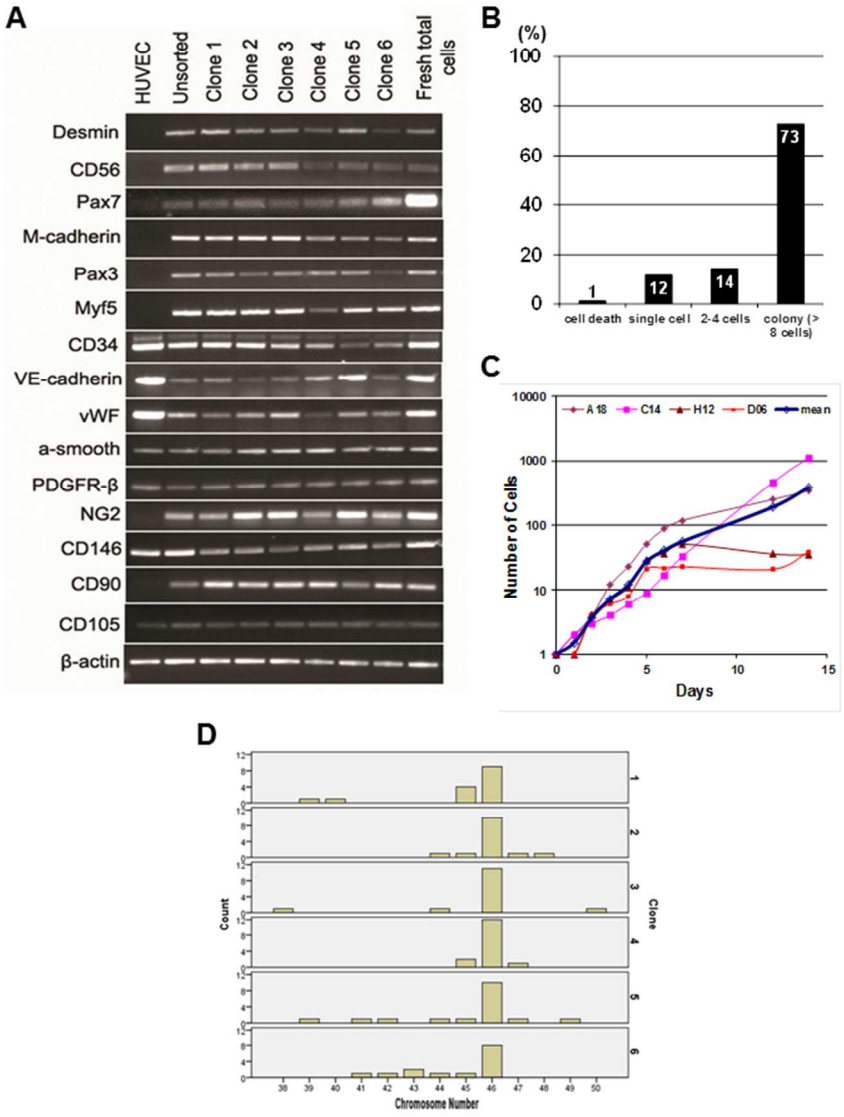

190x254mm (96 x 96 DPI)

Figure 2

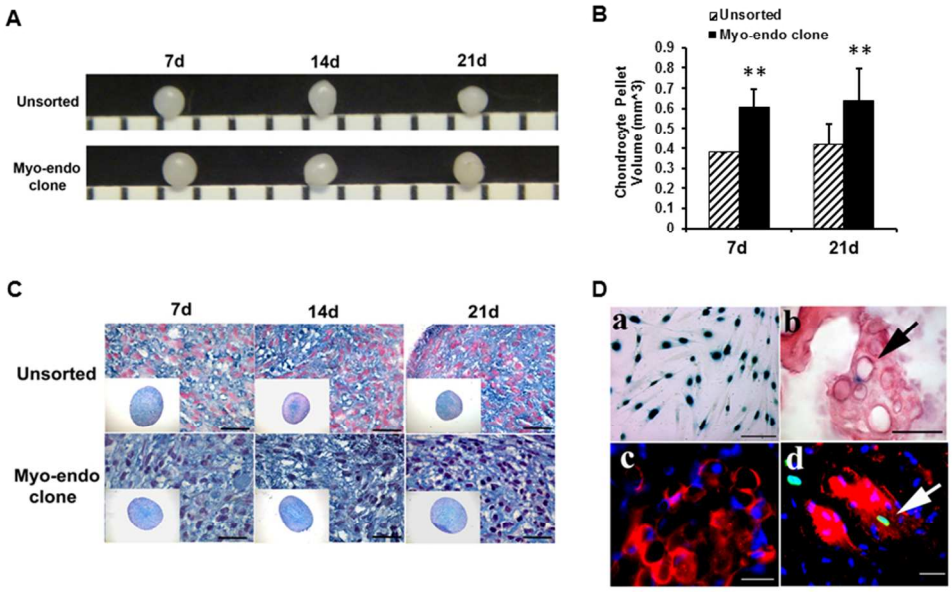

246x168mm (96 x 96 DPI)

Figure 3

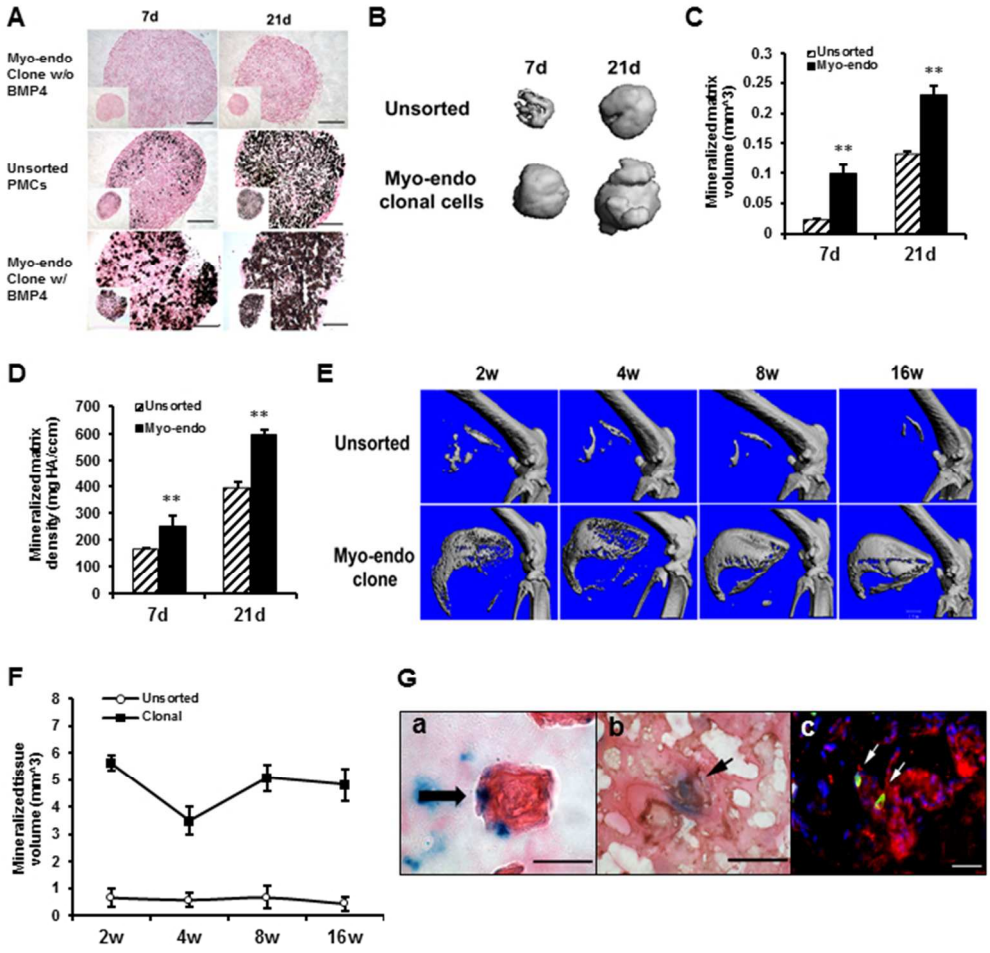

190x194mm (96 x 96 DPI)

Progression of muscular dystrophy in dystrophin/utrophin-/- mice is associated with rapid muscle progenitor cell exhaustion

Aiping Lu; Jonathan Proto; Xiaodong Mu; Ying Tang; Minakshi Poddar; Bing Wang; Johnny Huard
Stem Cell Research Center, Department of Orthopaedic Surgery, University of Pittsburgh, Pittsburgh, PA

Introduction

Duchenne muscular dystrophy (DMD) is a deadly genetic disease characterized by a lack of dystrophin expression and progressive weakening and wasting of the skeletal muscles. Researchers have observed that despite the lack of dystrophin at birth, the histopathological signs of muscle weakness do not become apparent until 4-8 years of age, which happens to coincide with the exhaustion of the muscle progenitor cell (MPC) pool (1).In this study we isolated MPCs from the skeletal muscle of young (2 weeks) and old (6 weeks) dKO (dystrophin/utrophin double knock out) mice, which have a maximum lifespan of 6 to 8 weeks and is a mouse model of DMD that closely recapitulates the disease progression observed in DMD patients. We found that MPCs isolated from old dKO mice have a reduced ability to proliferate and differentiate compared to MPCs isolated from young dKO mice. In addition, Pax7 staining (a muscle progenitor cell marker) indicated that the MPC population significantly decreased during disease progression. These observations suggest that blocking the exhaustion of the MPC pool could be a new approach to improve muscle weakness in DMD patients, despite their continued lack of dystrophin expression.

Methods

1. Cell Isolation: MPCs were isolated from dKO mice at 2 and 6 weeks of age, as previously described via a modified preplate technique (2).

2. Cell proliferation: Proliferation behavior of the MPCs isolated from the skeletal muscle of dKO mice was examined and compared by using a robotic time-lapsed live-cell imaging system (LCI).

3. ***Immunohistocytochemistry:***

Cryosections were stained for mouse Pax7 and the nuclei were revealed by DAPI staining.

4. Myogenic differentiation assay: Myogenic differentiation capacity of the MPCs was assessed by switching the proliferation medium to fusion medium (DMEM containing 2% fetal bovine serum). After 3 days, the cells were stained for fast myosin heavy chain (MyHCf), which is a marker of terminal myogenic differentiation. Myogenic differentiation levels were quantified as the percentage of the number of nuclei in MyHCf positive myotubes relative to the total number of nuclei.

5. Single fiber isolation: Skeletal muscle tissue isolated from 6 week old dKO and 9 week old WT control mice were incubated in a solution of 0.2% collagenase type I for 40 minutes at 37°C. When the muscle was sufficiently digested the muscles were triturated with heat polished glass pipettes to liberate single fibers and then transferred to a matrigel coated 12 well plate with proliferation medium.

Results

1. MPCs isolated from aged dKO mice display limited proliferation ability.

We examined the proliferation kinetics of both populations *in vitro* using LCI (3) and we observed a significant reduction in the proliferation capacity of the old dKO MPCs compared to young dKO MPCs (**Figure 1**)

2. Pax7 positive cells undergo a rapid decline in the skeletal muscle of dKO mice during aging and disease progression.

The results from the Pax7 staining showed that there is a rapid statistically significant decline in the population of Pax7 positive cells in the skeletal muscle of dKO mice from 4 to 8 weeks of age in contrast to that observed in *mdx* skeletal muscle ($p<0.05$) (**Figure 2A**).

3. Isolated muscle fibers from dKO mice show a reduction in muscle progenitor cells.

The single muscle fibers were isolated from 6 weeks old dKO and WT control mice. We observed that there were more cell nuclei in the WT muscle fibers compared to the dKO muscle fibers. In addition, 5 days post-culturing, the WT muscle fibers were able to release myogenic progenitor cells forming new myotubes, in contrasts to that observed with the dKO muscle fibers. These results support both a reduction in the number and myogenic potential of the MPCs derived from the dKO mice when compared to the WT MPCs (**Figure 2B**)

4. MPCs isolated from aged dKO mice display a limited myogenic differentiation ability.
We observed that the MPCs isolated from young dKO mice formed numerous, large multi-nucleated myotubes compared to the MPCs isolated from the old dKO mice. The degree of myogenic differentiation was significantly reduced in the old dKO MPCs relative to the MPCs isolated from young dKO mice ($P < 0.001$).(**Figure 3**)

Discussion:

It is interesting to note that despite the lack of dystrophin at birth, the initiation of any signs of muscle weakness does not occur in DMD patients until later in childhood which happens to coincide with the exhaustion of the muscle progenitor cell pool (1). In this study we demonstrated that MPCs isolated from the skeletal muscle of old dKO mice have a reduced ability to proliferate and differentiate compared to MPCs isolated from young mice. Moreover, the numbers of Pax7 positive cells *in vivo* undergo a rapid decline in the skeletal muscle of dKO mice during aging and disease progression. Since dKO mice can only live 6-8 weeks, stem cell exhaustion could represent the main mechanism for the rapid progress of this disease. Blocking the exhaustion of muscle progenitor cells and stem cell-mediated therapy may represent a potential strategy for treating these muscle diseases.

Significance:

This study suggested that the exhaustion of stem cells contributes to the histopathology associated with DMD and that blocking the exhaustion of muscle progenitor cells and stem cell-mediated therapy could be used as a potential clinical strategy to treat muscle disease.

Figure 1

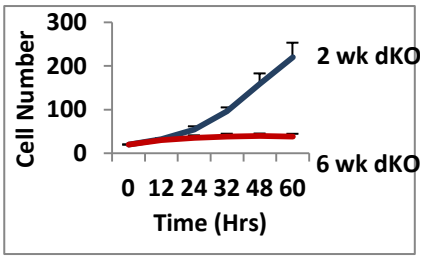

Figure 2A

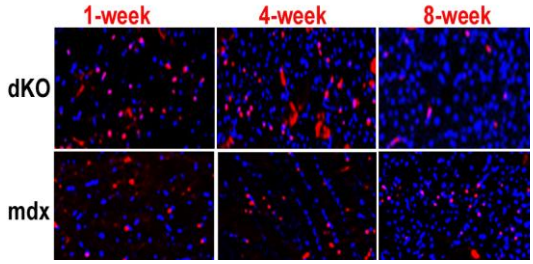

Figure 2B

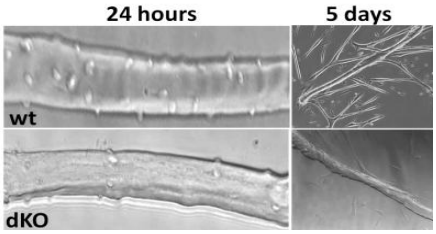

Figure 3

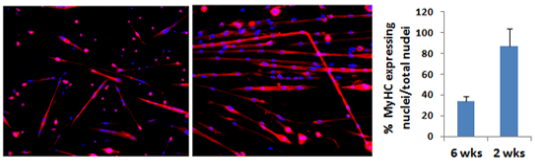

Reference

1. McLoon LK. Focusing on fibrosis: halofuginone-induced functional improvement in the mdx mouse model of Duchenne muscular dystrophy. Am J Physiol Heart Circ Physiol. 2008;294(4):H1505-7.
2. Gharaibeh B, Lu A, Tebbets J, Zheng B, Feduska J, Crisan M, et al. Isolation of a slowly adhering cell fraction containing stem cells from murine skeletal muscle by the preplate technique. Nat Protoc. 2008;3(9):1501-9.
3. Deasy BM, Jankowski RJ, Payne TR, Cao B, Goff JP, Greenberger JS, et al. Modeling stem cell population growth: incorporating terms for proliferative heterogeneity. Stem Cells. 2003;21(5):536-45.

TITLE:
Muscle-derived cells (MDCs) responsible for myogenesis differ from MDCs involved in adipogenesis in dystrophin/utrophin-/- mice

AUTHORS:
Jihee Sohn, Ying Tang, Bing Wang, Aiping Lu, +Johnny Huard
Department of Orthopaedic Surgery, University of Pittsburgh, Pittsburgh, Pennsylvania, United States, 15260 and [2]Department of Bioengineering and McGowan Institute for Regenerative Medicine, University of Pittsburgh, Pittsburgh, Pennsylvania, United States, 15260.
jhuard@pitt.edu

ABSTRACT BODY:
INTRODUCTION: Duchenne muscular dystrophy (DMD) is a genetic disease characterized by progressive weakening of the skeletal and cardiac muscles. The predominant symptoms seen in advanced cases of DMD are sarcopenia and pseudohypertrophy with fatty infiltration in skeletal muscle. Ectopic fat accumulation in skeletal muscle can be seen not only in myopathies but also in several disorders, including obesity and ageing-related sarcopenia; however, the origin of ectopic adipocytes, nor the stimulus that trigger their formation in disease, is known. In our lab, we utilize utrophin/dystrophin double knockout (dys-/-utro-/-, dKO) mice, which better emulates the phenotype seen in DMD patients. Several types of cells, including satellite cells, can be isolated from skeletal muscle and based on a previously published preplate technique (1) we isolated two types of cells; rapidly adhering cells (RACs) ,which are PDGFRα + mesenchymal progenitor cells, and slowly adhering cells (SACs), which are Pax7+ myogenic progenitor cells, from skeletal muscle of dKO and wild type (wt) mice. Previously, we have shown that dKO-SACs have reduced proliferation and myogenic and adipogenic differentiation abilities compared to wt-SACs. These observations suggested that SACs in dKO mice are exhausted and potentially are the main mechanism for the rapid progress of sarcopenia; however, the cells involved in pseudohypertrophy in dKO mice remains unclear. In this study, we examined the proliferation and adipogenic differentiation capabilities of RACs since adipose cells are thought to be derived from mesenchymal stem cells. We observed increased proliferation and adipogenic differentiation capabilities in dKO-RACs compared to wt-RACs. Our results suggest that muscle progenitor cells, SACs, may be more involved in muscle fiber regeneration or degeneration while mesenchymal progenitor cells, RACs, may be the origin of the cell population that is involved in adipogenesis in dKO muscle.

METHODS:

Cell Isolation: Cells were isolated from dKO (dys-/-utro-/-) and wild type (wt) mice at 6 weeks of age, as previously described via a modified preplate technique [1]. After 24hrs, the RACs were obtained and after 7 days, the SACs were obtained. Both cells were cultured in proliferation medium (DMEM supplemented with 10% fetal bovine serum, 10% horse serum, 0.5% chicken embryo extract and 1% penicillin-streptomycin).

Cell proliferation: Proliferation behavior of the dKO-SACs, dKO-RACs, wt-SACs, and wt-RACs were examined by using a robotic time-lapsed microscopic live-cell imaging system (LCI) and MTT assay.

Flow cytometry analysis and Immunofluorescent staining: 100,000 RACs and SACs were used to analyze their PDGFRα expressions. Cells were harvested and stained with PDGFRα-PE (eBioscience) antibody. 10,000 cells/well RACs and SACs were seeded on 24 well collagen type-1 coated plates and stained with mouse-monoclonal primary Pax7 antibody (1:400).

Multi-lineage Differentiation:

Adipogenic: 25,000 cells were cultured on 24 well plates for 21days in adipogenic induction media (Lonza) and then tested for adipogenesis with an AdipoRed reagent.

Myogenic: Myogenic differentiation capacity of the MDSCs was assessed by switching the proliferation medium into fusion medium (DMEM containing 2% fetal bovine serum). After 3 days, we analyzed myotube formation.

RESULTS:

dKO-RACs had increased PDGFRα expression compared to dKO-SACs. Flow cytometry analysis was used to evaluate the expression of PDGFRα, a marker for mesenchymal cells, of the RACs and SACs from both dKO and wt mice. dKO-RACs were about 98% positive for the PDGFRα surface protein, while much lower expression levels were detected in the SACs (Figure 1).

dKO-RACs displayed increased proliferation ability. The proliferation of the RACs and SACs were examined in vitro using an LCI system and MTT assay. We observed a significant increase in the proliferation of the dKO-RACs compared to the wt-RACs.

Increased in vitro adipogenic potential was detected in dKO-RACs. RACs and SACs from both dKO and wt mice were cultured in adipogenic differentiation medium for 21 days. AdipoRed staining was observed in the cytoplasm of the cells, around the nuclei. The degree of adipogenic differentiation was significantly increased in PDGFRα+ dKO-RACs compared to the dKO-SACs (Figure 2).

DISCUSSION: In dKO mice, an animal model of DMD, we observed severe peri-muscular adipose tissue on the surface of the gastrocneminus muscles (GM) as well as lipid accumulation inside of skeletal muscle myofibers. Intramyocellular lipid accumulation could be observed in the cardiac muscle of dKO mice; however, the source of the ectopic fat tissue within the skeletal muscle is unknown. In this study, we provide evidence that the RACs, PDGFRα + mesenchymal progenitor cells, are responsible for increased fat cell formation in the skeletal muscle of dKO mice. We observed that dKO-RACs had increased proliferation and adipogenic differentiation capabilities. This result suggests that dKO-RACs are prone to form adipocytes in skeletal muscle.

SIGNIFICANCE: This study suggests that dKO-RACs, mesenchymal progenitor cells in skeletal muscle, may contribute to adipogenesis and are responsible for ectopic fat cell formation within skeletal muscle in pathological conditions such as DMD. Therefore, targeting RACs to block adipogenesis in skeletal muscle may open new opportunities to treat muscle diseases.

REFERENCE:
[1] Gharaibeh, et al. Nat Protoc. 2008; 3:1501-9
[2] Uezumi, et al. Nat Cell biology. 2010; 2:143-152

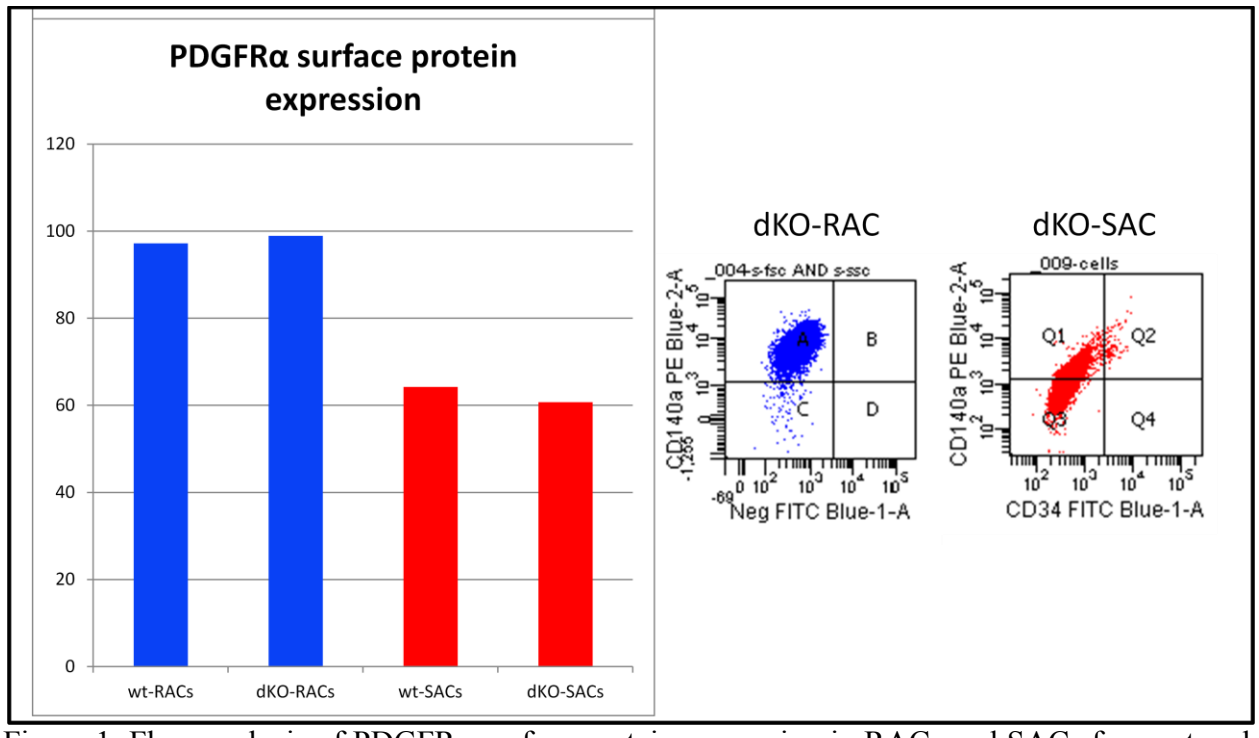

Figure 1. Flow analysis of PDGFRα surface protein expression in RACs and SACs from wt and dKO mice.

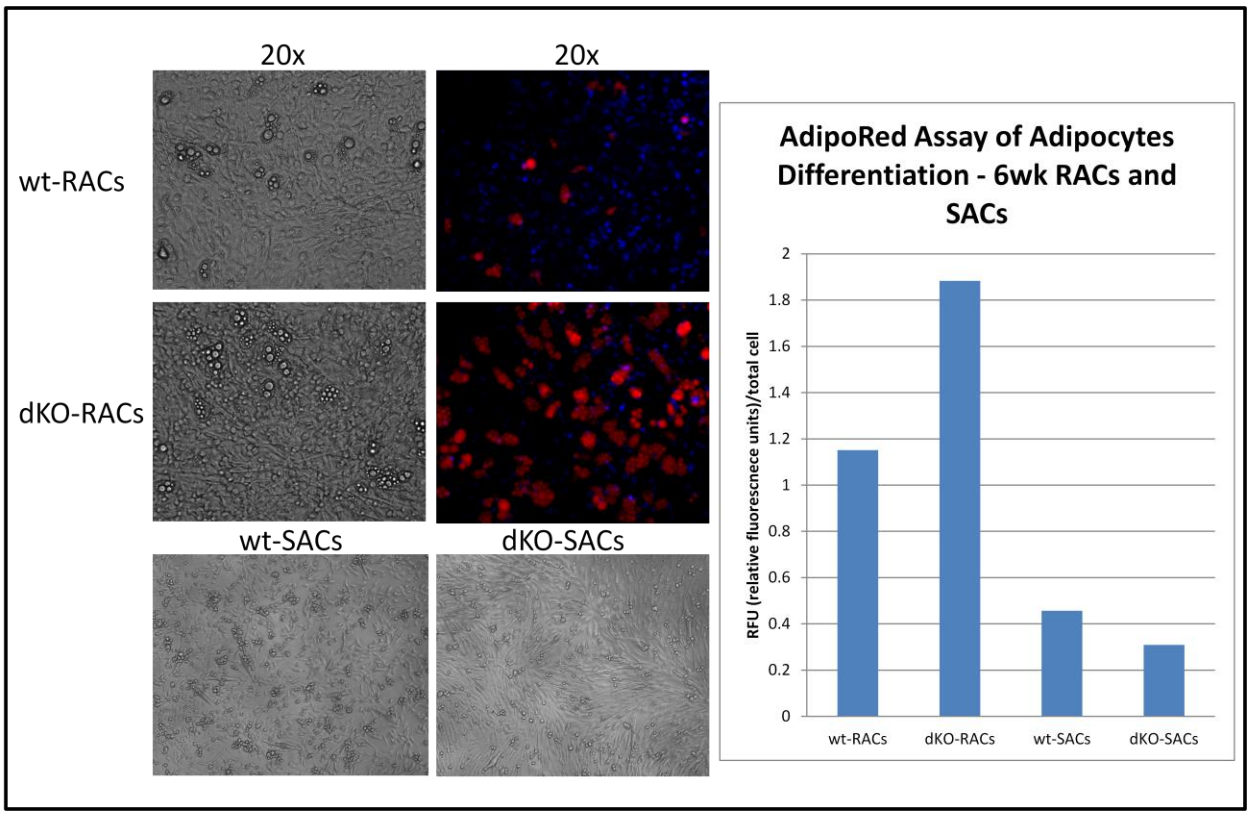

Figure 2. Adipogenesis of RACs and SACs. Bright field pictures and AdipoRed staining. Quantification of AdipoRed assay is shown.

RhoA signaling regulates heterotopic ossification and fatty infiltration in dystrophic skeletal muscle

Xiaodong Mu, Arvydas Usas, Ying Tang, Aiping Lu, Jihee Sohn, Bing Wang, Kurt Weiss, and Johnny Huard
Stem Cell Research Center, Department of Orthopaedic Surgery, University of Pittsburgh

Introduction: Frequent heterotopic ossification (HO) or fatty infiltration is observed in the dystrophic muscle of many animal models of human Duchenne muscular dystrophy (DMD); however, little is known about the correlated molecular mechanisms involved in the process. The RhoA-Rho kinase (ROCK) signaling pathway has been shown to function as a commitment switch of the osteogenic and adipogenic differentiation of mesenchymal stem cells (MSCs). Activation of RhoA-ROCK signaling in cultured MSCs *in vitro* induces their osteogenesis but inhibits the potential of adipogenesis, while the application of Y-27632, a specific inhibitor of ROCK, reversed the process. Inflammation has been shown to be one of main contributors to HO, while the role of RhoA signaling in inflammation reaction has been demonstrated. The objective of the current study is to investigate the potential role of RhoA signaling in regulating HO and fatty infiltration in dystrophic skeletal muscle.

Methods: 1.Mice models**:** Animal experiments were approved by IACUC of University of Pittsburgh. mdx mice (dystrophin-deficient) and dKO (Dystrophin/Utrophin double knockout) mice are both important mouse models of DMD; however, in contrast to the mild phenotype of mdx mice, dKO mice display a far more severe phenotype as is observed in human DMD patients, including a much shorter life span (~ 8 weeks compared to 2 years), more necrosis and fibrosis in the skeletal muscle, etc. 2. Tissue histological analysis: The gastrocnemius muscles (GM) of the mice were used for histological analysis. Alizarin red stain shows calcium deposition caused by HO or during osteogenic differentiation, Oil Red O stain shows fatty infiltration in muscle or fat cells, and Trichrome stain shows fibrosis. 3. Statistics: N >=6 for each group in animal study. Student's T-test was used to evaluate the significance.

Results: 1. Skeletal muscle of dKO mice features more HO but less fatty infiltration than mdx mice (Fig. 1). Both μ-CT scan of animals (**Fig. 1A**) and Alizarn Red stain (**Fig. 1B**) of the muscle tissues revealed greatly enriched HO in the dystrophic muscles of the dKO mice. While, Oil Red O stain (**Fig. 1C**) and Trichrome stain **(Fig. 1D)** of the muscle tissues revealed reduced fatty infiltration and a number of normal muscle fibers in the muscle of dKO mice.

2. RhoA signaling is more activated in both skeletal muscle and muscle-derived stem cells (MDSCs) from dKO mice. Both semi-quantitative PCR and immunohistochemistry study demonstrated that RhoA signaling is more activated in the muscles of dKO mice, as well as dKO MDSCs.

3. *In vitro* RhoA inactivation of cultured MDSCs from dKO mice decreases the osteogenesis potential and increases adipogenesis and myogenesis potential (Fig. 2). Semi-quantitative PCR study showed that Y27632 treatment *(*10 μM) of dKO-MDSCs down-regulated the expression of RhoA, BMP2 and 4, and inflammatory factors such as TNF-α and IL-6 (**Fig. 2A**). Osteogenesis potential was repressed while the adipogenesis and myogenesis potential of the dKO-MDSCs were increased by Y27632 (**Fig. 2B**).

4. RhoA inactivation in the skeletal muscle of dKO mice decreased HO and increased both fatty infiltration and muscle regeneration. GM muscles of 6 dKO mice were injected with Y27632 (5mM in 20μL of DMSO) (left limb) or control (20μL of DMSO) DMSO (right limb). Injections were conducted 3 times a week for 3 weeks. The skeletal muscles that received Y27632 injection demonstrated much slower development of HO and improved muscle regeneration, as well as reduced fibrosis formation.

Discussion: Our current results revealed that DMD mouse models featuring different severity of muscular dystrophy may have varied potentials for developing HO or fatty infiltration in the dystrophic muscle, and RhoA signaling might be a critical mediator of the determining these differential fates, including the progression towards HO, fatty infiltration, or normal muscle regeneration. RhoA inactivation is shown to have a great potential to repress HO and improve the phenotypes of dystrophic muscle. The status of RhoA activation in the skeletal muscle of human DMD patients and the potential effect of RhoA inactivation in human dystrophic muscle requires further investigation.

Significance: Our data reveals the involvement of RhoA signaling in regulating the process of heterotopic ossification, and indicates that RhoA may serve as a potential target for repressing injury-induced and congenital heterotopic ossification in humans.

Fig 1

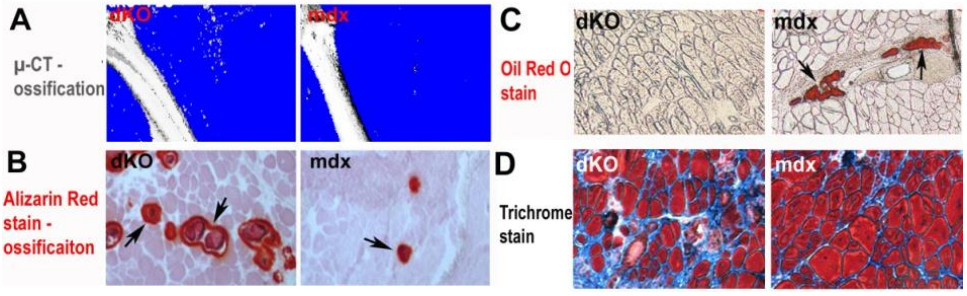

Fig 2

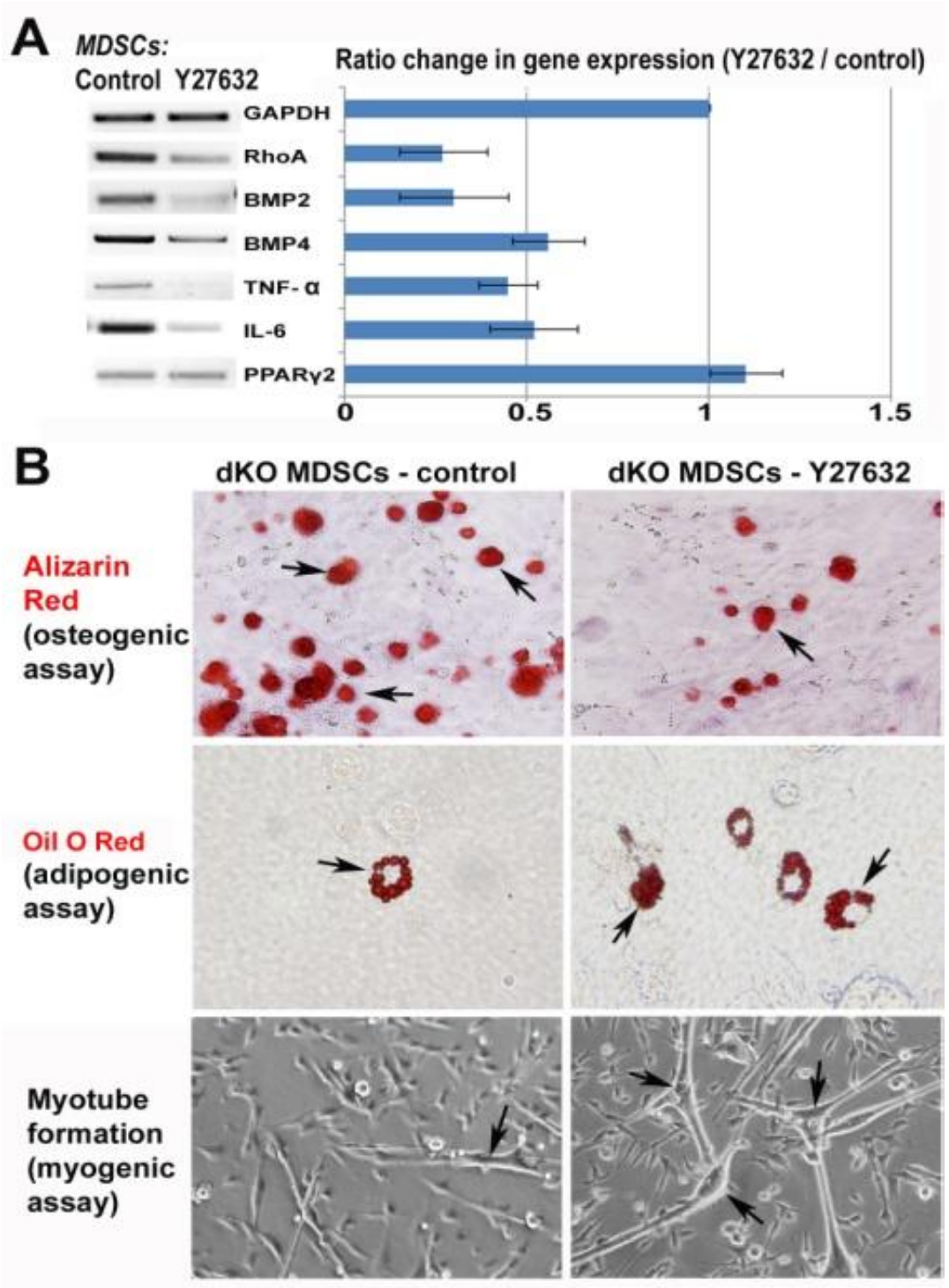
A
MDSCs:
Control Y27632
GAPDH
RhoA
BMP2
BMP4
TNF-α
IL-6
PPARγ2
Ratio change in gene expression (Y27632 / control)
0
0.5
1
1.5
B
dKO MDSCs - control
dKO MDSCs - Y27632
Alizarin Red (osteogenic assay)
Oil O Red (adipogenic assay)
Myotube formation (myogenic assay)

Suppression of skeletal muscle inflammation by muscle stem cells is associated with hepatocyte growth factor in wild type and *mdx*;p65$^{+/-}$ mice

[1]Proto, J.; [1]Tang, Y; [1]Lu, A.; [2]Robbins, P.D.; [1]Wang, B. [1]+Huard, J.
[1]+ Stem Cell Research Center, Children's Hospital of Pittsburgh, and Department of Orthopedic Surgery;
[2]Department of Metabolism and Aging, The Scripps Research Institute, Jupiter, FLA
jhuard@pitt.edu

INTRODUCTION

Persistent, unresolved inflammation can lead to secondary tissue damage. Recently, we reported that intramuscular (i.m.) injection of muscle-derived stem cells (MDSCs) heterozygous for the NF-kB subunit p65 (p65$^{+/-}$) reduced host inflammation and fiber necrosis seven days following muscle injury, relative to wild type (WT) MDSC injection [1]. In this investigation, we looked closer at the role of secreted factors in this observation. Using a murine cardiotoxin muscle injury model, we observed that delivery of p65$^{+/-}$ MDSCs accelerated the resolution of inflammation, relative to WT MDSCs. *In vitro* inflammation assays demonstrated that MDSCs secrete factors that modulate cytokine expression in LPS-activated macrophages, and genetic reduction of p65 enhanced this effect. Finally, deletion of one p65 allele in a murine model of Duchenne muscular dystrophy (mdx) increased the expression of the anti-inflammatory factor hepatocyte growth factor (HGF) and was associated with disease improvement.

MATERIALS AND METHODS

Mice: C57Bl/6 (WT) mice were purchased from the Jackson Laboratory (Bar Harbor, ME). P65$^{+/-}$ mice were bred with *mdx* mice to produce mdx/p65$^{+/-}$ and mdx/p65$^{+/+}$ mice. PCR analysis of tail samples was used for genotyping.

Cell Isolation: MDSCs were isolated from five month old (n=3) *p65*$^{+/+}$ or *p65*$^{+/-}$ mice via a modified preplate technique [2]. A population of slowly adhering cells was obtained and expanded in proliferation medium (PM, DMEM containing 10% fetal bovine serum (FBS), 10% horse serum, 1% penicillin-streptomycin, and 0.5% chick embryo extract).

In vivo regeneration assay: Muscle injury was induced in C57Bl/6J mice by the injection of cardiotoxin (4uM) into the gastrocnemius muscle. One day later, MDSCs were injected into the injured muscles. Muscles were harvested 1, 3, and 7 days post-injury. Serial cryosections were prepared and immunohistochemistry was performed to assess inflammation (F480, Gr-1). Gross tissue histology was performed by hematoxylin and eosin (H&E) staining.

In vitro Inflammation Model: MDSCs were grown for 24 hours in proliferation medium, after which the medium was collected and sterile filtered. RAW264.7 cells, immortal murine macrophage-like cells, were activated by exposure to 100 ng/mL LPS in either PM, *p65*$^{+/+}$-, or *p65*$^{+/-}$- conditioned medium for 30 min, 3 hours, and 24 hours. At each time point, RNA was collected for real time RT-PCR analysis or lysates were collected for western blot.

RESULTS

Confirming our previous report [1], we found that by 7 days, p65$^{+/-}$ cell engraftments were associated with reduced numbers of F4/80+ cells, compared to WT cell engraftments (Fig 1A). This can be further demonstrated histologically by H&E staining, revealing a reduction in mono-nuclear cells at sites of injury one week post injection (Fig 1B).

To look at the direct effects of MDSC-secreted factors, we performed *in vitro* inflammation assays. Briefly, RAW264.7 macrophages were activated with LPS (100ng/mL) in normal PM or WT or p65$^{+/-}$ conditioned medium (CM) (Fig 2A). The expression of the cytokines IL-1β and IL-6 was determined by real time (RT-PCR). Our results demonstrated that MDSC-CM significantly attenuates cytokine expression (Fig 2B).

Figure 1.

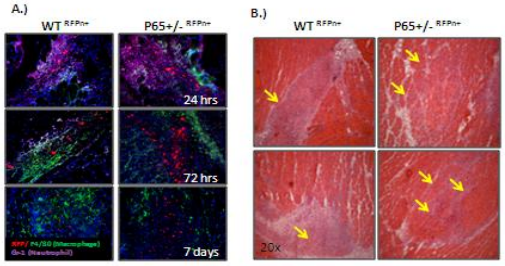

Although WT and p65$^{+/-}$ CM had a similar effect, we found that p65$^{+/-}$ CM exerted a stronger suppression of IL-6 expression. Previous reports have found that the activation of inflammatory macrophages is attenuated by the phosphorylation and subsequent inactivation of GSK3β [3]. By western blot, we found that upon treatment with LPS in WT-CM, the fraction of pS9-GSK3beta modestly increased within 30mins and was maintained through 24 hours. Furthermore, p65$^{+/-}$-CM demonstrated an even stronger induction of phosphorylation.

Figure 2.

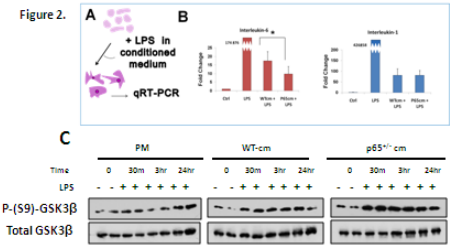

Hepatocyte growth factor (HGF) is one of the factors previously demonstrated to modulate inflammation via pS9-GSK3beta. We examined HGF expression in MDSCs and found elevated levels in p65$^{+/-}$ cells compared to the WT cells. Acharyya and colleagues have reported that haploinsufficiency of p65 in an mdx background improves dystrophic pathology [4]. As we had hypothesized, HGF expression was significantly increased. Based on our *in vitro* and *in vivo* inflammatory studies, HGF could be one of the contributing factors to disease improvement.

Figure 3.

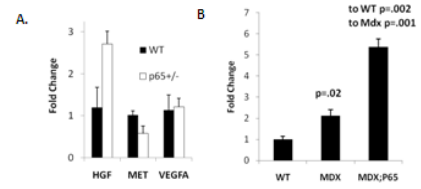

DISCUSSION

These findings indicate that NF-kB has a broader role in muscle stem and progenitor cells than previously thought, and that the anti-inflammatory molecules secreted by stem cells, such as HGF, could potentially be harnessed to control secondary pathologies of muscle diseases such as DMD.

REFERENCES

[1]Lu, A., et al, Mol Ther 2012, 20(3);661-68. [2] Gharaibeh, et al. Nat Protoc. 2008; 3:1501-9. [3] Beurel, E., et al, Trends Immunol 2010; 3-(1):24-31 [4]Acharyya, S., et al., J Clin Invest 2007, 117:889-901.

Hindawi Publishing Corporation
Stem Cells International
Volume 2013, Article ID 983059, 18 pages
http://dx.doi.org/10.1155/2013/983059

Review Article

Cellular Kinetics of Perivascular MSC Precursors

William C. W. Chen,[1,2] Tea Soon Park,[3] Iain R. Murray,[4,5] Ludovic Zimmerlin,[3] Lorenza Lazzari,[6] Johnny Huard,[1,7] and Bruno Péault[4,5,8]

[1] *Stem Cell Research Center, Department of Orthopaedic Surgery, School of Medicine, University of Pittsburgh, Pittsburgh, PA 15219, USA*
[2] *Department of Bioengineering, University of Pittsburgh, Pittsburgh, PA 15260, USA*
[3] *Institute for Cell Engineering and Department of Pediatric Oncology, School of Medicine, Johns Hopkins University, Baltimore, MD 21205, USA*
[4] *Centre for Regenerative Medicine, University of Edinburgh, Edinburgh, EH16 4TJ, UK*
[5] *Orthopaedic Hospital Research Center and David Geffen School of Medicine at UCLA, University of California at Los Angeles, 615 Charles E. Young Drive South, Los Angeles, CA 90095-7358, USA*
[6] *Cell Factory, Fondazione Ospedale Maggiore Policlinico, 20122 Milan, Italy*
[7] *McGowan Institute for Regenerative Medicine, Pittsburgh, PA 15219, USA*
[8] *Centre for Cardiovascular Science, University of Edinburgh, Queen's Medical Research Institute, 47 Little France Crescent, Edinburgh EH16 4TJ, UK*

Correspondence should be addressed to Bruno Péault; bpeault@mednet.ucla.edu

Received 14 May 2013; Accepted 13 July 2013

Academic Editor: Donald G. Phinney

Mesenchymal stem/stromal cells (MSCs) and MSC-like multipotent stem/progenitor cells have been widely investigated for regenerative medicine and deemed promising in clinical applications. In order to further improve MSC-based stem cell therapeutics, it is important to understand the cellular kinetics and functional roles of MSCs in the dynamic regenerative processes. However, due to the heterogeneous nature of typical MSC cultures, their native identity and anatomical localization in the body have remained unclear, making it difficult to decipher the existence of distinct cell subsets within the MSC entity. Recent studies have shown that several blood-vessel-derived precursor cell populations, purified by flow cytometry from multiple human organs, give rise to *bona fide* MSCs, suggesting that the vasculature serves as a systemic reservoir of MSC-like stem/progenitor cells. Using individually purified MSC-like precursor cell subsets, we and other researchers have been able to investigate the differential phenotypes and regenerative capacities of these contributing cellular constituents in the MSC pool. In this review, we will discuss the identification and characterization of perivascular MSC precursors, including pericytes and adventitial cells, and focus on their cellular kinetics: cell adhesion, migration, engraftment, homing, and intercellular cross-talk during tissue repair and regeneration.

1. Introduction

The availability of mesenchymal stem/stromal cells (MSCs) and MSC-like multipotent stem/progenitor cells marked a major milestone in stem cell therapies [1, 2]. For more than a decade, MSC has been a highly promising stem cell source and extensively investigated for its therapeutic potentials [3, 4]. Unlike embryonic stem cells (ESCs) or induced pluripotent stem cells (iPSCs), MSCs are inherently more relevant to clinical applications due to the lack of ethical and safety issues, despite lower developmental versatility [5]. MSCs and similar mesodermal stem/progenitor cells have been shown to repair and/or regenerate a wide variety of damaged/defective organs, including bone, cartilage, muscle, heart, and skin [6–10]. MSCs have also been reported to support hematopoiesis and suppress immune reaction after cell/organ transplantation [11–14].

Nevertheless, owing to the nature of MSC isolation by plastic adherence in tissue culture, the native identity and anatomical localization of MSCs have remained unclear for

years [15]. Recently, several studies have indicated that MSCs represent a heterogeneous entity in culture, and a number of multipotent precursor cells potentially contributing to the MSC pool have been identified *in vivo* [16, 17]. Increasing evidence further suggests that MSCs and some tissue-specific progenitor cells are anatomically and functionally associated with vascular/perivascular niches in various tissues [18–21]. Following the hypothesis that blood vessels throughout the body serve as a systemic reservoir of multipotent stem/progenitor cells, we and other researchers have identified, purified, and characterized distinct populations of MSC-like multilineage precursors from the vasculature of multiple human organs [17, 22]. These human blood vessel-derived precursor cell subsets, including pericytes (PCs) [23], adventitial cells (ACs) [24], and myogenic endothelial cells (MECs) [25], can be isolated via fluorescence-activated cell sorting (FACS) based on their unique expression of cell surface antigens. Purified PCs, ACs, and MECs not only exhibit typical mesodermal multipotency in culture but also demonstrate robust regenerative capacities in animal disease models. Consequently these precursor cell subsets, particularly PCs and ACs that can be universally derived from definitive structures of blood vessel walls, represent active contributors to the MSC entity [17].

In this review, we will discuss the identification and characterization of perivascular MSC precursors (i.e., PCs and ACs) from multiple organs and focus on their cellular kinetics during regenerative events, including cell adhesion, migration, engraftment, homing, and intercellular cross-talk.

2. Native Distribution of MSCs and MSC-Like Multipotent Stem/Progenitor Cells

MSCs and MSC-like stem/progenitor cells have been found in nearly all organs in the human body. Despite slight differences in phenotypes and cellular functions, MSCs and MSC-like cells from various ontogenies share basic features in general, including selective plastic adherence, expression of typical MSC surface markers, and mesenchymal multipotency such as osteogenesis, chondrogenesis, and adipogenesis. Some of the most common MSCs and MSC-like multilineage cells are briefly introduced here.

2.1. Bone Marrow-Derived MSCs (BM-MSCs). Bone marrow (BM) harbors multiple types of stem/progenitor cells, including hematopoietic stem cells (HSCs), endothelial progenitor cells (EPCs), and BM-MSCs [26, 27]. As a standard MSC population, BM-MSCs are defined as nonhematopoietic, plastic adherent progenitor cells that self-renew, differentiate into typical mesodermal cell lineages including osteogenic, chondrogenic, and adipogenic lineages, and express CD73, CD90, and CD105 but are negative for CD11b, CD14, CD19, CD34, CD45, CD79α, and HLA-DR1 [28]. Estimated by the colony forming unit fibroblasts assay (CFU-F) *in vitro,* BM-MSCs typically exist at a very low frequency within the BM mononucleated cell population (0.01%–0.1% of total BM cells) but can be efficiently expanded in culture, making them one of the most investigated autologous stem/progenitor cell populations. Interestingly, multipotent BM-MSC clones retain approximately twofold higher CD146 expression level than unipotent clones [29].

2.2. Adipose-Derived Stem/Stromal Cells (ASCs). The stromal vascular fraction (SVF) of adipose can be isolated via enzymatic digestion of intact fat tissue or lipoaspirate, followed by the depletion of mature adipocytes through centrifugation. The SVF embodies a broad and heterogeneous cellular compartment, including vascular cells (endothelial and perivascular populations), hematopoietic cells (resident and circulating cells), and stromal fibroblasts. In 1976, human adipogenic progenitors (aka preadipocytes) were successfully isolated by two independent groups from the adipose SVF by selective adherence to culture plastics [30, 31]. The adherent fraction of the adipose SVF was later identified as a source of mesenchymogenic progenitors [32], termed adipose-derived stem/stromal cells (ASC) [33]. ASCs are defined *in vitro* using the same criteria as *bona fide* BM-MSCs [34], including their selective plastic adherence, mesenchymal differentiation capacities and immunophenotypes [32], although ASCs only resemble BM-MSCs at subsequent passages in culture [35]. Unlike BM-MSCs, early-passage ASCs temporarily retain expression of mucosialin (CD34) [35], a well-established marker for stem/progenitor cells in both hematopoietic [36] and endothelial [37] cell lineages. On another note, the temporary retention of CD34 expression in primary ASCs led to confusion regarding their origin *in situ*. This misperception was accentuated in light of the recent characterization of CD34-negative PCs as a source of MSCs in a variety of mesodermal tissues, including fat [23]. While the adipogenic activity is mainly exhibited by the prevalent CD34+/CD31− subset of the adipose SVF [38], the CD34-negative fraction can also generate ASCs *in vitro* [24, 39, 40]. Immunohistochemical studies have confined these mesenchymogenic subpopulations to the adipose microvasculature where they coexist, respectively, in the media and adventitia in an annular fashion [24, 39, 41, 42]. Both PCs and an outer supra-adventitial layer of CD34-positive cells (adventitial cells/supra-adventitial stromal cells, ACs) possess high adipogenic potential *in vitro* [39, 43] and may contribute together to replenish the pool of adipocytes essential to sustain the high fat turnover *in vivo* [44].

2.3. Umbilical Cord-Derived Mesenchymal Stem/Stromal Cells (UC-MSCs). Stem/progenitor cells isolated from disposable perinatal tissues, including amnion/amniotic fluid, umbilical cord blood, placental tissue, umbilical cord blood vessels, and the Wharton's jelly, have been deemed promising for clinical applications because of the minimal safety and ethical concerns [45, 46]. MSCs and MSC-like cells have been isolated from different compartments of the umbilical cord, including umbilical vein subendothelial zone, umbilical cord blood, and specifically, Wharton's jelly [45, 47]. Wharton's jelly is the parenchyma within the umbilical cord, a mucoid connective tissue surrounding umbilical cord arteries and vein [45]. The Wharton's jelly can be further divided into three anatomical regions where MSCs can be derived from the perivascular

zone, the intervascular zone, and the subamnion [47]. Similar to BM-MSCs, MSCs derived from Wharton's jelly exhibit plastic adherence, mesenchymal multipotency, and expression of CD10, CD13, CD29, CD44, CD73, CD90, CD105, and HLA-class I but are negative for CD11b, CD14, CD19, CD31, CD34, CD45, CD56, CD79, and HLA class II [45–47].

3. Blood Vessels as a Source of MSC Precursors

The similarities between MSCs derived from many different tissues aroused the idea that a common reservoir of MSCs may exist in the body. The blood vessel, which typically consists of three structural layers: *tunica intima*, *tunica media*, and *tunica adventitia* [48], is distributed throughout nearly all human organs and therefore represents a favorable candidate. Early evidence supporting the hypothesis that the vascular wall serves as a systemic source of stem cells came from a study of the emerging hematopoietic system in the embryo and fetus, where hematopoietic cells emerged in close vicinity to vascular endothelial cells (ECs) in both intra- and extraembryonic blood-forming tissues [22]. Recently, several studies have indicated the possibility that blood vessels in different organs contain multilineage precursors that possess MSC-like features and contribute to tissue repair/regeneration [49, 50]. New evidence further pointed out that tissue-specific multipotent stem/progenitor cells, including osteogenic, neural, odontoblastic, and adipogenic progenitors, may originate from and/or associate with vascular/perivascular niches *in vivo* [18–21].

Microvascular pericytes (PCs), a set of perivascular mural cells surrounding *the intima* of microvessels and capillaries, are traditionally regarded as a structural component of blood vessels, regulating vascular contractility, stability, and integrity [51, 52]. Intimate interactions between PCs and ECs tightly regulate vascular growth, maturation, and remodeling [51, 53–55]. Recently, PCs have been implicated in a number of pathological conditions, making them potential targets for therapeutic interventions [55, 56]. On the other hand, the *tunica adventitia*, the outermost layer of large blood vessels, has long been considered as a structural bystander, consisting of loosely structured collagen-rich extracellular matrix (ECM), which embeds stromal cells/fibroblasts, the *vasa vasorum*, and perivascular nerves [57]. The importance of the *tunica adventitia* was recently reevaluated due to a number of studies reporting its active role in vascular remodeling, immune response mediation, cell trafficking, and atherosclerosis [57–59]. In a vascular remodeling setting following an injury, it has been shown that adventitial cells (ACs) start a process of proliferation, migration into the tunicae media and intima, and differentiation into smooth muscle cells [60–62]. Recently, we and several other groups reported new strategies for the identification and purification of the elusive PCs and ACs [23, 24, 39, 63–65]. Using immunohistochemistry and flow cytometry, we identified human PCs and ACs *in situ* and purified these cells to homogeneity based on their unique expressions of cell surface antigens. Details of the isolation and characterization of PCs and ACs will be described in the following sections.

Unlike the *tunicae media* and *adventitia*, the subendothelial zone of *tunica intima* has previously been suggested as one of the sources of EPCs [66, 67]. Apart from PCs and ACs, some of us have also reported a rare but distinct subset of blood-vessel-derived stem cells, that is, myogenic endothelial cells (MECs), residing within the intima of microvasculature in human skeletal muscle [25]. MECs, presumably the human counterpart of murine muscle derived stem cells (MDSCs), not only express the myogenic cell marker, CD56, but also display endothelial cell markers, CD34 and CD144. Following purification by FACS, MECs (CD34+/CD56+/CD144+/CD45−) can be clonally expanded and exhibited osteo-, chondro-, adipo-, and myogenic differentiation capacities *in vitro* [25]. Furthermore, MECs exhibited superior cardiac repair capacity in ischemic hearts and myogenic regeneration in injured skeletal muscle than conventional CD56+ myoblasts and ECs [25, 68, 69]. Nevertheless, despite their MSC-like features and tissue reparative/regenerative capability, whether MECs contribute significantly to the MSC entity remains to be clarified due to their restricted presence in skeletal muscle.

4. Identification and Purification of Perivascular MSC Precursors

4.1. Placenta. While placenta and umbilical cord are often discarded at birth, these extraembryonic tissues contain large numbers of stem/progenitor cells, making them attractive sources of donor cells for regenerative medicine. We and others have isolated multipotent PCs (CD146+/CD34−/CD45−/CD56−) from these tissues and utilized them toward multiple tissue repair/regeneration, including skeletal muscle [70], lung [71], dermal [72], and nervous tissues [73].

Placenta is a highly vascularized extraembryonic tissue, which serves as fetomaternal interface to sustain proper oxygen transportation, waste disposal, and nutrient delivery. The placental vasculature has been thoroughly characterized throughout fetal development previously and consists of all sizes/types of blood vessels and both pericytes/perivascular cells and ECs at all stages [74, 75]. Placenta PCs are critical to maintain blood vessel homeostasis and promote angiogenesis [76, 77]. PC abnormity in placenta capillaries leads to defects in sinusoidal integrity, a phenotype often observed during pregnancy complications due to diabetes, postmaturity, or preeclampsia [78]. In addition to their supportive role in the fetal vasculature, placental PCs have also been identified as a source of MSCs [23, 70, 79]. Our previous studies have discriminated mesenchymogenic placental PCs based on the expression of the cell adhesion molecule CD146 and lack of EC markers: CD34, CD144, and vWF [23, 70]. Similarly, Castrechini et al. described a perivascular population residing in human fetal and term placenta, which coexpressed MSC/PC markers (Stro-1, 3G5, CD105, CD106, CD146, CD49a, α-SMA) but not hematovascular markers (CD117, CD34, vWF) and were competent for trilineage mesenchymal differentiation [79]. In our hands, human fetal and term chorionic villi

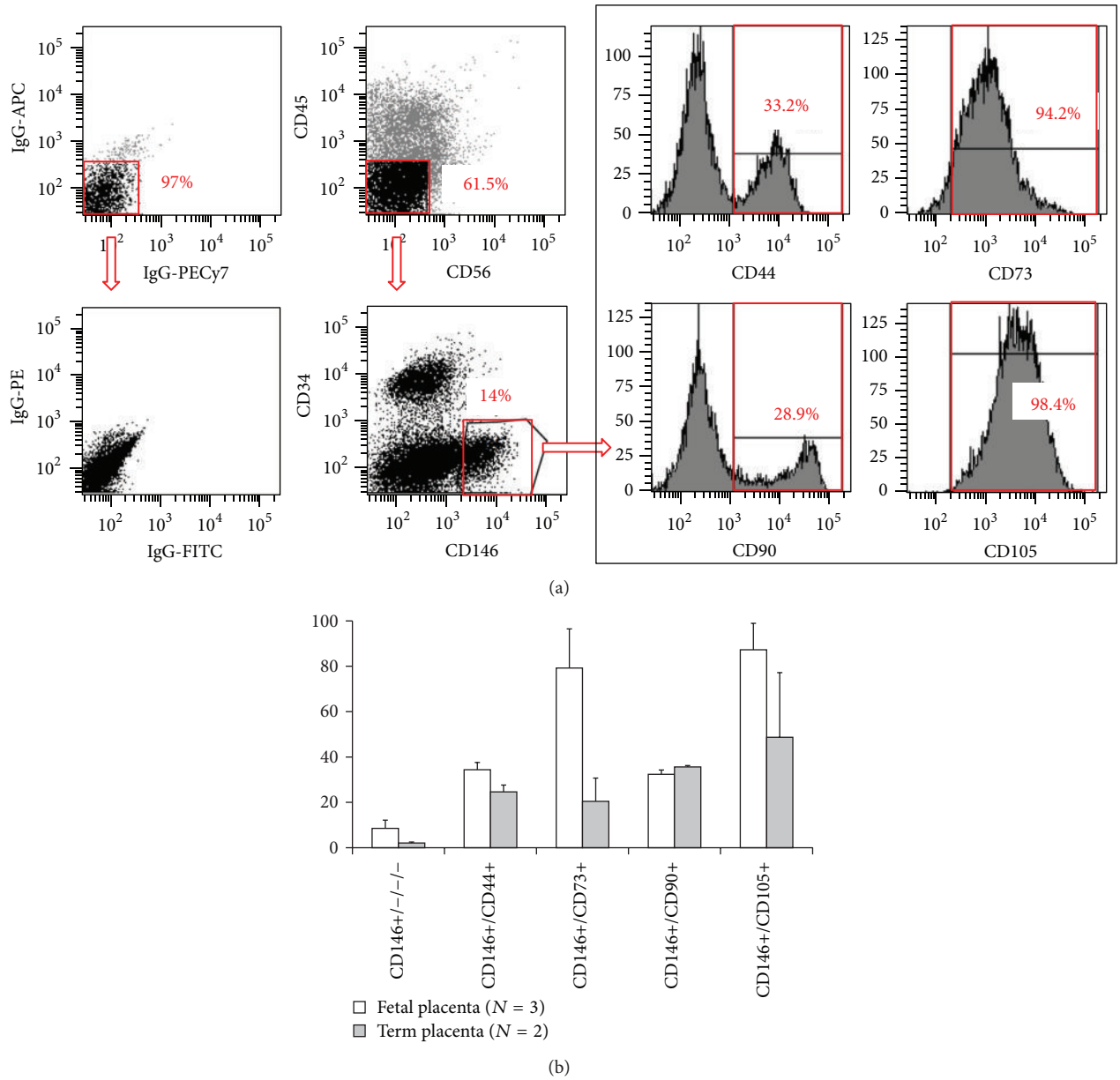

Figure 1: Flow cytometry analysis of mesenchymal stem cell marker expression in freshly isolated fetal and term placental pericytes. (a) Representative flow cytometry analysis of human placenta that was mechanically dissociated and enzymatically digested and subsequently stained for CD45, CD56, CD34, and CD146 along with CD44, CD73, CD90, or CD105. Matching isotype controls were shown in the left column. (b) Human fetal placenta ($N = 3$, average 20 weeks of gestation) and term placenta ($N = 2$, average 39 weeks of gestation) were used to isolate subsets of pericytes using surface expression of CD146+/CD34−/CD45−/CD56− (CD146+/−/−/−) and colabeled with one of the mesenchymal stem cell markers (CD146+/CD44+, CD146+/CD73+, CD146+/CD90+, CD146+/CD105+) as shown in (a). Values are mean ± standard error.

of placentas included 8.5 ± 3.66% ($N = 3$, 19 to 21 weeks of gestation) and 2.1 ± 0.43% ($N = 2$, 39 weeks of gestation) of PCs (CD146+/CD34−/CD45−/CD56−), respectively (Figure 1).

The native expression of CD146 by mesenchymogenic PCs in many tissues including bone marrow, fetal and term placentas has been reported [23, 70]. Using FACS, we purified PCs from mechanically and enzymatically dissociated placental chorionic villi [23, 70]. Freshly isolated placenta PCs natively expressed MSC markers (CD44, CD73, CD90, and CD105) at varying levels (30 to 87% of fetal and 20 to 48% of term placental CD146+/CD34−/CD45−/CD56− PCs) (Figure 1). We have previously demonstrated that when placed onto ECM-coated plates, dissected fetal placental villi release a population of vascular cells, which possess high migratory activity and robust capacity to regenerate skeletal muscle fibers in dystrophic mice [70]. The cells migrating out of placental villi included predominantly CD146+ cells

which coexpressed PC (NG2 and PDGFRβ) and MSC (CD44, CD73, CD90, and CD105) surface antigens and were deprived of EC antigens (CD31, CD34, CD144, and vWF) [70]. Maier et al. employed a similar approach to isolate PCs from the cellular outgrowth of human term placenta explants [80]. Consistently with fetal placenta, term placenta PCs expressed high levels of PC/MSC markers (CD146, PDGFRβ, NG2, CD90, and calponin), including 65 transcripts that are highly expressed in undifferentiated MSCs, and lacked endothelial/hematopoietic cell marker expression (CD31, CD34, and CD45) [80].

4.2. Umbilical Cord. Human umbilical cord (HUC) has been known as an abundant source of ECs as well as MSCs derived from the Wharton's jelly. Recently some of us demonstrated that human full-term UCs and, at a higher frequency, fetal (preterm) UCs contain perivascular cells that exhibit features of MSCs. These perivascular smooth muscle-like cells present in the HUC co-expressed CD146 and alpha-smooth muscle actin (αSMA) but did not express the established EC markers: CD144, CD34, CD31, and Ulex europaeus agglutinin (UEA-1) receptor. Using FACS, Montemurro et al. isolated a population of PCs (CD146+/NG2+/PDGFRβ+) from umbilical cords of preterm newborns [71]. These HUC-derived perivascular cells (HUCPCs) can be maintained in long-term culture, exhibiting classical spindle-shape PC morphology. When characterized by flow cytometry during subsequent passages, they maintained the expression of CD44, CD90, CD73, CD105, HLA class I, CD146, NG2, αSMA, and PDGFRβ as well as retained their multipotency to differentiate towards different cell types, including osteogenic, adipogenic, and myogenic cell lineages [71].

4.3. Skeletal Muscle. Skeletal muscle has been shown to harbor several adult stem/progenitor cell populations in mammals including humans, in addition to the typical muscle stem cells, that is, satellite cells [81–83]. Many studies have demonstrated that muscle derived stem/progenitor cells are capable of differentiating into a variety of cell lineages *in vitro* and *in vivo*, including blood cells and fat [25, 81, 84–86]. Using similar immunohistochemical and flow cytometry strategies, we first identified microvascular PCs *in situ* within human skeletal muscle and subsequently purified them from mechanically and enzymatically dissociated muscle biopsies via FACS [23]. Similar to PCs sorted from other tissues, muscle PCs (CD146+/CD34−/CD45−/CD56−) expressed typical PC markers: CD146, NG2, PDGFR-β, alkaline phosphatase (ALP), and α-smooth muscle actin (α-SMA), with the absence of EC markers: CD31, CD34, CD144, and vWF as well as the hematopoietic cell marker CD45 and myogenic cell marker CD56. Muscle PCs can be efficiently expanded in culture, at the clonal level, while maintaining robust mesodermal developmental potentials. Freshly isolated and long-term cultured muscle PCs both displayed robust myogenic capacity *in vitro* and *in vivo*. Moreover, muscle PCs natively and in culture expressed classic MSC markers: CD44, CD73, CD90, and CD105, indicating their developmental status as MSC ancestors [23].

4.4. Adipose. Vasculogenic CD34+/CD31− cell populations have been described in the adventitial *vasa vasorum* of large blood vessels such as the vena saphena [65] and the thoracic aorta [67], but microvascular CD34+ ACs seem to be a specific feature of the adipose and subcutaneous tissue [87]. Apart from CD34 expression and their adjacent anatomical localization within the blood vessel wall, ACs can be discriminated from adipose PCs due to the lack of native expression of PC markers (αSMA, CD146, NG2, PDGFRβ) [24, 39, 42]. The high prevalence (~50%) of CD34+/CD146− progenitor cells in the nonhematopoietic adipose SVF [39, 88, 89] and their limited clonogenicity and heterogeneous proliferative capacity [24] do not preclude the possibility that distinct CD34+ stem/progenitor cells exist within adult adipose tissue. Using a peroxisome proliferator-activated receptor gamma (PPARγ) reporter mouse model, Tang et al. demonstrated that adipogenic progenitors emerge from CD34+ cells which later adopt a perivascular niche and express PC markers (αSMA, NG2, PDGFRβ) [21]. Similarly, human adipose CD34+/CD146− ACs can acquire PC markers (αSMA, CD146, NG2, PDGFRβ) *in vitro*, following treatment with angiotensin II or angiopoietin-2 [24].

While developmentally mesenchymogenic PCs may arise from transient CD34+ cell population(s), the persistence of such CD34+ precursors in the adult and their ontological relationship to the bulk of CD34+ ACs in human fat will require further investigation. Indeed, rare CD34+ mesenchymogenic cells have been reported in fetal [24, 90, 91] and adult [92, 93] bone marrow, as well as in fetal muscle and fetal lung [24]. A multipotent CD34+ cell population residing in the wall of dorsal aorta, the mesoangioblast, has been proposed to be an ancestor of adult mesenchymogenic PCs in the mouse [49, 81]. Some groups have reported the direct derivation of CD34+ primitive MSCs from human embryonic stem cells (hESC) [94, 95], while Vodyanik et al. described the emergence of a multipotent MSC precursor, the mesenchymoangioblast, from hESC-derived CD34+ cells in a stepwise differentiation system [96]. Furthermore, Dar et al. recently reported successful derivation of CD105+/CD90+/CD73+/CD31− multipotent mesodermal precursors from embryoid bodies of either human ESCs or iPSCs that exhibit clonogenicity, mesenchymal differentiation potentials, and *bona fide* pericyte features, including angiogenic/vasculogenic capacity and expression of CD146, NG2, and PDGFRβ but not αSMA, CD56, CD34, or EC markers [97]. These hPSC-derived PCs significantly facilitated vascular and muscle regeneration when transplanted into the ischemic limb of immunodeficient mice, with the presence of hPSC-PCs in both recovered vasculature and myofibers, indicating robust vasculogenic and myogenic capacities *in vivo* similar to their adult counterparts [97]. Yet, the reciprocity of all these fetal populations to all or part of adult MSC precursors remains to be clarified.

A rare CD34+/CD146+/CD31−/CD45− population of adipose PCs has also been characterized in the SVF [39, 98–103] and may represent a developmental intermediate between PCs and some or all ACs [102]. This elusive CD34+ PC population is not easily detected within the vascular wall by immunohistochemistry [24, 42] and requires

stringent rare-event strategies for its detection and isolation by flow cytometry [100, 103]. Traktuev et al. suggested the existence of CD34+ cells exhibiting a native pericytic phenotype [98]. They demonstrated that primary cultures of AC-like CD34+CD144−CD45− SVF cells can express PC markers (NG2, PDGFRα, PDGFRβ) without requirement of blood vessel remodeling growth factors in contrast to CD34+CD146− cells [24]. Though these disparities may be related to culture conditions, SVF isolation techniques, and cell sorting strategies, the intricacy and anatomical proximity of these distinct subpopulations highlight the necessity to use multidimensional strategies for their isolation via exclusion of hematopoietic (CD45) and endothelial (CD31, CD144) lineages and combinatory positive selection of pericytic (i.e., CD146, NG2, PDGFRβ), adventitial (CD34), or MSC (CD44, CD73, CD90, CD105) cell subsets. A number of studies have employed preliminary sorting strategies relying on single markers, such as CD146 [104, 105] or CD34 [40, 106, 107], which may be inadequate in regard to the overlapping phenotypes of the vascular/perivascular cell subsets populating the adipose tissue.

Recently, using a combination of above-mentioned positive and negative selection antigens, we performed advanced flow cytometry analyses and FACS in the adipose SVF in order to identify and simultaneously purify these MSC precursor subpopulations [23, 24, 39, 101]. Both CD146+/CD34−/CD45− PCs and CD34+/CD31−/CD45−/CD146− ACs purified from adipose SVF have been shown to express MSC markers *in vivo* and in culture [23, 24, 101]. Furthermore, our quantitative multiparameter studies showed that only a third of adipose PCs (CD146+/CD34−/CD31−/Lineage−/CD45−) natively coexpress the MSC markers CD73, CD90, and CD105, which reveals the cellular heterogeneity of the pericyte compartment [101]. In contrast, both CD146+ (putative PC-AC intermediates) and CD146− (ACs) subsets of CD34+/CD31−/Lineage−/CD45− SVF cells homogenously co-express MSC markers [101]. On the other hand, among these MSC-like perivascular cells, two subpopulations in the adipose SVF can be discerned on the basis of CD34 expression and further distinguished by their proliferation pattern: a low proliferative CD34− subset and a high proliferative CD34+ subset. While CD34− is a typical phenotype of multipotent mesenchymogenic PCs in adipose and most other tissues [23], the CD34+ phenotype may represent transit-amplifying intermediates between stem-like adipose PCs and highly prevalent ACs *in vivo* but require prudent interpretations in culture due to its instability.

5. Adhesion and Migration of Perivascular MSC Precursors

In view of future stem cell-based approaches and therapies, it is crucial to identify predictive parameters that allow the researchers and clinicians to foresee the *in vivo* action of stem/progenitor cells. Since cell adhesion and migration capacities are tightly correlated with *in vivo* cell trafficking and homing, these parameters represent potential predictors for the clinical outcome of stem cell-treated patients and require further investigation [108–110]. Herein we discuss recent progresses in the understanding of perivascular MSC precursors in regard to cell adhesion, migration, and response to hypoxia.

5.1. Cell Adhesion. Anatomically, PCs closely surround ECs populating the vascular intima with specific adhesion and migration properties that allow them to regulate the blood vessel stability/integrity as well as the proliferation and motility of adjacent ECs [51]. Up to 1000 contacts can be secured by peg-sockets to a juxtaposing EC via cytoplasmic fingers inserted into endothelial invaginations [111]. Pericytic elongated terminal arms include adhesion plaques that strongly embed into the basement membrane and EC body to secure their location [111]. Different molecules and pathways have been involved in mural cell motility and adhesion. Notably, ephB/ephrin-B interactions mediate human MSC/PC adhesion, migration, and differentiation [112, 113]. The eph/ephrin family of tyrosine kinase receptors has been identified as an important factor contributing to bone homeostasis and regulating MSC adhesion. Inhibition of ephrin-B signaling prevents MSC attachment and spreading by activation of Src-, PI3 Kinase-, and JNK-dependent signaling pathways [112]. Ephrin-B2-deficient mural cells display major defects in spreading, focal-adhesion formation, and polarized migration as well as exhibiting increased motility [113]. Our group investigated adhesion molecules and proteins involved in PC migratory capacity. We demonstrated that CD146+/NG2+/PDGFRβ+/CD144− PCs exhibited more robust adherence to extracellular matrix substrates (e.g., collagen type-I, gelatin, and fibronectin) and greater migratory capacity than the CD146− population. Enhanced adherence and migratory capacities may result from high expression levels of alpha and beta subunits of integrin and matrix metalloproteinase (MMP)-2, respectively [70]. On the other hand, PCs express intercellular adhesion molecule 1 (ICAM-1) and upregulate its expression in response to tumor necrosis factor (TNF) and pattern-recognition receptor (PRR) ligands. ICAM-1 also regulates interactions of neutrophils and monocytes with PCs *in vitro* [114]. Moreover, it has been suggested that arteriolar and capillary PCs can detect inflammatory stimuli and increase their adhesive interactions with innate leukocytes, implicating their role in the regulation of inflammatory responses [114, 115].

5.2. Cell Migration. PC recruitment and migration occur frequently in response to pathophysiological events such as wound healing, inflammation, or angiogenesis. During vascular development, ECs release PDGF-BB to recruit PCs and stabilize the newly formed blood vessels [116, 117]. Increase of PC density by activation of PDGF-BB/ PDGFRβ signaling pathways has also been detected during wound healing and tumor vascular remodeling [56, 111, 118]. Inversely, disruption of PDGF-BB/PDGFRβ pathways may occur during pathologic conditions (e.g., diabetic retinopathy), resulting in PC apoptosis and augmented permeability of the vascular wall [111, 119]. Upon inflammatory events, PCs control the pattern and efficiency of leukocyte interstitial migration *in vivo* [114,

120]. A recent study highlighted the constitutive expression of chemoattractants by NG2+ PCs: CSC-chemokine ligand-1 (CXCL1) and -8 (CXCL8), macrophage migration inhibitory factor (MIF), CC-chemokine ligand 2 (CCL2), and interleukin-6 (IL-6). PCs further upregulated the expression of these chemo-attractants following stimulation by PRR ligands [114, 115]. Therefore, PCs not only chemotactically migrate to the site of angiogenesis, injury, or inflammation but also actively recruit other proinflammatory participants, including myeloid leukocytes, neutrophils, and macrophages.

Using an *in vitro* model of tissue damage, some of us previously mimicked the ability of HUCPCs to migrate towards the injury site *in vivo* and predicted their capacity to secrete cytokines and trophic factors [71]. Envisioning a possible clinical application of stem cells in the context of extremely immature newborns with an acute lung injury, where alveolar type II cells crucial for producing surfactant and regulating alveolar fluid levels and host defense are damaged, HUC can be readily considered as a convenient source of stem cells. Consequently, a coculture model of pulmonary tissue damage was set up, where an alveolar type II cell line was damaged with bleomycin, an anticancer drug with known pulmonary toxicity [71]. Dye-labeled HUCPCs in coculture were mobilized and migrated towards the damaged alveolar type II cells. HUCPCs showed a great ability to secrete angiogenic/antiapoptotic cytokines and trophic factors compared to the control, in particular high level of keratinocyte growth factor (KGF) [71]. KGF appears to play a crucial role mediating tissue improvement in a range of experimental lung injuries, presumably due to its versatile effects including cellular repair, cytoprotection, and alveolar fluid clearance modulation and immunomodulation [121, 122]. Similarly, skeletal muscle-derived PCs secrete high levels (superior to those of BM-MSCs) of KGF and vascular endothelial growth factor (VEGF) as well as heparin binding-epidermal growth factor (HB-EGF) and basic-fibroblast growth factor (bFGF), which are all considered playing critical roles during wound healing [123, 124].

The abundance of mesenchymogenic progenitors in the SVF of adipose tissue (5,000 CFU-F per gram) [125] provides a great advantage for the development of clinical applications without any *in vitro* expansion requirements [126, 127]. ASC-based therapeutic strategies have been proposed for either regenerative or targeted therapies and often rely on native tropism of ASCs for wound healing, inflammation, or cancer. Although investigations of cell adhesion and migration in purified ACs are currently ongoing, much can be learned from the unfractionated ASCs which have been shown to home to sites of injury and promote tissue repair following systemic injections in animal models of myocardial infarction [128, 129], liver injury [130, 131], olfactory dysfunction [132], hypoxia-ischemia induced brain damage [133], allergic rhinitis [134], inflammatory neuropathy [135], sciatic crush [136], cranial injury [137], and muscular dystrophy [138, 139]. The migratory activity of early-passage ASCs can be modulated by a set of chemokines and growth factors, including PDGF-AB, TGF-β1, and TNFα [140]. These soluble factors can stimulate ASCs via activation of an array of migration-associated receptors such as C-C chemokine receptor types 1 and 7 (CCR1, CCR7), C-X-C chemokine receptor types 4, 5, and 6 (CXCR4, CXCR5, CXCR6), EGF receptor, fibroblast growth factor receptor 1, TGF-β receptor 2, TNF receptor superfamily member 1A, and PDGF receptors α and β [140–142].

ASCs have been proposed to affect various neighboring cells within the subcutaneous tissue via paracrine signals during active remodeling processes such as wound healing [143–145]. In a recent study, ASC-conditioned medium promoted *in vitro* migration of vascular ECs, fibroblasts, and keratinocytes [146]. These data support the impact of ASCs on the proliferation and recruitment of these distinct cell subsets during wound healing via secretion of high levels of promigratory cytokines, including angiopoietin-like-1, EGF, FGF, HGF, TGFβ, SDF-1, and VEGF [145–149].

Similarly to BM-MSCs [150, 151], ASCs have been associated with enhanced migratory activities during tumorigenesis. ASC tropism towards various tumors such as glioma [152, 153], colon cancer [154], and prostate cancer [155] has been exploited to develop targeted therapies. On the other hand, ASCs can modulate the migration of cancer cells, promoting metastasis of breast cancer cells [156, 157] via CCR5/CCL5 signaling in animal models despite the inhibition of breast cancer metastasis in a different model [158]. An antimetastatic result was also observed with pancreas cancer cells [159].

5.3. Cellular Response to Hypoxia. Hypoxia has been shown to promote proliferation and migration of both PCs and MSCs [160, 161]. A recent study highlighted the involvement of the ERK signaling pathway during the modulation of mitogenic and chemotactic responses of human muscle PCs to a low oxygen concentration (6% O_2). This activation of ERK signaling and associated integrins occurred without any detectable alteration on the cell phenotypes or differentiation potentials [160, 162]. A number of growth factors, including PDGF, EGF, and FGF, can activate the Ras-Raf-MEK1/2-ERK signaling axis [163], which controls the adhesion dynamics and cell migratory properties via formation of protrusions within cell membrane and enhancement of the focal adhesion turnover [164]. Culture of MSCs in hypoxic conditions also resulted in higher survival and migration in a hind-limb ischemia model, presumably through Akt signaling [165]. The activation of the Akt pathway has been linked to the cell migratory ability and can be mediated by hepatocyte growth factor (HGF). MSCs under hypoxia exhibited higher expression of cMet, a critical HGF receptor [165, 166], and two receptors of the chemokine stromal-derived factor-1 (SDF-1), CXCR4 and CXCR7, whose expression can also be mediated by hypoxia via the hypoxia-inducible factor-1 alpha (HIF-1α) and Akt phosphorylation [167]. Additionally, even under a 2.5% O_2 hypoxia, the paracrine function of PCs remained highly active when compared to 21% O_2 normoxic culture, with increased expression of VEGF-A, PDGF-B, and TGFβ1 and decreased expression of angiopoietin-1, bFGF, EGF, HGF, and MCP-1, and similar levels of leukemia inhibitory factor (LIF), cyclooxygenase-2 (COX-2/PTGS-2, prostaglandin endoperoxide synthase-2), heme oxygenase-1

(HMOX-1), IL-6, HIF-1α, and MMP-2 [168]. Understanding cellular responses of perivascular MSC precursors and MSCs to hypoxia would help researchers and clinicians to develop better approaches to improve the efficacy of MSC-based cell therapy, including genetic modification, cellular preconditioning, and pharmacological adjunct therapy [9].

6. Migratory and Homing Characteristics of Perivascular MSC Precursors during Tissue Repair/Regeneration

Perivascular MSC precursors have recently been demonstrated as efficient regenerative/supportive units for tissue repair and regeneration. In particular, human muscle PCs and saphenous vein-derived ACs exhibited superior angiogenic, paracrine, and cardioprotective capacities and augmented functional recovery in murine myocardial infarction and hind-limb ischemia models when compared to myoblasts or unfractionated MSCs [65, 168, 169]. Additionally, muscle and placental PCs were shown to repair/regenerate injured and dystrophic muscles in animal disease models as well as contribute to the muscle stem cell (satellite cell) pool [23, 64, 70, 170]. Some of us also showed that HUCPCs prevented/rescued the oxygen-induced arrest in alveolar growth and restored lung function and architecture, primarily through their paracrine function [171]. Interestingly, CD146+ PCs extracted from adipose tissue were shown to support the long-term persistence of human hematopoietic stem/progenitor cells in coculture [172]. Moreover, purified human PCs and ACs exhibited bone formation or healing when implanted into animal models of ectopic bone formation or critical-sized calvarial bone injury, respectively [88, 89, 173]. In this section, we will discuss the current understanding of the cell engraftment, migration, and homing of transplanted perivascular MSC precursors during some of these regenerative events.

6.1. Cardiac Repair. When intramyocardially transplanted into a mouse model of acute myocardial infarction (AMI), purified human muscle PCs contributed to cardiac functional and anatomic recovery after infarction, presumably through multiple cardioprotective and regenerative mechanisms: reversal of ventricular remodeling, reduction of cardiac fibrosis, diminution of chronic inflammation, promotion of host angiogenesis, and small-scale myocardial regenerative events [168]. The engraftment ratio of intramyocardially injected GFP-labeled PCs was approximately 9% at the first week, decreasing to roughly 3% at 8 weeks after infarction. Above all, a fraction of donor PCs was identified in perivascular positions, juxtaposing host CD31+ ECs (Figure 2). In contrast to the engraftment ratio, the vessel-homing ratio of transplanted PCs slightly increased over time, implicating the potential benefit of niche-homing for long-term donor cell survival. Moreover, cellular interactions between donor PCs and host ECs were demonstrated by the expression of human-specific ephrin type-B receptor 2 (EphB2) in some GFP+ PCs adjacent to ECs as well as the formation of connexin 43 gap junctions with ECs [168]. Additionally, immune cells

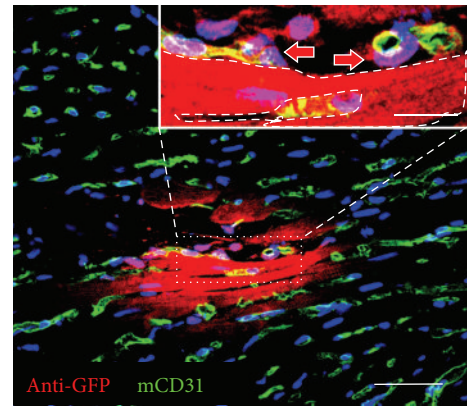

Figure 2: Human pericytes home to perivascular locations. Confocal microscopy showed that GFP+ human pericytes (red), identified by anti-GFP immunostaining, can be located at the interstitial space where host CD31+ capillaries (green) reside (main, scale bar = 50 μm). Some GFP+ donor cells (inset, red arrows) are in close contact with mouse CD31+ endothelial cells (green). Dash line in the inset picture delineates a putative GFP+ cardiomyocyte (inset, scale bar = 10 μm).

in the ischemic tissue release chemokines such as interleukins and monocyte chemoattractant protein-1 (MCP-1), which are involved in the homing of MSCs to the ischemic heart [174]. Moreover, the paracrine anti-inflammatory function of human MSCs was also demonstrated by the high expression of anti-inflammatory protein TSG-6 from MSCs embolized in lung, which led to decreased inflammatory responses, reduced infarct size, and improved cardiac function [175].

Similarly, Katare et al. reported that transplantation of human saphenous vein-derived ACs (hSV-ACs), a putative PC progenitor population, promoted functional improvement in a mouse model of MI, primarily through angiocrine activities and neovascularization via both donor and recipient cells as well as other cardioprotective mechanisms including improved myocardial blood flow, attenuated vascular permeability, and reduction of myocardial remodeling, cardiomyocyte apoptosis, and interstitial fibrosis [169]. hSV-ACs produced and released microRNA-132 (miR-132) as a paracrine agent, which exerts proangiogenic, prosurvival, and antifibrotic activities and likely plays a key role as an activator of cardiac healing. While retaining their original antigenic and perivascular phenotype, homing of hSV-ACs to perivascular locations was confirmed by Dil-labeled hSV-ACs juxtaposing isolectin-positive capillary ECs [169].

6.2. Muscle Regeneration. As mentioned previously, we have demonstrated that intramuscular injection of freshly sorted or cultured PCs derived from human adipose or skeletal muscle regenerated human myofibers efficiently in the mouse dystrophic or injured muscle [23]. In another study, we showed that intramuscular implantation of dissected human placental villi resulted in crude outgrowth of human cells in dystrophic mice [70]. Ample amount of cells of human origin released from placental villi fragments participated in host muscle regeneration, revealed by the

detection of human dystrophin-positive (hDys3t) and/or human spectrin-positive myofibers. Many of these human myofibers coexpressed human lamin A/C, indicating their sole human origin and not intermediate products of cell fusion. Surprisingly, human myofibers were located not only close to the implantation area (500 μm to 2 mm) but also in far more distant regions (up to 2 cm), suggesting active migration of outgrown human myogenic precursors over long distances. Similarly, freshly isolated placental PCs possessed high migratory activity and actively contributed to host skeletal muscle regeneration [70].

6.3. Pulmonary Repair. As mentioned previously, PCs isolated from umbilical cords migrated efficiently *in vitro* toward alveolar type II cells damaged by bleomycin, with an elevated secretion of KGF and VEGF [71]. Using a preclinical animal model of oxygen-arrested lung growth (exposure to 95% oxygen, i.e., hyperoxia), which mimics bronchopulmonary dysplasia (BPD), Pierro et al. tested the *in vivo* therapeutic potential of HUCPCs [171]. To examine suitable approaches for future clinical applications, two different administration strategies, prophylactic or therapeutic, as well as two different therapeutic modalities, direct cell transplantation or HUCPC-conditioned medium injection, were investigated. Intratracheal transplantation of HUCPCs prevented/rescued oxygen-induced arrested alveolar growth and restored normal alveolar architecture. However, immunofluorescence and qPCR revealed very few donor cells localized within the lung. This low cell engraftment suggested that cell replacement is not the primary mechanism of the observed therapeutic effects. Indeed similar therapeutic benefits can be achieved by daily intraperitoneal administration of conditioned medium, resulting in improved alveolar architecture and lung function. In both administration strategies, long-term efficacy and safety were demonstrated till 6 months with an improved exercise capacity and normal alveolar architecture. No suspicious tumor formation was noted by total body CT scans. In conclusion, the therapeutic potential of HUCPCs for pulmonary repair can be exploited by either direct cell therapy or the production of trophic factors, expanding new clinical perspectives for HUCPCs and other perivascular MSC precursors.

6.4. Skeletal Regeneration. To investigate their skeletal regenerative capacity, human PCs and ACs purified from lipoaspirate SVF have been seeded onto osteoinductive scaffolds and implanted into animal models of ectopic bone formation or critical-sized calvarial bone injury, respectively [88, 89, 176]. Significantly greater osteogenesis or bone healing by PCs and ACs in murine muscle pockets or calvarial defects than control SVF cells was observed, respectively. Additionally, the high osteogenic capability of human ACs and PCs can be further enhanced by Nel-like molecule-1 (NELL-1), an osteoinductive growth factor that is a direct transcriptional target of Runx2 [89, 173, 176, 177]. On the other hand, the role of the SDF-1/CXCR4 pathway in MSCs/PCs recruitment during the injury response has been established in a murine model of femoral bone graft, where SDF-1 deficient mice were unable to recruit MSCs at bone fracture sites and consequently limited their participation to local bone repair [178]. The role of the SDF-1/CXCR4 axis in PC recruitment has also been revealed during tumorigenesis [179]. Overexpression of PDGF-BB increased malignant PC growth via activation of the SDF-1/CXCR4 axis and induced expression of SDF-1 in ECs. The upregulation of SDF-1 was directly mediated by inhibition of the Akt/mTOR pathway or HIF-1α. Accordingly, both donor and host stem cell homing can be further enhanced by MSCs genetically modified to overexpress SDF-1 [180].

7. Angiogenic Capacities of Perivascular MSC Precursors and Cellular Interactions with ECs

7.1. Pericyte-EC Cellular Interactions: A Perivascular Niche for MSC Precursors. PCs are ubiquitously present in microvasculature where they extend primary cytoplasmic processes along the abluminal surface of the endothelial tube. They are enveloped in a basement membrane that is continuous with the EC basement membrane to which both cells contribute [181, 182]. The majority of the PC-EC interface is separated by basement membrane, with the two cell types contacting each other at discrete points through peg-socket type interactions, occluding contacts, gap junctions, and adhesion plaques [183, 184]. The intimate anatomical relationship between ECs and PCs suggests close interactions involving not only direct contact but also paracrine or juxtacrine signaling. EC-to-PC ratios in normal tissues vary between 1 : 1 to 10 : 1 and may be up to 100 : 1 (in skeletal muscle), while PC coverage of the endothelial abluminal surface ranges between 10% and 70% [185, 186]. PC density and coverage appear to correlate with endothelial barrier properties (i.e., brain > lungs > muscle) [111], EC turnover (large turnover leading to less coverage) [184], and orthostatic blood pressure (larger coverage in lower body parts) [185], in keeping with a role of PCs in regulating capillary barriers, endothelial proliferation, and capillary diameter [111]. Genetically modified mouse models have demonstrated that these two vascular cell types are interdependent: primary defects in one cell type have obligated consequences for the other. There is growing evidence to suggest that ECs can manipulate the migratory and angiogenic properties of PCs, while *in vitro* data highlighting EC influence on mesenchymal differentiation potential of PCs points to a possible role of ECs as gatekeepers within the context of an adult stem cell niche.

7.2. EC Interactions Regulate Pericyte Recruitment and Angiogenesis. The formation of new capillaries during angiogenesis requires a series of well-orchestrated cellular events allowing ECs and PCs to migrate into the perivascular space. In vessel sprouting, angiogenic factors (e.g., VEGF) stimulate ECs, which in turn secrete proteases that degrade basement membrane and allow EC invasion. An endothelial column, guided by a migrating EC at the very tip, then moves toward a VEGF gradient [183]. Studies of the *corpus luteum* indicate that PCs are also capable of guiding sprouting processes by migrating

Table 1: The influence of ECs on the multipotency of tissue-specific MSCs.

Niche Component	Model	Stem cell surrogate	Niche surrogate	Lineage assessed	Effect on differentiation	Context	Proposed mechanism	Investigator
Endothelial cell	3D	ASC	HUVEC	Osteogenesis	↓	Paracrine	↑Wnt	Rajashekhar et al. [203]
Endothelial cell	3D	ASC	HUVEC	Osteogenesis	↓	Juxtacrine	↑Wnt	Rajashekhar et al. [203]
Endothelial cell	2D	BMSC	HUVEC	Osteogenesis	↑	Paracrine	(Dkk1-Wnt, FGF, PDGF, BMP, TGFβ, Notch)	Saleh et al. [204]
Endothelial cell	2D	BMSC	HUVEC	Adipogenesis	—	Paracrine	—	Saleh et al. [205]
Endothelial cell	2D	BMSC	HUVEC	Osteogenesis	↑	Juxtacrine	—	Xue et al. [206]
Endothelial cell	2D	BMSC	HDMEC	Osteogenesis	↑	Juxtacrine	BMP-2	Kaigler et al. [207]
Endothelial cell	2D	BMSC	HDMEC	osteogenesis	—	Paracrine	—	Kaigler et al. [207]
Endothelial cell	2D	BMSC	HDMEC	Osteogenesis	↑	Juxtacrine	N-cadherin	Li et al. [208]
Endothelial cell	2D	BMSC	HDMEC	Osteogenesis	↑	Paracrine	VEGF	Grellier et al. [209]
Endothelial cell	2D	BMSC	HDMEC	Osteogenesis	↓	Paracrine	Osterix/OSX	Meury et al. [210]
Endothelial cell	2D	BMSC	HUVEC	Osteogenesis	↑	Juxtacrine	Cx43/gap junctions	Villars et al. [211]
Endothelial cell	2D	BMSC	HUVEC	Osteogenesis	↑	Juxtacrine	—	Villars et al. [212]
Endothelial cell	2D	HOP	HUVEC	Osteogenesis	↑	Juxtacrine	—	Guillotin et al. [213]
Endothelial cell	2D	HOP	EPC, HSVEC	Osteogenesis	↑	Juxtacrine	Cx43/gap junctions	Guillotin et al. [213]

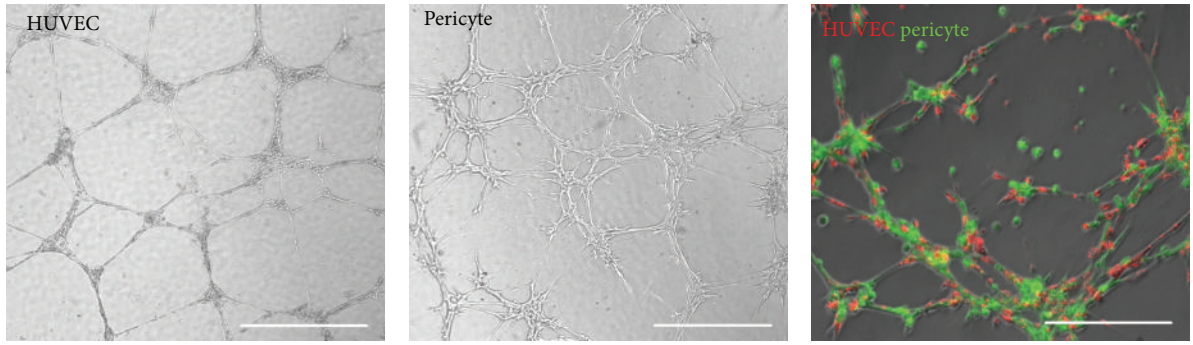

(a) (b) (c)

Figure 3: Human pericytes support formation of microvascular structures. (a) HUVECs seeded onto Matrigel-coated wells formed typical capillary-like structures after 24 hours (scale bar = 1 mm). (b) Human muscle pericytes formed morphologically similar network structures within 6–8 hours (scale bar = 1 mm). (c) Cocultured dye-labeled HUVECs (red) and pericytes (green) at 1 : 1 ratio on Matrigel showed coformation of capillary-like networks within 6–8 hours (scale bars = 500 μm).

ahead of ECs and expressing VEGF [187–189]. Emerging endothelial tubes then secrete growth factors, partly to attract PCs that envelop the vessel wall, and promote vessel maturation. Key pathways implicated in PC-EC signaling include PDGF/PDGFRβ, angiopoietins and Tie receptors, sphingosine-1-phosphate signaling, TGF-β signaling, Notch and Wnt [116, 186, 190, 191]. It is believed that PCs, because of their vessel-embracing position, are able to transfer angiogenic signals along the vessel length by contacting numerous ECs. The recruitment and contribution of PCs to developing endothelial tubes and angiogenic process can be observed *in vitro* through Matrigel culture. Human muscle PCs alone can form network structures in Matrigel culture that were morphologically similar to networks formed by ECs but at an accelerated fashion (Figures 3(a) and 3(b)). Coculture of dye-labeled PCs and ECs at 1 : 1 ratio in Matrigel showed network formation by both cell types, facilitated by the presence of PCs (Figure 3(c)). Blocki et al. further demonstrated that while the capacity to colocalize and/or coform network structures with endothelial tubules on Matrigel is not restricted to PCs, only PCs (CD146+/CD34−) effectively stabilize endothelial networks and improve endothelial sprout integrity [192]. Nevertheless, it is noteworthy that the EC-to-PC ratio may play an important role in the formation of vascular networks and PC functionality *in vitro*.

7.3. ECs: The Gatekeepers of Pericyte Mesenchymal Activation? A growing number of studies demonstrate that tissue resident stem cells reside in vascular niches, including neural, hematopoietic, and MSCs [19, 193–195]. Adult stem cell niche components provide signals that control the balance between quiescence, self-renewal, and differentiation [194]. A significant obstacle in identification of the perivascular origin of

MSCs was the reluctance of PCs to express mesenchymal phenotypes in their native microenvironment [196]. Although it is feasible that PCs acquire MSC potentials upon exiting the microvasculature, it is intuitive that MSC features are expressed by PCs *in situ* but environmentally downregulated. Studies using unfractionated SVF have demonstrated poor and unreliable tissue formation [197] or lower regeneration efficacy relative to prospectively isolated and purified MSCs [197], lending further support to a hypothesis that certain cellular component(s) of SVF have an inhibitory/adverse effect on differentiating MSCs. As such, the influence of ECs on the multipotency of tissue-specific MSCs is now under investigation even though preliminary results to date have been divergent (Table 1). Osteogenic and adipogenic differentiation is not seen within the perivasculature of healthy tissues where the PC-EC relationship is undisturbed. However, disturbed PC-EC interactions have been observed in conditions associated with pathological mineralization and adipogenesis, for example, heterotopic ossification and atherosclerosis [198, 199]. In addition, the ECM proteins, also present within a perivascular niche, have been shown to modify growth and differentiation of MSCs, with collagen type I-, fibronectin-, and vitronectin-treated plates enhancing mineralization *in vitro* [200]. The secretome and proteome of human MSCs have now been extensively documented [201] with studies identifying numerous transcription factors and multiple extracellular and intracellular signaling pathways that regulate adipogenesis and osteogenesis. Interestingly, inducers of differentiation along one lineage often inhibit differentiation along another. For example, the transcription factor PPARγ is a prime inducer of adipogenesis that inhibits osteogenesis, highlighting the mutual exclusivity of these lineages [202]. It is therefore likely that signaling mechanisms responsible for the mesenchymal fate of PCs will be multifactorial and distinct for different lineages.

8. Conclusion

In this review, we described the identification and characterization of perivascular MSC precursors with regard to their adhesion, migration, engraftment/homing, and intercellular cross-talk in culture and in experimental animal models. Although PCs and ACs both exhibit multilineage mesenchymogenic capacities and are derived from adjacent perivascular structural layers, further investigations are required to clarify their developmental relationship as well as the involvement of an ontogenic intermediate. Through the understanding of their unique cellular kinetics and regenerative potential, we will be able to define the pathophysiological role and therapeutic value of the individual blood-vessel-derived MSC precursor population under a particular pathological circumstance. Ultimately, through the purification and/or recombination of these distinct subsets of MSC precursors, it is feasible to further enhance stem cell therapy by eliminating cells with none or limited regenerative potentials in a specific disorder, creating a customized therapeutic modality for the personalized medicine.

Authors' Contribution

Iain R. Murray and Ludovic Zimmerlin contributed equally to this work.

References

[1] S. P. Bruder, D. Gazit, L. Passi-Even, I. Bab, and A. I. Caplan, "Osteochondral differentiation and the emergence of stage-specific osteogenic cell-surface molecules by bone marrow cells in diffusion chambers," *Bone and Mineral*, vol. 11, no. 2, pp. 141–151, 1990.

[2] P. A. Zuk, M. Zhu, H. Mizuno et al., "Multilineage cells from human adipose tissue: implications for cell-based therapies," *Tissue Engineering*, vol. 7, no. 2, pp. 211–228, 2001.

[3] A. I. Caplan and J. E. Dennis, "Mesenchymal stem cells as trophic mediators," *Journal of Cellular Biochemistry*, vol. 98, no. 5, pp. 1076–1084, 2006.

[4] J. García-Castro, C. Trigueros, J. Madrenas, J. A. Pérez-Simón, R. Rodriguez, and P. Menendez, "Mesenchymal stem cells and their use as cell replacement therapy and disease modelling tool," *Journal of Cellular and Molecular Medicine*, vol. 12, no. 6B, pp. 2552–2565, 2008.

[5] W. Prasongchean and P. Ferretti, "Autologous stem cells for personalised medicine," *New Biotechnology*, vol. 29, no. 6, pp. 641–650, 2012.

[6] A. F. Steinert, L. Rackwitz, F. Gilbert, U. Noth, and R. S. Tuan, "Concise review: the clinical application of mesenchymal stem cells for musculoskeletal regeneration: current status and perspectives," *Stem Cells Translational Medicine*, vol. 1, no. 3, pp. 237–247, 2012.

[7] L. Wu, X. Cai, S. Zhang, M. Karperien, and Y. Lin, "Regeneration of articular cartilage by adipose tissue derived mesenchymal stem cells: perspectives from stem cell biology and molecular medicine," *Journal of Cellular Physiology*, vol. 228, no. 5, pp. 938–944, 2013.

[8] W. M. Jackson, L. J. Nesti, and R. S. Tuan, "Potential therapeutic applications of muscle-derived mesenchymal stem and progenitor cells," *Expert Opinion on Biological Therapy*, vol. 10, no. 4, pp. 505–517, 2010.

[9] C. W. Chen, J. Huard, and B. Péault, "Mesenchymal stem cells and cardiovascular repair," in *Mesenchymal Stem Sells*, Y. Xiao, Ed., Nova Science Publishers, New York, NY, USA, 2011.

[10] W. M. Jackson, L. J. Nesti, and R. S. Tuan, "Concise review: clinical translation of wound healing therapies based on mesenchymal stem cells," *Stem Cells Translational Medicine*, vol. 1, no. 1, pp. 44–50, 2012.

[11] C. Pontikoglou, F. Deschaseaux, L. Sensebé, and H. A. Papadaki, "Bone marrow mesenchymal stem cells: biological properties and their role in hematopoiesis and hematopoietic stem cell transplantation," *Stem Cell Reviews and Reports*, vol. 7, no. 3, pp. 569–589, 2011.

[12] M. E. J. Reinders, T. J. Rabelink, and J. W. de Fijter, "The role of mesenchymal stromal cells in chronic transplant rejection after solid organ transplantation," *Current Opinion in Organ Transplantation*, vol. 18, no. 1, pp. 44–50, 2013.

[13] L. Wang, Y. Zhao, and S. Shi, "Interplay between mesenchymal stem cells and lymphocytes: implications for immunotherapy and tissue regeneration," *Journal of Dental Research*, vol. 91, no. 11, pp. 1003–1010, 2012.

[14] M. E. Bernardo and W. E. Fibbe, "Safety and efficacy of mesenchymal stromal cell therapy in autoimmune disorders,"

Annals of the New York Academy of Sciences, vol. 1266, no. 1, pp. 107–117, 2012.

[15] L. D. S. Meirelles, A. I. Caplan, and N. B. Nardi, "In search of the in vivo identity of mesenchymal stem cells," *Stem Cells*, vol. 26, no. 9, pp. 2287–2299, 2008.

[16] M. Pevsner-Fischer, S. Levin, and D. Zipori, "The origins of mesenchymal stromal cell heterogeneity," *Stem Cell Reviews and Reports*, vol. 7, no. 3, pp. 560–568, 2011.

[17] C.-W. Chen, M. Corselli, B. Péault, and J. Huard, "Human blood-vessel-derived stem cells for tissue repair and regeneration," *Journal of Biomedicine and Biotechnology*, vol. 2012, Article ID 597439, 9 pages, 2012.

[18] B. Sacchetti, A. Funari, S. Michienzi et al., "Self-renewing osteoprogenitors in bone marrow sinusoids can organize a hematopoietic microenvironment," *Cell*, vol. 131, no. 2, pp. 324–336, 2007.

[19] M. Tavazoie, L. van der Veken, V. Silva-Vargas et al., "A specialized vascular niche for adult neural stem cells," *Cell Stem Cell*, vol. 3, no. 3, pp. 279–288, 2008.

[20] S. Shi and S. Gronthos, "Perivascular niche of postnatal mesenchymal stem cells in human bone marrow and dental pulp," *Journal of Bone and Mineral Research*, vol. 18, no. 4, pp. 696–704, 2003.

[21] W. Tang, D. Zeve, J. M. Suh et al., "White fat progenitor cells reside in the adipose vasculature," *Science*, vol. 322, no. 5901, pp. 583–586, 2008.

[22] M. Tavian, B. Zheng, E. Oberlin et al., "The vascular wall as a source of stem cells," *Annals of the New York Academy of Sciences*, vol. 1044, pp. 41–50, 2005.

[23] M. Crisan, S. Yap, L. Casteilla et al., "A perivascular origin for mesenchymal stem cells in multiple human organs," *Cell Stem Cell*, vol. 3, no. 3, pp. 301–313, 2008.

[24] M. Corselli, C. W. Chen, B. Sun, S. Yap, J. P. Rubin, and B. Péault, "The tunica adventitia of human arteries and veins as a source of mesenchymal stem cells," *Stem Cells and Development*, vol. 21, no. 8, pp. 1299–1308, 2012.

[25] B. Zheng, B. Cao, M. Crisan et al., "Prospective identification of myogenic endothelial cells in human skeletal muscle," *Nature Biotechnology*, vol. 25, no. 9, pp. 1025–1034, 2007.

[26] C. B. Ballas, S. P. Zielske, and S. L. Gerson, "Adult bone marrow stem cells for cell and gene therapies: implications for greater use," *Journal of Cellular Biochemistry*, vol. 38, pp. 20–28, 2002.

[27] H. Chao and K. K. Hirschi, "Hemato-vascular origins of endothelial progenitor cells?" *Microvascular Research*, vol. 79, no. 3, pp. 169–173, 2010.

[28] Y.-H. Choi, A. Kurtz, and C. Stamm, "Mesenchymal stem cells for cardiac cell therapy," *Human Gene Therapy*, vol. 22, no. 1, pp. 3–17, 2011.

[29] K. C. Russell, D. G. Phinney, M. R. Lacey, B. L. Barrilleaux, K. E. Meyertholen, and K. C. O'Connor, "In vitro high-capacity assay to quantify the clonal heterogeneity in trilineage potential of mesenchymal stem cells reveals a complex hierarchy of lineage commitment," *Stem Cells*, vol. 28, no. 4, pp. 788–798, 2010.

[30] R. L. R. Van, C. E. Bayliss, and D. A. K. Roncari, "Cytological and enzymological characterization of adult human adipocyte precursors in culture," *Journal of Clinical Investigation*, vol. 58, no. 3, pp. 699–704, 1976.

[31] I. Dardick, W. J. Poznanski, I. Waheed, and G. Setterfield, "Ultrastructural observations on differentiating human preadipocytes cultured in vitro," *Tissue and Cell*, vol. 8, no. 3, pp. 561–571, 1976.

[32] P. A. Zuk, M. Zhu, P. Ashjian et al., "Human adipose tissue is a source of multipotent stem cells," *Molecular Biology of the Cell*, vol. 13, no. 12, pp. 4279–4295, 2002.

[33] S. R. Daher, B. H. Johnstone, D. G. Phinney, and K. L. March, "Adipose stromal/stem cells: basic and translational advances: the IFATS collection," *Stem Cells*, vol. 26, no. 10, pp. 2664–2665, 2008.

[34] M. Dominici, K. Le Blanc, I. Mueller et al., "Minimal criteria for defining multipotent mesenchymal stromal cells. The International Society for Cellular Therapy position statement," *Cytotherapy*, vol. 8, no. 4, pp. 315–317, 2006.

[35] J. B. Mitchell, K. McIntosh, S. Zvonic et al., "Immunophenotype of human adipose-derived cells: temporal changes in stromal-associated and stem cell-associated markers," *Stem Cells*, vol. 24, no. 2, pp. 376–385, 2006.

[36] C. I. Civin, L. C. Strauss, and C. Brovall, "Antigenic analysis of hematopoiesis. III. A hematopoietic progenitor cell surface antigen defined by a monoclonal antibody raised against KG-1a cells," *Journal of Immunology*, vol. 133, no. 1, pp. 157–165, 1984.

[37] T. Asahara, T. Murohara, A. Sullivan et al., "Isolation of putative progenitor endothelial cells for angiogenesis," *Science*, vol. 275, no. 5302, pp. 964–967, 1997.

[38] C. Sengenès, K. Lolmède, A. Zakaroff-Girard, R. Busse, and A. Bouloumié, "Preadipocytes in the human subcutaneous adipose tissue display distinct features from the adult mesenchymal and hematopoietic stem cells," *Journal of Cellular Physiology*, vol. 205, no. 1, pp. 114–122, 2005.

[39] L. Zimmerlin, V. S. Donnenberg, M. E. Pfeifer et al., "Stromal vascular progenitors in adult human adipose tissue," *Cytometry A*, vol. 77, no. 1, pp. 22–30, 2010.

[40] H. Suga, D. Matsumoto, H. Eto et al., "Functional implications of CD34 expression in human adipose-derived stem/progenitor cells," *Stem Cells and Development*, vol. 18, no. 8, pp. 1201–1209, 2009.

[41] C.-S. Lin, Z.-C. Xin, C.-H. Deng, H. Ning, G. Lin, and T. F. Lue, "Defining adipose tissue-derived stem cells in tissue and in culture," *Histology and Histopathology*, vol. 25, no. 6, pp. 807–815, 2010.

[42] G. Lin, M. Garcia, H. Ning et al., "Defining stem and progenitor cells within adipose tissue," *Stem Cells and Development*, vol. 17, no. 6, pp. 1053–1063, 2008.

[43] H. Li, L. Zimmerlin, K. G. Marra, V. S. Donnenberg, A. D. Donnenberg, and J. P. Rubin, "Adipogenic potential of adipose stem cell subpopulations," *Plastic and Reconstructive Surgery*, vol. 128, no. 3, pp. 663–672, 2011.

[44] K. L. Spalding, E. Arner, P. O. Westermark et al., "Dynamics of fat cell turnover in humans," *Nature*, vol. 453, no. 7196, pp. 783–787, 2008.

[45] M. Witkowska-Zimny and E. Wrobel, "Perinatal sources of mesenchymal stem cells: wharton's jelly, amnion and chorion," *Cellular and Molecular Biology Letters*, vol. 16, no. 3, pp. 493–514, 2011.

[46] R. R. Taghizadeh, K. J. Cetrulo, and C. L. Cetrulo, "Wharton's Jelly stem cells: future clinical applications," *Placenta*, vol. 32, no. 4, pp. S311–S315, 2011.

[47] D. L. Troyer and M. L. Weiss, "Concise review: wharton's Jelly-derived cells are a primitive stromal cell population," *Stem Cells*, vol. 26, no. 3, pp. 591–599, 2008.

[48] V. Kumar, N. Fausto, and A. Abbas, "Robbins and cotran pathologic basis of disease," in *Blood Vessels*, chapter 11, Saunders, Philadelphia, Pa, USA, 7th edition, 2004.

[49] G. Cossu and P. Bianco, "Mesoangioblasts: vascular progenitors for extravascular mesodermal tissues," *Current Opinion in Genetics and Development*, vol. 13, no. 5, pp. 537–542, 2003.

[50] D. Galli, A. Innocenzi, L. Staszewsky et al., "Mesoangioblasts, vessel-associated multipotent stem cells, repair the infarcted heart by multiple cellular mechanisms: a comparison with bone marrow progenitors, fibroblasts, and endothelial cells," *Arteriosclerosis, Thrombosis, and Vascular Biology*, vol. 25, no. 4, pp. 692–697, 2005.

[51] A. Armulik, A. Abramsson, and C. Betsholtz, "Endothelial/pericyte interactions," *Circulation Research*, vol. 97, no. 6, pp. 512–523, 2005.

[52] D. von Tell, A. Armulik, and C. Betsholtz, "Pericytes and vascular stability," *Experimental Cell Research*, vol. 312, no. 5, pp. 623–629, 2006.

[53] H. K. Rucker, H. J. Wynder, and W. E. Thomas, "Cellular mechanisms of CNS pericytes," *Brain Research Bulletin*, vol. 51, no. 5, pp. 363–369, 2000.

[54] P. Dore-Duffy and J. C. LaManna, "Physiologic angiodynamics in the brain," *Antioxidants and Redox Signaling*, vol. 9, no. 9, pp. 1363–1371, 2007.

[55] F. Kuhnert, B. Y. Y. Tam, B. Sennino et al., "Soluble receptor-mediated selective inhibition of VEGFR and PDGFRβ signaling during physiologic and tumor angiogenesis," *Proceedings of the National Academy of Sciences of the United States of America*, vol. 105, no. 29, pp. 10185–10190, 2008.

[56] P. Lindahl, B. R. Johansson, P. Levéen, and C. Betsholtz, "Pericyte loss and microaneurysm formation in PDGF-B-deficient mice," *Science*, vol. 277, no. 5323, pp. 242–245, 1997.

[57] M. W. Majesky, X. R. Dong, V. Hoglund, W. M. Mahoney Jr., and G. Daum, "The adventitia: a dynamic interface containing resident progenitor cells," *Arteriosclerosis, Thrombosis, and Vascular Biology*, vol. 31, no. 7, pp. 1530–1539, 2011.

[58] Y. Hu and Q. Xu, "Adventitial biology: differentiation and function," *Arteriosclerosis, Thrombosis, and Vascular Biology*, vol. 31, no. 7, pp. 1523–1529, 2011.

[59] Z. Tang, A. Wang, F. Yuan et al., "Differentiation of multipotent vascular stem cells contributes to vascular diseases," *Nature Communications*, vol. 3, article 875, 2012.

[60] Y. Hu, Z. Zhang, E. Torsney et al., "Abundant progenitor cells in the adventitia contribute to atherosclerosis of vein grafts in ApoE-deficient mice," *Journal of Clinical Investigation*, vol. 113, no. 9, pp. 1258–1265, 2004.

[61] Y. Shi, J. E. O'Brien Jr., A. Fard, J. D. Mannion, D. Wang, and A. Zalewski, "Adventitial myofibroblasts contribute to neointimal formation in injured porcine coronary arteries," *Circulation*, vol. 94, no. 7, pp. 1655–1664, 1996.

[62] S. Oparil, S.-J. Chen, Y.-F. Chen, J. N. Durand, L. Allen, and J. A. Thompson, "Estrogen attenuates the adventitial contribution to neointima formation in injured rat carotid arteries," *Cardiovascular Research*, vol. 44, no. 3, pp. 608–614, 1999.

[63] M. Crisan, J. Huard, B. Zheng et al., "Purification and culture of human blood vessel-associated progenitor cells," in *Current Protocols in Stem Cell Biology*, John Wiley and Sons, 2007.

[64] A. Dellavalle, M. Sampaolesi, R. Tonlorenzi et al., "Pericytes of human skeletal muscle are myogenic precursors distinct from satellite cells," *Nature Cell Biology*, vol. 9, no. 3, pp. 255–267, 2007.

[65] P. Campagnolo, D. Cesselli, A. Al Haj Zen et al., "Human adult vena saphena contains perivascular progenitor cells endowed with clonogenic and proangiogenic potential," *Circulation*, vol. 121, no. 15, pp. 1735–1745, 2010.

[66] D. Tilki, H.-P. Hohn, B. Ergün, S. Rafii, and S. Ergün, "Emerging biology of vascular wall progenitor cells in health and disease," *Trends in Molecular Medicine*, vol. 15, no. 11, pp. 501–509, 2009.

[67] E. Zengin, F. Chalajour, U. M. Gehling et al., "Vascular wall resident progenitor cells: a source for postnatal vasculogenesis," *Development*, vol. 133, no. 8, pp. 1543–1551, 2006.

[68] M. Okada, T. R. Payne, B. Zheng et al., "Myogenic endothelial cells purified from human skeletal muscle improve cardiac function after transplantation into infarcted myocardium," *Journal of the American College of Cardiology*, vol. 52, no. 23, pp. 1869–1880, 2008.

[69] B. Zheng, C. W. Chen, G. Li et al., "Isolation of myogenic stem cells from cultures of cryopreserved human skeletal muscle," *Cell transplantation*, vol. 21, no. 6, pp. 1087–1093, 2012.

[70] T. S. Park, M. Gavina, C.-W. Chen et al., "Placental perivascular cells for human muscle regeneration," *Stem Cells and Development*, vol. 20, no. 3, pp. 451–463, 2011.

[71] T. Montemurro, G. Andriolo, E. Montelatici et al., "Differentiation and migration properties of human foetal umbilical cord perivascular cells: potential for lung repair," *Journal of Cellular and Molecular Medicine*, vol. 15, no. 4, pp. 796–808, 2011.

[72] N. Zebardast, D. Lickorish, and J. E. Davies, "Human umbilical cord perivascular cells (HUCPVC): a mesenchymal cell source for dermal wound healing," *Organogenesis*, vol. 6, no. 4, pp. 197–203, 2010.

[73] M. M. Carvalho, F. G. Teixeira, R. L. Reis, N. Sousa, and A. J. Salgado, "Mesenchymal stem cells in the umbilical cord: phenotypic characterization, secretome and applications in central nervous system regenerative medicine," *Current Stem Cell Research and Therapy*, vol. 6, no. 3, pp. 221–228, 2011.

[74] E. Jauniaux, G. J. Burton, G. J. Moscoso, and J. Hustin, "Development of the early human placenta: a morphometric study," *Placenta*, vol. 12, no. 3, pp. 269–276, 1991.

[75] A. Bárcena, M. Kapidzic, M. O. Muench et al., "The human placenta is a hematopoietic organ during the embryonic and fetal periods of development," *Developmental Biology*, vol. 327, no. 1, pp. 24–33, 2009.

[76] R. Demir, P. Kaufmann, M. Castellucci, T. Erbengi, and A. Kotowski, "Fetal vasculogenesis and angiogenesis in human placental villi1," *Acta Anatomica*, vol. 136, no. 3, pp. 190–203, 1989.

[77] M. Wareing, "Effects of oxygenation and luminal flow on human placenta chorionic plate blood vessel function," *Journal of Obstetrics and Gynaecology Research*, vol. 38, no. 1, pp. 185–191, 2012.

[78] C. J. P. Jones and G. Desoye, "A new possible function for placental pericytes," *Cells Tissues Organs*, vol. 194, no. 1, pp. 76–84, 2011.

[79] N. M. Castrechini, P. Murthi, N. M. Gude et al., "Mesenchymal stem cells in human placental chorionic villi reside in a vascular Niche," *Placenta*, vol. 31, no. 3, pp. 203–212, 2010.

[80] C. L. Maier, B. R. Shepherd, T. Yi, and J. S. Pober, "Explant outgrowth, propagation and characterization of human pericytes," *Microcirculation*, vol. 17, no. 5, pp. 367–380, 2010.

[81] B. Péault, M. Rudnicki, Y. Torrente et al., "Stem and progenitor cells in skeletal muscle development, maintenance, and therapy," *Molecular Therapy*, vol. 15, no. 5, pp. 867–877, 2007.

[82] B. M. Deasy, Y. Li, and J. Huard, "Tissue engineering with muscle-derived stem cells," *Current Opinion in Biotechnology*, vol. 15, no. 5, pp. 419–423, 2004.

[83] M. Sampaolesi, S. Blot, G. D'Antona et al., "Mesoangioblast stem cells ameliorate muscle function in dystrophic dogs," *Nature*, vol. 444, no. 7119, pp. 574–579, 2006.

[84] B. Cao, B. Zheng, R. J. Jankowski et al., "Muscle stem cells differentiate into haematopoietic lineages but retain myogenic potential," *Nature Cell Biology*, vol. 5, no. 7, pp. 640–646, 2003.

[85] H. Oshima, T. R. Payne, K. L. Urish et al., "Differential myocardial infarct repair with muscle stem cells compared to myoblasts," *Molecular Therapy*, vol. 12, no. 6, pp. 1130–1141, 2005.

[86] A. Uezumi, S.-I. Fukada, N. Yamamoto, S. Takeda, and K. Tsuchida, "Mesenchymal progenitors distinct from satellite cells contribute to ectopic fat cell formation in skeletal muscle," *Nature Cell Biology*, vol. 12, no. 2, pp. 143–152, 2010.

[87] M. P. Pusztaszeri, W. Seelentag, and F. T. Bosman, "Immunohistochemical expression of endothelial markers CD31, CD34, von Willebrand factor, and Fli-1 in normal human tissues," *Journal of Histochemistry and Cytochemistry*, vol. 54, no. 4, pp. 385–395, 2006.

[88] A. W. James, J. N. Zara, M. Corselli et al., "An abundant perivascular source of stem cells for bone tissue engineering," *Stem Cells Translational Medicine*, vol. 1, no. 9, pp. 673–684, 2012.

[89] A. W. James, J. N. Zara, X. Zhang et al., "Perivascular stem cells: a prospectively purified mesenchymal stem cell population for bone tissue engineering," *Stem Cells Translational Medicine*, vol. 1, no. 6, pp. 510–519, 2012.

[90] E. K. Waller, J. Olweus, F. Lund-Johansen et al., "The "common stem cell" hypothesis reevaluated: human fetal bone marrow contains separate populations of hematopoietic and stromal progenitors," *Blood*, vol. 85, no. 9, pp. 2422–2435, 1995.

[91] E. K. Waller, S. Huang, and L. Terstappen, "Changes in the growth properties of CD34+, CD38– bone marrow progenitors during human fetal development," *Blood*, vol. 86, no. 2, pp. 710–718, 1995.

[92] D. J. Simmons, P. Seitz, L. Kidder et al., "Partial characterization of rat marrow stromal cells," *Calcified Tissue International*, vol. 48, no. 5, pp. 326–334, 1991.

[93] S. Kaiser, B. Hackanson, M. Follo et al., "BM cells giving rise to MSC in culture have a heterogeneous CD34 and CD45 phenotype," *Cytotherapy*, vol. 9, no. 5, pp. 439–450, 2007.

[94] R. A. Kopher, V. R. Penchev, M. S. Islam, K. L. Hill, S. Khosla, and D. S. Kaufman, "Human embryonic stem cell-derived CD34+ cells function as MSC progenitor cells," *Bone*, vol. 47, no. 4, pp. 718–728, 2010.

[95] R. Barbet, I. Peiffer, A. Hatzfeld, P. Charbord, and J. A. Hatzfeld, "Comparison of gene expression in human embryonic stem cells, hESC-derived mesenchymal stem cells and human mesenchymal stem cells," *Stem Cells International*, vol. 2011, Article ID 368192, 9 pages, 2011.

[96] M. A. Vodyanik, J. Yu, X. Zhang et al., "A mesoderm-derived precursor for mesenchymal stem and endothelial cells," *Cell Stem Cell*, vol. 7, no. 6, pp. 718–729, 2010.

[97] A. Dar, H. Domev, O. Ben-Yosef et al., "Multipotent vasculogenic pericytes from human pluripotent stem cells promote recovery of murine ischemic limb," *Circulation*, vol. 125, no. 1, pp. 87–99, 2012.

[98] D. O. Traktuev, S. Merfeld-Clauss, J. Li et al., "A population of multipotent CD34-positive adipose stromal cells share pericyte and mesenchymal surface markers, reside in a periendothelial location, and stabilize endothelial networks," *Circulation Research*, vol. 102, no. 1, pp. 77–85, 2008.

[99] H. Yamanishi, S. Fujiwara, and T. Soma, "Perivascular localization of dermal stem cells in human scalp," *Experimental Dermatology*, vol. 21, no. 1, pp. 78–80, 2012.

[100] L. Zimmerlin, V. S. Donnenberg, and A. D. Donnenberg, "Rare event detection and analysis in flow cytometry: bone marrow mesenchymal stem cells, breast cancer stem/progenitor cells in malignant effusions, and pericytes in disaggregated adipose tissue," *Methods in Molecular Biology*, vol. 699, pp. 251–273, 2011.

[101] L. Zimmerlin, V. S. Donnenberg, J. P. Rubin, and A. D. Donnenberg, "Mesenchymal markers on human adipose stem/progenitor cells," *Cytometry A*, vol. 83, no. 1, pp. 134–140, 2012.

[102] L. Zimmerlin, V. S. Donnenberg, and A. D. Donnenberg, "Pericytes: a universal adult tissue stem cell?" *Cytometry A*, vol. 81, no. 1, pp. 12–14, 2012.

[103] K. Yoshimura, T. Shigeura, D. Matsumoto et al., "Characterization of freshly isolated and cultured cells derived from the fatty and fluid portions of liposuction aspirates," *Journal of Cellular Physiology*, vol. 208, no. 1, pp. 64–76, 2006.

[104] D. T. Covas, R. A. Panepucci, A. M. Fontes et al., "Multipotent mesenchymal stromal cells obtained from diverse human tissues share functional properties and gene-expression profile with CD146+ perivascular cells and fibroblasts," *Experimental Hematology*, vol. 36, no. 5, pp. 642–654, 2008.

[105] A. C. W. Zannettino, S. Paton, A. Arthur et al., "Multipotential human adipose-derived stromal stem cells exhibit a perivascular phenotype in vitro and in vivo," *Journal of Cellular Physiology*, vol. 214, no. 2, pp. 413–421, 2008.

[106] M. Maumus, J.-A. Peyrafitte, R. D'Angelo et al., "Native human adipose stromal cells: localization, morphology and phenotype," *International Journal of Obesity*, vol. 35, no. 9, pp. 1141–1153, 2011.

[107] G. Astori, F. Vignati, S. Bardelli et al., "'In vitro' and multicolor phenotypic characterization of cell subpopulations identified in fresh human adipose tissue stromal vascular fraction and in the derived mesenchymal stem cells," *Journal of Translational Medicine*, vol. 5, article 55, 2007.

[108] A. O. Sahin and M. Buitenhuis, "Molecular mechanisms underlying adhesion and migration of hematopoietic stem cells," *Cell Adhesion and Migration*, vol. 6, no. 1, pp. 39–48, 2012.

[109] A. Augello, T. B. Kurth, and C. de Bari, "Mesenchymal stem cells: a perspective from in vitro cultures to in vivo migration and niches," *European Cells and Materials*, vol. 20, pp. 121–133, 2010.

[110] S. K. Kang, I. S. Shin, M. S. Ko, J. Y. Jo, and J. C. Ra, "Journey of mesenchymal stem cells for homing: atrategies to enhance efficacy and safety of stem cell therapy," *Stem Cells International*, vol. 2012, Article ID 342968, 11 pages, 2012.

[111] A. Armulik, G. Genové, and C. Betsholtz, "Pericytes: developmental, physiological, and pathological perspectives, problems, and promises," *Developmental Cell*, vol. 21, no. 2, pp. 193–215, 2011.

[112] A. Arthur, A. Zannettino, R. Panagopoulos et al., "EphB/ephrin-B interactions mediate human MSC attachment, migration and osteochondral differentiation," *Bone*, vol. 48, no. 3, pp. 533–542, 2011.

[113] S. S. Foo, C. J. Turner, S. Adams et al., "Ephrin-B2 controls cell motility and adhesion during blood-vessel-wall assembly," *Cell*, vol. 124, no. 1, pp. 161–173, 2006.

[114] K. Stark, A. Eckart, S. Haidari et al., "Capillary and arteriolar pericytes attract innate leukocytes exiting through venules and "instruct" them with pattern-recognition and motility programs," *Nature Immunology*, vol. 14, no. 1, pp. 41–51, 2013.

[115] Y. Bordon, "Cell migration: pericytes: route planners," *Nature Reviews Immunology*, vol. 13, no. 1, p. 5, 2013.

[116] M. Hellström, M. Kalén, P. Lindahl, A. Abramsson, and C. Betsholtz, "Role of PDGF-B and PDGFR-β in recruitment of vascular smooth muscle cells and pericytes during embryonic blood vessel formation in the mouse," *Development*, vol. 126, no. 14, pp. 3047–3055, 1999.

[117] M. Enge, M. Bjarnegård, H. Gerhardt et al., "Endothelium-specific platelet-derived growth factor-B ablation mimics diabetic retinopathy," *EMBO Journal*, vol. 21, no. 16, pp. 4307–4316, 2002.

[118] A. Abramsson, P. Lindblom, and C. Betsholtz, "Endothelial and nonendothelial sources of PDGF-B regulate pericyte recruitment and influence vascular pattern formation in tumors," *Journal of Clinical Investigation*, vol. 112, no. 8, pp. 1142–1151, 2003.

[119] S. Ejaz, "Importance of pericytes and mechanisms of pericyte loss during diabetes retinopathy," *Diabetes, Obesity and Metabolism*, vol. 10, no. 1, pp. 53–63, 2008.

[120] K. le Blanc, "Immunomodulatory effects of fetal and adult mesenchymal stem cells," *Cytotherapy*, vol. 5, no. 6, pp. 485–489, 2003.

[121] L. B. Ware and M. A. Matthay, "Keratinocyte and hepatocyte growth factors in the lung: roles in lung development, inflammation, and repair," *The American Journal of Physiology*, vol. 282, no. 5, pp. L924–L940, 2002.

[122] G. F. Curley, M. Hayes, B. Ansari et al., "Mesenchymal stem cells enhance recovery and repair following ventilator-induced lung injury in the rat," *Thorax*, vol. 67, no. 6, pp. 496–501, 2012.

[123] C.-W. Chen, E. Montelatici, M. Crisan et al., "Perivascular multi-lineage progenitor cells in human organs: regenerative units, cytokine sources or both?" *Cytokine and Growth Factor Reviews*, vol. 20, no. 5-6, pp. 429–434, 2009.

[124] M. Takeoka, W. F. Ward, H. Pollack, D. W. Kamp, and R. J. Panos, "KGF facilitates repair of radiation-induced DNA damage in alveolar epithelial cells," *The American Journal of Physiology*, vol. 272, no. 6, pp. L1174–L1180, 1997.

[125] B. M. Strem, K. C. Hicok, M. Zhu et al., "Multipotential differentiation of adipose tissue-derived stem cells," *Keio Journal of Medicine*, vol. 54, no. 3, pp. 132–141, 2005.

[126] D. Matsumoto, K. Sato, K. Gonda et al., "Cell-assisted lipotransfer: supportive use of human adipose-derived cells for soft tissue augmentation with lipoinjection," *Tissue Engineering*, vol. 12, no. 12, pp. 3375–3382, 2006.

[127] P. van Pham, K. H.-T. Bui, D. Q. Ngo, L. T. Khuat, and N. K. Phan, "Transplantation of nonexpanded adipose stromal vascular fraction and platelet-rich plasma for articular cartilage injury treatment in mice model," *Journal of Medical Engineering*, vol. 2013, Article ID 832396, 7 pages, 2013.

[128] L. Cai, B. H. Johnstone, T. G. Cook et al., "IFATS collection: human adipose tissue-derived stem cells induce angiogenesis and nerve sprouting following myocardial infarction, in conjunction with potent preservation of cardiac function," *Stem Cells*, vol. 27, no. 1, pp. 230–237, 2009.

[129] U. Kim, D.-G. Shin, J.-S. Park et al., "Homing of adipose-derived stem cells to radiofrequency catheter ablated canine atrium and differentiation into cardiomyocyte-like cells," *International Journal of Cardiology*, vol. 146, no. 3, pp. 371–378, 2011.

[130] A. Banas, T. Teratani, Y. Yamamoto et al., "IFATS collection: in vivo therapeutic potential of human adipose tissue mesenchymal stem cells after transplantation into mice with liver injury," *Stem Cells*, vol. 26, no. 10, pp. 2705–2712, 2008.

[131] D. H. Kim, C. M. Je, J. Y. Sin, and J. S. Jung, "Effect of partial hepatectomy on in vivo engraftment after intravenous administration of human adipose tissue stromal cells in mouse," *Microsurgery*, vol. 23, no. 5, pp. 424–431, 2003.

[132] Y. M. Kim, Y. S. Choi, J. W. Choi et al., "Effects of systemic transplantation of adipose tissue-derived stem cells on olfactory epithelium regeneration," *Laryngoscope*, vol. 119, no. 5, pp. 993–999, 2009.

[133] W. Xing, D. Zhimei, Z. Liming et al., "IFATS collection: the conditioned media of adipose stromal cells protect against hypoxia-ischemia-induced brain damage in neonatal rats," *Stem Cells*, vol. 27, no. 2, pp. 478–488, 2009.

[134] K.-S. Cho, H.-K. Park, H.-Y. Park et al., "IFATS collection: immunomodulatory effects of adipose tissue-derived stem cells in an allergic rhinitis mouse model," *Stem Cells*, vol. 27, no. 1, pp. 259–265, 2009.

[135] P. Sacerdote, S. Niada, S. Franchi et al., "Systemic administration of human adipose-derived stem cells reverts nociceptive hypersensitivity in an experimental model of neuropathy," *Stem Cells and Development*, vol. 22, no. 8, pp. 1252–1263, 2013.

[136] S. Marconi, G. Castiglione, E. Turano et al., "Human adipose-derived mesenchymal stem cells systemically injected promote peripheral nerve regeneration in the mouse model of sciatic crush," *Tissue Engineering A*, vol. 18, no. 11-12, pp. 1264–1272, 2012.

[137] B. Levi, A. W. James, E. R. Nelson et al., "Studies in adipose-derived stromal cells: migration and participation in repair of cranial injury after systemic injection," *Plastic and Reconstructive Surgery*, vol. 127, no. 3, pp. 1130–1140, 2011.

[138] N. M. Vieira, M. Valadares, E. Zucconi et al., "Human adipose-derived mesenchymal stromal cells injected systemically into GRMD dogs without immunosuppression are able to reach the host muscle and express human dystrophin," *Cell Transplantation*, vol. 21, no. 7, pp. 1407–1417, 2012.

[139] N. M. Vieira, C. R. Bueno Jr., V. Brandalise et al., "SJL dystrophic mice express a significant amount of human muscle proteins following systemic delivery of human adipose-derived stromal cells without immunosuppression," *Stem Cells*, vol. 26, no. 9, pp. 2391–2398, 2008.

[140] S. J. Baek, S. K. Kang, and J. C. Ra, "In vitro migration capacity of human adipose tissue-derived mesenchymal stem cells reflects their expression of receptors for chemokines and growth factors," *Experimental and Molecular Medicine*, vol. 43, no. 10, pp. 596–603, 2011.

[141] C. Garrovo, N. Bergamin, D. Bates et al., "In vivo tracking of murine adipose tissue-derived multipotent adult stem cells and ex vivo cross-validation," *International Journal of Molecular Imaging*, vol. 2013, Article ID 426961, 13 pages, 2013.

[142] N. Kakudo, S. Kushida, K. Suzuki et al., "Effects of transforming growth factor-beta1 on cell motility, collagen gel contraction, myofibroblastic differentiation, and extracellular matrix expression of human adipose-derived stem cell," *Human Cell*, vol. 25, no. 4, pp. 87–95, 2012.

[143] P. R. Baraniak and T. C. McDevitt, "Stem cell paracrine actions and tissue regeneration," *Regenerative Medicine*, vol. 5, no. 1, pp. 121–143, 2010.

[144] L. Casteilla, V. Planat-Benard, P. Laharrague, and B. Cousin, "Adipose-derived stromal cells: their identity and uses in clinical trials, an update," *World Journal of Stem Cells*, vol. 3, no. 4, pp. 25–33, 2011.

[145] S. H. Lee, S. Y. Jin, J. S. Song, K. K. Seo, and K. H. Cho, "Paracrine effects of adipose-derived stem cells on keratinocytes and

dermal fibroblasts," *Annals of Dermatology*, vol. 24, no. 2, pp. 136–143, 2012.

[146] L. Hu, J. Zhao, J. Liu, N. Gong, and L. Chen, "Effects of adipose stem cell-conditioned medium on the migration of vascular endothelial cells, fibroblasts and keratinocytes," *Experimental and Therapeutic Medicine*, vol. 5, no. 3, pp. 701–706, 2013.

[147] S. S. Collawn, N. Sanjib Banerjee, J. de la Torre, L. Vasconez, and L. T. Chow, "Adipose-derived stromal cells accelerate wound healing in an organotypic raft culture model," *Annals of Plastic Surgery*, vol. 68, no. 5, pp. 501–504, 2012.

[148] K. M. Moon, Y. H. Park, J. S. Lee et al., "The effect of secretory factors of adipose-derived stem cells on human keratinocytes," *International Journal of Molecular Sciences*, vol. 13, no. 1, pp. 1239–1257, 2012.

[149] X. Fu, L. Fang, H. Li, X. Li, B. Cheng, and Z. Sheng, "Adipose tissue extract enhances skin wound healing," *Wound Repair and Regeneration*, vol. 15, no. 4, pp. 540–548, 2007.

[150] A. E. Karnoub, A. B. Dash, A. P. Vo et al., "Mesenchymal stem cells within tumour stroma promote breast cancer metastasis," *Nature*, vol. 449, no. 7162, pp. 557–563, 2007.

[151] A. Nakamizo, F. Marini, T. Amano et al., "Human bone marrow-derived mesenchymal stem cells in the treatment of gliomas," *Cancer Research*, vol. 65, pp. 3307–3318, 2005.

[152] C. Pendleton, Q. Li, D. A. Chesler, K. Yuan, H. Guerrero-Cazares, and A. Quinones-Hinojosa, "Mesenchymal stem cells derived from adipose tissue vs bone marrow: in vitro comparison of their tropism towards gliomas," *PLoS ONE*, vol. 8, no. 3, Article ID e58198, 2013.

[153] M. Lamfers, S. Idema, F. van Milligen et al., "Homing properties of adipose-derived stem cells to intracerebral glioma and the effects of adenovirus infection," *Cancer Letters*, vol. 274, no. 1, pp. 78–87, 2009.

[154] L. Kucerova, V. Altanerova, M. Matuskova, S. Tyciakova, and C. Altaner, "Adipose tissue-derived human mesenchymal stem cells mediated prodrug cancer gene therapy," *Cancer Research*, vol. 67, no. 13, pp. 6304–6313, 2007.

[155] I. T. Cavarretta, V. Altanerova, M. Matuskova, L. Kucerova, Z. Culig, and C. Altaner, "Adipose tissue-derived mesenchymal stem cells expressing prodrug-converting enzyme inhibit human prostate tumor growth," *Molecular Therapy*, vol. 18, no. 1, pp. 223–231, 2010.

[156] F. L. Muehlberg, Y.-H. Song, A. Krohn et al., "Tissue-resident stem cells promote breast cancer growth and metastasis," *Carcinogenesis*, vol. 30, no. 4, pp. 589–597, 2009.

[157] S. Pinilla, E. Alt, F. J. Abdul Khalek et al., "Tissue resident stem cells produce CCL5 under the influence of cancer cells and thereby promote breast cancer cell invasion," *Cancer Letters*, vol. 284, no. 1, pp. 80–85, 2009.

[158] B. Sun, K.-H. Roh, J.-R. Park et al., "Therapeutic potential of mesenchymal stromal cells in a mouse breast cancer metastasis model," *Cytotherapy*, vol. 11, no. 3, pp. 289–298, 2009.

[159] B. Cousin, E. Ravet, S. Poglio et al., "Adult stromal cells derived from human adipose tissue provoke pancreatic cancer cell death both in vitro and in vivo," *PLoS ONE*, vol. 4, no. 7, Article ID e6278, 2009.

[160] S. Tottey, M. Corselli, E. M. Jeffries, R. Londono, B. Peault, and S. F. Badylak, "Extracellular matrix degradation products and low-oxygen conditions enhance the regenerative potential of perivascular stem cells," *Tissue Engineering A*, vol. 17, no. 1-2, pp. 37–44, 2011.

[161] B. Annabi, Y.-T. Lee, S. Turcotte et al., "Hypoxia promotes murine bone-marrow-derived stromal cell migration and tube formation," *Stem Cells*, vol. 21, no. 3, pp. 337–347, 2003.

[162] R. K. Assoian and M. A. Schwartz, "Coordinate signaling by integrins and receptor tyrosine kinases in the regulation of G1 phase cell-cycle progression," *Current Opinion in Genetics and Development*, vol. 11, no. 1, pp. 48–53, 2001.

[163] I. Hunger-Glaser, R. S. Fan, E. Perez-Salazar, and E. Rozengurt, "PDGF and FGF induce focal adhesion kinase (FAK) phosphorylation at Ser-910: dissociation from Tyr-397 phosphorylation and requirement for ERK activation," *Journal of Cellular Physiology*, vol. 200, no. 2, pp. 213–222, 2004.

[164] C. Huang, K. Jacobson, and M. D. Schaller, "MAP kinases and cell migration," *Journal of Cell Science*, vol. 117, no. 20, pp. 4619–4628, 2004.

[165] I. Rosová, M. Dao, B. Capoccia, D. Link, and J. A. Nolta, "Hypoxic preconditioning results in increased motility and improved therapeutic potential of human mesenchymal stem cells," *Stem Cells*, vol. 26, no. 8, pp. 2173–2182, 2008.

[166] S. Neuss, E. Becher, M. Wöltje, L. Tietze, and W. Jahnen-Dechent, "Functional expression of HGF and HGF receptor/c-met in adult human mesenchymal stem cells suggests a role in cell mobilization, tissue repair, and wound healing," *Stem Cells*, vol. 22, no. 3, pp. 405–414, 2004.

[167] H. Liu, W. Xue, G. Ge et al., "Hypoxic preconditioning advances CXCR4 and CXCR7 expression by activating HIF-1α in MSCs," *Biochemical and Biophysical Research Communications*, vol. 401, no. 4, pp. 509–515, 2010.

[168] C. W. Chen, M. Okada, J. D. Proto, X. Gao et al., "Human pericytes for ischemic heart repair," *Stem Cells*, vol. 31, no. 2, pp. 305–316, 2013.

[169] R. Katare, F. Riu, K. Mitchell et al., "Transplantation of human pericyte progenitor cells improves the repair of infarcted heart through activation of an angiogenic program involving micro-RNA-132," *Circulation Research*, vol. 109, no. 8, pp. 894–906, 2011.

[170] A. Dellavalle, G. Maroli, D. Covarello et al., "Pericytes resident in postnatal skeletal muscle differentiate into muscle fibres and generate satellite cells," *Nature Communications*, vol. 2, no. 1, article 499, 2011.

[171] M. Pierro, L. Ionescu, T. Montemurro, A. Vadivel et al., "Short-term, long-term and paracrine effect of human umbilical cord-derived stem cells in lung injury prevention and repair in experimental bronchopulmonary dysplasia," *Thorax*, vol. 68, no. 5, pp. 475–484, 2013.

[172] M. Corselli, C. J. Chin, C. Parekh, A. Sahaghian et al., "Perivascular support of human hematopoietic stem/progenitor cells," *Blood*, vol. 121, no. 15, pp. 2891–2901, 2013.

[173] X. Zhang, B. Péault, W. Chen et al., "The nell-1 growth factor stimulates bone formation by purified human perivascular cells," *Tissue Engineering A*, vol. 17, no. 19-20, pp. 2497–2509, 2011.

[174] E. Chavakis, C. Urbich, and S. Dimmeler, "Homing and engraftment of progenitor cells: a prerequisite for cell therapy," *Journal of Molecular and Cellular Cardiology*, vol. 45, no. 4, pp. 514–522, 2008.

[175] R. H. Lee, A. A. Pulin, M. J. Seo et al., "Intravenous hMSCs improve myocardial infarction in mice because cells embolized in lung are activated to secrete the anti-inflammatory protein TSG-6," *Cell Stem Cell*, vol. 5, no. 1, pp. 54–63, 2009.

[176] A. Askarinam, A. W. James, J. N. Zara et al., "Human perivascular stem cells show enhanced osteogenesis and vasculogenesis

with nel-like molecule I protein," *Tissue Engineering A*, vol. 19, no. 11-12, pp. 1386–1397, 2013.

[177] X. Zhang, K. Ting, C. M. Bessette et al., "Nell-1, a key functional mediator of Runx2, partially rescues calvarial defects in Runx2+/– mice," *Journal of Bone and Mineral Research*, vol. 26, no. 4, pp. 777–791, 2011.

[178] T. Kitaori, H. Ito, E. M. Schwarz et al., "Stromal cell-derived factor 1/CXCR4 signaling is critical for the recruitment of mesenchymal stem cells to the fracture site during skeletal repair in a mouse model," *Arthritis and Rheumatism*, vol. 60, no. 3, pp. 813–823, 2009.

[179] N. Song, Y. Huang, H. Shi et al., "Overexpression of platelet-derived growth factor-BB increases tumor pericyte content via stromal-derived factor-1α/CXCR4 axis," *Cancer Research*, vol. 69, no. 15, pp. 6057–6064, 2009.

[180] E. Chavakis, M. Koyanagi, and S. Dimmeler, "Enhancing the outcome of cell therapy for cardiac repair: progress from bench to bedside and back," *Circulation*, vol. 121, no. 2, pp. 325–335, 2010.

[181] A. N. Stratman, A. E. Schwindt, K. M. Malotte, and G. E. Davis, "Endothelial-derived PDGF-BB and HB-EGF coordinately regulate pericyte recruitment during vasculogenic tube assembly and stabilization," *Blood*, vol. 116, no. 22, pp. 4720–4730, 2010.

[182] A. N. Stratman, K. M. Malotte, R. D. Mahan, M. J. Davis, and G. E. Davis, "Pericyte recruitment during vasculogenic tube assembly stimulates endothelial basement membrane matrix formation," *Blood*, vol. 114, no. 24, pp. 5091–5101, 2009.

[183] H. Gerhardt and C. Betsholtz, "Endothelial-pericyte interactions in angiogenesis," *Cell and Tissue Research*, vol. 314, no. 1, pp. 15–23, 2003.

[184] L. Díaz-Flores, R. Gutiérrez, J. F. Madrid et al., "Pericytes. Morphofunction, interactions and pathology in a quiescent and activated mesenchymal cell niche," *Histology and Histopathology*, vol. 24, no. 7, pp. 909–969, 2009.

[185] D. E. Sims, "The pericyte-A review," *Tissue and Cell*, vol. 18, no. 2, pp. 153–174, 1986.

[186] K. Gaengel, G. Genové, A. Armulik, and C. Betsholtz, "Endothelial-mural cell signaling in vascular development and angiogenesis," *Arteriosclerosis, Thrombosis, and Vascular Biology*, vol. 29, no. 5, pp. 630–638, 2009.

[187] G. Rajashekhar, D. O. Traktuev, W. C. Roell, B. H. Johnstone, S. Merfeld-Clauss, B. van Natta et al., "IFATS collection: adipose stromal cell differentiation is reduced by endothelial cell contact and paracrine communication: role of canonical Wnt signaling," *Stem Cells*, vol. 26, no. 10, pp. 2674–2681, 2008.

[188] F. A. Saleh, M. Whyte, P. Ashton, and P. G. Genever, "Regulation of mesenchymal stem cell activity by endothelial cells," *Stem Cells and Development*, vol. 20, no. 3, pp. 391–403, 2011.

[189] F. A. Saleh, M. Whyte, and P. G. Genever, "Effects of endothelial cells on human mesenchymal stem cell activity in a three-dimensional in vitro model," *Journal of European Cells and Materials*, vol. 22, pp. 242–257, 2011.

[190] Y. Xue, Z. Xing, S. Hellem, K. Arvidson, and K. Mustafa, "Endothelial cells influence the osteogenic potential of bone marrow stromal cells," *BioMedical Engineering Online*, vol. 8, article 34, 2009.

[191] D. Kaigler, P. H. Krebsbach, E. R. West, K. Horger, Y. C. Huang, and D. J. Mooney, "Endothelial cell modulation of bone marrow stromal cell osteogenic potential," *FASEB Journal*, vol. 19, no. 6, pp. 665–667, 2005.

[192] H. Li, R. Daculsi, M. Grellier, R. Bareille, C. Bourget, and J. Amedee, "Role of neural-cadherin in early osteoblastic differentiation of human bone marrow stromal cells cocultured with human umbilical vein endothelial cells," *The American Journal of Physiology*, vol. 299, no. 2, pp. 422–430, 2010.

[193] M. Grellier, N. Ferreira-Tojais, C. Bourget, R. Bareille, F. Guillemot, and J. Amedee, "Role of vascular endothelial growth factor in the communication between human osteoprogenitors and endothelial cells," *Journal of Cellular Biochemistry*, vol. 106, no. 3, pp. 390–398, 2009.

[194] T. Meury, S. Verrier, and M. Alini, "Human endothelial cells inhibit BMSC differentiation into mature osteoblasts in vitro by interfering with osterix expression," *Journal of Cellular Biochemistry*, vol. 98, no. 4, pp. 992–1006, 2006.

[195] F. Villars, B. Guillotin, T. Amedee, S. Dutoya, L. Bordenave, R. Bareille et al., "Effect of HUVEC on human osteoprogenitor cell differentiation needs heterotypic gap junction communication," *The American Journal of Physiology*, vol. 282, no. 4, pp. 775–785, 2002.

[196] F. Villars, L. Bordenave, R. Bareille, and J. Amedee, "Effect of human endothelial cells on human bone marrow stromal cell phenotype: role of VEGF?" *Journal of Cellular Biochemistry*, vol. 79, no. 4, pp. 672–685, 2000.

[197] B. Guillotin, C. Bourget, M. Remy-Zolgadri, R. Bareille, P. Fernandez, V. Conrad et al., "Human primary endothelial cells stimulate human osteoprogenitor cell differentiation," *Cellular Physiology and Biochemistry*, vol. 14, no. 4–6, pp. 325–332, 2004.

[198] U. Ozerdem and W. B. Stallcup, "Early contribution of pericytes to angiogenic sprouting and tube formation," *Angiogenesis*, vol. 6, no. 3, pp. 241–249, 2003.

[199] U. Ozerdem, K. A. Grako, K. Dahlin-Huppe, E. Monosov, and W. B. Stallcup, "NG2 proteoglycan is expressed exclusively by mural cells during vascular morphogenesis," *Developmental Dynamics*, vol. 222, no. 2, pp. 218–227, 2001.

[200] L. P. Reynolds, A. T. Grazul-Bilska, and D. A. Redmer, "Angiogenesis in the corpus luteum," *Endocrine*, vol. 12, no. 1, pp. 1–9, 2000.

[201] M. Enge, M. Bjarnegård, H. Gerhardt et al., "Endothelium-specific platelet-derived growth factor-B ablation mimics diabetic retinopathy," *EMBO Journal*, vol. 21, no. 16, pp. 4307–4316, 2002.

[202] K. K. Hirschi, S. A. Rohovsky, L. H. Beck, S. R. Smith, and P. A. D'Amore, "Endothelial cells modulate the proliferation of mural cell precursors via platelet-derived growth factor-BB and heterotypic cell contact," *Circulation Research*, vol. 84, no. 3, pp. 298–305, 1999.

[203] A. Blocki, Y. Wang, M. Koch et al., "Not all MSCs can act as pericytes: functional in vitro assays to distinguish pericytes from other mesenchymal stem cells in angiogenesis," *Stem Cells and Development*, vol. 22, no. 17, 2013.

[204] M. Corselli, C.-W. Chen, M. Crisan, L. Lazzari, and B. Péault, "Perivascular ancestors of adult multipotent stem cells," *Arteriosclerosis, Thrombosis, and Vascular Biology*, vol. 30, no. 6, pp. 1104–1109, 2010.

[205] A. Ehninger and A. Trumpp, "The bone marrow stem cell niche grows up: mesenchymal stem cells and macrophages move in," *Journal of Experimental Medicine*, vol. 208, no. 3, pp. 421–428, 2011.

[206] S. Ergün, D. Tilki, and D. Klein, "Vascular wall as a reservoir for different types of stem and progenitor cells," *Antioxidants and Redox Signaling*, vol. 15, no. 4, pp. 981–995, 2011.

[207] A. I. Caplan, "All MSCs are pericytes?" *Cell Stem Cell*, vol. 3, no. 3, pp. 229–230, 2008.

[208] A. M. Müller, A. Mehrkens, D. J. Schäfer et al., "Towards an intraoperative engineering of osteogenic and vasculogenic grafts from the stromal vascular fraction of human adipose tissue," *European Cells and Materials*, vol. 19, pp. 127–135, 2010.

[209] V. Marthiens, I. Kazanis, L. Moss, K. Long, and C. Ffrench-Constant, "Adhesion molecules in the stem cell niche: more than just staying in shape?" *Journal of Cell Science*, vol. 123, no. 10, pp. 1613–1622, 2010.

[210] J. P. Kirton, F. L. Wilkinson, A. E. Canfield, and M. Y. Alexander, "Dexamethasone downregulates calcification-inhibitor molecules and accelerates osteogenic differentiation of vascular pericytes: implications for vascular calcification," *Circulation Research*, vol. 98, no. 10, pp. 1264–1272, 2006.

[211] S. Mathews, R. Bhonde, P. K. Gupta, and S. Totey, "Extracellular matrix protein mediated regulation of the osteoblast differentiation of bone marrow derived human mesenchymal stem cells," *Differentiation*, vol. 84, no. 2, pp. 185–192, 2012.

[212] S. H. Ranganath, O. Levy, M. S. Inamdar, and J. M. Karp, "Harnessing the mesenchymal stem cell secretome for the treatment of cardiovascular disease," *Cell Stem Cell*, vol. 10, no. 3, pp. 244–258, 2012.

[213] I. Takada, A. P. Kouzmenko, and S. Kato, "PPAR-γ signaling crosstalk in mesenchymal stem cells," *PPAR Research*, vol. 2010, Article ID 341671, 6 pages, 2010.

The FASEB Journal article fj.13-233460. Published online May 23, 2013.

Appendix 12

RhoA mediates defective stem cell function and heterotopic ossification in dystrophic muscle of mice

Xiaodong Mu, Arvydas Usas, Ying Tang, Aiping Lu, Bing Wang, Kurt Weiss, and Johnny Huard[1]

Stem Cell Research Center, Department of Orthopaedic Surgery, University of Pittsburgh, Pittsburgh, Pennsylvania, USA

ABSTRACT **Heterotopic ossification (HO) and fatty infiltration (FI) often occur in diseased skeletal muscle and have been previously described in various animal models of Duchenne muscular dystrophy (DMD); however, the pathological mechanisms remain largely unknown. Dystrophin-deficient *mdx* mice and dystrophin/utrophin double-knockout (dKO) mice are mouse models of DMD; however, *mdx* mice display a strong muscle regeneration capacity, while dKO mice exhibit a much more severe phenotype, which is similar to patients with DMD. Our results revealed that more extensive HO, but not FI, occurred in the skeletal muscle of dKO mice versus *mdx* mice, and RhoA activation specifically occurred at the sites of HO. Moreover, the gene expression of RhoA, BMPs, and several inflammatory factors were significantly up-regulated in muscle stem cells isolated from dKO mice; while inactivation of RhoA in the cells with RhoA/ROCK inhibitor Y-27632 led to reduced osteogenic potential and improved myogenic potential. Finally, inactivation of RhoA signaling in the dKO mice with Y-27632 improved muscle regeneration and reduced the expression of BMPs, inflammation, HO, and intramyocellular lipid accumulation in both skeletal and cardiac muscle. Our results revealed that RhoA represents a major molecular switch in the regulation of HO and muscle regeneration in dystrophic skeletal muscle of mice.—Mu, X., Usas, A., Tang, Y., Lu, A., Wang, B., Weiss, K., Huard, J. RhoA mediates defective stem cell function and heterotopic ossification in dystrophic muscle of mice. *FASEB J.* 27, 000–000 (2013). www.fasebj.org**

Key Words: ROCK · mdx · utrophin$^{-/-}$ *· intramyocellular lipid accumulation*

HETEROTOPIC OSSIFICATION (HO) and/or fatty infiltration (FI) are two distinct histological processes that often occur in diseased muscle tissues. HO refers to the formation of bone in the soft tissues of the body and can occur as a result of trauma, surgery, neurological injury, or genetic abnormalities (1). FI has been reported to be associated with aging, inactivity, obesity, and various diseases, such as diabetes, and results in the accumulation of fat cells outside the typical fat stores (2–3). FI located within skeletal muscle is often the result of disordered lipid metabolism (3); however, abnormal lipid metabolism can also cause another type of abnormal lipid deposition in skeletal muscle, known as intramyocellular lipid accumulation (IMCL; refs. 4–5). Notably, IMCL in cardiac muscle, (intramyocardial lipid accumulation) can be caused by lipid overload, which has the potential to lead to lipotoxicity and progressive cardiac dysfunction (6–9). However, the pathological mechanisms regulating these distinct processes in diseased muscles remain largely unknown.

Duchenne muscular dystrophy (DMD) features progressive muscle degeneration and has no cure yet. Obesity occurs in >50% of patients wtih DMD after 14 yr of age, and a reduction in myocardial fatty acid metabolism has been observed in ~50% of patients wtih DMD (10, 11). FI is commonly observed in the skeletal muscles of patients wtih DMD, and it is one of the main factors responsible for patients' decline in muscular strength (12). Lipid mapping analysis of the hearts and skeletal muscles of patients wtih DMD revealed IMCL within the most damaged areas of the dystrophic muscles (11, 13); however, there are very few studies on the mechanisms and prevention of IMCL in patients wtih DMD. Although less documented in human patients wtih DMD, the presence of HO has been reported in the skeletal muscles of various animal models of human DMD, including *mdx* mice and golden retriever muscular dystrophy (GRMD) dogs

Abbreviations: BMP, bone morphogenetic protein; dKO, dystrophin/utrophin double knockout; DMD, Duchenne muscular dystrophy; FBS, fetal bovine serum; FI, fatty infiltration; GM, gastrocnemius muscle; GRMD, golden retriever muscular dystrophy; HO, heterotopic ossification; IMCL, intramyocellular lipid accumulation; MDSC, muscle-derived stem cell; *mdx*, dystrophin-deficient; micro-CT, micro-computed tomography; MSC, mesenchymal stem cell; NF-κB, nuclear factor-κB; PPARγ, peroxisome proliferator-activated receptor γ

[1] Correspondence: Stem Cell Research Center, Department of Orthopaedic Surgery, University of Pittsburgh, Bridgeside Point 2, Ste. 206, 450 Technology Dr., Pittsburgh, PA 15219, USA. E-mail: jhuard@pitt.edu

doi: 10.1096/fj.13-233460

This article includes supplemental data. Please visit *http://www.fasebj.org* to obtain this information.

(14–16). *In vitro* studies with muscle stem cells showed that bone morphogenetic protein (BMPs) or adipogenic media can promote the differentiation of muscle stem cells into osteogenic and adipogenic cells, respectively (17), suggesting that muscle stem cells may represent a cell source of HO and/or FI in skeletal muscle.

The experiments described in this article were conducted using two animal models of human DMD, dystrophin-deficient (*mdx*) mice and dystrophin/utrophin double-knockout (dKO) mice (14, 18–20). Compared with *mdx* mice, which actually feature potent muscle regeneration capacity, the phenotype of dKO mice is more severe and more closely resembles the phenotype seen in patients wtih DMD (19–20). For example, dKO mice feature a much shorter life span (~8 wk compared with ~2 yr), more necrosis and fibrosis in their skeletal muscles, scoliosis/kyphosis of the spine, and severe cardiac involvement and eventual cardiac failure (14, 19, 20). The occurrence of FI and HO in the skeletal muscles of *mdx* mice has been previously described (15), and more extensive HO in dKO mice has also been recently reported by our group (21). IMCL, on the other hand, has not been studied in either *mdx* or dKO mice or in any other DMD animal models. It is also clear that the knowledge about the molecular regulation of HO, fatty infiltration, and IMCL in dystrophic muscle remains limited.

Inflammation is directly involved in the dystrophic process and represents an important therapeutic target to treat DMD. For example, corticosteroids are capable of repressing systematic inflammation and are the only known effective drugs that can provide relief of the symptoms of DMD (22). Inflammation has been identified as a main contributor of HO (23); hence, the administrations of various anti-inflammatory medications have been used to prevent HO (24–25). For example, Cox-2 inhibitors were found to be effective at preventing HO after total hip arthroplasty (THA) and following spinal cord injury (26–27). Although inflammation and FI often occur simultaneously in diseased or injured skeletal muscles, inflammation has not been directly linked to FI (28–29). On the other hand, it has been well established, in studies of diabetes and obesity, that there is a close association between the occurrence of IMCL and chronic systematic inflammation during the progression of cardiac disease (30, 31). Similarly, lipid peroxidation has been shown to activate nuclear factor-κB (NF-κB), and consequently, has contributed to the histopathological cascade observed in *mdx* muscles (32). Finally, inflammatory cytokines have been shown to inhibit myogenic differentiation through the activation of NF-κB (33–34), and the activation of NF-κB signaling in skeletal muscle has been correlated with muscular dystrophies and inflammatory myopathies (34, 35).

In the current study, we examined the role that RhoA signaling pathway plays in regulating HO, FI, and IMCL in these models of DMD (dKO and *mdx* mice), due to the fact that RhoA signaling has been shown to play an important role in regulating osteogenesis, adipogenesis, myogenesis, and inflammation. RhoA is a small G protein in the Rho family that regulates cell morphology and migration by reorganizing the actin cytoskeleton in response to extracellular signaling (36). The RhoA signaling pathway is involved in the commitment of mesenchymal stem cells (MSCs) toward their osteogenic or adipogenic differentiation (37). RhoA signaling activation in MSCs *in vitro* induces osteogenesis potential and inhibits adipogenic potential of the cells; however, the application of Y-27632, a specific inhibitor of RhoA/Rho kinase (ROCK), reverses this process (37–39). RhoA also mediates BMP-induced signaling in MSCs and promotes osteoblastic cell survival (40, 41). Moreover, the inhibition of RhoA with Y-27632 was found to induce the adipogenic differentiation of muscle-derived cells *in vitro*, and resulted in the manifestation of FI in skeletal muscle (42). RhoA is also activated by Wnt5a, which results in the induction of osteogenic differentiation of human adipose stem cells (ASCs) and the repression of adipogenic differentiation (43). RhoA's role in the inflammatory process has been previously described, where TNF-α induces the activation of RhoA signaling in smooth muscle cells (44), RhoA regulates Cox-2 activity in fibroblasts (45), and RhoA induces the expression of inflammatory cytokines in adipocytes (46). Moreover, involvement of RhoA in mediating myocardial and pulmonary fibrosis has been described (47–48). In addition, previous studies have indicated that the sustained activation of the RhoA pathway can block the differentiation of muscle cells by inhibiting myoblast fusion (49–51).

Because of RhoA's potential involvement in the regulation of osteogenesis, adipogenesis, and myogenesis of stem cells and inflammation, we hypothesized that RhoA may act as a critical regulator of these processes in dystrophic muscle. In the current study, we investigated the status of HO, FI, IMCL, and muscle regeneration in the skeletal muscle of *mdx* and dKO mice, as well as the potential role that RhoA signaling plays in regulating these processes.

MATERIALS AND METHODS

Animals

Wild-type (C57BL/10J) mice were obtained from the Jackson Laboratory (Bar Harbor, ME, USA). The *mdx* and dKO (*mdx*; *utrn*$^{-/-}$) mice were derived from our in-house colony. Mice were housed in groups of 4 on a 12:12-h light-dark cycle at 20–23°C. At least 6 mice were used in each experimental sample group. All procedures were approved by the Institutional Animal Care and Use Committee (IACUC) at the University of Pittsburgh.

Stem cell isolation from skeletal muscle

Muscle-derived stem cells (MDSCs) were isolated from the skeletal muscle of dKO and *mdx* mice (4 wk old) *via* a modified preplate technique (52). Mice were sacrificed in a carbon dioxide chamber, as described in the IACUC proto-

col. Cells were cultured in proliferation medium [DMEM supplemented with 20% fetal bovine serum (FBS), 1% penicillin-streptomycin antibiotics, and 0.5% chicken embryo extract (CEE)].

Micro-computed tomography (micro-CT)

To observe HO in the soft tissues of *mdx* and dKO mice, 8-wk-old mice were anesthetized with 3% isoflurane in O_2 gas (1.5 L/min), and the lower extremities, including the pelvis, were scanned using the Viva CT 40 (Scanco, Wangen-Brüttisellen, Switzerland) with the following settings: energy, 70 kVp; intensity, 114 μA; integration time, 200 ms; isotropic voxel size, 35 μm; threshold, 163.

In vitro RhoA inactivation with Y-27632 and multipotent differentiation assays

dKO MDSCs cultured *in vitro* were treated with the RhoA/Rock inhibitor Y-27632 (10 μM; EMD Millipore, Billerica, MA, USA) in proliferation medium for 2 d, before being plated in 12-well flasks and set up for osteogenesis, adipogenesis, or myogenesis assays. The osteogenesis assay was conducted with osteogenic medium (DMEM supplemented with 110 μg/ml sodium pyruvate, 584 μg/ml L-glutamine, 10% FBS, 1% penicillin/streptomycin, 10^{-7} μM dexamethasone, 50 μg/ml ascorbic-acid-2-phosphate, and 10^{-2} μM β-glycerophosphate), supplemented with BMP2 (50 ng/ml for 7 d). Calcium deposition was assessed with alizarin red stain. Adipogenesis assay was conducted with adipogenic induction medium (Lonza, Basel, Switzerland) for 10 d and tested for lipid droplets with Oil red O stain (Sigma, St. Louis, MO, USA). The myogenesis assay was conducted by switching the proliferation medium into myogenic differentiation medium (DMEM containing 2% horse serum). Myotube formation was tracked during the following 4 d. 10 μM of Y-27632 was continuously present in the differentiation medium.

mRNA analysis with reverse transcriptase-PCR

Total RNA was obtained from MDSCs or the skeletal muscles of mice using a RNeasy Mini Kit (Qiagen, Valencia, CA, USA), according to the manufacturer's instructions. Reverse transcription was performed using the iScript cDNA synthesis kit (Bio-Rad, Hercules, CA, USA). PCR reactions were performed using an iCycler Thermal Cycler (Bio-Rad). The cycling parameters used for all primers were as follows: 95°C for 10 min; PCR, 40 cycles of 30 s at 95°C for denaturation, 1 min at 54°C for annealing, and 30 s at 72°C for extension. Products were separated by size, and they were visualized on 1.5% agarose gels stained with ethidium bromide. All data were normalized to the expression of *GAPDH*. Genes and primers used in the study included *GAPDH*: TCCATGACAACTTTGGCATTG (sense) and TCACGCCACAGCTTTCCA (antisense); *RhoA*: GTAGAGTTGGCTTTATGGGACAC (sense), and TGGAGTCCATTTTTCTGGGATG (antisense); BMP2: TCTTCCGGGAACAGATACAGG (sense), and TGGTGTCCAATAGTCTGGTCA (antisense); *BMP4*: ATTCCTGGTAACCGAATGCTG (sense), and CCGGTCTCAGGTATCAAACTAGC (antisense); *TNF-α*: GATTATGGCTCAGGGTCCAA (sense), and CTCCCTTTGCAGAACTCAGG (antisense); *IL6*: GGAAATCGTGGAAATGAG (sense), and GCTTAGGCATAACGCACT (antisense); *Klotho*: CCCAAACCATCTATGAAAC (sense), and CTACCGTATTCTATGCCTTC (antisense); and peroxisome proliferator-activated receptor γ (*PPARγ*): CCACCAACTTCGGAATCAGCT (sense) and TTTGTGGATCCGGCAGTTAAGA (antisense).

In vivo RhoA inactivation with Y-27632

Intramuscular injections into the gastrocnemius muscles (GMs) of dKO mice were conducted with Y-27632 (5 mM in 30 μl of PBS solution; left limb) or control (30 μl of PBS; right limb), starting from 4 wk of age. Intramuscular injections were conducted 3×/wk for 4 wk. Differential HO formation in the skeletal muscle with or without Y-27632 treatment was assessed by micro-CT scan or alizarin red stain. Systematic inhibition of RhoA signaling was conducted by intraperitoneal injection of Y-27632 (5 mM in PBS, 10 mg/kg/mouse) or control (PBS only) into dKO mice from 3 wk of age. Intraperitoneal injections into dKO mice were conducted 3×/wk for 4 wk.

Histology

Cryostat sections (10 μm) were prepared using standard techniques from GMs of mice. HO in muscle tissue was assessed by alizarin red stain: tissue sections of skeletal muscle were fixed with 4% formalin (10 min) and rinsed with ddH_2O; slides were then incubated with alizarin red working solution for 10 min before being washed with ddH_2O. FI was detected by Oil red O stain: fixed tissue sections were rinsed with ddH_2O and 60% isopropanol; slides were then incubated with Oil red O working solution for 15 min before being rinsed with 60% isopropanol and ddH_2O. The IMCL was detected by AdipoRed assay reagent (Lonza): fixed tissue sections were rinsed with PBS and incubated with AdipoRed assay reagent for 15 min before being washed with PBS. For immunofluorescent staining of tissue sections, the sections were blocked with horse serum (10%) for 1 h, and the primary antibodies RhoA (Santa Cruz Biotechnology, Santa Cruz, CA, USA), CD68 (Abcam, Cambridge, MA, USA), or MyoD (Santa Cruz Biotechnology) were applied at 1:100–1:200. Negative controls were performed concurrently with all immunohistochemical staining. Necrosis with damaged myofibers in muscle was assayed by incubating with biotinylated anti-mouse IgG (1:300; Vector Laboratory, Burlingame, CA, USA) for 1 h at room temperature, which was followed by a 15-min incubation with streptavidin Cy3 conjugate (1:500; Sigma-Aldrich). All incubations were performed at room temperature. All slides were analyzed using fluorescent microscopy (Leica Microsystemic, Buffalo Grove, IL, USA) and photographed at ×4–40 view.

Measurement of results and statistical analysis

The measurement of results from images was performed using commercially available software (Northern Eclipse 6.0; Empix Imaging, Mississauga, ON, Canada) and ImageJ 1.32j (U.S. National Institutes of Health, Bethesda, MD, USA). Data from ≥3 samples from each subject were pooled for statistical analysis. Results are given as means ± SD. Statistical significance of any difference was calculated using Student's t test. Values of $P < 0.05$ were considered statistically significant.

RESULTS

Extensive intramuscular HO and IMCL occurred in the skeletal muscle of dKO mice

Micro-CT scan and alizarin red staining revealed extensive HO in the hind-limb muscles (*i.e.*, GMs) of dKO mice at 8 wk of age (**Fig. 1*A*, *B***), while in age-matched *mdx* mice, only mild HO was observed (Fig. 1*A*, *B*). Oil

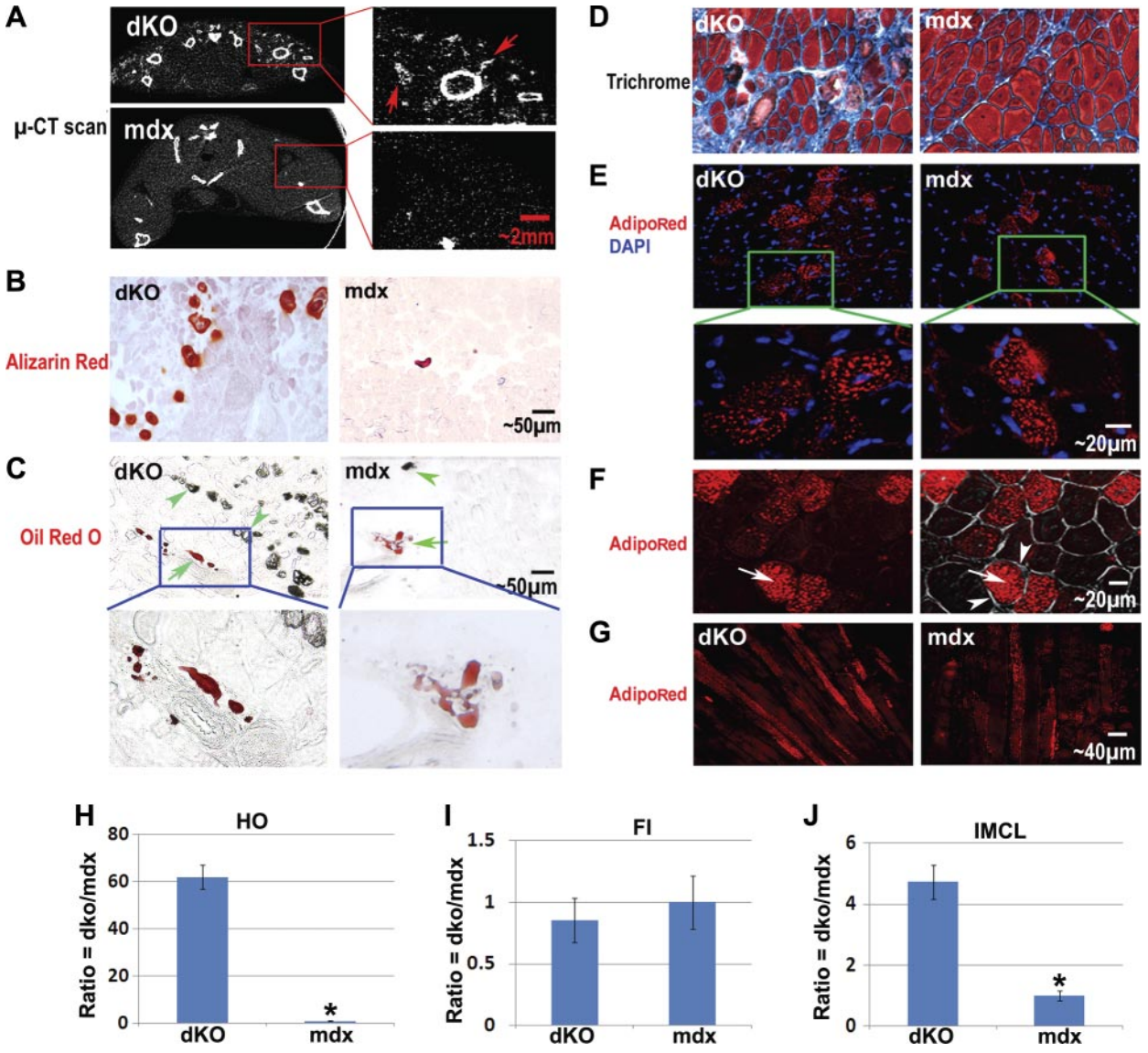

Figure 1. Differential formation of HO, FI, fibrosis, and IMCL in the skeletal muscle of dKO mice and *mdx* mice. *A*) Micro-CT scan revealed extensive HO formation (arrows) in the hind-limb skeletal muscles of dKO mice (8 wk of age), especially in the thigh and GM. Much less HO was observed in *mdx* mice (8 wk of age). *B*) Alizarin red stain of muscle tissue sections also showed more extensive HO formation in the GMs of the dKO mice. *C*) Oil red O stain revealed comparable amounts of intramuscular FI in dKO and *mdx* mice (but a much lower ratio of fat/HO), and the distinct localization of fat and HO (HO is visible with brightfield light). Arrows denote FI; arrowheads denote HO. *D*) Trichrome stain showed more fibrotic tissue (blue) and less normal myofibers in the skeletal muscle of dKO mice. *E*) AdipoRed stain indicated that IMCL occurred in the skeletal muscle of both *mdx* and dKO mice but was more extensive in the dKO mice. *F*) Representative images showing the localization of lipids (arrows) inside the membrane (arrowheads) of myofibers. Left panel: fluorescent image showing AdipoRed signal. Right panel: overlay of fluorescent and brightfield images. *G*) AdipoRed stain of longitudinal sections of GMs, verifying that the identity of the cells with positive signals were myofibers and not fat cells. *H*) Statistics of HO in GMs of dKO mice compared to *mdx* mice. *I*) Statistics of FI in GMs of dKO mice compared to *mdx* mice. *J*) Statistics of IMCL in GMs of dKO mice compared to *mdx* mice. $*P < 0.05$.

red O stain revealed mild intramuscular FI in the GMs of both 8-wk-old *mdx* and dKO mice (Fig. 1*C*). Notably, the FI/HO ratio was much lower in the dKO mice, and the sites of intramuscular HO and FI did not colocalize (Fig. 1*C* and Supplemental Fig. S1*A*). The fact that HO and FI never colocalized in the muscle suggests that these two processes are mutually exclusive and could implicate different cell types and/or niches involved in the two processes. In addition, trichrome staining of the skeletal muscle tissue further revealed more fibrosis in the skeletal muscle of dKO mice when compared with skeletal muscle of the *mdx* mice (Fig. 1*D*). These observations suggest that the microenvironment differs between dKO and *mdx* skeletal muscle, and the micromilieu in the dKO skeletal muscle is more conductive to osteogenesis or fibrogenesis processes. Much like our observation in the dKO mice, other important animal models of human DMD, including the GRMD dog and the canine X-linked muscular dystrophy (CXMD) dog, feature extensive HO and mild FI in their skeletal

muscle, especially before the age of 4–6 mo (16, 53–54).

Interestingly, contrary to the mild FI observed in the skeletal muscles of dKO mice, extensive IMCL was observed; while in the skeletal muscle of *mdx* mice, less extensive amounts of IMCL were noted (Fig. 1*E–G*). This severe lipid accumulation in the mature muscle cells (myofibers) of dKO muscle is indicative of disordered lipid metabolism in their skeletal muscle (55).

In addition, intramuscular HO and FI development was compared between the dKO and *mdx* mice at different ages (dKO mice at 4 or 8 wk and *mdx* mice at 4 wk or 24 mo). Eight weeks and 24 mo represent ~100% of the life span of the dKO and *mdx* mice, respectively. Results showed that HO increased with age in the dKO mice within their very short life span, but it remained mild in the *mdx* mice across their entire life span (**Fig. 2*A*, *C*, *D***). Meanwhile, FI increased with age in both the *mdx* and dKO mice and became quite excessive in aged *mdx* mice but not in the 8-wk-old dKO mice (Fig. 2*B–D*). Notably, in both the 4- and 8-wk-old dKO mice, the presence of FI was much less extensive than HO (Fig. 2*C*), while in *mdx* mice, FI became more extensive than HO with aging (Fig. 2*D*).

HO localizes at the sites of necrosis and fibrosis in the skeletal muscle of dKO mice

Alizarin red or hematoxylin and eosin staining was performed on serial sections of the skeletal muscle of 8-wk-old dKO mice, and HO generally localized at the sites enriched with damaged myofibers, but not in areas where normal myofibers existed (Fig. 2*E*). Also, Trichrome stain and IgG stain further indicated that localization of HO is generally surrounded by fibrotic tissues (Supplemental Fig. S1*B*) or necrotic tissues (Supplemental Fig. S1*C*). Therefore, it appears that

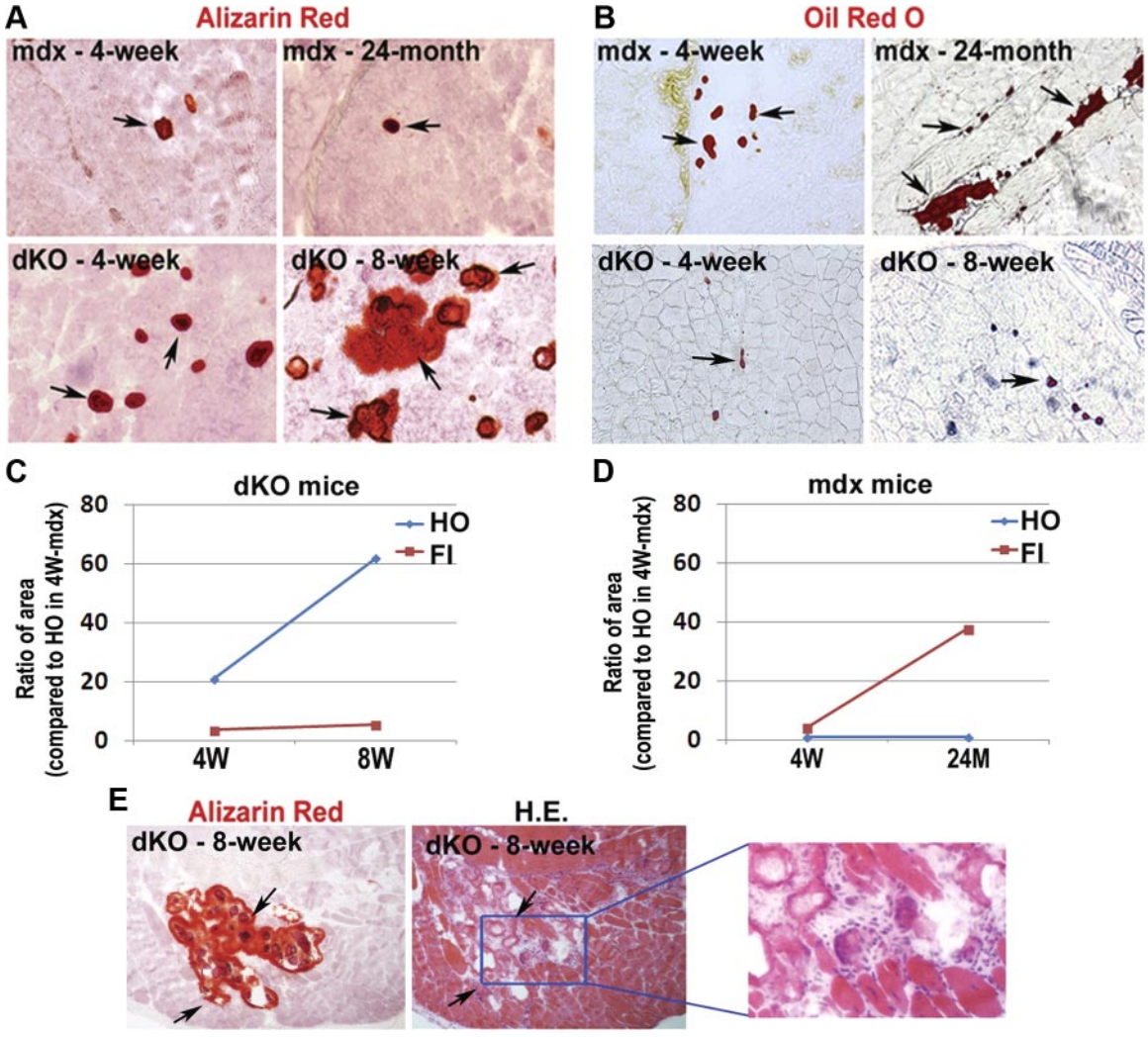

Figure 2. Development of HO and FI in the skeletal muscle of "younger" and "older" dKO mice (4 and 8 wk) and *mdx* mice (4 wk and 24 mo). *A*) HO (arrows) increased significantly with age in dKO mice but not in *mdx* mice. *B*) FI (arrows) increased with age in both *mdx* mice and dKO mice, but to a lesser extent in the dKO mice. *C*) Statistics on the change of HO and FI with aging in dKO mice. *D*) Statistics on the change of HO and FI with aging in *mdx* mice. *E*) Serial sections of the skeletal muscle of 8-wk-old dKO mice were stained with either alizarin red or hematoxylin and eosin (H.E.); it shows that HO was generally localized at the sites enriched with damaged myofibers and fibrosis (arrows) but not at the sites possessing normal myofibers.

HO formation in the skeletal muscle of dKO mice is concurrent with necrosis and fibrosis.

RhoA signaling was activated in the skeletal muscle of dKO mice and RhoA$^+$ cells specifically localized at the sites of necrosis and HO

Semiquantitative RT-PCR analyses revealed that the expression of the inflammatory factor TNF-α, and osteogenesis-related factors BMP2, BMP4, and RhoA were all up-regulated in the dKO skeletal muscle, when compared to the age-matched *mdx* skeletal muscle (**Fig. 3*A***). BMPs are known to induce HO in damaged skeletal muscle, and elevated BMP signaling has been observed in satellite cells of patients wtih DMD (56). We also found that the expression of Klotho, an antiinflammatory and antiaging factor (57), was down-regulated in the dKO skeletal muscle when compared to the *mdx* skeletal muscle (Fig. 3*A*). Because inflammation has been implicated as an important contributor to HO (1, 27, 58), it is possible that highly activated inflammation signaling in the dKO skeletal muscle is involved with the extensive HO observed in this animal model. A similar differential expression of these genes was found in MDSCs isolated from dKO and *mdx* mice.

Furthermore, immunofluorescent staining for the RhoA protein revealed an increased number of RhoA$^+$ cells in the skeletal muscle of dKO mice when compared to *mdx* mice (Fig. 3*B, C*), further confirming elevated RhoA signaling in the dKO skeletal muscle. Notably, it was noted that RhoA$^+$ cells were usually localized at the sites of excessive necrosis and HO (Fig. 3*B* and Supplemental Fig. S2), but not in area of FI, indicating potential involvement of RhoA$^+$ cells in the progression of HO.

In addition, through colocalization analyses, it was demonstrated that RhoA$^+$ cells do not colocalize with CD68$^+$ inflammatory cells (Fig. 3*D*) and MyoD$^+$ myogenic cells (Fig. 3*E*), indicating that the RhoA$^+$ cells did not represent inflammatory or myogenic cells.

RhoA inactivation of dKO MDSCs decreased their osteogenic potential, while it increased their adipogenic and myogenic potentials

Similar to what was observed with skeletal muscle tissues, immunofluorescent staining of MDSCs isolated from dKO and *mdx* mice for MyoD and RhoA also demonstrated a greater number of RhoA$^+$ cells in the MDSCs isolated from the dKO mice than the *mdx* mice (**Fig. 4*A***). Therefore, we hypothesized that the inactiva-

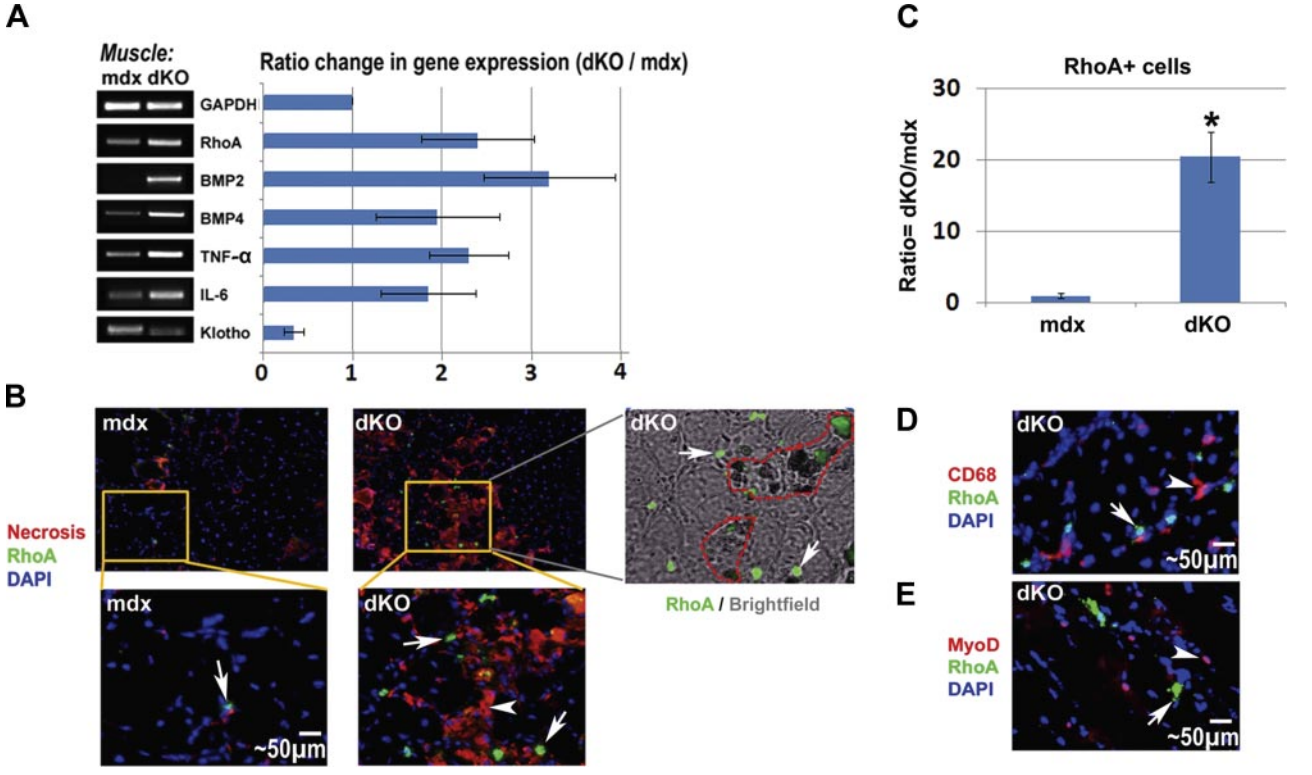

Figure 3. RhoA$^+$ cells in the skeletal muscle of dKO and *mdx* mice. *A*) RT-PCR of mRNA isolated from the skeletal muscle of dKO and *mdx* mice (8 wk of age) showed that the expression of RhoA, BMP2/4, TNF-α, IL-6 was up-regulated in dKO mice, and the expression of the anti-inflammation factor Klotho was down-regulated. *B*) Immunofluorescent staining of RhoA demonstrated a greater number of RhoA$^+$ cells (arrows) in the skeletal muscle of dKO mice. Necrotic areas (arrowheads) were localized by staining with fluorescent anti-mouse IgG, and RhoA$^+$ cells were found to localize at or around the necrotic areas; overlay of images of brightfield and immunofluorescent staining of RhoA further revealed that the same areas enriched with RhoA$^+$ cells (arrows) are the area of HO (circled) too. *C*) Statistics of RhoA$^+$ cells in *mdx* and dKO skeletal muscle. *D*) Representative image of immunofluorescent staining of CD68 and RhoA in the dKO muscle demonstrated that CD68$^+$ cells (arrowheads) and RhoA$^+$ cells (arrows) were two different cell populations. *E*) Representative image of immunofluorescent staining of MyoD and RhoA in the dKO muscle demonstrated that MyoD$^+$ cells (arrowheads) and RhoA$^+$ cells (arrows) were two different cell populations. *$P < 0.05$.

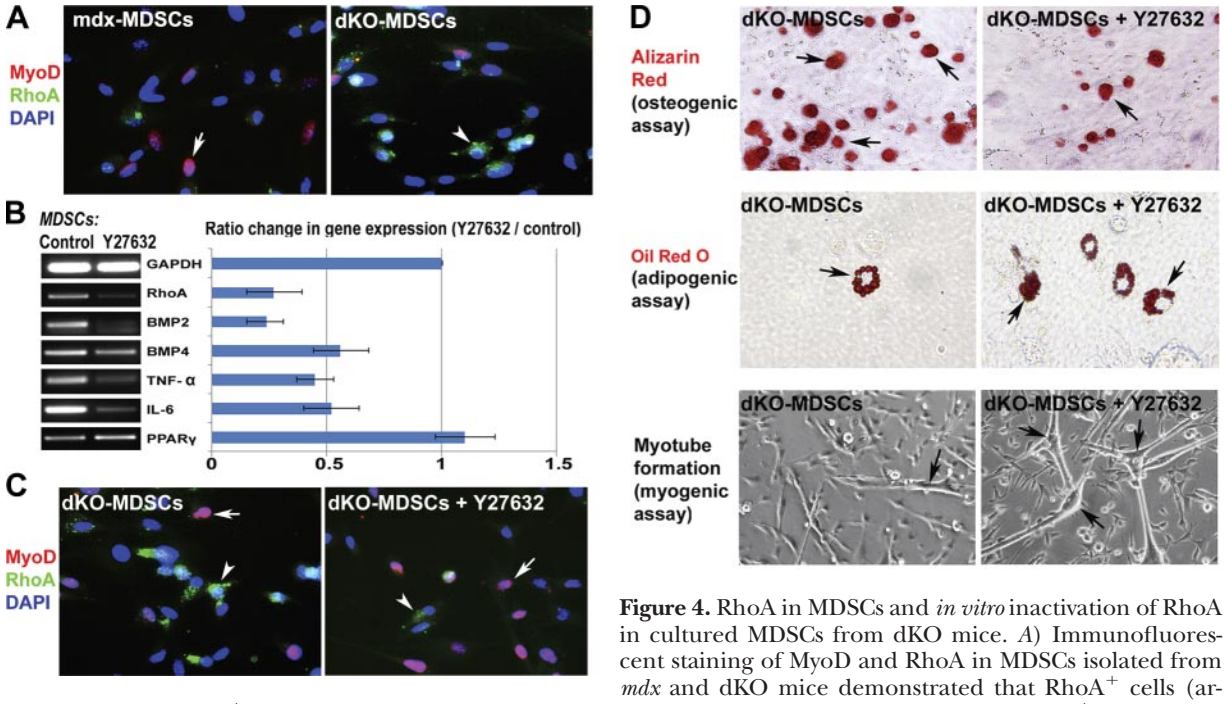

Figure 4. RhoA in MDSCs and *in vitro* inactivation of RhoA in cultured MDSCs from dKO mice. *A*) Immunofluorescent staining of MyoD and RhoA in MDSCs isolated from *mdx* and dKO mice demonstrated that RhoA$^+$ cells (arrowhead) and MyoD$^+$ cells (arrow) were two distinct cell populations, and there were more RhoA$^+$ cells in the MDSCs isolated from dKO mice than *mdx* mice. *B*) Pretreatment of dKO-MDSCs with the RhoA/Rock inhibitor Y-27632 in proliferation medium for 2 d down-regulated the expression of RhoA, BMP2/4, TNF-α, and IL-6, and up-regulated the expression of PPARγ. *C*) Y-27632 treatment decreased the number of RhoA$^+$ cells (arrowheads) and increased the number of MyoD$^+$ cells (arrows). *D*) *In vitro* osteogenesis, adipogenesis, and myogenesis assays indicated that, Y-27632 pretreated dKO-MDSCs demonstrated decreased osteogenic potential (less cells with positive alizarin red signal) in osteogenic medium and increased adipogenesis potential (more cells with positive Oil red O signal) in adipogenic medium, as well as increased myogenic potential (more myotube formation) in the myogenic medium.

tion of RhoA signaling in the MDSCs may change the osteogenic, adipogenic, and myogenic potentials of the cells because RhoA is a proosteogenic and antiadipogenic/myogenic signaling pathway. To test the hypothesis, dKO MDSCs were cultured in proliferation medium and pretreated with the RhoA/Rock inhibitor, Y-27632, for 2 d before undergoing osteogenic, adipogenic, and myogenic assays. Y-27632 pretreatment of dKO MDSCs significantly down-regulated the expression of the inflammation-related genes (TNF-α and IL-6), BMPs, and RhoA (Fig. 4*B*). Also, Y-27632 pretreatment up-regulated the expression of the key adipogenic factor, PPARγ, which is known to have anti-inflammatory activities (59). Immunostaining of RhoA and MyoD showed that RhoA$^+$ cells and MyoD$^+$ cells were 2 distinct cell populations, and the number of RhoA$^+$ cells was decreased, while the number of MyoD$^+$ cells was increased with Y-27632 treatment (Fig. 4*C*), indicating decreased osteogenic but increased myogenic potentials of the treated cell population. Osteogenesis and adipogenesis assays revealed a decreased osteogenic potential and increased adipogenic potential of the MDSCs treated with Y-27632 (Fig. 4*D*). Meanwhile, the dKO MDSCs treated with Y-27632 showed an increase in their myogenic potential (Fig. 4*D*).

RhoA inactivation in dKO skeletal muscle decreased HO and IMCL, while it increased muscle regeneration

The RhoA/Rock inhibitor Y-27632 was injected intramuscularly into the GM muscles of 4-wk-old dKO mice to determine the effect of RhoA inactivation on the development of HO, FI, IMCL, and muscle regeneration. Four weeks after the administration of Y-27632, we observed slower development of HO in the dKO skeletal muscle, as determined by micro-CT scanning and histological staining (**Fig. 5*A, B***). At the same time, skeletal muscle regeneration was enhanced in the treated dKO skeletal muscle (Fig. 5*C*) despite slightly increased FI (Fig. 5*D*). Notably, the increase of FI in the dKO muscle with Y-27632 administration was mild compared to the increase of muscle regeneration, and the overall phenotype of the dystrophic muscle was greatly improved (Fig. 5). Finally, IMCL was decreased (Fig. 5*E*), indicating improved fatty acid metabolism in the skeletal muscle with RhoA inactivation. Immunofluorescent staining of RhoA revealed that the number of RhoA$^+$ cells decreased with the administration of Y-27632 (Fig. 5*F*), which may correlate with the reduced number of osteogenic cells in the skeletal muscle. Furthermore, the number of CD68$^+$ inflammatory cells (mainly macrophages; ref. 60) was also reduced after the administration of Y-27632 (Fig. 5*G*). In addition, semiquantitative RT-PCR showed that the expression of RhoA, BMPs, and inflammation-related factors were down-regulated in skeletal muscle treated with Y-27632, while the expression of PPARγ was up-regulated (Fig. 5*H*). PPARγ activation may have improved fatty acid metabolism and reduced the accumulation of lipid within the muscle cells (61–62). The overall pheno-

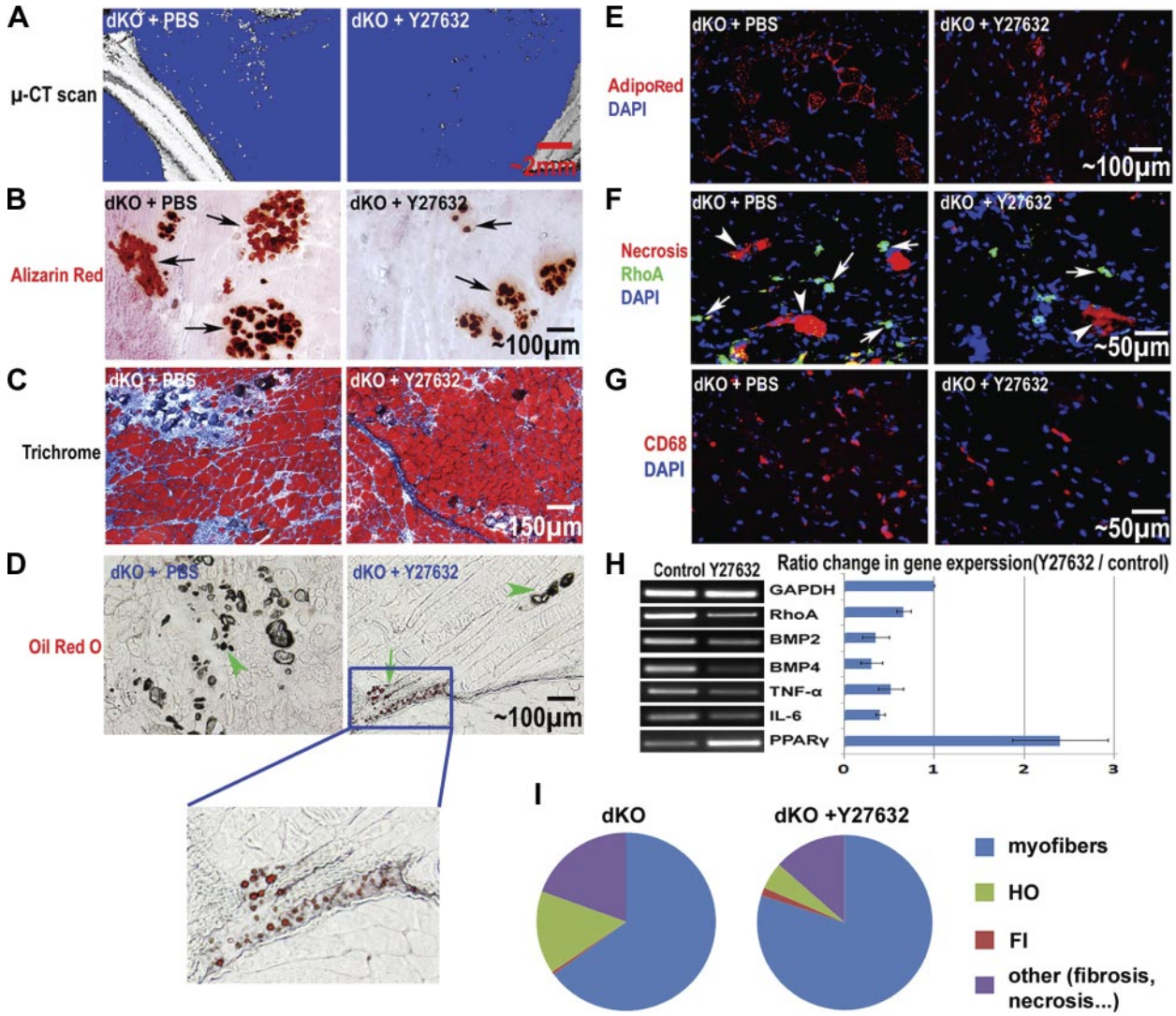

Figure 5. *In vivo* inactivation of RhoA in the skeletal muscle of dKO mice. *A*) Micro-CT scan of the hind-limb skeletal muscles, including the GM, 4 wk after beginning the administration of the RhoA/Rock inhibitor Y-27632 in dKO mice (from 4 to 8 wk of age) showed a reduction in HO. *B*) Alizarin red stain of muscle tissues also revealed greatly reduced HO (arrows) in the GM muscles with Y-27632 treatment. *C*) Hematoxylin and eosin stain showed improved muscle regeneration with Y-27632 treatment. *D*) Oil red O stain showed slightly increased FI (arrows) with Y-27632 treatment. HO is also visible with brightfield microscopy (arrowheads). *E*) AdipoRed stain showed reduced IMCL in dKO mice with Y-27632 treatment. *F*) Immunofluorescent stain showed reduced numbers of $RhoA^+$ cells (arrows) and necrotic myofibers (arrowheads) with Y-27632 treatment. *G*) Immunofluorescent stain showed reduced numbers of $CD68^+$ inflammatory cells with Y-27632 treatment. *H*) RT-PCR of the muscle tissues revealed down-regulated expression of RhoA, BMP2/4, TNF-α, and IL-6, and up-regulated expression of PPARγ with Y-27632 treatment. *I*) The overall phenotypic change of the muscle treated with Y-27632 is summarized in the pie graph, including myofibers, HO, FI, and other (fibrosis and necrosis). It is clear that HO, fibrosis, and necrosis were reduced with Y-27632 treatment, while muscle regeneration was improved; FI was also increased, but only very slightly.

typic change in the dKO skeletal muscle treated with Y-27632 is summarized in Fig. 5*I*.

dKO cardiac muscle featured increased IMCL, fibrosis, and HO when compared to *mdx* mice

Cardiac involvement is the leading cause of early death in patients wtih DMD (63), and intramyocardial lipid accumulation in cardiac muscle has been observed in patients wtih DMD, especially in the most damaged areas of the hearts (11, 13). We hypothesized that IMCL observed in the *mdx* and dKO mice was not limited to the skeletal muscle but would also be found in cardiac muscle and could be related to the formation of fibrosis observed in the dystrophic hearts (cardiomyopathy) of the mice.

Trichrome staining of cardiac muscles from 8-wk-old WT, *mdx*, and dKO mice was conducted to characterize ECM collagen deposition, and it revealed that fibrosis formation is generally severe in dKO mice, mild in *mdx* mice, and absent in WT mice (**Fig. 6*A***). Alizarin red staining of the cardiac muscle revealed occurrences of HO in the dKO mice (Fig. 6*B*), but not in the WT or *mdx* mice (data not shown). Meanwhile, we did not observe any FI in the cardiac muscles in these three

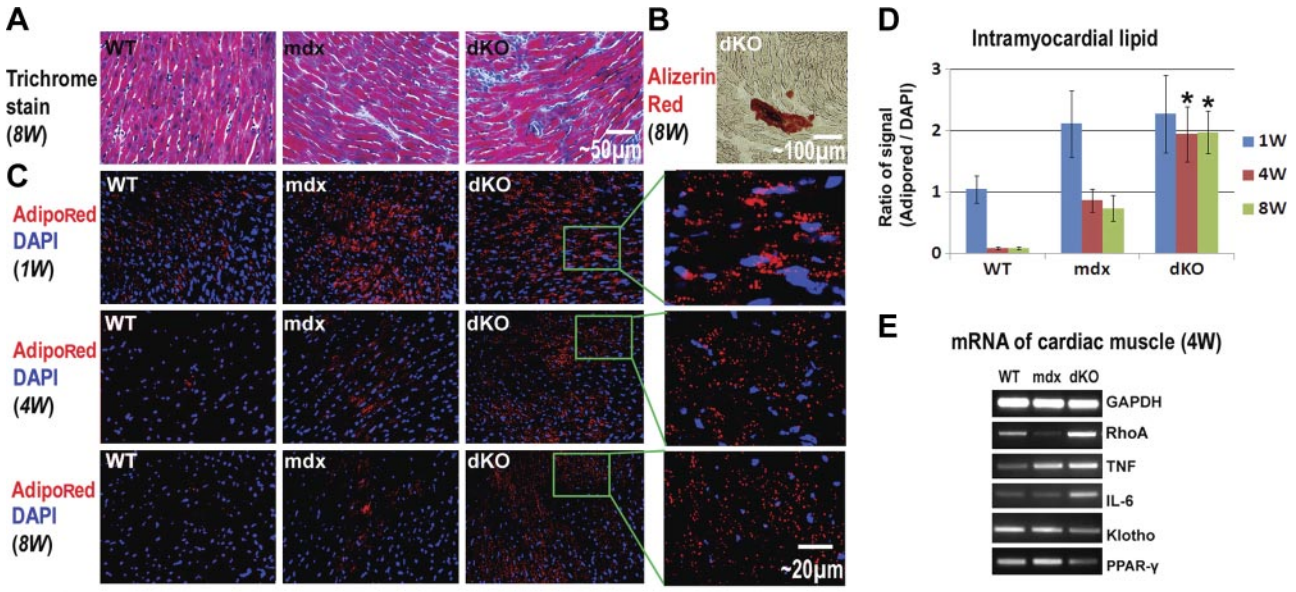

Figure 6. Fibrosis formation and intramyocardial lipid accumulation in the cardiac muscles of WT, *mdx*, and dKO mice. *A*) Trichrome stain showed the progression of fibrosis formation (collagen deposition, blue) in the cardiac muscles as dKO > *mdx* > WT. *B*) Alizarin red stain revealed HO (although mild) in the cardiac muscle of dKO mice. *C*) High levels of intramyocardial lipids were observed in all three mouse models at 1 wk after birth. At 4 and 8 wk after birth, intramyocardial lipid accumulation decreased to an undetectable level in WT mice and decreased to a moderate level in *mdx* mice but still maintained a very high level in the dKO mice. *D*) Statistical analysis of the percentage of area positive for lipid accumulation in WT, *mdx*, and dKO mice of different ages. *E*) RT-PCR results showed that the expression of inflammatory factors (TNF-α and IL-6) were up-regulated in the cardiac muscles of *mdx* and dKO mice, compared with WT mice. The strongest up-regulation of TNF-α and IL-6 occurred to the dKO mice. The expression of the anti-inflammatory factor Klotho was down-regulated in the cardiac muscle of mdx and dKO mice, compared to WT mice. $*P < 0.05$.

mouse models (data not shown), but we did observe intramyocardial lipid accumulation in both the *mdx* and dKO mice (Fig. 6*C*, *D*).

Extensive intramyocardial lipid accumulation at 1 wk of age was observed in all 3 mouse models (Fig. 6*C*). Intramyocardial lipid accumulation in fetal WT mice is a common occurrence because, unlike adult hearts, the fetal hearts use glucose instead of fatty acids as a source of energy (64). Intramyocardial lipid accumulation was found to decrease rapidly in WT mice 1 wk after birth and became nearly undetectable at 4 wk of age (Fig. 6*C*); however, in both *mdx* and dKO mice, intramyocardial lipid accumulation was still observed at 4 wk of age, and the dKO mice exhibited more intramyocardial lipid accumulation than the *mdx* mice (Fig. 6*C*, *D*). Compared to the WT and *mdx* mice, the expression of RhoA and inflammation related factors (TNF-α and IL-6) were also found to be up-regulated in the dKO cardiac muscle, while the expression of the *Klotho* gene was down-regulated (Fig. 6*E*). We suggest that the activation of RhoA and inflammation signaling in dKO cardiac muscle may account for higher levels of HO, intramyocardial lipid accumulation, and fibrosis.

Systemic RhoA inactivation *via* intraperitoneal injection (IP) of Y-27632 reduced IMCL, fibrosis, and HO in dKO cardiac muscle

We hypothesized that RhoA inactivation could reduce HO, IMCL, and fibrosis in the dKO cardiac muscle. To confirm this hypothesis, Y-27632 was injected intraperitoneally (IP) to achieve the systemic inhibition of RhoA signaling in 3-wk-old dKO mice. As expected, after 4 wk of continuous injection. IMCL, fibrosis, and HO in the cardiac muscle decreased compared to nontreated mice (**Fig. 7*A–F***). Actually, involvement of RhoA/ROCK in mediating myocardial fibrosis in type 2 diabetes has been previously demonstrated (48). Semiquantitative PCR further revealed that the expression of RhoA and inflammatory factors were down-regulated with Y-27632 administration, while the expression of Klotho and PPARγ was up-regulated (Fig. 7*G*).

DISCUSSION

Heterotopic ossification (HO) and ectopic fatty infiltration (FI) have been reported in the dystrophic muscle of patients wtih DMD and related animal models (12, 14–16, 65). Our results revealed that mouse models of DMD featuring differing severities of muscular dystrophy have varied potentials for developing HO and FI, and that RhoA signaling could represent a critical mediator in the process, including progression toward HO, FI, and normal muscle regeneration. We noted that the inactivation of RhoA repressed the development of HO and IMCL and improved muscle regeneration in dKO mice. RhoA signaling was previously demonstrated to promote the osteogenic potential of MSCs, while preventing their adipogenic and myogenic potentials (37, 40). Here, we further identified a similar

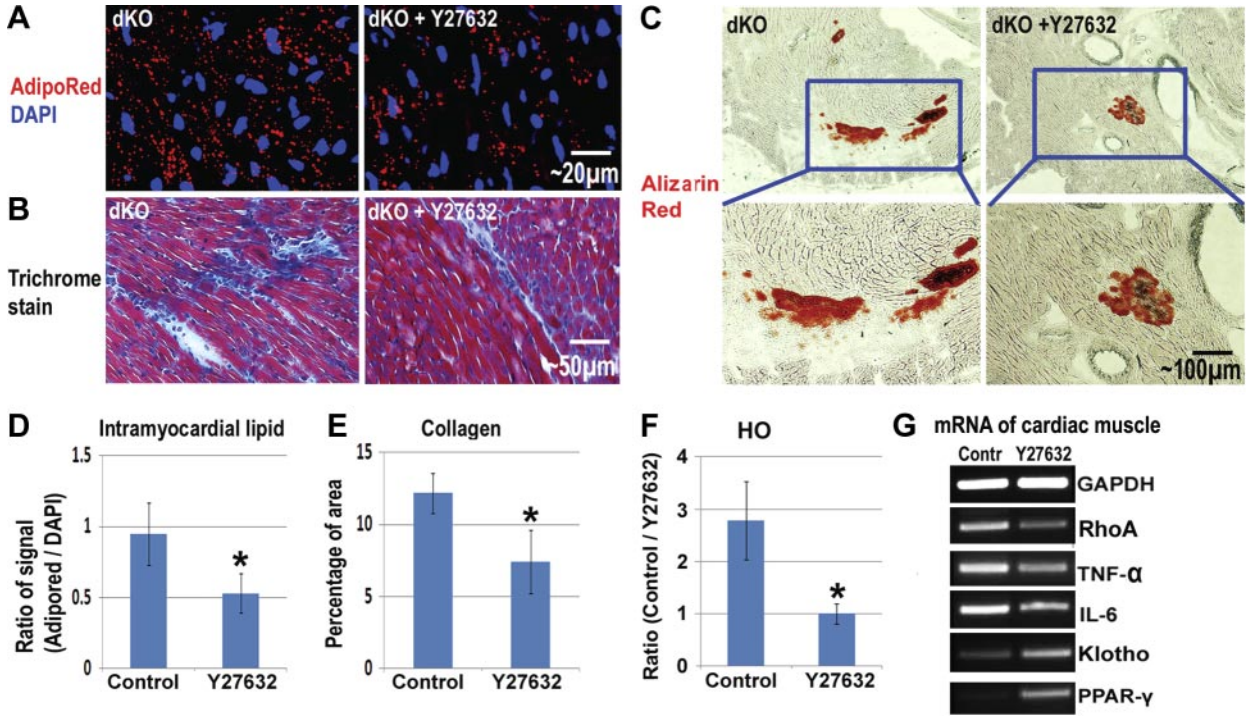

Figure 7. Reduction of intramyocardial lipid accumulation and fibrosis in the cardiac muscles of dKO mice with inactivated RhoA. *A*) AdipoRed stain showed that intramyocardial lipid accumulation in dKO mice was reduced 4 wk after the initiation of Y-27632 administration. *B*) Trichrome stain showed that fibrosis formation was reduced with Y-27632 administration. *C*) Alizarin red stain showed that HO formation in the cardiac muscles of dKO mice was reduced with Y-27632 administration. *D*) Statistical analysis of the percentage of areas positive for IMCL in dKO mice, with and without Y-27632 administration. *E*) Statistical analysis of the percentage of dKO mice positive for HO in their cardiac muscles, with and without Y-27632 administration. *F*) RT-PCR of mRNA from the cardiac muscles showed that the expression of RhoA and inflammatory factors (TNF-α and IL-6) were down-regulated with Y-27632 administration, while the expressions of Klotho and PPAR-γ were up-regulated. *Significant difference, $P < 0.05$.

role of RhoA signaling in muscle stem cells. We suggest that HO in skeletal muscle could be a cell-mediated process involving the transdifferentiation of myogenic cells into osteogenic cells in a stressful microenvironment. The potential mechanisms underlying our current results are proposed in **Fig. 8**.

Muscle stem cells from normal mice are known to possess multipotent differentiation potentials and can

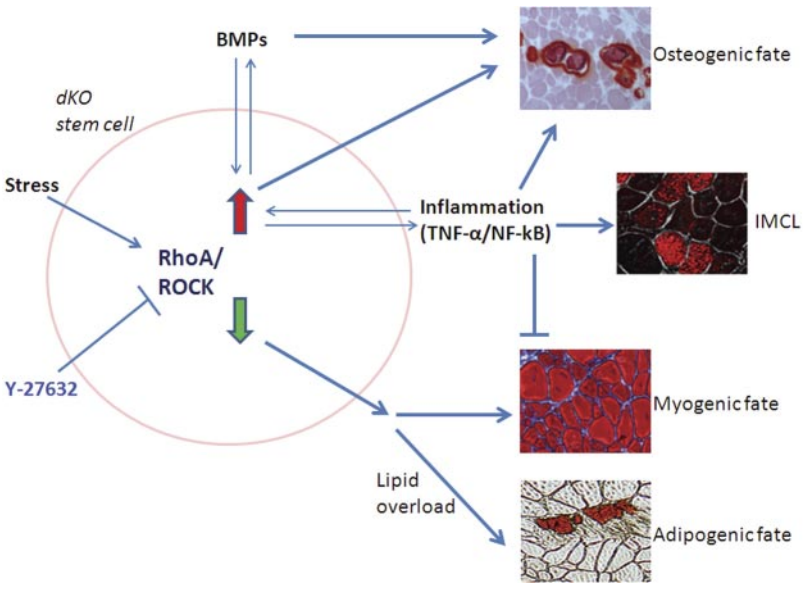

Figure 8. Schematic diagram of the potential mechanism involving RhoA/ROCK signaling in regulating HO, FI, and muscle regeneration in the dystrophic muscle of dKO mice. RhoA/ROCK is responsive to a variety of stresses. Multipotent stem cells, either local stem cells in the dystrophic muscle, bone-marrow-derived stem cells mobilized to the dystrophic muscle of dKO mice, or stem cells of other origins, may be stimulated to differentiate into an osteogenic lineage and may participate in HO formation by highly activated RhoA/Rock signaling, whereas normal myogenic differentiation or potential adipogenic differentiation in dKO mice were repressed by RhoA/Rock signaling. Critical HO-inducing factors, such as BMPs and inflammatory signaling, are interactive with RhoA/Rock signaling, and contribute to HO formation by stem cells or other progenitor cells. RhoA/Rock inactivation with Y-27632 has the potential to reverse the progression of differentiation of the stem cells toward HO, and improve myogenic or adipogenic differentiation. Inflammation-induced IMCL may be directly responsible for HO formation in the muscle (72).

differentiate into osteogenic, chrondrogenic, adipogenic, and myogenic lineages with appropriate induction stimuli (66). In the current study, we observed that the osteogenic potential of muscle stem cells appeared to be promoted, while adipogenic and myogenic potentials appeared to be repressed in the severely dystrophic muscle of dKO mice, a process likely mediated, at least in part, by RhoA activation. RhoA activation was shown to occur in response to stresses, including mechanical stress and oxidative stress (67, 68), suggesting that RhoA activation in the dystrophic muscle of dKO mice could be related to the multiple stresses to which the skeletal muscle of dKO mice is exposed. Compared to *mdx* mice, stresses in the dystrophic muscle of dKO mice may include more myofiber damage and abnormal neuromuscular junctions created by the absence of utrophin; stronger production of profibrotic factors, such as TGF-β1; and severe inflammation caused by extensive muscle degeneration and an abnormally high fat-to-skeletal muscle ratio.

Inactivation of RhoA signaling could be beneficial for improving the severe myopathological phenotype present in dKO mice. Interestingly, RhoA signaling was found to be increased in the spinal cord of an intermediate spinal muscular atrophy (SMA) mouse model, and the inactivation of RhoA signaling with Y-27632 improved the survival of these SMA mice (69). Our results showed that RhoA inactivation in dKO mice led to a less severe dystrophic muscle phenotype that more closely resembled the phenotype observed in *mdx* mice. RhoA signaling has been found to interact with inflammatory signaling and acts as a proinflammatory factor (46, 70). In our current study, we found the level of inflammation to be higher in dKO mice compared to *mdx* mice. By inactivating RhoA with Y-27632, we observed that TNF-α and IL-6 were down-regulated, while Klotho and PPAR-γ were up-regulated in both dKO muscle stem cells and skeletal muscle tissues, indicating a repression of inflammation (59). Therefore, we suggest that the improved muscle phenotype of dKO mice with RhoA inactivation is at least partially due to a reduction in inflammation. Moreover, the up-regulation of PPARγ expression *via* RhoA inactivation could also improve the metabolism of fatty acids in dystrophic muscle since PPARγ was previously reported to increase free fatty acid (FFA) disposal in skeletal muscle through oxidation augmentation, resulting in the reduction of IMCL (71). PPARγ activation in muscle has also been reported to prevent IMCL normally observed in both fat-fed wild-type mice, as well as in the muscles of obese diabetic patients (61, 62). Thus, the up-regulation of PPARγ *via* RhoA inactivation in dKO muscle improved fat metabolism by promoting the uptake of lipids by fat cells and not by muscle cells. Since obesity, inflammation, and IMCL have also been commonly observed in human DMD, we suggest that DMD should also be investigated for the prevention of IMCL by reducing obesity, inflammation, and metabolic abnormalities.

Previous researchers have demonstrated that intramyocardial lipid accumulation is potentially involved with cardiac dysfunction in the dystrophic heart. Cardiac failure is the leading cause for early death of patients wtih DMD (63), and it has been reported that intramyocardial lipid accumulation occurs in the damaged areas of cardiac muscle in patients wtih DMD (11); however, research is sparse regarding the mechanisms and prevention of intramyocardial lipid accumulation. Compared with *mdx* mice, the dKO mouse model exhibits a more severe abnormal cardiac phenotype (*i.e.*, fibrosis formation) and is considered to be an important model for studying DMD-associated cardiomyopathy (14, 19, 20). Our results showed that, when comparing the cardiac muscles of WT, *mdx*, and dKO mice, the severity of intramyocardial lipid accumulation appeared to be closely related to progressive cardiac muscle degeneration. More importantly, our results indicate that intramyocardial lipid accumulation can be reduced by inactivating RhoA, an effect potentially associated with repressed systematic inflammation.

In summary, our results indicated that RhoA signaling could play a major role in regulating the processes of HO, FI, IMCL, and muscle regeneration in the dystrophic skeletal muscle of mice, and consequently, RhoA inactivation may represent a therapeutic target to improve the muscle histopathology associated with DMD. Moreover, RhoA signaling may also serve as a potential target for repressing the development of HO in cases of trauma, neurological injury, and genetic abnormalities. The status of RhoA activation in human patients wtih DMD and the potential effect of RhoA inactivation are, therefore, very promising but require further investigation. FJ

This research was supported, in part, by the Henry J. Mankin endowed chair at the University of Pittsburgh, and the William F. and Jean W. Donaldson endowed chair at the Children's Hospital of Pittsburgh. The authors also thank Ms. Bria King and Mr. James Cummins for their editorial assistance in completing this manuscript.

REFERENCES

1. Cipriano, C. A., Pill, S. G., and Keenan, M. A. (2009) Heterotopic ossification following traumatic brain injury and spinal cord injury. *J. Am. Acad. Orthop. Surg.* **17,** 689–697
2. Marcus, R. L., Addison, O., Kidde, J. P., Dibble, L. E., and Lastayo, P. C. (2010) Skeletal muscle fat infiltration: impact of age, inactivity, and exercise. *J. Nutr. Health Aging* **14,** 362–366
3. Miljkovic-Gacic, I., Wang, X., Kammerer, C. M., Gordon, C. L., Bunker, C. H., Kuller, L. H., Patrick, A. L., Wheeler, V. W., Evans, R. W., and Zmuda, J. M. (2008) Fat infiltration in muscle: new evidence for familial clustering and associations with diabetes. *Obesity* **16,** 1854–1860
4. Savage, D. B., Petersen, K. F., and Shulman, G. I. (2007) Disordered lipid metabolism and the pathogenesis of insulin resistance. *Physiol. Rev.* **87,** 507–520
5. Hulver, M. W., and Dohm, G. L. (2004) The molecular mechanism linking muscle fat accumulation to insulin resistance. *Proc. Nutr. Soc.* **63,** 375–380
6. Schulze, P. C. (2009) Myocardial lipid accumulation and lipotoxicity in heart failure. *J. Lipid Res.* **50,** 2137–2138
7. Axelsen, L. N., Lademann, J. B., Petersen, J. S., Holstein-Rathlou, N. H., Ploug, T., Prats, C., Pedersen, H. D., and Kjolbye, A. L. (2010) Cardiac and metabolic changes in long-term high fructose-fat fed rats with severe obesity and extensive

intramyocardial lipid accumulation. *Am. J. Physiol. Regul. Integr. Comp. Physiol.* **298,** R1560–R1570
8. Ruberg, F. L. (2007) Myocardial lipid accumulation in the diabetic heart. *Circulation* **116,** 1110–1112
9. Sharma, S., Adrogue, J. V., Golfman, L., Uray, I., Lemm, J., Youker, K., Noon, G. P., Frazier, O. H., and Taegtmeyer, H. (2004) Intramyocardial lipid accumulation in the failing human heart resembles the lipotoxic rat heart. *FASEB J.* **18,** 1692–1700
10. Momose, M., Iguchi, N., Imamura, K., Usui, H., Ueda, T., Miyamoto, K., and Inaba, S. (2001) Depressed myocardial fatty acid metabolism in patients with muscular dystrophy. *Neuromusc. Disord.* **11,** 464–469
11. Saini-Chohan, H. K., Mitchell, R. W., Vaz, F. M., Zelinski, T., and Hatch, G. M. (2012) Delineating the role of alterations in lipid metabolism to the pathogenesis of inherited skeletal and cardiac muscle disorders: Thematic Review Series: Genetics of Human Lipid Diseases. *J. Lipid Res.* **53,** 4–27
12. Ionasescu, V., Monaco, L., Sandra, A., Ionasescu, R., Burmeister, L., Deprosse, C., and Stern, L. Z. (1981) Alterations in lipid incorporation in Duchenne muscular dystrophy. Studies of fresh and cultured muscle. *J. Neurol. Sci.* **50,** 249–251
13. Tahallah, N., Brunelle, A., De La Porte, S., and Laprevote, O. (2008) Lipid mapping in human dystrophic muscle by cluster-time-of-flight secondary ion mass spectrometry imaging. *J. Lipid Res.* **49,** 438–454
14. Duan, D. (2006) Challenges and opportunities in dystrophin-deficient cardiomyopathy gene therapy. *Hum. Mol. Genet.* **15**(Spec. 2), R253–R261
15. Kikkawa, N., Ohno, T., Nagata, Y., Shiozuka, M., Kogure, T., and Matsuda, R. (2009) Ectopic calcification is caused by elevated levels of serum inorganic phosphate in *mdx* mice. *Cell Struct. Funct.* **34,** 77–88
16. Nguyen, F., Cherel, Y., Guigand, L., Goubault-Leroux, I., and Wyers, M. (2002) Muscle lesions associated with dystrophin deficiency in neonatal golden retriever puppies. *J. Comp. Pathol.* **126,** 100–108
17. Starkey, J. D., Yamamoto, M., Yamamoto, S., and Goldhamer, D. J. (2011) Skeletal muscle satellite cells are committed to myogenesis and do not spontaneously adopt nonmyogenic fates. *J. Histochem. Cytochem.* **59,** 33–46
18. Sicinski, P., Geng, Y., Ryder-Cook, A. S., Barnard, E. A., Darlison, M. G., and Barnard, P. J. (1989) The molecular basis of muscular dystrophy in the *mdx* mouse: a point mutation. *Science* **244,** 1578–1580
19. Grady, R. M., Teng, H., Nichol, M. C., Cunningham, J. C., Wilkinson, R. S., and Sanes, J. R. (1997) Skeletal and cardiac myopathies in mice lacking utrophin and dystrophin: a model for Duchenne muscular dystrophy. *Cell* **90,** 729–738
20. Deconinck, A. E., Rafael, J. A., Skinner, J. A., Brown, S. C., Potter, A. C., Metzinger, L., Watt, D. J., Dickson, J. G., Tinsley, J. M., and Davies, K. E. (1997) Utrophin-dystrophin-deficient mice as a model for Duchenne muscular dystrophy. *Cell* **90,** 717–727
21. Isaac, C., Wright, A., Usas, A., Li, H., Tang, Y., Mu, X., Greco, N., Dong, Q., Vo, N., Kang, J., Wang, B., and Huard, J. (2013) Dystrophin and utrophin "double knockout" dystrophic mice exhibit a spectrum of degenerative musculoskeletal abnormalities. *J. Orthop. Res.* **31,** 343–349
22. Muntoni, F., Fisher, I., Morgan, J. E., and Abraham, D. (2002) Steroids in Duchenne muscular dystrophy: from clinical trials to genomic research. *Neuromusc. Disord.* **12**(Suppl. 1), S162–S165
23. Mavrogenis, A. F., Soucacos, P. N., and Papagelopoulos, P. J. (2011) Heterotopic ossification revisited. *Orthopedics* **34,** 177
24. Neal, B., Rodgers, A., Dunn, L., and Fransen, M. (2000) Non-steroidal anti-inflammatory drugs for preventing heterotopic bone formation after hip arthroplasty. *Cochrane Database Syst. Rev.*, CD001160
25. Dahners, L. E., and Mullis, B. H. (2004) Effects of nonsteroidal anti-inflammatory drugs on bone formation and soft-tissue healing. *J. Am. Acad. Orthop. Surg.* **12,** 139–143
26. Vasileiadis, G. I., Sioutis, I. C., Mavrogenis, A. F., Vlasis, K., Babis, G. C., and Papagelopoulos, P. J. (2011) COX-2 inhibitors for the prevention of heterotopic ossification after THA. *Orthopedics* **34,** 467
27. Banovac, K., Williams, J. M., Patrick, L. D., and Levi, A. (2004) Prevention of heterotopic ossification after spinal cord injury with COX-2 selective inhibitor (rofecoxib). *Spinal Cord* **42,** 707–710
28. Joe, A. W., Yi, L., Natarajan, A., Le Grand, F., So, L., Wang, J., Rudnicki, M. A., and Rossi, F. M. (2010) Muscle injury activates resident fibro/adipogenic progenitors that facilitate myogenesis. *Nat. Cell Biol.* **12,** 153–163
29. Cox, F. M., Reijnierse, M., van Rijswijk, C. S., Wintzen, A. R., Verschuuren, J. J., and Badrising, U. A. (2011) Magnetic resonance imaging of skeletal muscles in sporadic inclusion body myositis. *Rheumatology* **50,** 1153–1161
30. Mei, M., Zhao, L., Li, Q., Chen, Y., Huang, A., Varghese, Z., Moorhead, J. F., Zhang, S., Powis, S. H., and Ruan, X. Z. (2011) Inflammatory stress exacerbates ectopic lipid deposition in C57BL/6J mice. *Lipids Health Dis.* **10,** 110
31. Hotamisligil, G. S., Shargill, N. S., and Spiegelman, B. M. (1993) Adipose expression of tumor necrosis factor-alpha: direct role in obesity-linked insulin resistance. *Science* **259,** 87–91
32. Messina, S., Altavilla, D., Aguennouz, M., Seminara, P., Minutoli, L., Monici, M. C., Bitto, A., Mazzeo, A., Marini, H., Squadrito, F., and Vita, G. (2006) Lipid peroxidation inhibition blunts nuclear factor-kappaB activation, reduces skeletal muscle degeneration, and enhances muscle function in *mdx* mice. *Am. J. Pathol.* **168,** 918–926
33. Langen, R. C., Schols, A. M., Kelders, M. C., Wouters, E. F., and Janssen-Heininger, Y. M. (2001) Inflammatory cytokines inhibit myogenic differentiation through activation of nuclear factor-κB. *FASEB J.* **15,** 1169–1180
34. Lu, A., Proto, J. D., Guo, L., Tang, Y., Lavasani, M., Tilstra, J. S., Niedernhofer, L. J., Wang, B., Guttridge, D. C., Robbins, P. D., and Huard, J. (2012) NF-κB negatively impacts the myogenic potential of muscle-derived stem cells. *Mol. Ther.* **20,** 661–668
35. Monici, M. C., Aguennouz, M., Mazzeo, A., Messina, C., and Vita, G. (2003) Activation of nuclear factor-κB in inflammatory myopathies and Duchenne muscular dystrophy. *Neurology* **60,** 993–997
36. Ridley, A. J. (2001) Rho GTPases and cell migration. *J. Cell Sci.* **114,** 2713–2722
37. McBeath, R., Pirone, D. M., Nelson, C. M., Bhadriraju, K., and Chen, C. S. (2004) Cell shape, cytoskeletal tension, and RhoA regulate stem cell lineage commitment. *Dev. Cell.* **6,** 483–495
38. Khatiwala, C. B., Kim, P. D., Peyton, S. R., and Putnam, A. J. (2009) ECM compliance regulates osteogenesis by influencing MAPK signaling downstream of RhoA and ROCK. *J. Bone. Miner. Res.* **24,** 886–898
39. Meyers, V. E., Zayzafoon, M., Douglas, J. T., and McDonald, J. M. (2005) RhoA and cytoskeletal disruption mediate reduced osteoblastogenesis and enhanced adipogenesis of human mesenchymal stem cells in modeled microgravity. *J. Bone Miner. Res.* **20,** 1858–1866
40. Wang, Y. K., Yu, X., Cohen, D. M., Wozniak, M. A., Yang, M. T., Gao, L., Eyckmans, J., and Chen, C. S. (2012) Bone morphogenetic protein-2-induced signaling and osteogenesis is regulated by cell shape, RhoA/ROCK, and cytoskeletal tension. *Stem Cells Dev.* **21,** 1176–1186
41. Fromigue, O., Hay, E., Modrowski, D., Bouvet, S., Jacquel, A., Auberger, P., and Marie, P. J. (2006) RhoA GTPase inactivation by statins induces osteosarcoma cell apoptosis by inhibiting p42/p44-MAPKs-Bcl-2 signaling independently of BMP-2 and cell differentiation. *Cell Death Differ.* **13,** 1845–1856
42. Hosoyama, T., Ishiguro, N., Yamanouchi, K., and Nishihara, M. (2009) Degenerative muscle fiber accelerates adipogenesis of intramuscular cells via RhoA signaling pathway. *Differentiation* **77,** 350–359
43. Santos, A., Bakker, A. D., de Blieck-Hogervorst, J. M., and Klein-Nulend, J. (2010) WNT5A induces osteogenic differentiation of human adipose stem cells via rho-associated kinase ROCK. *Cytotherapy* **12,** 924–932
44. Goto, K., Chiba, Y., Sakai, H., and Misawa, M. (2009) Tumor necrosis factor-alpha (TNF-alpha) induces upregulation of RhoA via NF-κB activation in cultured human bronchial smooth muscle cells. *J. Pharmacol. Sci.* **110,** 437–444
45. Slice, L. W., Bui, L., Mak, C., and Walsh, J. H. (2000) Differential regulation of COX-2 transcription by Ras- and Rho-family of GTPases. *Biochem. Biophys. Res. Commun.* **276,** 406–410
46. Nakayama, Y., Komuro, R., Yamamoto, A., Miyata, Y., Tanaka, M., Matsuda, M., Fukuhara, A., and Shimomura, I. (2009) RhoA

induces expression of inflammatory cytokine in adipocytes. *Biochem. Biophys. Res. Commun.* **379,** 288–292
47. Zhou, Y., Huang, X., Hecker, L., Kurundkar, D., Kurundkar, A., Liu, H., Jin, T. H., Desai, L., Bernard, K., and Thannickal, V. J. (2013) Inhibition of mechanosensitive signaling in myofibroblasts ameliorates experimental pulmonary fibrosis. *J. Clin. Invest.* **123,** 1096–1108
48. Zhou, H., Li, Y. J., Wang, M., Zhang, L. H., Guo, B. Y., Zhao, Z. S., Meng, F. L., Deng, Y. G., and Wang, R. Y. (2011) Involvement of RhoA/ROCK in myocardial fibrosis in a rat model of type 2 diabetes. *Acta Pharmacol. Sin.* **32,** 999–1008
49. Charrasse, S., Comunale, F., Grumbach, Y., Poulat, F., Blangy, A., and Gauthier-Rouviere, C. (2006) RhoA GTPase regulates M-cadherin activity and myoblast fusion. *Mol. Biol. Cell* **17,** 749–759
50. Castellani, L., Salvati, E., Alema, S., and Falcone, G. (2006) Fine regulation of RhoA and Rock is required for skeletal muscle differentiation. *J. Biol. Chem.* **281,** 15249–15257
51. Beqaj, S., Jakkaraju, S., Mattingly, R. R., Pan, D., and Schuger, L. (2002) High RhoA activity maintains the undifferentiated mesenchymal cell phenotype, whereas RhoA down-regulation by laminin-2 induces smooth muscle myogenesis. *J. Cell Biol.* **156,** 893–903
52. Gharaibeh, B., Lu, A., Tebbets, J., Zheng, B., Feduska, J., Crisan, M., Peault, B., Cummins, J., and Huard, J. (2008) Isolation of a slowly adhering cell fraction containing stem cells from murine skeletal muscle by the preplate technique. *Nat. Protoc.* **3,** 1501–1509
53. Thibaud, J. L., Monnet, A., Bertoldi, D., Barthelemy, I., Blot, S., and Carlier, P. G. (2007) Characterization of dystrophic muscle in golden retriever muscular dystrophy dogs by nuclear magnetic resonance imaging. *Neuromusc. Disord.* **17,** 575–584
54. Valentine, B. A., Cooper, B. J., Cummings, J. F., and de Lahunta, A. (1990) Canine X-linked muscular dystrophy: morphologic lesions. *J. Neurol. Sci.* **97,** 1–23
55. Greenberg, A. S., Coleman, R. A., Kraemer, F. B., McManaman, J. L., Obin, M. S., Puri, V., Yan, Q. W., Miyoshi, H., and Mashek, D. G. (2011) The role of lipid droplets in metabolic disease in rodents and humans. *J. Clin. Invest.* **121,** 2102–2110
56. Lounev, V. Y., Ramachandran, R., Wosczyna, M. N., Yamamoto, M., Maidment, A. D., Shore, E. M., Glaser, D. L., Goldhamer, D. J., and Kaplan, F. S. (2009) Identification of progenitor cells that contribute to heterotopic skeletogenesis. *J. Bone Joint Surg. Am.* **91,** 652–663
57. Arking, D. E., Krebsova, A., Macek, M., Sr., Macek, M., Jr., Arking, A., Mian, I. S., Fried, L., Hamosh, A., Dey, S., McIntosh, I., and Dietz, H. C. (2002) Association of human aging with a functional variant of klotho. *Proc. Natl. Acad. Sci. U. S. A.* **99,** 856–861
58. Salisbury, E., Rodenberg, E., Sonnet, C., Hipp, J., Gannon, F. H., Vadakkan, T. J., Dickinson, M. E., Olmsted-Davis, E. A., and Davis, A. R. (2011) Sensory nerve induced inflammation contributes to heterotopic ossification. *J. Cell. Biochem.* **112,** 2748–2758
59. Straus, D. S., and Glass, C. K. (2007) Anti-inflammatory actions of PPAR ligands: new insights on cellular and molecular mechanisms. *Trends Immunol.* **28,** 551–558
60. Holness, C. L., and Simmons, D. L. (1993) Molecular cloning of CD68, a human macrophage marker related to lysosomal glycoproteins. *Blood* **81,** 1607–1613
61. Amin, R. H., Mathews, S. T., Camp, H. S., Ding, L., and Leff, T. (2010) Selective activation of PPARgamma in skeletal muscle induces endogenous production of adiponectin and protects mice from diet-induced insulin resistance. *Am. J. Physiol. Endocrinol. Metab.* **298,** E28–E37
62. Ye, J. M., Doyle, P. J., Iglesias, M. A., Watson, D. G., Cooney, G. J., and Kraegen, E. W. (2001) Peroxisome proliferator-activated receptor (PPAR)-α activation lowers muscle lipids and improves insulin sensitivity in high fat-fed rats: comparison with PPAR-γ activation. *Diabetes* **50,** 411–417
63. Finsterer, J., and Stollberger, C. (2003) The heart in human dystrophinopathies. *Cardiology* **99,** 1–19
64. Lehman, J. J., and Kelly, D. P. (2002) Transcriptional activation of energy metabolic switches in the developing and hypertrophied heart. *Clin. Exp. Pharmacol. Physiol.* **29,** 339–345
65. Ahmad, N., Bygrave, M., De Zordo, T., Fenster, A., and Lee, T. Y. (2010) Detecting degenerative changes in myotonic murine models of Duchenne muscular dystrophy using high-frequency ultrasound. *J. Ultrasound. Med.* **29,** 367–375
66. Qu-Petersen, Z., Deasy, B., Jankowski, R., Ikezawa, M., Cummins, J., Pruchnic, R., Mytinger, J., Cao, B., Gates, C., Wernig, A., and Huard, J. (2002) Identification of a novel population of muscle stem cells in mice: potential for muscle regeneration. *J. Cell Biol.* **157,** 851–864
67. Smith, P. G., Roy, C., Zhang, Y. N., and Chauduri, S. (2003) Mechanical stress increases RhoA activation in airway smooth muscle cells. *Am. J. Respir. Cell Mol. Biol.* **28,** 436–442
68. Aghajanian, A., Wittchen, E. S., Campbell, S. L., and Burridge, K. (2009) Direct activation of RhoA by reactive oxygen species requires a redox-sensitive motif. *PLoS One* **4,** e8045
69. Bowerman, M., Beauvais, A., Anderson, C. L., and Kothary, R. (2010) Rho-kinase inactivation prolongs survival of an intermediate SMA mouse model. *Hum. Mol. Genet.* **19,** 1468–1478
70. Segain, J. P., Raingeard de la Bletiere, D., Sauzeau, V., Bourreille, A., Hilaret, G., Cario-Toumaniantz, C., Pacaud, P., Galmiche, J. P., and Loirand, G. (2003) Rho kinase blockade prevents inflammation via nuclear factor κB inhibition: evidence in Crohn's disease and experimental colitis. *Gastroenterology* **124,** 1180–1187
71. Ciaraldi, T. P., Cha, B. S., Park, K. S., Carter, L., Mudaliar, S. R., and Henry, R. R. (2002) Free fatty acid metabolism in human skeletal muscle is regulated by PPARγ and RXR agonists. *Ann. N. Y. Acad. Sci.* **967,** 66–70
72. Demer, L. L. (2002) Vascular calcification and osteoporosis: inflammatory responses to oxidized lipids. *Int. J. Epidemiol.* **31,** 737–741

Received for publication April 18, 2013.
Accepted for publication May 14, 2013.

The Role of Muscle Progenitor Cell Exhaustion in the Rapid Disease Progression Observed in Dystrophic *mdx/utrophin*$^{-/-}$ Mice

Progression of muscular dystrophy is associated with Muscle Progenitor Cell Exhaustion and over-activated mTOR signaling

Aiping Lu♣; Xiaodong Mu♣; Ying Tang; Minakshi Poddar; Jonathan D. Proto; Jihee Sohn; Nicholas Oyster; Koji Takayama; Bing Wang; Weiss Kurt; Johnny Huard*

Department of Orthopaedic Surgery, University of Pittsburgh, Pittsburgh, PA 15219, USA

*To whom correspondence should be addressed at: Department of Orthopaedic Surgery, University of Pittsburgh, Pittsburgh, Bridgeside Point 2, 450 Technology Dr. Pittsburgh, PA, 15219, USA. Tel: +1 412-648-2641; Fax: +1 412-648-4066; Email: jhuard@pitt.edu

♣ The first two authors contributed equally

The title has to be less than 15 words

Abstract

Duchenne muscular dystrophy (DMD) patients lack dystrophin at birth; however, muscle weakness does not occur until 4-8 years of age, which coincides with the exhaustion of the muscle progenitor cell (MPC) pool. In this study we tested if the decline in MPC function is associated with disease progression by utilizing two DMD murine models including: dystrophin/utrophin double Knock-Out (dKO) mice (severe phenotype) and dystrophin deficient *mdx* mice (mild phenotype). We found that MPCs isolated from dKO mice are defective in proliferation, oxidative stress resistance, and multilineage differentiation capacities when compared to age-matched *mdx* mice, indicating the rapid disease progression is strongly correlated to MPC exhaustion. Furthermore, we observed that dKO MPC exhaustion was associated with over-activated mTOR signaling and that prednisolone treatment repressed mTOR activity, which prevents the exhaustion of the MPC pool. These results suggest that the beneficial use of steroids is related, at least in part, to a delay in stem cell exhaustion for DMD patients.

158 words (has to be less than 150 words)

Introduction

Duchenne muscular dystrophy (DMD) is the most common form of muscular dystrophy which is caused by a deficiency of dystrophin. The loss of sarcolemmal dystrophin in DMD patients promotes muscle fiber damage during muscle contraction [1, 2, 3], and recurrent myofiber damage elicits a constant need for regeneration, thus giving way to the exhaustion of the muscle progenitor cell (MPC) pool and the loss of functional muscle regeneration. Eventually, muscle tissue is replaced by fibrotic tissue, calcium deposits, and adipose accumulation, which exacerbate the wasting process in DMD [4]. It is interesting to note that despite the lack of dystrophin at birth, the onset of muscle weakness in DMD patients does not occur until 4-8 years of age, which happens to coincide with the exhaustion of the MPC pool. Previous studies have shown that myoblasts in DMD patients are impaired and exhibit a severe proliferation deficit *in vitro* which becomes more pronounced with patient age [5, 6]. We believe that the exhaustion of the MPC pool during the progression of DMD represents a form of accelerated aging which may be the pathophysiological cause for the failure of the repair process to properly occur in the skeletal muscles. Normally, skeletal muscle possesses a robust regenerative capacity due to the presence of adult MPCs which play an important role in postnatal muscle growth and repair. Many MPC populations have been found which possess myogenic regenerative capacities in skeletal muscle; however, they are found in different locations within the muscle. Satellite cells are located between the basal lamina and muscle fiber plasma membrane [7] and were the first defined major source of MPCs that regulate postnatal skeletal muscle growth and regeneration [7, 8]; however, other myogenic progenitors, such as bone marrow-derived circulating stem cells and cell populations residing in the muscle interstitium and blood vessels have also been identified as potential cell populations for muscle repair [9, 10, 11]. These MPCs are capable of adopting a skeletal myogenic fate following engraftment into damaged or diseased muscle. Researchers have isolated MPCs utilizing a variety of different methods including cell culture selection techniques and flow cytometry-based sorting using cell surface markers or Hoechst dye exclusion [12, 13, 14]. Our research group has reported the isolation of muscle derived stem cells (MDSCs) via through the use of the preplate technique[15] which segregates cells based on their adhesion characteristics. MDSCs, which are found with the slow adhering fraction of cells, are capable of undergoing multilineage differentiation [14, 16, 17, 18] and have been shown to be superior to myoblasts for muscle regeneration [15]; moreover, they have also been isolated from Pax7

deficient mice [19], which suggests a distinct population from satellite cells. Myoblasts are more committed toward a myogenic lineage (late muscle progenitors) and readily fuse together or with injured mature myofibers to repair the injured muscle.

A major challenge for developing effective therapies for DMD is the lack of a small animal model that closely recapitulates the disease progression seen in humans. The *mdx* mouse is the most widely used animal model of DMD, and like DMD patients, the *mdx* mouse lacks only functional dystrophin due to a point mutation in the dystrophin gene [20, 21, 22]; however, these mice only exhibit a mild dystrophic phenotype when compared to DMD patients. Moreover, these mice often live up to 2 years of age, which is comparable to the life span of normal wild type (WT) mice. Furthermore, these *mdx* mice do not exhibit accelerating loss of muscle strength and early death observed in DMD patients[23, 24]. In addition, various features such as, pseudohypertrophy, scoliosis and cardiomyopathy, typical of DMD patients, are not observed in young *mdx* mice[25, 26, 27]. The data from many investigators have suggested that *mdx* mice compensate for the lack of dystrophin by increasing their expression of utrophin, a protein structurally related to dystrophin [28, 29, 30]. Utrophin localizes to the sarcolemma of skeletal muscle fibers during fetal development, but by birth, dystrophin replaces utrophin at the sarcolemma; however, utrophin persists at the neuromuscular and myotendinous junctions (NMJ and MTJ) under homeostatic conditions[31, 32]. It has been reported that high levels of utrophin are present around the sarcolemma of regenerating myofibers in adult *mdx* skeletal muscle and utrophin up-regulation may compensate for the dystrophin deficiency[29, 30, 33]. It is believed that the utrophin reserve the structural integrity of dystrophic muscle fibers, cause a delay in MPCs exhaustion. In support of this, reducing the telomerase activity in *mdx* MPCs, lead to a rapid exhaustion of MPCs and occurrence of pathophysiology of DMD[34]. Previous studies have reported that dystrophin and utrophin double-Knock Out (dKO) mice (*dystrophin*$^{-/-}$*/utrophin*$^{-/-}$) show many more of the clinical signs of DMD compared to *mdx* mice [35], however, it is not clear whether the progression of muscular dystrophy is due to MPC exhaustion in dKO mice.

Despite some extensive evidence for MPC exhaustion occurring in DMD patients as they age, the mechanism is unknown. The mammalian Target of Rapamycin (mTOR) is an anabolic pathway, and is essential for cell proliferation and tissue growth; however, hyper-function of mTOR has been revealed as a mediator of aging, and its inhibition with rapamycin has been shown to extend the longevity of several mouse disease models [36, 37, 38]. mTOR has also been

found to promote the exhaustion and senescence of stem cells [36, 39, 40]. Interestingly, a study has shown that rapamycin inactivated mTOR is able to ameliorate the dystrophic phenotype of *mdx* mice [41], suggesting that mTOR may play an important role in stem cell exhaustion in DMD. Hence, the inhibition of mTOR could be used as a potential therapeutic target for the treatment of muscular dystrophies.

The glucocorticoids have been suggested as standard medications for treating DMD patients for over the past two decade[42, 43]; however, the molecular mechanism underlying the beneficial effects steroids impart has not yet been fully elucidated, including the relationship between glucocorticoids and mTOR signaling. It has been demonstrated that mTOR signaling in normal skeletal muscle is responsive to glucocorticoids[44], and crosstalk between the glucocorticoid receptor and mTOR signaling in skeletal muscle is crucial for coordinating catabolic and anabolic metabolism [45]. Therefore, we suggest that the beneficial effects of glucocorticoids that have been observed in dystrophic muscle could be associated with the repression of the anabolic mTOR pathway.

In the present study, we tested the hypothesis that the rapid progression of the pathophysiology in dKO mice is associated with rapid muscle progenitor cell exhaustion, and compared this model to *mdx* mice in order to further investigate which model more closely recapitulated the disease progression seen in humans. The results demonstrated that dKO muscle is far more severely affected than the muscles of *mdx* mice, which includes the accumulation of necrotic myofibers, fibrosis, and calcium deposits within their skeletal muscle; moreover their life span is greatly reduced. Importantly, we show here that the severity of the phenotype in dKO mice progressively worsens with age and is associated with the exhaustion of MPCs including early and late myogenic progenitors (MDSCs, satellite cells and myoblasts). In addition, we also observed that mTOR was over-activated in both dKO muscle and MDSCs isolated from the muscle, which correlated to muscle stem cell exhaustion and cell senescence. These results suggest that over-activated mTOR promotes a decline in stem cell number and function and increases the occurrence of cellular senescence during disease progression. Furthermore, we demonstrated that prednisolone treatment not only reduced inflammation in dystrophic muscle, but also repressed mTOR activity which prevents the exhaustion of MPCs.

Results

Severe muscle histopathology in dKO mice

In order to assess the severity of muscular dystrophy in the dKO mice, we first characterized the histopathology that developed in the skeletal muscles of dKO mice (6-8 week old) which were compared to age-matched *mdx* and WT mice. H&E staining revealed little evidence of muscle regeneration (centrally nucleated fibers), large areas of necrotic myofibers, massive cellular infiltration, and the deposition of connective tissue within the dKO skeletal muscles when compared to age-matched WT and *mdx* mice (**Fig. 1a**). Mouse IgG positive muscle fibers, which indicate necrotic muscle fibers, were markedly increased in the dKO muscles compared to age-matched *mdx* and WT mice (**Fig. 1b**). Calcium deposition (**Fig. 1c**) and fibrosis (**Fig. 1d**) were substantially increased in the dKO muscles compared to age-matched WT and *mdx* mice. These results indicate that, in contrast to age-match WT and *mdx* mice, the dKO mice rapidly develop a muscle histopathological phenotype similar to DMD patients.

We also observed that dKO mice developed rapid muscle weakness, marked kyphosis, weight loss (**Fig. 1e**), and had a severely shortened lifespan (**Fig. 1f**) when compared to WT and *mdx* mice. To assess muscle performance, we measured the isometric torque of the anterior crural muscles and found that muscle function was significantly decreased in the dKO mice in contrast to age-matched WT and *mdx* mice (**Fig. 1g**). This result provides direct evidence for severe muscle weakness in the dKO muscles. In contrast, the function of the anterior crural muscles from *mdx* mice were greater than the muscles from the WT control mice, which is consistent with a previous study [46].

Muscle progenitor cells from dKO skeletal muscles are exhausted

To test whether the severe muscle damage seen in the dKO mice is associated with rapid MPC exhaustion, MPCs were isolated from the limb muscles of 6-8 week old dKO, *mdx*, and WT mice followed by flow cytometry analysis using antibodies against CD34, Sca-1, and CD45. The CD34+/Sca-1-/CD45- cells were classified as MPCs [47]. Our analysis revealed that the percentage of CD34+/Sca-1-/CD45- cells from dKO mice was significantly reduced (**Fig. 2a, 2b**), when compared to age-matched *mdx* muscle. The myogenic potential of the CD34+/Sca-1-/CD45- cell fractions were further tested for their ability to differentiate into myotubes (**Fig. 2c**).

Pax7 positive muscle satellite cells represent a population of MPCs responsible for postnatal growth, repair, and maintenance of skeletal muscle. We analyzed the Pax7 positive

cells in the diaphragm muscles of the dKO, WT and *mdx* mice in order to determine if the dKO's severe histopathological phenotype was related to a satellite cell defect. We observed that the number of Pax7 positive cells was significantly reduced in the diaphragm muscles of dKO mice (**Fig. 2d**, **2e**) compared to the *mdx* and WT mice. Moreover, the results from real-time PCR confirmed that there was a rapid, significant decline in Pax7 mRNA expression in the diaphragm muscles of dKO mice isolated from 4 to 8 week old mice in contrast to that observed in the *mdx* and WT diaphragm muscles (**Fig. 2f**). These results demonstrate that myogenic progenitor cells undergo a rapid decline in the skeletal muscles of dKO mice during the rapid progression of the disease, which probably contributes to the severe dystrophic phenotype observed in these mice.

Impaired proliferation and differentiation capacity of MPCs isolated from dKO single muscle fibers

To further determine whether the progression of muscular dystrophy in dKO mice is caused by a reduction MPC proliferation and differentiation potentials, we assessed the myogenic potential of MPCs derived from single isolated muscle fibers. First, we observed more damaged muscle fibers in the dKO muscles (53%±12%) compared to the *mdx* muscles (34%±8%) 24 hours after the single fibers attached to the matri-gel coated plates (**Fig. 3a**). The proliferative potential of the MPCs migrating from the isolated myofibers were analyzed after 4 days in culture. The MPCs were immunostained for desmin and the result reveal that the number of desmin positive cells from the single fibers was significantly decreased in the dKO mice compared to the *mdx* mice (**Fig. 3b, 3c**), indicating that the MPCs derived from the single myofibers of dKO muscle exhibited a reduced proliferative potential compared to the *mdx* MPCs. In addition, 7 days post-culturing, immunostaining for fast myosin heavy chain (MyHCf), a terminal myogenic differentiation marker, was performed to determine the myogenic differentiation capacity of the MPCs. We observed that the MPCs released from the *mdx* muscle fibers formed more MyHCf+ multinucleated myotubes in contrast to those migrating from the dKO muscle fibers (**Fig. 3d, 3e, 3f**). These results support both a reduction in the proliferation and differentiation potentials of the MPCs derived from the dKO mice and provides more evidence to suggest that the defective proliferation and differentiation capacities of MPCs in dKO mice leads to a reduction in muscle repair, similar to what is seen in DMD patients [5].

The function of myoblasts is impaired in dKO mice

Next, we asked whether myoblast dysfunction can also be observed in dKO mice. We isolated MPCs including myoblasts from 6 week old WT, *mdx* and dKO mice using the preplate technique as previously described and observed that the number of preplate population 5 and 6 (PP5, PP6) isolated from the dKO muscle, which contain mostly muscle stem cells [15, 48], were decreased (**Fig. 4a**). We further tested the rapidly adhering cell populations (PP3 and PP4), which contain mostly satellite cell and myoblasts [15, 48], for their differentiation capacity *in vitro* and found that the rapidly adhering cells isolated from the WT and *mdx* mice formed numerous, large multi-nucleated myotubes while the cells isolated from the dKO mice formed fewer and smaller myotubes (**Fig. 4b**). This finding indicated that the myogenic differentiation potential of the dKO myoblasts was significantly reduced relative to the myoblasts isolated from the *mdx* and WT mice ($P<0.05$) (**Fig. 4c**). This result demonstrated that myoblasts isolated from dKO mice are also impaired in their differentiation capacity, which is similar to what is observed in myoblasts isolated from DMD patients.

Muscle derived stem/progenitor cells isolated from dKO mice are functionally defective

We next assessed the slowly adhering cell populations of cells isolated from 6-8 week old dKO, *mdx*, and WT mice, which contains the MDSCs [15, 19], and examined their functionality by measuring relative differences in their capacities for proliferation, myogenic differentiation, resistance to oxidative stress, and multilineage differentiation capacities. We examined the proliferation kinetics of the cell populations *in vitro* using the LCI system described above [49] and observed a significant reduction in the proliferation capacity of the dKO MDSCs when compared to the *mdx* and WT MDSCs (**Fig. 5a**). In order to determine the myogenic differentiation capacity of the MDSCs isolated from the dKO, *mdx* and WT mice *in vitro*, equal numbers of cells from each group were plated in a 24-well plate and switched to differentiation medium once the cells adhered. After 3 days, the majority of the WT (72%) and *mdx* cells (80%) had differentiated into myotubes, as determined by immunodetection of MyHCf (**Fig. 5b**). The differentiation potential of the dKO MDSCs was observed to be significantly lower (38%), compared to the WT and *mdx* MDSCs ($P < 0.01$; **Fig. 5c)**. Next, we examined the cells' resistance to hydrogen peroxide (400μM) induced oxidative stress. In comparison with MDSCs isolated from the *mdx* and WT mice, the dKO MDSCs displayed a reduced resistance to oxidative stress (**Fig. 5d**). Furthermore, the ability of the MDSCs to undergo multi-lineage differentiation was examined, and the results indicated that there was a reduction in the

adipogenic, osteogenic, and chondrogenic differentiation capacities of the MDSCs isolated from the dKO mice compared to the MDSCs isolated from the *mdx* and WT mice (**Fig. 5e**). Together, these data suggest that the functionality of the dKO MDSCs are defective when compared to WT and *mdx* mice.

Impaired muscle regeneration in dKO mice

In vivo muscle regeneration and inflammation were next determined by assessing embryonic myosin heavy chain (eMyHC) and F4/80 (macrophage marker) expression in young and old dKO muscle. eMyHC is expressed almost exclusively in newly regenerated muscle fibers, which is expressed following acute muscle injury or damage caused by inflammation. Normally in dystrophic muscle, eMyHC positive fibers are surrounded by F4/80 positive macrophages, during muscle regeneration. The gastrocnemius muscle sections from young (4 week old) and old (6-8 week old) dKO mice were examined for eMyHC and F4/80 expression. Our results revealed that the number of eMyHC positive fibers significantly declined in the dKO muscles from 4 to 8 weeks (**Fig. 6a, 6b**), but macrophage infiltration increased with age and correlated with the progression of the disease state (**Fig. 6a, 6c**). Meanwhile, to further confirm this observation, real-time PCR for F4/80 and eMyHC from 6-8 week old dKO mice was performed. In support of the immunohistochemical findings, the level of inflammation (F4/80 positive macrophage infiltration) increased, whereas muscle regeneration (eMyHC positive fibers) decreased from 6-8 weeks. These data indicate that the dKO mice display a reducing ability to regenerate myofibers.

Excessive mTOR activation and stem cell senescence observed in dKO mice

The above data provides strong evidence suggesting that the progression of muscular dystrophy in dKO mice is associated with rapid muscle progenitor cell exhaustion; however, the mechanism responsible for stem cells exhaustion is still unclear. Studies have demonstrated that mTOR is a major contributor to stem cell exhaustion and senescence during aging[36, 39, 40] and we next investigate whether mTOR was involved in the exhaustion of the MPC pool during the progression of muscular dystrophy in the dKO mice. It has been reported that higher amounts of the p-4E-BP1 protein (mTOR downstream target) in the muscle cells reflect higher activities of mTOR signaling[50]. Therefore, we examined p-4E-BP1 and p-mTOR expression in MDSCs populations isolated from WT, *mdx* and dKO mice. Immunostaining for p-4E-BP1 showed that the percentage of p-4E-BP1 positive cells was significantly higher in dKO MDSCs in contrast to

WT and *mdx* MDSCs (**Fig. 7a, 7b**). Meanwhile, a cell senescence assay showed that very few senescent cells (β-galactosidase/β-gal+) were found in the WT MDCSs and *mdx* MDSCs in contrast to dKO MDSCs (**Fig. 7a, 7c**). These observations suggest that over-activation of mTOR in the dKO MDSCs may have caused uncontrolled and accelerated proliferation of the cells, which could have resulted in the premature cell senescence. We also examined p-4E-BP1 expression in the gastrocnemius (GM) muscles and found this protein is highly expressed in dKO skeletal muscle (**Fig. 7d, 7e**), which was accompanied by increased numbers of necrotic myofibers compared to either WT or *mdx* muscle. Similarly, there were more cells positive with p-mTOR in the dKO skeletal muscle, compared to that of WT and mdx mice (**Fig. 7d, 7f**). A cell senescence assay was also conducted on the GM muscles and the presence of β-gal+ senescent cells was only observed in dKO skeletal muscle (**Fig. 7d, 7g)**. Furthermore, many Pax7 expressing satellite cells in the GM muscles of 4-week old dKO mice were also positive for mTOR expression (**Fig. 7h**), suggesting that accelerated proliferation of satellite cells occurred early in dKO mice. In order to confirm our findings, semi-quantitative PCR was performed. The results revealed that the expressions of TNF-α and mTORC1 were up-regulated in the skeletal muscles of the 8-week old dKO mice, while the expression of Pax7 was down-regulated (**Fig. 7i, 7j)** . The up-regulated expression of TNF-α reflects an elevated inflammatory reaction in the skeletal muscle of dKO mice, which may contribute to the histopathological sign seen in the dKO mice. Together, these results indicate that mTOR signaling is a contributor of MPC exhaustion during the rapid disease progression of muscular dystrophy observed in dKO mice.

Prednisolone administration repressed mTOR activity and improved histopathology in dKO mice

Glucocorticoid corticosteroids have been demonstrated as effective medications for treating DMD patients, however, except for the anti-inflammation effect[51], little is understood about the molecular mechanism(s) underlying the beneficial effects steroids impart. To assess the effect that glucocorticoids have on mTOR activity, we carried out prednisolone administration on dKO mice and MDSCs isolated from 6-week old dKO mice. Prednisolone treated dKO MDSCs showed a significantly decreased number of p-4E-BP1+ and β-gal+ senescent cells compared to the untreated dKO MDSCs (**Fig. 8a, 8b, 8c**). Next we treated dKO mice with prednisolone via intraperitoneal injection. We observed that p-4E-BP1+ cells, necrotic myofibers (**Fig. 8d**, **8e**), CD68+ inflammatory cells (**Fig. 8d, 8f**), and β-gal+ senescent cells (**Fig. 8d, 8g**) were all

significantly decreased in the GM's of the dKO mice with prednisolone treatment; however, the number of Pax7+ cells was increased (**Fig. 8d, 8h**). Also, mRNA expression of TNF-α and mTOR were found down-regulated, while the expression of Pax7 was up-regulated with prednisolone treatment (**Fig. 8i, 8j**). The effects of glucocorticoids on TNF-α expression and anti-inflammation are consistent with previous findings[51]. These results suggest that prednisolone treatment not only reduced inflammation, but also repressed mTOR activity which prevented the exhaustion of the muscle stem cell pool.

Discussion

In order to investigate whether the progression of muscular dystrophy is due to MPC exhaustion in DMD patients, an animal model that closely recapitulates the disease progression seen in humans is required. The most commonly utilized model of DMD is the dystrophin deficient *mdx* mouse; however, it has a relatively mild dystrophic phenotype [52]. Helen Blau' group has recently reported that the mild mouse *mdx* phenotype results from greater MPC reserve fueled by longer telomeres[34]. They generated *mdx* mice lacking telomerase activity (mdx/mTR) and show that dystrophin deficiency coupled with telomere dysfunction recapitulates the severe phenotypic characteristics of muscular dystrophy in humans with the progressive exhaustion of functional MPCs. It is also believed that *mdx* mice compensate for the lack of dystrophin through the up-regulation of other proteins including MyoD and the structurally related protein utrophin [53]. In this study we demonstrated that the dystrophin/utrophin double knock-out mice more closely recapitulates the DMD phenotype than the *mdx* model as evidenced by their severe, progressive loss of muscle function. Histopathological analysis of dKO muscle sections show many of the characteristic features described in DMD biopsies, including variations in muscle fiber size, infiltration of inflammatory cells, presence of necrotic fibers, calcium deposits, replacement of functional tissue with fibrotic tissue. Many of the features seen in the dKO mice such as marked myopathy, joint contractures, kyphosis, loss of body weight and muscle function, as well as premature death are all similar to what is observed in DMD patients. This is similar to what is seen in mdx/mTR mice; however, these mice have a much longer lifespan than the dKO model[34]. Indeed, we also found that the telomerase activity in dKO MDSCs was significantly reduced, when compared to MDSCs isolated from age matched WT and *mdx* mice (data not shown). As utrophin has been knocked out in this animal model, the genotype is not the same as that found in DMD, which only lacks dystrophin, yet the dKO mice show all of the clinical features of DMD. In addition, studies have shown that the utrophin deficient mice are healthy and show no signs of weakness, living up to 2 years of age [54]. This can rule out other possible abnormalities caused by utrophin deficiency.

We have proposed that the severe muscle wasting phenotype observed in this dKO mouse model is due to the impaired function of the MPC pool. Here we determined, both *in vitro* and *in vivo,* that MPCs, including satellite cells, early myogenic progenitors (MDSCs), and myoblasts from aged dKO mice, are defective in their functionality. *In vivo* we confirmed that there is a

rapid decline of satellite cells during disease progression in dKO mouse muscles from 4 to 8 weeks of age in contrast to that observed in *mdx* skeletal muscle. *In vitro*, the proliferation and differentiation defects were marked by a reduction in the number of satellite cells capable of being derived from dKO single muscle fibers, and also a reduction in the formation of MyHCf positive myotubes in culture. MDSCs display unique characteristics that are associated with non-committed progenitor cells. We have previously shown that MDSCs express markers associated with stem cells and are capable of self-renewal *in vitro* [15]. Furthermore, MDSCs have been shown to be capable of replenishing myogenic progenitors when injected into dystrophic murine muscle and contribute to the persistent restoration of dystrophin within the transplanted muscles [15, 55]. In this study, we show that MDSCs isolated from dKO mice also exhibited deficiencies in their proliferation and differentiation capacities including deficiencies in their myogenic, adipogenic, osteogenic and chondrogenic differentiation capacities, and a reduction in their oxidative stress resistance. These data obtained from the dKO mouse model differ from the data obtained from the mdx/mTRG2 mouse model which show no alterations in satellite cell number per myofiber at 8 weeks of age [34], but demonstrate a markedly reduced number of satellite cells when the mice reach 60 weeks of age, indicating that MPC exhaustion appears at a much earlier age in the dKO mice. Further *in vivo* histological analysis revealed that the amount of inflammatory infiltration was substantially increased in the muscles of the dKO mice from 4 to 8 weeks of age, while the number of newly regenerated muscle fibers was significantly reduced, indicating an inability of the muscle to appropriately respond to injury. Importantly, unlike the *mdx* mice, but similar to DMD patients, we observed a large amount of variability between the dKO mice; however, the occurrence of severe muscle histopathology in the dKO mice was always associated with the exhaustion of the MPC pool. When taken together this study demonstrated, both *in vitro* and *in vivo,* that MPCs isolated from dKO mice suffer from severe functional defects and that the progressive loss of MPCs plays a major role in determining the severity of the dystrophic phenotype. Indeed, the concept of stem cell exhaustion as a potential cause for the rapid progression of muscle weakness in DMD has been recently reported[5]. Thus we believe that the dKO model represents an excellent murine model of muscle stem cell exhaustion, allowing for the study of potential therapies to treat DMD patients.

Interestingly, we observed that the percentages of Sca-1 and PDGFRα positive mesenchymal interstitial cells were significantly higher in aged dKO muscle compared to WT

and *mdx* muscle (data not shown), suggesting that their severe dystrophic phenotype is muscle specific and not the result of a functional defect in other cell types. Moreover, the increase in muscle-derived mesenchymal stem cells within the skeletal muscle of the dKO mice may be responsible for the heterotopic ossification and ectopic fat formation observed in the dystrophic muscle of dKO mice. There are several reports to support our hypothesis showing that mesenchymal progenitor cells are a major contributor of ectopic fat cell formation [56] in skeletal muscle and are a predominant source of progenitors that drive heterotopic ossification in this mouse model [57]; however further investigation is required.

The mechanisms that may contribute to the severe phenotype observed in the dKO mice which are associated with muscle progenitor cell exhaustion are unknown. mTOR controls protein synthesis in muscle [58], and is a key molecule for regulating cellular energy metabolism [59, 60, 61]. However, many studies have shown that over-activation of mTOR mediates aging and senescence of various types of stem cells, and that the inactivation of mTOR with rapamycin is effective for delaying stem cell exhaustion and senescence; hence, extending the life span of animal models of various diseases [36, 37, 39]. Interestingly, mTOR activity has recently been shown to be associated with muscular dystrophy and its inactivation with rapamycin was shown to ameliorate the dystrophic phenotype exhibited by *mdx* mice [41]. In our current study, we found over-activated mTOR signaling in both MDSCs isolated from dKO muscle and the skeletal muscle of dKO mice, which exhibits severe stem cell exhaustion and senescence, however over-activated mTOR was not found in *mdx* nor WT mice in either their MDSCs or skeletal muscles. These results suggest that mTOR may contribute to the rapid muscle stem cell exhaustion observed in the dKO model. Strategies to repress mTOR signaling may therefore reduce stem cell loss during aging and disease progression.

It is well-established that glucocorticoids, such as prednisolone, are effective at reducing inflammation and delaying disease progression in DMD patients [62]; however, little is known about their cellular and molecular regulatory mechanism(s). A previous study has shown that the treatment of *mdx* mice with anabolic steroids increased muscle damage in their muscles [63], suggesting a potentially beneficial effect of inhibiting anabolic factors in dystrophic muscle. In contrast to anabolic factors like mTOR [64] and anabolic steroids [63], glucocorticoids are catabolic steroids, which have been shown to repress mTOR signaling in skeletal muscle [45]. Based on the previously observed crosstalk that exists between glucocorticoid and mTOR signaling [45], we

postulated that prednisolone treatment could rescue dKO mice from stem cell exhaustion by repressing mTOR activation. In this study, we provided evidence that strongly supported our hypothesis. Here we showed that prednisolone treatment not only decreased inflammation, necrosis and cell senescence, but also increased the number of Pax7 positive satellite cells, all of which correlated with the inhibition of mTOR activation. This data suggests that muscle atrophy in the dKO mice could be the result of mTOR-mediated stem cell deficiency, and the replenished Pax7+ satellite cell pool in the dystrophic muscle after prednisolone treatment could therefore be the result of decreased mTOR activation. However, despite the increased number of muscle stem cells present after prednisolone treatment, the numbers of embryonic MyHC+ and MyoD+ cells in the GM muscles were not increased (data not shown). These observations indicate that although there was enrichment in the number of satellite cells, their activation is inhibited by prednisolone which has been reported[65]. Therefore, we suggest that improved glucocorticoid therapies for treating DMD would be desirable in combination with enhancing muscle satellite cell activation.

In summary, we provided evidence that the severe progression of the muscle pathology observed in dKO mice, a mouse model that recapitulates the disease progression seen in human DMD patients, is the consequence of a loss of functional muscle stem cells. We also found that the rapid exhaustion of the MPC pool is related to the over activation of mTOR signaling, and more importantly, that the administration of prednisolone proved to be effective at preventing the exhaustion of the MPC pool by repressing mTOR activation. Therapeutic interventions should consider both mTOR activity as well as cell source for potential myogenic regeneration. Together, these data provide strong experimental evidence that the rapid disease progression in DMD is associated with stem cell exhaustion, which is driven by dystrophin deficiency.

should<5000 words

Materials and methods

Animals

dKO mice are generated by crossing (utr+/−, dys−/−) mice, which have been obtained by crossing utr−/− mice with *mdx* mice in our lab[26, 66]. Wild type mice (WT, C57BL/10J) were ordered from Jackson Laboratories. All animal protocols used for these experiments were approved by the University of Pittsburgh's Animal Care and Use Committee.

Isolation of MDSCs

The mice were sacrificed at 6-8 weeks of age and MDSC isolation was performed as previously described via a modified preplate technique[67, 68]. Briefly, the skeletal muscle tissue was minced and processed through a series of enzymatic dissociations: 0.2% of collagenase type XI (Sigma-Aldrich) for 1 hour, 2.4 units/ml of dispase (Invitrogen) for 45 minutes, and 0.1% of trypsin-EDTA (Invitrogen) for 30 minutes at 37°C. After enzymatic dissociation, the muscle cells were centrifuged and resuspended in proliferation medium (Dulbecco's modified Eagle's medium (DMEM, Invitrogen) supplemented with 10% fetal bovine serum (FBS, Invitrogen), 10% horse serum (HS, Invitrogen), 0.5% chicken embryo extract (CEE, Accurate Chemical Co.) and 1% penicillin-streptomycin (Invitrogen). The cells were then plated in collagen type I (Sigma-Aldrich) coated flasks. Different populations of muscle-derived cells were isolated based on their variable adhesion characteristics. After 7 days, late preplate populations (slow-adhering cells) were obtained and cultured in proliferation medium, which have previously been described to contain the MDSC fraction of cells [15].

Immunostaining flow cytometry and cell sorting analyses

Fluorescence-activated cell sorting (FACS Aria II SORP; BD) was used to analyze the expression of CD34, Sca-1 (stem cell antigen-1) and CD45. The mice were sacrificed at 6-8 weeks of age and muscle cell isolation was performed as previously described via a modified preplate technique [67, 68]. After enzymatic dissociation, the muscle cells were centrifuged and resuspended in proliferation medium, the cells were then plated in collagen type I coated flasks. After 24 hours, the floating cells were collected, which contain the myogenic progenitor cells, centrifuged, washed with PBS containing 2% FBS and counted. The cell suspension was divided into equal aliquots and centrifuged, and then placed on ice and resuspended in a 1:10 dilution of mouse serum (Sigma-Aldrich) in phosphate-buffered saline (PBS). The suspensions were incubated for 10 min. FITC-conjugated rat anti-mouse CD34 (BD), PE-conjugated rat anti-

mouse Sca-1(BD) and APC-conjugated rat anti-mouse CD45 (Invitrogen) were added to each tube and incubated for 30min. Just before analysis, propidium iodide (PI, BD) was added to each tube for dead cell exclusion and live cell events were collected and analyzed. CD34+/Sca-1-/CD45- cells were sorted after analysis. Single color of antibody was used to optimize fluorescence compensation settings for multi-color analyses and sorts.

Single fiber isolation

Mice were sacrificed at 6-8 weeks of age and the extensor digitorum longus (EDL) muscles were isolated from dKO and *mdx* mice and incubated in a solution of 0.2% collagenase type I (Sigma-Aldrich) for 50 minutes at 37°C while shaking the mixture at 40rpm. When the muscles were sufficiently digested they were triturated with heat polished glass pipettes to liberate single fibers. The muscle fibers were then transferred to a matri-gel (Fisher) coated 24 well plate with proliferation medium.

In vitro assessment of cell proliferation

In order to compare the proliferative potential of the dKO MDSCs to WT and *mdx* MDSCs, we used a previously described Live Cell Imaging system (Kairos Instruments LLC)[49, 69]. Bright field images were taken at 100× magnification at 10min intervals over a 72-hour period in three fields of view per well, with three wells per population. Proliferation was assessed by manually counting the number of cells per field of view over 60 hours.

Myogenic differentiation assay and fast myosin heavy chain staining

The cells were plated on 24 well plates (30,000 cells/well) with DMEM supplemented with 2% FBS to stimulate myotube formation. Three days after plating, immunocytochemical staining for fast myosin heavy chain (MyHCf) was performed. After rinsing two times with PBS, cells were fixed for 2 minutes in cold methanol (-20°C), blocked with 10% horse serum (Vector) for 1 hour and then incubated with a mouse anti-MyHCf (1:250; Sigma-Aldrich) antibody for 2 hours at RT. The primary antibody was detected with a 594-conjugated anti-mouse IgG antibody (1:500; Molecular probes) for 30 minutes. The nuclei were revealed by 4, 6-diamidino-2- phenylindole (DAPI, 100ng/ml, Sigma-Aldrich) counter staining. The percentage of differentiated myotubes was quantified as the number of nuclei in MyHCf positive myotubes relative to the total number of nuclei. This method was also used for analyzing myotube formation from single muscle fibers.

Survival analysis of MDSCs

Cells were exposed to oxidative stress by treating them with 400uM hydrogen peroxide. In order to visualize cell death, propidium iodide (PI), a DNA-binding dye, was added to the culture medium according to manufacturer's protocol (BD Bioscience). Using the LCI system described above, 100x bright field and fluorescence images were taken at 10 minute intervals over 24 hours. Identifying the number of PI+ cells per field of view out of the total cell number determined the percentage of cell death over time.

Cell senescence assay:

A cell senescence assay was performed on MDSCs and muscle tissues and was conducted with a Senescence β-Galactosidase (β-gal) Staining Kit (Cell Signaling Technology) following the manufacturer's protocol. The number of cells positive for β-gal activity at pH6, a known characteristic of senescent cells, but not found in pre-senescent, quiescent, or immortal cells, was determined.

Immunocytochemistry:

MPCs migrating off from the single myofibers were stained for the myogenic marker desmin at 96 hours after the single fibers attached to the matri-gel coated 24-well plates. The myofibers and cells were fixed in 5% formalin for 5min and blocked with 10% donkey serum (Jackson ImmunoResearch) in PBS for 1 hour at room temperature (RT). Rabbit anti-desmin (1:200; Sigma-Aldrich) was incubated for 3 hours at RT, followed by PBS washes and incubation with a secondary antibody, donkey anti rabbit IgG conjugated with Alexa Fluor 488 (1:500, Molecular probes) for 30min. mTOR activity in the MDSCs was measured by staining for phosphorylated 4E-binding protein 1 (p-4E-BP1), a mTOR downstream target. The MDSCs were formalin fixed, blocked with serum, and incubated with rabbit anti-p-4E-BP1 (1:200, Cell Signaling Technology) for 2 hours at RT, followed by incubation with goat anti-rabbit IgG Alexa Fluor 594 (1:500, Invitrogen). Nuclei were revealed with DAPI staining. Following staining, the total number of p-4E-BP1 and desmin positive cells derived from each of the analyzed fibers was counted manually.

Immunohistochemistry

Muscle samples were frozen in 2-methylbutane pre-cooled in liquid nitrogen and stored at –80°C. Ten micrometer cryosections from the gastrocnemius and diaphragm were fixed in a 1:1 cold (–20°C) acetone/methanol mixture for 5min and blocked with 10% donkey serum (Jackson ImmunoResearch) for 1 hour at RT. Primary antibodies including rat anti-F4/80 (1:500;

Secrotec), rabbit anti-p-4E-BP1 (1:200, Cell Signaling Technology), rabbit anti-p-mTOR (1:200, Cell Signaling Technology), rat anti-CD68 (1:200, Abcam), rabbit anti-Collagen IV (1:200, Abcam) and biotinglated anti mouse IgG (1:300; Vector,) were incubated for 3 hours at RT. Secondary antibodies followed by incubating with 594-conjugated donkey anti-rat or anti-rabbit IgG (1:500; Molecular probes), and 594-conjugated streptavidin (1:500; Molecular probes) for 30 min at RT. A MOM kit (Vector, Inc.) was used for Pax7 and embryonic myosin heavy chain (eMyHC) staining following the manufacturers protocol. Pax7 (1:100, Developmental Studies Hybridoma Bank) and eMyHC (1:50; Developmental Studies Hybridoma Bank) were used as primary antibodies, the Cy3-streptavidin (1:500, Sigma-Aldrich) was added for detecting Pax7 and eMyHC, and the nuclei were stained with DAPI. All the stained sections were visualized on a Nikon Eclipse E800 fluorescence microscope. Ten random pictures per slide were taken and the number of Pax7+, p-mTOR+, CD68+ cells and eMyHC+ myofibers were counted manually. The F4/80+ and p-4E-BP1 areas were measured and quantified as the percentage of F4/80+ macrophage infiltration area per image using Northern Eclipse software.

Adipogenesis assay

A total of 60,000 MDSCs were cultured on 24 well collagen type I coated plates for 21 days in adipogenic differentiation medium (Lonza). At 100% confluence, 3 cycles of induction/maintenance stimulated optimal adipogenic differentiation. Each cycle consisted of feeding the MDSCs with supplemented adipogenesis induction medium and cultured for 3 days followed by 1-3 days of culture in supplemented adipogenic maintenance medium. Then, MDSCs were tested for adipogenesis with AdipoRed reagent (30ul/ml, Fisher) following the manufacturer's protocols.

Osteogenesis assay

A total of 50,000 cells were cultured in osteogenic medium (OM: control medium supplemented with dexamethasone (0.1 μM, Sigma-Aldrich), abscorbic-acid-2-phosphate (50 μg/ml, Sigma-Aldrich), 10mM B-glycerophosphate (BMP2, 100ng/ml, Sigma-Aldrich). Cells were stained for calcium deposition (Alizarin Red) after 7 and 10 days of culture, respectively.

Chondrogenesis assay

MDSCs were centrifuged into pellets (250,000 cells/pellet) and cultured for 4 weeks in chondrogenic induction media (200ul/pellet, Lonza) supplemented with 100ng/ml BMP2 and 20ng/ml TGFβ3 (Invitrogen). Pellets were frozen in embedding medium and cryosectioned. The

sections were then stained with alcian blue to confirm chondrogenesis. To further confirm that the pellets chondrogenecity, a GAG assay was performed to verify the presence of proteoglycans.

Reverse Transcriptase-PCR and Real-time PCR

Total RNA was obtained from MDSCs or the skeletal muscles of mice using the RNeasy Mini Kit (Qiagen, Inc., Valencia, CA) according to the manufacturer's instructions. Reverse transcription was performed using the iScript cDNA Synthesis Kit (Bio-Rad Laboratories, Inc., Hercules, CA). The sequences of primers are given in Table 1, including: mTORC1, TNF-α, Pax7, and GAPDH (glyceraldehydes 3-phosphate dehydrogenase). PCR reactions were performed using an iCycler Thermal Cycler (Bio-Rad Laboratories, Inc.). The cycling parameters used for all primers were as follows: 95°C for 10 minutes; PCR, 40 cycles of 30 seconds at 95°C for denaturation, 1 minute at 52-55°C for annealing, and 30 seconds at 72°C for extension. Products were separated by size, and visualized on a 1.5% agarose gel stained with ethidium bromide. All data were normalized to the expression of GAPDH. For real-time PCR, the total RNA was isolated using TRizol Reagent (Invitrogen) and reverse transcribed using a Maxima first strand cDNA synthesis kit (Fermentas) according to the manufacturer's protocol. Real-time PCR was carried out using the Maxima SYBR® Green Assay kit (Fermentas) with an iQ5 thermocycler (Biorad). Primers were designed using PRIMER-Blast (NCBI) and can be found in Table 1.

Prednisolone treatment in vitro and in vivo

MDSCs from 6-week old dKO mice were cultured in the presence of prednisolone (Sigma, St Louis, MO) (10μg/ml) [70, 71] for 7 days. Cells cultured without prednisolone served as controls. Prednisolone treatment of the cells was refreshed every 2 days by changing the medium (PM). dKO MDSCs were then fixed and analyzed for their expression of p-4E-BP1, β-gal, and LC3. For in vivo treatment, prednisolone was solved in PBS (1.6mg/mL) [72] and injected intraperitoneally (1mg/kg) into dKO mice from 3-weeks of age, 3 times per week. The dKO mice receiving an equal amount of PBS served as the controls. IP injection of prednisolone was continued until the mice reached 8-weeks of age, or the end of their lifespan.

Histochemistry

H&E, alizarin red and trichrome staining were performed according to the manufacturer's instructions.

Skeletal muscle functional measurements

Animals were anesthetized with 2-3% isoflurane and maintained in a surgical plane during the procedure with 1.5% isoflurane. The lower hind limbs were shaved and the animal was placed on an *in situ* muscle physiology test apparatus (Model 806-B, Aurora Scientific) with only the right hind limb being tested. The animal was laid in a supine position and the foot was secured to the force plate with adhesive tape. The knee was positioned and secured at 90 degrees of flexion and the ankle was at 0 degrees of flexion. Twenty-seven gauge needle electrodes were placed intramuscularly into the tibialis anterior. Force-frequency curves were generated by stimulating the muscles with 9 volts at varying frequencies from 1Hz up to 200Hz with a 2 minute rest between each of the frequency stimulations. Data were recorded and analyzed with DMC software (Aurora Scientific).

Statistical analysis

All results are given as the mean ± standard deviation (SD). Means from dKO, *mdx* or WT were compared using Student's *t*-test. Differences were considered statistically significant when the *P* value was < 0.05.

2000 words (Should<3000 words)

References

1. Koenig M, Kunkel LM. Detailed analysis of the repeat domain of dystrophin reveals four potential hinge segments that may confer flexibility. *J Biol Chem* **265**, 4560-4566 (1990).

2. Miranda AF*, et al.* Dystrophin immunocytochemistry in muscle culture: detection of a carrier of Duchenne muscular dystrophy. *Am J Med Genet* **32**, 268-273 (1989).

3. Lapidos KA, Kakkar R, McNally EM. The dystrophin glycoprotein complex: signaling strength and integrity for the sarcolemma. *Circ Res* **94**, 1023-1031 (2004).

4. McLoon LK. Focusing on fibrosis: halofuginone-induced functional improvement in the mdx mouse model of Duchenne muscular dystrophy. *Am J Physiol Heart Circ Physiol* **294**, H1505-1507 (2008).

5. Blau HM, Webster C, Pavlath GK. Defective myoblasts identified in Duchenne muscular dystrophy. *Proc Natl Acad Sci U S A* **80**, 4856-4860 (1983).

6. Webster C, Blau HM. Accelerated age-related decline in replicative life-span of Duchenne muscular dystrophy myoblasts: implications for cell and gene therapy. *Somatic cell and molecular genetics* **16**, 557-565 (1990).

7. Mauro A. Satellite cell of skeletal muscle fibers. *The Journal of biophysical and biochemical cytology* **9**, 493-495 (1961).

8. Zammit PS*, et al.* Pax7 and myogenic progression in skeletal muscle satellite cells. *Journal of cell science* **119**, 1824-1832 (2006).

9. Dellavalle A*, et al.* Pericytes of human skeletal muscle are myogenic precursors distinct from satellite cells. *Nat Cell Biol* **9**, 255-267 (2007).

10. Mitchell KJ*, et al.* Identification and characterization of a non-satellite cell muscle resident progenitor during postnatal development. *Nat Cell Biol* **12**, 257-266 (2010).

11. Pannerec A, Formicola L, Besson V, Marazzi G, Sassoon DA. Defining skeletal muscle resident progenitors and their cell fate potentials. *Development* **140**, 2879-2891 (2013).

12. Asakura A, Seale P, Girgis-Gabardo A, Rudnicki MA. Myogenic specification of side population cells in skeletal muscle. *J Cell Biol* **159**, 123-134 (2002).

13. Tamaki T*, et al.* Skeletal muscle-derived CD34+/45- and CD34-/45- stem cells are situated hierarchically upstream of Pax7+ cells. *Stem cells and development* **17**, 653-667 (2008).

14. Lee JY*, et al.* Clonal isolation of muscle-derived cells capable of enhancing muscle regeneration and bone healing. *J Cell Biol* **150**, 1085-1100 (2000).

15. Qu-Petersen Z*, et al.* Identification of a novel population of muscle stem cells in mice: potential for muscle regeneration. *J Cell Biol* **157**, 851-864 (2002).

16. Usas A, Huard J. Muscle-derived stem cells for tissue engineering and regenerative therapy. *Biomaterials* **28**, 5401-5406 (2007).

17. Kuroda R*, et al.* Cartilage repair using bone morphogenetic protein 4 and muscle-derived stem cells. *Arthritis Rheum* **54**, 433-442 (2006).

18. Cao B*, et al.* Muscle stem cells differentiate into haematopoietic lineages but retain myogenic potential. *Nat Cell Biol* **5**, 640-646 (2003).

19. Lu A*, et al.* Isolation of myogenic progenitor populations from Pax7-deficient skeletal muscle based on adhesion characteristics. *Gene therapy* **15**, 1116-1125 (2008).

20. Bulfield G, Siller WG, Wight PA, Moore KJ. X chromosome-linked muscular dystrophy (mdx) in the mouse. *Proceedings of the National Academy of Sciences of the United States of America* **81**, 1189-1192 (1984).

21. Hoffman EP, Brown RH, Jr., Kunkel LM. Dystrophin: the protein product of the Duchenne muscular dystrophy locus. *Cell* **51**, 919-928 (1987).

22. Ryder-Cook AS*, et al.* Localization of the mdx mutation within the mouse dystrophin gene. *The EMBO journal* **7**, 3017-3021 (1988).

23. DiMario JX, Uzman A, Strohman RC. Fiber regeneration is not persistent in dystrophic (MDX) mouse skeletal muscle. *Developmental biology* **148**, 314-321 (1991).

24. Straub V, Rafael JA, Chamberlain JS, Campbell KP. Animal models for muscular dystrophy show different patterns of sarcolemmal disruption. *The Journal of cell biology* **139**, 375-385 (1997).

25. Khouzami L*, et al.* Delayed cardiomyopathy in dystrophin deficient mdx mice relies on intrinsic glutathione resource. *Am J Pathol* **177**, 1356-1364 (2010).

26. Isaac C*, et al.* Dystrophin and utrophin "double knockout" dystrophic mice exhibit a spectrum of degenerative musculoskeletal abnormalities. *Journal of orthopaedic research : official publication of the Orthopaedic Research Society* **31**, 343-349 (2013).

27. Kornegay JN*, et al.* The paradox of muscle hypertrophy in muscular dystrophy. *Physical medicine and rehabilitation clinics of North America* **23**, 149-172, xii (2012).

28. Nguyen TM, Le TT, Blake DJ, Davies KE, Morris GE. Utrophin, the autosomal homologue of dystrophin, is widely-expressed and membrane-associated in cultured cell lines. *FEBS Lett* **313**, 19-22 (1992).

29. Ferretti R, Neto HS, Marques MJ. Expression of utrophin at dystrophin-deficient neuromuscular synapses of mdx mice: a study of protected and affected muscles. *Anat Rec (Hoboken)* **294**, 283-286 (2011).

30. Baban D, Davies KE. Microarray analysis of mdx mice expressing high levels of utrophin: therapeutic implications for dystrophin deficiency. *Neuromuscul Disord* **18**, 239-247 (2008).

31. Bewick GS, Nicholson LV, Young C, O'Donnell E, Slater CR. Different distributions of dystrophin and related proteins at nerve-muscle junctions. *Neuroreport* **3**, 857-860 (1992).

32. Law DJ, Allen DL, Tidball JG. Talin, vinculin and DRP (utrophin) concentrations are increased at mdx myotendinous junctions following onset of necrosis. *Journal of cell science* **107 (Pt 6)**, 1477-1483 (1994).

33. Deol JR*, et al.* Successful compensation for dystrophin deficiency by a helper-dependent adenovirus expressing full-length utrophin. *Mol Ther* **15**, 1767-1774 (2007).

34. Sacco A*, et al.* Short telomeres and stem cell exhaustion model Duchenne muscular dystrophy in mdx/mTR mice. *Cell* **143**, 1059-1071 (2010).

35. Deconinck AE*, et al.* Utrophin-dystrophin-deficient mice as a model for Duchenne muscular dystrophy. *Cell* **90**, 717-727 (1997).

36. Pani G. From growing to secreting: new roles for mTOR in aging cells. *Cell cycle* **10**, 2450-2453 (2011).

37. Harrison DE*, et al.* Rapamycin fed late in life extends lifespan in genetically heterogeneous mice. *Nature* **460**, 392-395 (2009).

38. Blagosklonny MV. Big mice die young but large animals live longer. *Aging (Albany NY)* **5**, 227-233 (2013).

39. Blagosklonny MV. Aging, stem cells, and mammalian target of rapamycin: a prospect of pharmacologic rejuvenation of aging stem cells. *Rejuvenation Res* **11**, 801-808 (2008).

40. Iglesias-Bartolome R*, et al.* mTOR inhibition prevents epithelial stem cell senescence and protects from radiation-induced mucositis. *Cell Stem Cell* **11**, 401-414 (2012).

41. Eghtesad S, Jhunjhunwala S, Little SR, Clemens PR. Rapamycin ameliorates dystrophic phenotype in mdx mouse skeletal muscle. *Mol Med* **17**, 917-924 (2011).

42. Manzur AY, Kuntzer T, Pike M, Swan A. Glucocorticoid corticosteroids for Duchenne muscular dystrophy. *The Cochrane database of systematic reviews*, CD003725 (2004).

43. Kang J. [Glucocorticoid therapy in Duchenne muscular dystrophy]. *Rinsho shinkeigaku = Clinical neurology* **36**, 1338-1340 (1996).

44. Schakman O, Gilson H, Thissen JP. Mechanisms of glucocorticoid-induced myopathy. *The Journal of endocrinology* **197**, 1-10 (2008).

45. Shimizu N*, et al.* Crosstalk between glucocorticoid receptor and nutritional sensor mTOR in skeletal muscle. *Cell Metab* **13**, 170-182 (2011).

46. Dellorusso C, Crawford RW, Chamberlain JS, Brooks SV. Tibialis anterior muscles in mdx mice are highly susceptible to contraction-induced injury. *J Muscle Res Cell Motil* **22**, 467-475 (2001).

47. Kallestad KM, Hebert SL, McDonald AA, Daniel ML, Cu SR, McLoon LK. Sparing of extraocular muscle in aging and muscular dystrophies: a myogenic precursor cell hypothesis. *Exp Cell Res* **317**, 873-885 (2011).

48. Jankowski RJ, Haluszczak C, Trucco M, Huard J. Flow cytometric characterization of myogenic cell populations obtained via the preplate technique: potential for rapid isolation of muscle-derived stem cells. *Hum Gene Ther* **12**, 619-628 (2001).

49. Chirieleison SM*, et al.* Automated live cell imaging systems reveal dynamic cell behavior. *Biotechnology progress* **27**, 913-924 (2011).

50. Gingras AC*, et al.* Regulation of 4E-BP1 phosphorylation: a novel two-step mechanism. *Genes Dev* **13**, 1422-1437 (1999).

51. Hussein MR, Hamed SA, Mostafa MG, Abu-Dief EE, Kamel NF, Kandil MR. The effects of glucocorticoid therapy on the inflammatory and dendritic cells in muscular dystrophies. *Int J Exp Pathol* **87**, 451-461 (2006).

52. Lefaucheur JP, Pastoret C, Sebille A. Phenotype of dystrophinopathy in old mdx mice. *Anat Rec* **242**, 70-76 (1995).

53. Matsumura K, Ervasti JM, Ohlendieck K, Kahl SD, Campbell KP. Association of dystrophin-related protein with dystrophin-associated proteins in mdx mouse muscle. *Nature* **360**, 588-591 (1992).

54. Deconinck AE*, et al.* Postsynaptic abnormalities at the neuromuscular junctions of utrophin-deficient mice. *J Cell Biol* **136**, 883-894 (1997).

55. Deasy BM*, et al.* Long-term self-renewal of postnatal muscle-derived stem cells. *Molecular biology of the cell* **16**, 3323-3333 (2005).

56. Uezumi A, Fukada S, Yamamoto N, Takeda S, Tsuchida K. Mesenchymal progenitors distinct from satellite cells contribute to ectopic fat cell formation in skeletal muscle. *Nat Cell Biol* **12**, 143-152 (2010).

57. Wosczyna MN, Biswas AA, Cogswell CA, Goldhamer DJ. Multipotent progenitors resident in the skeletal muscle interstitium exhibit robust BMP-dependent osteogenic activity and mediate heterotopic ossification. *J Bone Miner Res* **27**, 1004-1017 (2012).

58. Lawrence JC, Jr. mTOR-dependent control of skeletal muscle protein synthesis. *Int J Sport Nutr Exerc Metab* **11 Suppl**, S177-185 (2001).

59. Buller CL*, et al.* A GSK-3/TSC2/mTOR pathway regulates glucose uptake and GLUT1 glucose transporter expression. *Am J Physiol Cell Physiol* **295**, C836-843 (2008).

60. Lai YC, Liu Y, Jacobs R, Rider MH. A novel PKB/Akt inhibitor, MK-2206, effectively inhibits insulin-stimulated glucose metabolism and protein synthesis in isolated rat skeletal muscle. *Biochem J* **447**, 137-147 (2012).

61. Yue T, Yin J, Li F, Li D, Du M. High glucose induces differentiation and adipogenesis in porcine muscle satellite cells via mTOR. *BMB Rep* **43**, 140-145 (2010).

62. Manzur AY, Kuntzer T, Pike M, Swan A. Glucocorticoid corticosteroids for Duchenne muscular dystrophy. *The Cochrane database of systematic reviews*, CD003725 (2008).

63. Krahn MJ, Anderson JE. Anabolic steroid treatment increases myofiber damage in mdx mouse muscular dystrophy. *J Neurol Sci* **125**, 138-146 (1994).

64. Iadevaia V, Huo Y, Zhang Z, Foster LJ, Proud CG. Roles of the mammalian target of rapamycin, mTOR, in controlling ribosome biogenesis and protein synthesis. *Biochem Soc Trans* **40**, 168-172 (2012).

65. Betters JL*, et al.* Nitric oxide reverses prednisolone-induced inactivation of muscle satellite cells. *Muscle & nerve* **37**, 203-209 (2008).

66. Wang B, Li J, Fu FH, Xiao X. Systemic human minidystrophin gene transfer improves functions and life span of dystrophin and dystrophin/utrophin-deficient mice. *J Orthop Res* **27**, 421-426 (2009).

67. Lavasani M, Lu A, Thompson SD, Robbins PD, Huard J, Niedernhofer LJ. Isolation of muscle-derived stem/progenitor cells based on adhesion characteristics to collagen-coated surfaces. *Methods Mol Biol* **976**, 53-65 (2013).

68. Gharaibeh B*, et al.* Isolation of a slowly adhering cell fraction containing stem cells from murine skeletal muscle by the preplate technique. *Nat Protoc* **3**, 1501-1509 (2008).

69. Deasy BM*, et al.* Modeling stem cell population growth: incorporating terms for proliferative heterogeneity. *Stem Cells* **21**, 536-545 (2003).

70. Moller B*, et al.* Prednisolone induces interleukin-18 expression in mononuclear blood and myeloid progenitor cells. *Inflamm Res* **51**, 457-463 (2002).

71. Metzinger L, Passaquin AC, Leijendekker WJ, Poindron P, Ruegg UT. Modulation by prednisolone of calcium handling in skeletal muscle cells. *Br J Pharmacol* **116**, 2811-2816 (1995).

72. Zhang S, Kodama M, Hanawa H, Izumi T, Shibata A, Masani F. Effects of cyclosporine, prednisolone and aspirin on rat autoimmune giant cell myocarditis. *J Am Coll Cardiol* **21**, 1254-1260 (1993).

Blank Page

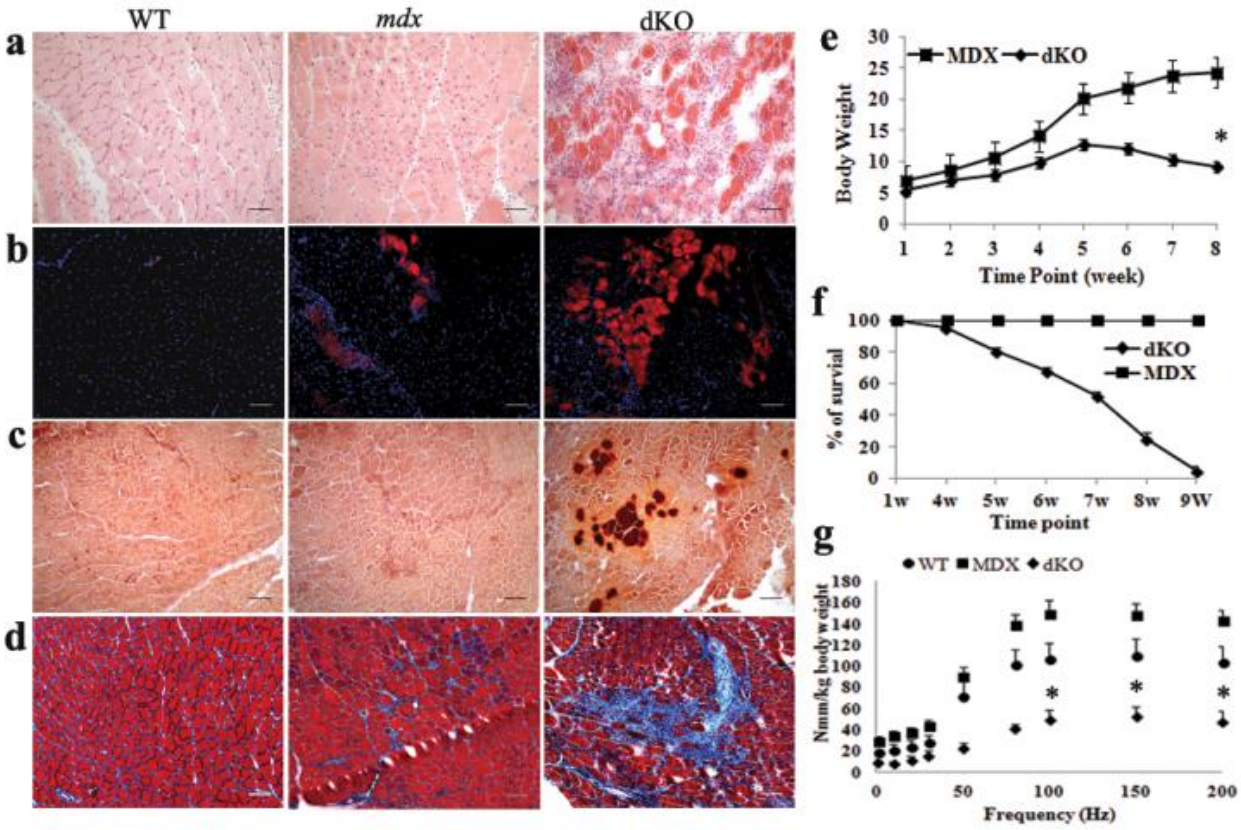

Figure1: Muscle histopathology and muscular dystrophy are more severe in dKO mice in contrast to WT and *mdx* mice

(a) H&E staining show severe muscle damage in the gastrocnemius muscles of 8 week old dKO mice and have less centrally nucleated fibers compared to age matched WT and *mdx* muscles. (**b**) Necrotic areas in the gastrocnemius muscles was identified by mouse IgG staining. (**c**) Alizarin red staining to visualize calcium deposits in 8 week old WT, *mdx* and dKO muscles. (**d**) Trichrome staining of muscle sections to identify fibrotic regions. (**e**) The body weight of the dKO mice significantly decreased after 5-6 weeks. Error bars indicate "mean ± SD"; n=10. P<0.05. (**f**) dKO mice have a significantly shorter life span than WT and *mdx* mice. Error bars indicate "mean ± SD"; n=30. (**g**) The results from muscle physiology testing showed a significant decrease in muscle strength in the dKO mice. n=6. Error bars indicate "mean ± SD." p<0.05. In panel "**a**", all scale bars = 50μm, in panel "**b, c, d**", all scale bars=100um.

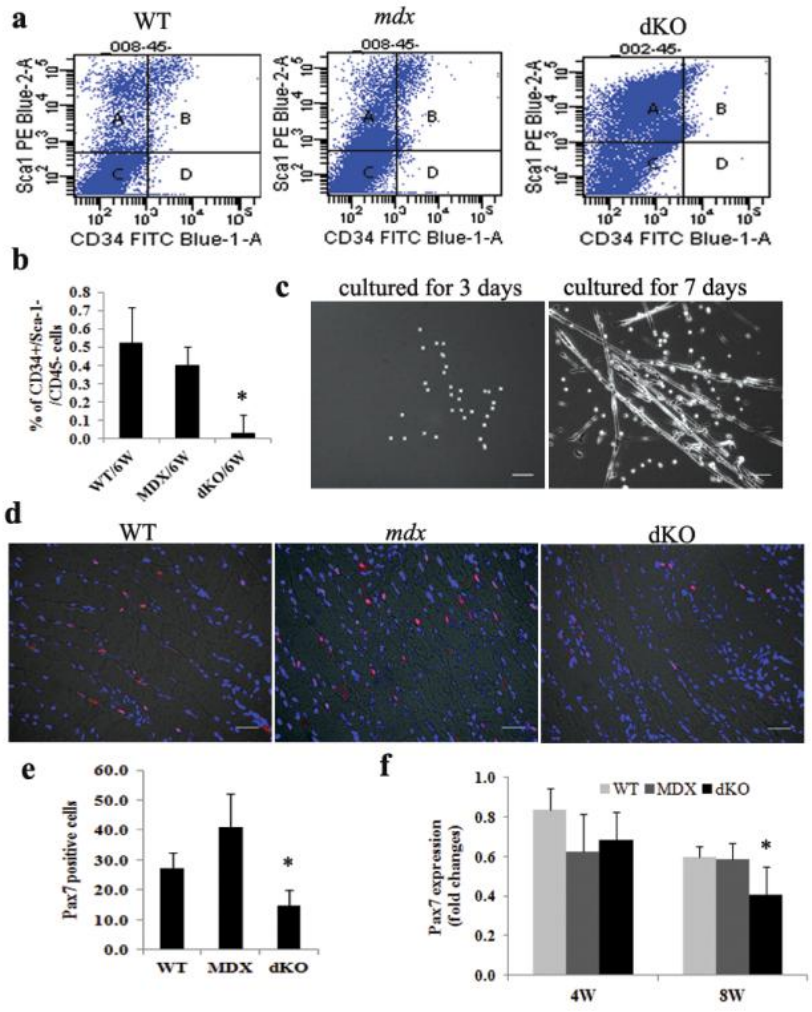

Figure 2: Muscle progenitor cells are exhausted in old dKO mice

(**a**) Fluorescence activated cell sorting (FACS) plots show that almost no CD34+/Sca-1- cells could be detected in 6 week old dKO muscles. (**b**) Quantification of FACs results. Error bars indicate "mean ± SD", n=3, $p<0.01$. (**c**) CD34+/Sca-1-/CD45- cells were cultured for 3 and 7 days, multinucleated myotubes were monitored using bright field microscopy. (**d**) Diaphragmatic cryosections from 8 week old dKO, *mdx* and WT mice were immuno-stained for the myogenic progenitor cell marker Pax7. (**e**) Quantitation of Pax7 positive cells in the diaphragm muscle of 8 week old mice. The number of Pax7 positive cells was quantified based on the total number of Pax7 positive cells per image (the data represent 3 muscles per group). Error bars indicate "mean ± SD." $p<0.05$. (**f**) Graph showing the results of Real-time PCR. RNA was isolated from three diaphragms of each genotype. In panel "**c**", all scale bar = 100um and in panel "**d"** all scale bars = 25μm.

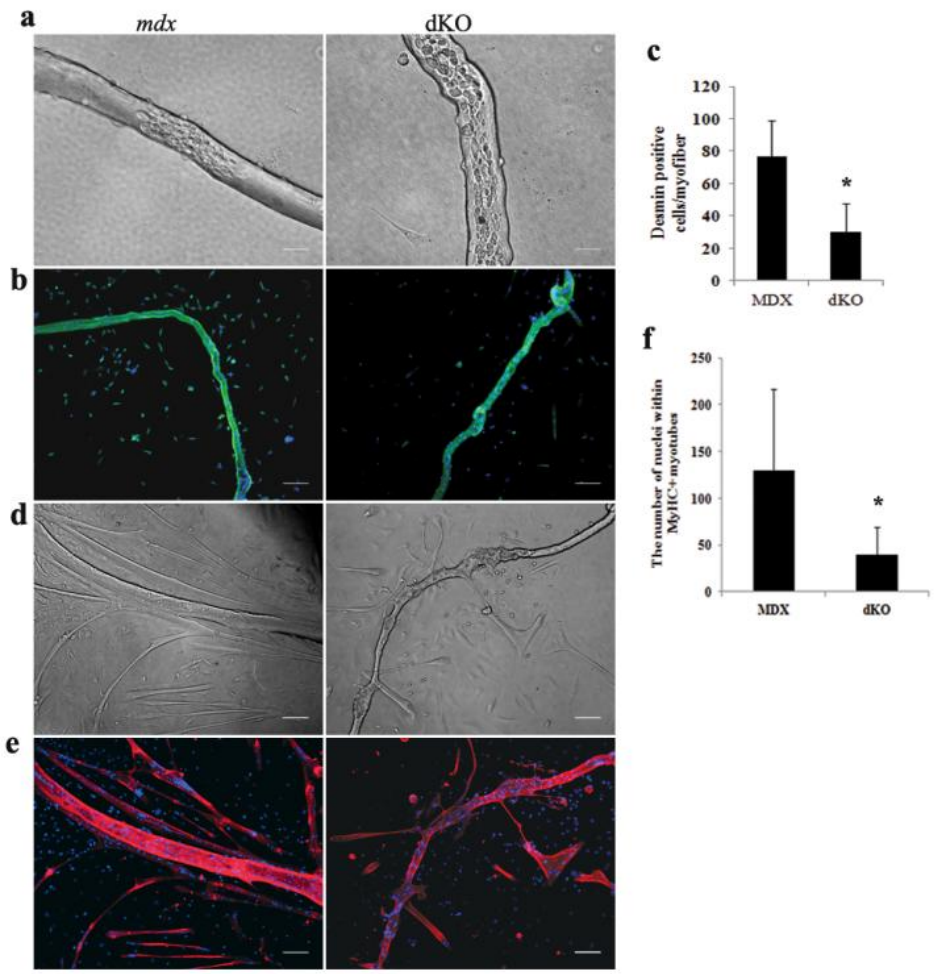

Figure 3: MPCs from single muscle fibers isolated from dKO mice exhibit proliferation and differentiation defects

(**a**) Single muscle fibers isolated from 6-8 week old mice. Abnormal single muscle fibers are shown in bright field. (**b**) Desmin was stained after 96 hours of culture (green cells). Representative images show a proliferation defect in the dKO muscles, compared to *mdx* muscles. (**c**) Quantification of desmin positive cells derived per fiber. n=3. Error bars indicate "mean ± SD." $p<0.05$. (**d**) Single muscle fibers were cultured for 7 days. Representative images showing myotube formation in cultured both dKO and *mdx* fibers (bright field). (**e**) Representative images of immunofluorescent staining for fast myosin heavy chain (MyHCf) (red) and nuclei (blue) indicated myogenic differentiation. (**f**) Graph showing quantification of the differentiation capacity as the total number of nuclei in MyHCf positive myotubes derived per muscle fiber after 7 days of culture. n=5. In panel "**a**" all scale bars = 25um and in panels "**b, d** and **e**" all scale bars = 100um.

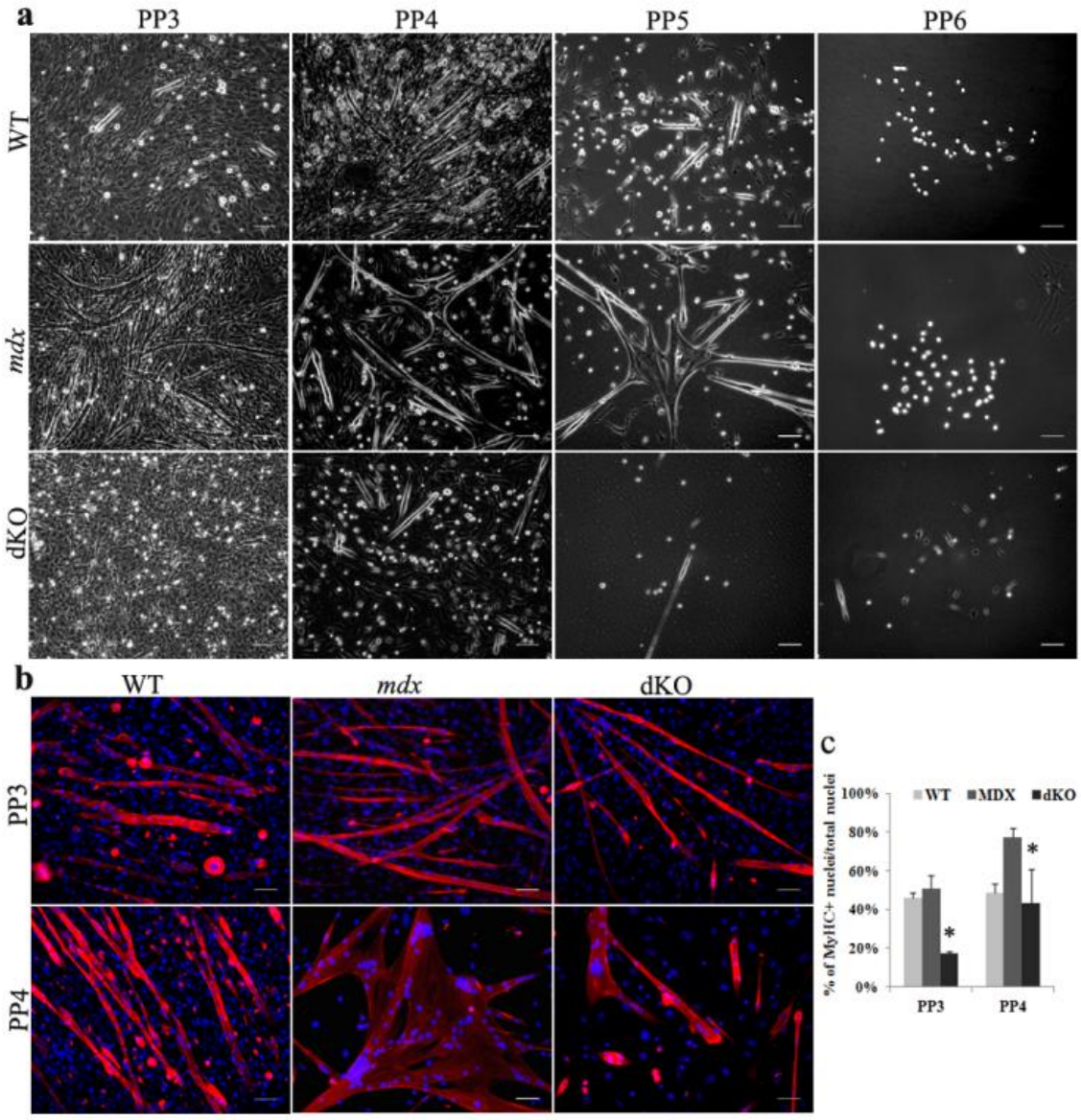

Figure 4: dKO muscle progenitor cells are impaired in their differentiation capacity

(**a**) Various populations of muscle derived cells were isolated according to their adhesion characteristics by the preplate technique. Representative images showing different MPC populations isolated from WT, *mdx* and dKO mice. (**b**) Representative images of PP3 and PP4 cell populations isolated from WT, *mdx* and dKO mice at 6 weeks of age and immuno-stained for MyHCf (red) and DAPI (blue). (**c**) Graph showing quantification of the cells differentiation capacity as the number of nuclei in MyHCf positive myotubes relative to the total number of nuclei. n=5. Error bars indicates "mean ± SD." $p<0.05$. In panel "**a**" all scale bars = 100um, in panel "**b**" all scale bars = 50um.

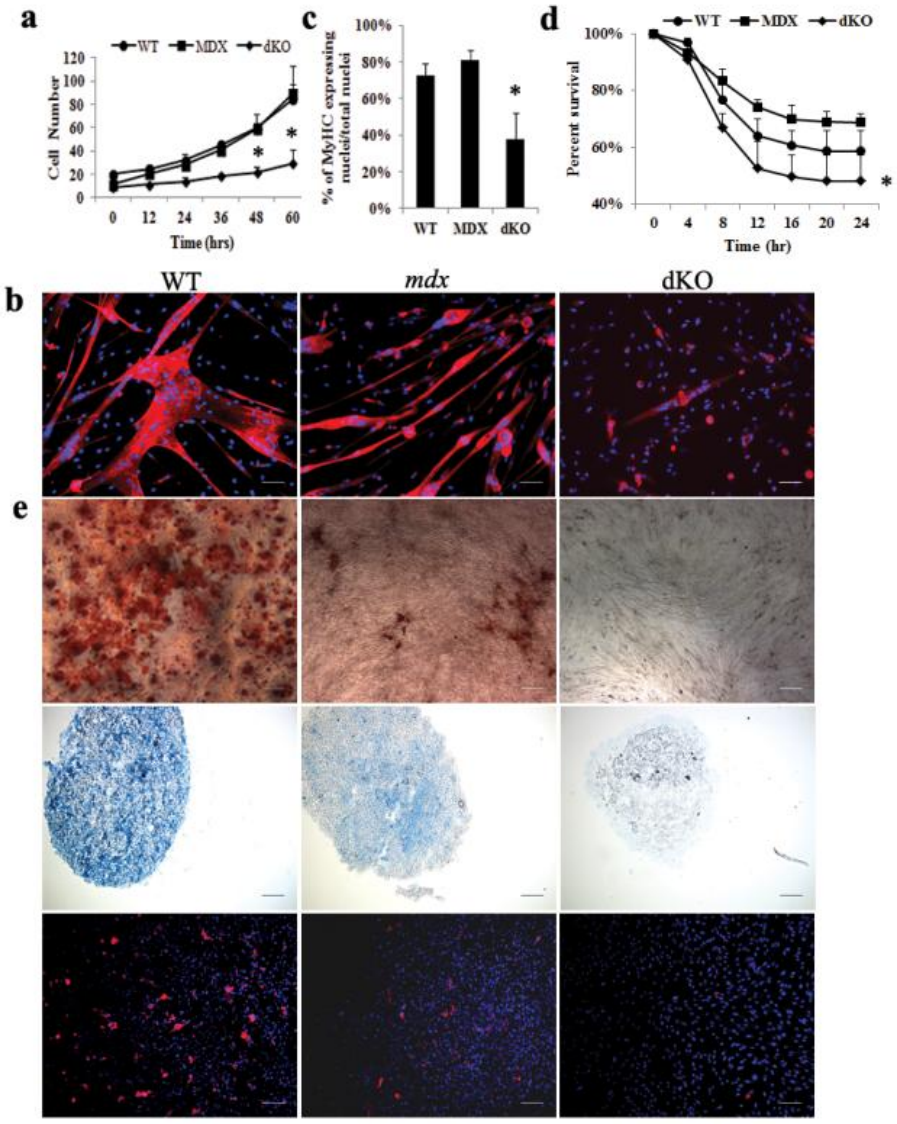

Figure 5: Muscle derived stem cells (MDSCs) isolated from aged dKO muscle exhibit a reduction of their functionality.

(**a**) Cell proliferation rate was measured using a Live Cell Imaging (LCI) system. (**b**) MDSCs were cultured in myogenic differentiation medium for 3 days, during which cell fusion into multinucleated myotubes was determined by immuno-staining of MyHCf. (**c**) Quantification of MyHCf positive myotubes. The percentage of differentiated myotubes was quantified as the number of nuclei in MyHCf positive myotubes relative to the total number of nuclei. A total of three populations of WT, *mdx* and dKO MDSCs were tested ($p<0.01$). Error bars indicate "mean ±SD." (**d**) Each cell population (dKO, *mdx* and WT) were exposed to 400µM hydrogen peroxide in proliferation medium containing PI. Using the LCI system, 10x bright field and fluorescence

images were taken at 10 minute intervals over 24 hours. Identifying the number of PI+ cells per field of view out of the total cell number determined the percentage of cell death over time. (**e**) Multi-lineage differentiation of MDSCs. These cells were cultured in insulin mediated adipogenic differentiation medium, BMP2 supplemental osteogenic medium and chondrogenic induction media supplemented with BMP2 and TGFβ3, respectively, and then alizarin red (top), alcian blue (middle) and AdipoRed (bottom) staining were performed. In panel "**b**" all scale bars = 50um. In panel "**e**", scale bar=50um for alizarin red and alcian blue, scale bar=100um for AdipoRed.

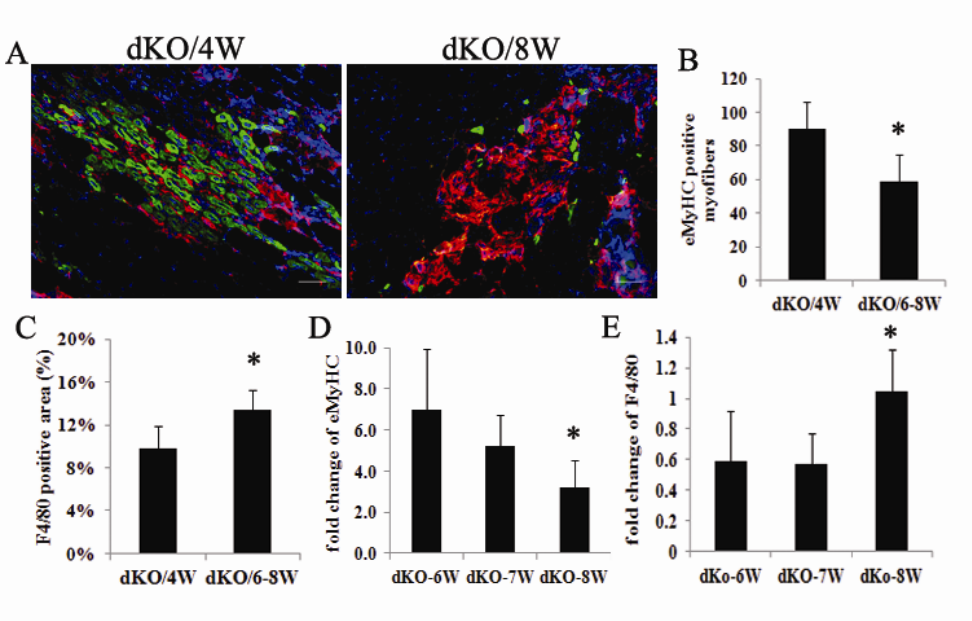

Figure 6: Limited muscle regeneration potential of MPCs in dKO mice in vivo

(a) Representative images showing cryosections from young (4 week old) and old (6-8 week old) dKO gastrocnemius muscle and stained for eMyHC (green) and F4/80 (red). Scale bars = 50um. (**b**) Graph showing quantification of eMyHC positive fibers. n=5, error bars indicate "mean ± SD." $p<0.05$. (**c**) Graph showing quantification of F4/80 positive macrophages. Macrophage infiltration areas in the gastrocnemius muscles were quantified based on the total positive area per image (the data represent 5 muscles per group). $p<0.05$. (**d**) Graph showing the results of real-time PCR for eMyHC expression. RNA was isolated from 3-6 gastrocnemius muscles from dKO mice. (**e**) Graph showing the results of real-time PCR for F4/80 expression. RNA was isolated from 3-6 gastrocnemius muscles from dKO mice. Error bars indicate "mean ± SD."

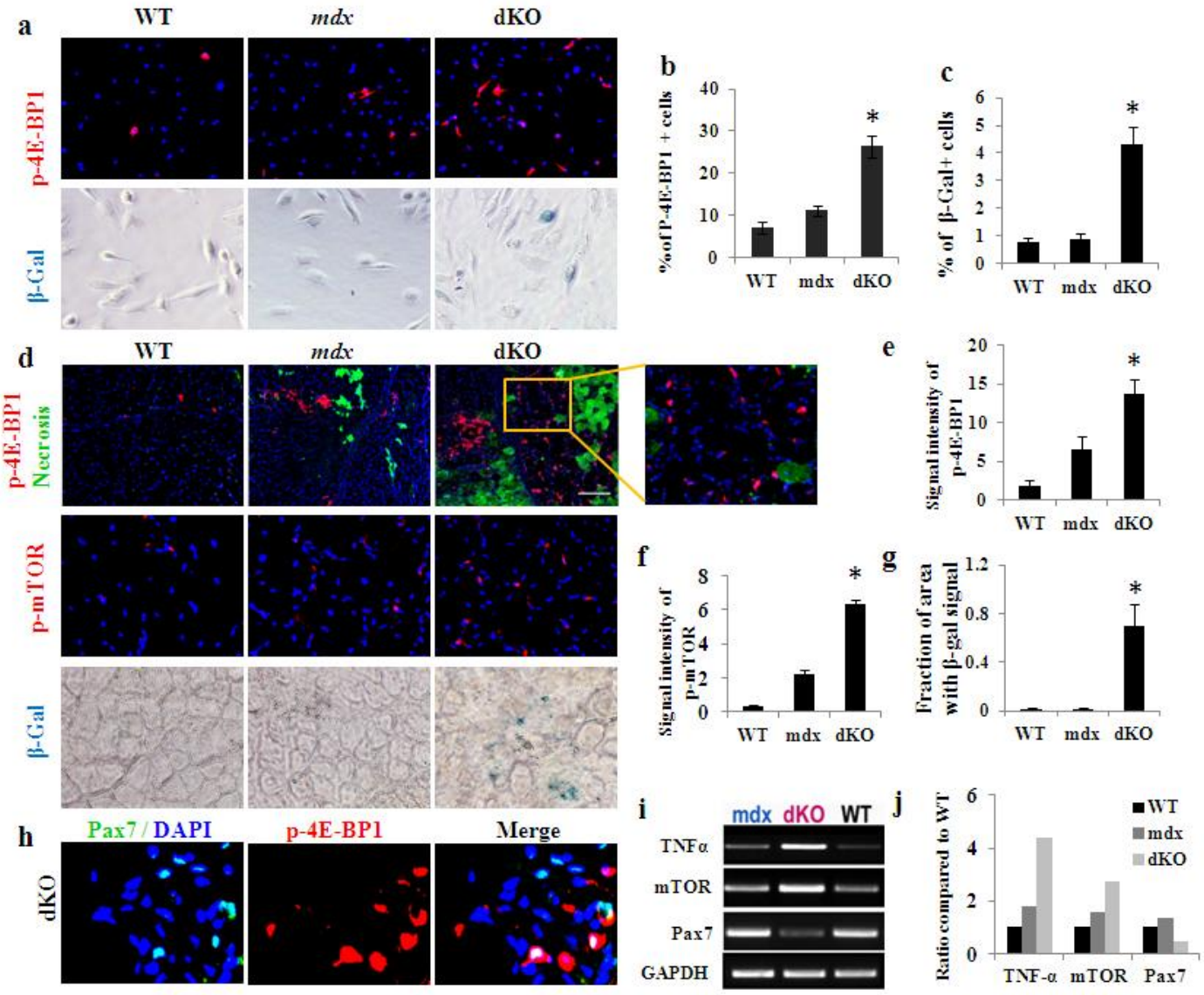

Figure 7. mTOR activity and cell senescence in the MDSCS and skeletal muscle of WT, mdx and dKO mice. (a) immunostaining of p-4E-BP1 in MDSCs from 6-week old WT, mdx, and dKO mice showed a greater number of p-4E-BP1+ cells (red) in MDSCs isolated from dKO mice. Also, a cell senescence assay showed that β-gal+ cells were generally absent in MDSCs isolated from WT or mdx mice, but present in MDSCs isolated from dKO mice. **(b)** Quantification of the number of p-4E-BP1+ cells in MDSCs isolated from the 3 mouse models. **(c)** Quantification of the number of β-gal+ cells in MDSCs isolated from the 3 mouse models. **(d)** immunostaining of p-4E-BP1 in the GM muscles of 8-week old WT, mdx, and dKO mice showed a slight increase in p-4E-BP1+ cells (red) in the mdx mice and an excessive increase of p-4E-BP1+ cells in the dKO mice; necrotic myofibers (green) were immunostained with anti-

mouse IgG and were found to be present in both mdx and dKO mice, though significantly more necrotic myofibers was observed in the dKO muscle. Immunostaining of p-mTOR in the GM muscle of 8-week old mice showed a slight increase in p-mTOR+ cells (red) in the mdx mice, and an excessive increase of p-mTOR+ cells in the dKO mice. The cell senescence assay in the GM muscles of 8-week old mice revealed the presence of senescent cells (β-gal+) in the dKO mice but not in the WT or mdx mice. **(e)** Quantification of p-4E-BP1+ signaling in the muscle of the 3 mouse models. **(f)** Quantification of p-mTOR+ signaling in the muscle of the 3 mouse models. **(g)** Quantification of the β-gal+ area in the GM muscles of the 3 mouse models. **(h)** Co-immunostaining of Pax7 and p-4E-BP1 in skeletal muscle of 4-week old dKO mice revealed that some Pax7+ cells (muscle stem cell) are positive with p-4E-BP1. **(i)** RT-PCR showed the up-regulated expression of TNF-α, mTOR, and Beclin1, and down-regulated expression of Pax7 in the GM muscles of 8-week old dKO mice, compared to that of the WT and mdx mice**. (j)** Quantification of the mRNA level of TNF-α, mTOR and Pax7 in muscles of the 3 mouse models. " * " on the bar charts indicates the difference is significant ($p<0.05$).

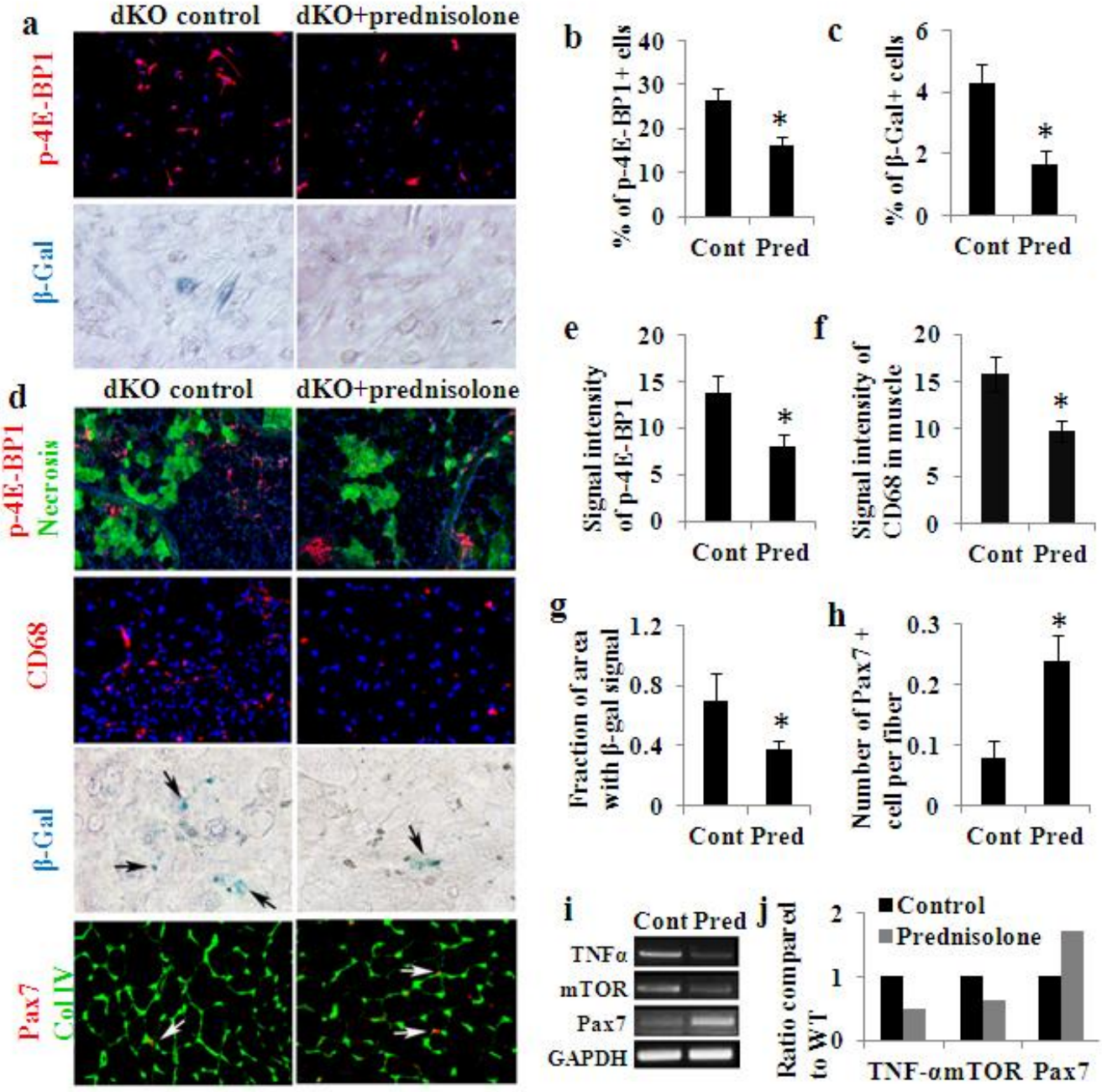

Figure 8. Effects of *in vitro* prednisolone treatment of dKO-MDSCs and *in vivo* prednisolone treatment of dKO mice. (a) immunostaining of p-4E-BP1 in MDSCs isolated from 6-week old dKO mice showed that prednisolone treatment for 7 days reduced the number of p-4E-BP1+ cells. A cell senescence assay showed that prednisolone treatment for 7 days reduced the number of β-gal+ cells in dKO MDSCs. **(b)** Quantification of the number of p-4E-BP1+ cells in MDSCs with and without prednisolone treatment. **(c)** Quantification of the number

of β-gal+ cells in MDSCs with and without prednisolone treatment. **(d)** Immunostaining of p-4E-BP1+ in skeletal muscle of 8-week old dKO mice showed prednisolone treatment reduced the number of p-4E-BP1+ cells (red) and necrotic myofibers (green). Immunostaining also revealed a reduction in the number of CD68+ cells in the skeletal muscle with prednisolone treatment. A cell senescence assay showed a reduction in the number of β-gal+ cells in the skeletal muscles with prednisolone treatment. Immunostaining revealed increased numbers of Pax7+ cells in the skeletal muscles with prednisolone treatment. **(e)** Quantification of the p-4E-BP1+ signal in the muscles of dKO mice with and without prednisolone treatment. **(f)** Quantification of the CD68+ signal in the muscles of dKO mice with and without prednisolone treatment. **(g)** Quantification of the β-gal+ area in the muscles of dKO mice with and without prednisolone treatment. **(h)** Quantification of the number of Pax7+ cells in the muscles of dKO mice with and without prednisolone treatment. **(i)** RT-PCR assay showed that prednisolone treatment of dKO mice down-regulated the expression of TNF-α and mTOR in the skeletal muscle, while up-regulating the expression of Pax7. **(j)** Quantification of the mRNA level of TNF-α, mTOR and Pax7 in the muscles of dKO mice with and without prednisolone treatment.

Table 1 Primers used for real time PCR

Gene	Forward primers	Reverse primers	Location
Pax7*	GTGCCCTCAGTGAGTTCGAT	CCACATCTGAGCCCTCATCC	499-667
Pax7	TCCATGACAACTTTGGCATTG	TCACGCCACAGCTTTCCA	540-642
FGF2	GGCTGCTGGCTTCTAAGTGT	GTCCCGTTTTGGATCCGAGT	463-615
eMyHC	GGAGGCTGATGAACAAGCCA	GCTAGAGGTGAAGTCACGGG	5696-5897
F4/80	CGGGGCTATGGGATGCATAA	TCAGCAACCTCGTGTCCTTG	2375-2564
TNF-α	GATTATGGCTCAGGGTCCAA	CTCCCTTTGCAGAACTCAGG	944-1120
mTOR	CAGTTCGCCAGTGGACTGAAG	GCTGGTCATAGAAGCGAGTAGAC	190-319
GAPDH	TCCATGACAACTTTGGCATTG	TCACGCCACAGCTTTCCA	540-642
β-Actin	TCAGAAGGACTCCTATGTGG	TCTTTGATGTCACGCACGAT	234–722

*primer for real time PCR

CONTROL ID: 1473466

TITLE: Enhanced myogenic potential of human dental pulp and amniotic fluid stem cells by use of a demethylation agent and conditioned media.

AUTHORS (LAST NAME, FIRST NAME): Pisciotta, Alessandra[1, 2]; Lu, Aiping[2]; Gharaibeh, Burhan[2,]; De Pol, Anto[1]; Huard, Johnny[2]

INSTITUTIONS (ALL): 1. Department of Surgical, Medical, Dental and Morphological Sciences with interest in Transplant, Oncology and Regenerative Medicine, University of Modena and Reggio Emilia, Modena, Italy.
2. Stem Cell Research Center, Department of Orthopaedic Surgery, University of Pittsburgh, Pittsburgh, PA, United States.

CURRENT PRIMARY CATEGORY: Muscle

AWARDS:

KEYWORDS: Muscle, Cell and Molecular Imaging, Orthopaedic Pathology.

ABSTRACT BODY:

Introduction: Duchenne muscular dystrophy (DMD) is a genetic mutation resulting in muscle degeneration that leads to death by the mid-twenties. Cell therapy can be used to reintroduce dystrophin to repair damaged muscle fibers. Human dental pulp (hDPSCs) and amniotic fluid stem cells (hAFSCs) may represent an alternative, less controversial source to embryonic stem cells. HDPSCs can be isolated from adult human dental pulp of the third molars during routine extraction. HAFSCs, which represent 1% of the cells in human amniocentesis specimens, can be obtained by immunoselecting the antigen c-Kit (CD117) positive population, via magnetic cell sorting. HDPSCs and hAFSCs have been shown to be self-renewing and multipotent (1, 2), therefore they may represent promising tools for muscular dystrophy therapies.
This study evaluated the myogenic potential of hDPSCs and hAFSCs using different conditions which optimized the most effective protocol to differentiate the cells towards a myogenic lineage by means of demethylation. The results of the current study provide the basis for subsequent in vivo uses of hDPSCs and hAFSCs to enhance skeletal muscle repair in animal models and human DMD patients.

Methods: Human DPSCs were isolated as described by Riccio et al (3). The STRO-1+ DPSC population was obtained by magnetic cell sorting. AFSCs were isolated as previously described by De Coppi et al (2): hAFSCs cultures, from supernumerary amniocentesis specimens, were subjected to c-Kit immuno-selection by MACS technology. The STRO-1+ DPSC and the c-kit+

AFSC populations were used in this study.
Direct co-culture: To test the ability of hAFSCs and hDPSCs to form new myotubes, the cells were differentiated in a direct co-culture system with C2C12 myoblasts. Human cells and C2C12 cells, seeded at a 10:1 ratio, were maintained in proliferation medium (PM: DMEM High Glucose + 10% FBS) until confluent, the medium was then replaced with fusion medium (FM: DMEM High Glucose + 1% FBS + 10nM insulin).
Demethylation and differentiation: To evaluate whether hAFSCs and hDPSCs can be committed to the myogenic lineage, cells were seeded at 3000 cells/cm2 in PM until confluent. Subsequently, the medium was replaced with low serum differentiation medium supplemented with 10µM 5-Aza-2'-deoxycytidine (5-Aza) for 24 hours, to induce DNA demethylation. After removing 5-Aza, medium was replaced with low serum differentiation medium supplemented with 10 nM insulin. Cells were differentiated in a) low serum medium plus 10 nM insulin and b) pre-filtered conditioned FM from the C2C12 culture + fresh differentiation medium + 10 nM insulin.
To verify myogenic differentiation, staining for human Nuclei (huNu) and myosin heavy chain (MyHC) was performed. Myogenic differentiation after demethylation was verified by myogenin and MyHC immune-fluorescent (IF) staining. Human cells were processed for IF staining as previously described (3).

Results: When differentiated in a direct co-culture with C2C12 cells, human AFSCs and DPSCs were able to undergo myogenic differentiation, as demonstrated by the positive staining of the myotubes with anti-huNu ab (Fig. 1A-B). Human cells which were not co-cultured with C2C12 did not undergo myogenic differentiation and did not fuse in myotubes (Fig. 1C-D).
Data from the IF analysis of myogenic differentiation after treatment with 10µM 5-Aza showed that hAFSCs are driven to the myogenic lineage and express myogenin, a myogenic differentiation marker, after 14 days of differentiation (Fig. 2A), while the hDPSCs underwent myogenic differentiation expressing myogenin after 21 days of differentiation under the same conditions (Fig. 2C). Moreover, some hAFSCs also showed positive staining for MyHC (Fig. 2B). Immunofluorescence labeling also showed that when conditioned medium from the differentiating C2C12 cells was added to fresh myogenic medium, the human cells pre-treated with 5-Aza started to express myogenin after 14 and 21 days of differentiation (Fig. 2D-2F) respectively. Furthermore, some of the hAFSCs also showed positive staining for MyHC (Fig. 2E). Cells not demethylated demonstrated no positive staining for muscle specific markers (Fig. 2G-H).

Discussion: The IF image data in this study demonstrated the ability of the hAFSCs and hDPSCs stem cell populations to actively participate in the formation of myotubes. These human cells were capable of fusing with murine C2C12, as demonstrated by the positive IF staining of the

multi-nucleated cells to anti-huNu ab. These results showed the potential of these cells for skeletal muscle repair.
Previous studies have demonstrated that the genes related to skeletal myogenic differentiation are controlled by DNA methylation and that the use of the demethylation agent, 5-Aza, was able to induce adult human bone marrow stem cells to differentiate towards a cardiomyogenic lineage (4, 5).
This study demonstrated that demethylation treatment could effectively induce a myogenic commitment of hAFSCs and hDPSCs, in two different conditions, as shown by IF staining: hAFSCs underwent myogenic differentiation earlier than hDPSCs, and reached a more mature differentiation status as shown by their expression of MyHC.
These results demonstrate that hAFSCs and hDPSCs can be induced to differentiate towards a myogenic lineage in vitro, and suggests that modulating the myogenic potential of these stem cells can be achieved by combining demethylation treatment, which increases the expression of muscle regulatory factors (MRFs), with the addition of a conditioned medium from differentiating C2C12 cells, which contains numerous soluble factors, such as IGF-II that promotes the myogenic differentiation process (6).

Significance: This study demonstrated the utility of demethylation to induce hAFSCs and hDPSCs to differentiate towards the myogenic lineage in vitro. Human AFSCs and DPSCs are suitable, non-controversial sources of stem cells that could be very useful for translational strategies to enhance the repair of injured skeletal muscle in DMD or trauma patients.

References: 1. Zhang et al. 2006. Tissue Eng 12, 2813. 2. De Coppi et al. 2007 Nat Biotechnol 25, 100. 3. Riccio et al. 2010. Eur J Histochem 54, 4. 4. N.S. Ye et al. 2006. Stem Cells Dev 15, 665. 5. Antonitsis et al. 2008 Thorac Cardiovasc Surg 56, 77. 6. Duan et al. 2010. Gen Comp Endocrinol 167, 344.

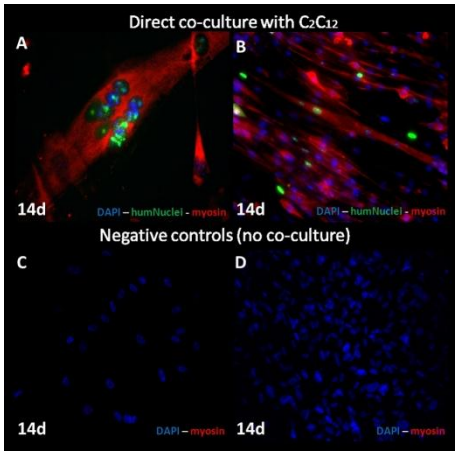

Analysis of co-culture of hAFSCs (A) and hDPSCs (B) with C2C12 cells after14 days of inducing

differentiation. Incorporation of hAFSCs and hDPSCs into myotubes stained against huNu (green), and MyHC (red). C, D. hAFSCs and hDPSCs not co-cultured with C2C12. Nuclei were stained with DAPI (blue).

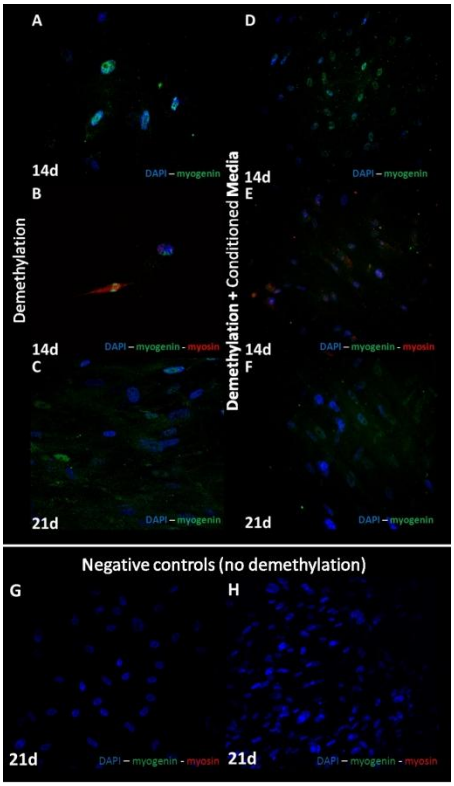

Analysis of myogenic differentiation of hAFSCs and hDPSCs after demethylation (A-C), and after demethylation plus conditioned medium from differentiating C2C12 (D-F). A-B, D-E. hAFSCs at day 14, positively stained with: myogenin (green) (A, D); myogenin (green) and MyHC (red) (B, E). C, F: hDPSCs at day 21, positive stained against myogenin (green).
G, H: hAFSCs and hDPSCs not demethylated. Nuclei were stained with DAPI.

IMAGE CAPTION:
Analysis of co-culture of hAFSCs (A) and hDPSCs (B) with C2C12 cells at 14 days of differentiation. Incorporation of hAFSCs and hDPSCs into myotubes stained against huNu (green), and MyHC (red). C, D. hAFSCs and hDPSCs not co-cultured with C2C12. Nuclei were stained with DAPI (blue).

Analysis of myogenic differentiation of hAFSCs and hDPSCs after demethylation (A-C), and after demethylation plus conditioned medium from differentiating C2C12 (D-F). A-B, D-E. hAFSCs at day 14, positive stained against: myogenin (green) (A, D); myogenin (green) and MyHC (red) (B, E). C, F: hDPSCs at day 21, positive stained against myogenin (green).
G, H: hAFSCs and hDPSCs not demethylated. Nuclei were stained with DAPI.

Proliferation and Differentiation Capacities of Muscle Derived Stem/Progenitor Cells Cultured on Polydimethylsiloxane Substrates of Varying Elastic Modulus and Protein Coating

Seth David Thompson[1], Mitra Lavasani[1,2], Bahar Ahani[1], Prerana Reddy[3], Yan Sun[4], Quentin Jallerat[4], Adam W. Feinberg[4,5], Johnny Huard[1,2].

[1]Stem Cell Research Center, Department of Orthopaedic Surgery, University of Pittsburgh, Pittsburgh, PA, USA,
[2]Department of Bioengineering, University of Pittsburgh, Pittsburgh, PA, USA,
[3]Department of Biological Sciences, Carnegie Mellon University, Pittsburgh, PA, USA,
[4]Department of Biomedical Engineering, Carnegie Mellon University, Pittsburgh, PA, USA,
[5]Department of Materials Science and Engineering, Carnegie Mellon University, Pittsburgh, PA, USA.

Abstract:

Introduction:

Muscle derived stem/progenitor cells (MDSPCs) are multipotent murine cells that display a capacity for long term proliferation. They have been utilized to regenerate bone[1], cartilage[2], skeletal[1] and cardiac muscles[3], as well as ameliorate the effects of aging[4]. MDSPCs are isolated and cultured on collagen I coated polystyrene flasks, but recent publications have shown that culturing progenitor cells on substrates with anatomically relevant elasticities and protein coatings can vastly alter their ability to proliferate and differentiate *in vitro* as well as engraft *in vivo*[5,6,7]. PDMS (polydimethylsiloxane) blends have shown to be a readily tunable substrate creating reproducible culture surfaces at anatomically relevant elasticities[7]. These blends can be adjusted across three orders-of-magnitude, surpassing what is capable with other hydrogel or PDMS systems. This study was designed to observe the effects of altering the culture surface conditions on MDSPCs *in vitro* and determine how to translate these findings to improve tissue regeneration with MDSPCs *in vivo*.

Methods:

Creating variable stiffness PDMS substrates and protein coated culture surfaces: PDMS substrates and protein coatings were prepared using previously defined methods7. Briefly, blends of Sylgard 527 and Sylgard 184 (Dow Corning) were mixed to create PDMS substrates with elastic modulus of 5 kPa, 50 kPa, 830 kPa, and 1.72 MPa. These blends were cured in 12 well plates with one of each protein coating, collagen type I (Col-1), collagen type IV and laminin (Col-4/Lam), or fibronectin (FN).

Proliferation of MDSPCs: MDSPC proliferation was investigated for 3 days on 12-well plates using a Live Cell Imaging (LCI) system. Time-lapse images were acquired every 15 minutes over 72 hours and cell numbers quantified at 6-hour intervals using ImageJ (NIH). Counts were averaged for each time point from at least 6 separate images and experiments were performed in duplicate.

Myogenic differentiation of MDSPCs: Myogenic differentiation potential was assessed by inducing *in vitro* myotubes formation after switching the proliferation medium (Dulbecco's modified Eagle's medium [DMEM] containing 10% fetal bovine serum [FBS], 10% horse serum, 1% Penicillin/Streptomycin, and 0.5% chick embryo extract) to fusion medium (DMEM containing 2% FBS and 1% penicillin/streptomycin). After 2-3 days, cells were fixed in cold methanol and immunostained for skeletal fast myosin heavy chain (f-MyHC)-positive myotubes (1:400, Sigma) and counterstained with DAPI (1:1000, Sigma). Images were taken on a Leica DM-IRB inverted microscope with a 20x objective.

Results:

Culture surfaces with PDMS substrates and protein coatings increase the proliferative capacity of MDSPCs: MDSPCs were observed on 13 separate combinations of protein coating and substrate elastic modulus, including the negative control of tissue culture plastic with no substrate or coating, to evaluate their effects on rate of proliferation (**Figure 1**). Significance in comparison to the negative control (plastic) is denoted with * ($p< 0.05$) and # ($p<0.001$). The highest proliferation rate from each group of substrate elastic modulus came from the condition including the coating of collagen type I. The combination of collagen type I coating on the 50 kPa PDMS provided the optimal condition for MDSPC proliferation.

Qualitative differences in myotube formation between substrate elasticities and protein coatings: MDSPCs were differentiated into myotubes on the various PDMS substrates and protein coatings for 2-3 days, displaying a dynamic range of myotube dimensions (**Figure 2**). MDSPCs cultured on collagen type I and collagen type IV/laminin coatings created more robust and elongated myotubes. Myotubes formed on stiffer substrates (830 kPa and 1.72 MPa) were more numerous, but also more slender, than their broader counterparts formed on softer PDMS.

Discussion:

These findings support the view that optimizing the *in vitro* environment, by modulating the surface culture conditions with a variable stiffness PDMS substrate and protein coating, can augment stem cell proliferation and differentiation capacities. Culture methods such as this may be used to prime MDSPCs towards specific lineages, by simulating tissue conditions of their natural niche, to improve cellular engraftment for therapeutic cell transplantations.

Significance:

Future cell therapies implemented for tissue repair may significantly benefit from the application of primary cells isolated and expanded on PDMS surfaces with protein coatings.

Acknowledgments:

This work was supported in part by the NIH, the Henry J. Mankin Endowed Chair at the University of Pittsburgh, and the Dowd-ICES Fellowship from Carnegie Mellon University.

References:

[1] Lee JY, et al., *J Cell Bio* 150, 1085-1100 (2000). [2] Kuroda R, et al., *Arthritis Rheum* 54, 433-422 (2006). [3] Oshima H, etl al., *Mol Ther* 12, 1130-1141. [4] Lavasani M, et al., *Nat Comm* 3: e608 (2012). [5] Gilbert PM, et al., *Science* 329, 1078-1081 (2010). [6] Engler AJ, et al., *Cell* 126, 677-689 (2006). [7] Palchesko RN, et al., *PLoS ONE* 7(12): e51499 (2012).

Figure 1

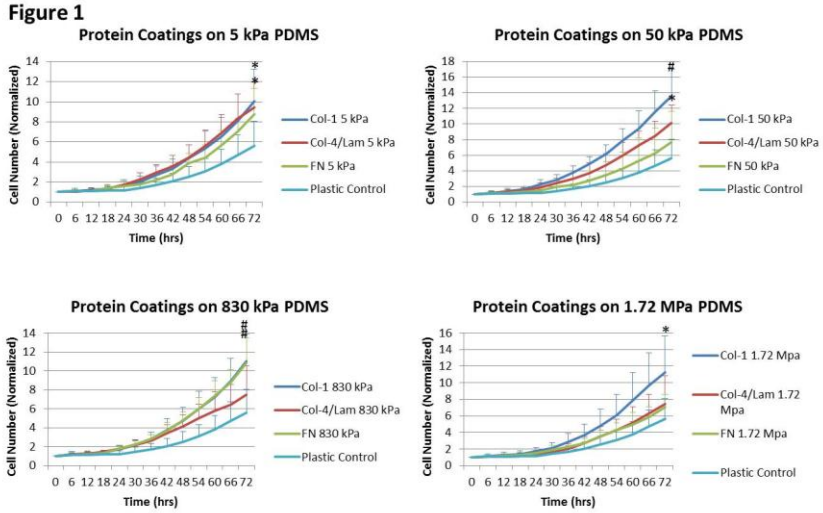

Figure 2